Final Design Report

Cal Poly Wind Power – Balancing System

By

Caleb Cross (*ccross01@calpoly.edu*)

Ethan Czuppa (*eczuppa@calpoly.edu*)

(wpcbalancingteam@gmail.com)

Sponsor: Sophie Spencer

Advisor: John Fabijanic

Mechanical Engineering Department

California Polytechnic State University

Submitted: 3/19/2021

Revised Submission: 3/31/2021

Statement of Disclaimer

Since this project is a result of a class assignment, it has been graded and accepted as fulfillment of the course requirements. Acceptance does not imply technical accuracy or reliability. Any use of information in this report is done at the risk of the user. These risks may include catastrophic failure of the device or infringement of patent or copyright laws. California Polytechnic State University at San Luis Obispo and its staff cannot be held liable for any use or misuse of the project.

Acknowledgments

Caleb and Ethan would like to thank the following individuals for their meritorious contributions that supported this senior project's completion.

Dr. Xi (Julia) Wu – Vibrations Lab Coordinator
Thank you for your patience in office hours, on weekends, and during all our meetings while you helped us understand the intricacies of rotordynamics – at least what we needed for our senior project. We are incredibly grateful for you.

Michael Mullen – PG&E Rotordynamics Engineer and CP SLO Alumni
Thank you for your willingness to help us develop the balancing mechanism and procedure by sharing your knowledge of the literature, relevant ISO standards, and time to review our design. We are incredibly grateful for you.

Jessica Dent – Previous Sponsor
Thank you for this fantastic project, your continued support, your willingness to help us find points of contact within the club! We are incredibly grateful for you.

Sophie Spencer – Current Sponsor
Thank you so much for your support and willingness to accommodate the current situation with regards to our scope. Also, the transition from Jess to you as our sponsor was seamless largely because of your leadership and communication abilities. Jess has passed on the CPWPC to good hands. It was a blast getting to know you and Dunk through 6 months of routine meetings about the status of our project! These meetings were added motivation for our team to do our best in meeting the weeks goals as we looked forward to both updating you on our progress and hearing about the clubs from you and Dunk. We are incredibly grateful for you.

Zach Dunkelberger – CPWPC Mechanical Team Lead
Thank you for putting up with all of our turbine shaft-related questions!! You ran and are running the mechanical team like a champ; keep up the great work! Thank you also for the fun you brought to all of our meetings. We are incredibly grateful for you.

Professor John Fabijanic – Senior Project Advisor
Thank you for the guidance and perspective that you have given Caleb and I throughout this project. Even to the questions you did not know, you had helpful insight into where we might start looking. We appreciate your willingness to be flexible with our timeline and scope. We are sorry that we did not listen to you regarding limiting our scope, in our case, we needed to learn this lesson by doing it wrong. Overall, your advising has been highly formative to both of us, and while you may not miss our meetings, we certainly will. We are incredibly grateful for you.

Abstract

The Cal Poly Wind Power club is anticipating joining the annual Collegiate Wind Competition in the year 2021. This competition hosts schools from all around the country, who meet and compete against each other by testing the wind turbines they have made throughout the academic school year. Tasks included in the competition test the wind turbine's efficiency, power generation, overall design, and stability in extreme conditions.

Cal Poly is planning to implement a formal balancing system to support their 2021 wind turbine. Our senior project team undertook mitigating mass imbalance in the wind turbine; mass imbalance occurs when the center of mass of a rotating object does not lie on the axis of rotation. Our project's original goal was to develop a balancing system to minimize mass unbalance in the wind turbine's rotor assembly and optimize power collection while keeping the turbine safe to operate. While we were able to develop this mechanism and provide design documentation to the CPWPC, we were unable to balance the competition wind turbine.

In this report, we discuss the preliminary research conducted regarding wind turbine rotary systems and rotational imbalances. Furthermore, we will break down our understanding of the project and our approach to completing it, as well as our ideation and down-selection processes. Then, we will detail our plans to cheaply manufacture and accurately balance the wind turbine. Finally, we will outline the next steps needed to thoroughly verify the final design, as well as officially balance the completed 2021 wind turbine.

Contents

1.0 Introduction 4

2.0 Background Research 5

2.1 Summary of Customer & Subject Matter Expert Meetings 5

2.2 Existing Products & Designs 12

2.3 Patent Research 14

2.4 Summary of relevant technical literature 15

2.5 Applicable Industry Standards 19

3.0 Objectives 22

3.1 Problem Statement 22

3.2 Boundary Diagram 23

3.3 Summary of Customer Needs and Wants 24

3.4 QFD Process & Results 25

4.0 Modeling and Preliminary Analysis 30

4.1 Modeling Rationale and Approach 30

4.2 Rigid Shaft Parametric Study 31

4.3 Preliminary ADAMS Model 40

4.4 SolidWorks Frequency Analysis – Critical Speeds 42

4.5 ABAQUS Linear Static and Linear Dynamic Modeling of Rotor Shaft System 48

5.0 Concept Design 50

5.1 Initial Ideation & Concept Block Diagram 50

5.2. Go-No-Go Down Selection 53

5.3 Pugh Matrices Down Selection 55

5.4 Weighted Decision Matrix Down Selection 65

5.5 Selected Balancing Mechanism Finalist Design Descriptions 69

5.6 Final Balancing Mechanism Design Selection 78

5.7 Grooved Plate Final Concept Design 79

5.8 Concept Design of Test Mass Positioner 80

5.9 Balancing System Concept Design 84

6.0 Final Design 89

6.1 Selected Design – Balancing Mechanism & Test Mass Positioner 89

6.2 Grooved Plate Design Justifications 94

6.3 Design Verification Calculations for Grooved Plate 95

6.4 Proposed Balancing System Design 96
6.5 Maintenance and Safety Concerns 100
7.0 Manufacturing 102
7.1 Manufacturing Set-Up 102
7.2 Post-Print Inspection 103
7.3 Manufacturing Considerations 103
8.0 Proposed Testing 104
8.1 Proposed Instrumentation and Measurements to Characterize Mass Imbalance 104
8.2 Testing Procedure 107
8.3 Calibration MATLAB Code 108
9.0 Proposed Design Verification 109
9.1 Update Simulation in ABAQUS 109
9.2 Proposed Testing and Verification Plans 109
10.0 Project Management 112
11.0 Conclusion 113
11.1 Next Steps 114
Works Cited 116
Appendix A - Preliminary Design Flowchart 120
Appendix B - House of Quality 122
Appendix C - Gantt Chart for CPWP Balance 123
Appendix D – Rigid Shaft Parametric Study 124
Appendix E – SolidWorks Frequency Analysis Results 130
Appendix F – Initial Concept Block Diagram & Ideation 135
Appendix G – Mass Eccentricity Derivation 153
Appendix H – Go-No-Go Down Selection 154
Appendix I – Notes on Imbalance Determinants 155
Appendix J – Notes on Michael Mullen's Recommended Testing Procedure 158
Appendix K – ABAQUS Simulation Plan 161
Appendix L – ABAQUS Simulation Report 163
Appendix M – Grooved Plate & Vibrations Test Bed Design Calculations 196
Appendix O – Manufacturing Inspection Log 220
Appendix P – MATLAB Calibration Code 221
Appendix Q – Product Literature 224

Appendix R – Final Project Budget..... 227

Appendix S – Failure Modes & Effects Analysis + Risk Assessment (DesignSafe and Preliminary FMEA)..... 228

Appendix T – Design Hazard Checklist..... 236

Appendix U – Testing Procedure..... 237

Appendix V – The Theory and Practice of Miniature Wind Turbine Balancing 249

Appendix W – Cura © 4.7.1 Slicer Settings..... 259

1.0 Introduction

The Cal Poly Wind Power club (CPWP) was founded to design and manufacture miniature wind turbines. The club aims to provide a thoughtful design experience and build teamwork skills among its members. For the first time in the club's career, the CPWP will be competing in the 2021 Collegiate Wind Competition (CWC). Hosted by the U.S. Department of Energy, the annual competition pits multiple schools against each other in a myriad of competitions to test their turbine's stability, efficiency, and adaptivity to different wind speeds. The winner of each year's competition receives a cash reward for their participation and aptitude.

The first set of rules published by the CWC in preparation for the 2021 competition introduced a new test to the competition: the runaway test. The runaway test specified that each turbine would be subjected to 22 m/s windspeeds while idle. This procedure was added for safety purposes to address safety issues that had arisen in previous competitions preemptively. In part, this test's onerous nature motivated the CPWP to recruit a balancing team to specifically address and analyze the problem of imbalance in the wind turbine. However, the NREL competition committee decided to remove the runaway test and institute an analysis requirement in place of it. In addition to going through our senior project's work over the past year, this report will also provide analysis supporting the verification of this 22 m/s wind speed requirement for the CPWP wind turbine.

For our senior project, we completed the design of a balancing system for the CPWP's 2021 wind turbine. However, we could not balance the turbine due to changing COVID protocols and a significant timeline offset between our senior project and the CPWP. This report covers our senior project's scope of work, background research, problem specification, modeling, design development, final design, manufacturing, and the outcome of our efforts. Finally, we seek our sponsor's permission to accept our final design and prototype balancing mechanism along with the procedure for using it in the Cal Poly mechanical vibrations lab despite the currently unproven state of our deliverables.

2.0 Background Research

Vibrational analysis of an overhung rotating assembly requires complex analysis and a deep understanding of rotordyanmics. Because of this, we placed an early emphasis on developing a foundational understanding regarding the technical aspects of vibrational analysis and the approach that others have taken to balance similar systems. This section will summarize the meetings we hosted with vibrations experts and project leads. We will also discuss the preliminary research we conducted to understand our project and our specific system.

2.1 Summary of Customer & Subject Matter Expert Meetings

Introductory Meeting with Sponsor 4/13/2020:

Our first meeting with the Cal Poly Wind Power club's point of contact (Jess Dent) relayed a few critical goals for the project. Firstly, the wind turbine must complete the CWC's runaway test proficiently and safely. At the beginning of the competition, this test involves rotating the wind turbine at 4000-5000 RPM to ensure the safety of operation during all other tests at the competition. Since the NREL competition committee removed the runaway test from the competition, the turbine's theoretical analysis under runaway test conditions is required instead. The safety criteria emphasized by the initial inclusion of the test and further emphasized by Jess highlights the fact that one of the primary initiatives for our project is to assure the safety of the turbine during operation and the safety of others operating the turbine throughout the competition.

The addition of a thoroughly designed balancing system for the Cal Poly wind turbine is a relatively novel idea. While many CWC participants throughout the previous years of participation have used tail vanes in their final design, many teams do not include a formal balancing system for their turbine. However, with the recent addition of the runaway test before the competition begins, it is more important than ever to ensure that each turbine is safe and stable during testing.

Slack/Email Exchanges with Jess:

From our correspondence with Jess outside of scheduled meeting times, we received the following clarifications on project:

- Our primary deliverable is a balanced wind turbine rotor assembly, a balancing system to balance it on, and a procedure/training for how to use the balancing system.
- Additionally, we are to suggest designs for balance adjustment mechanisms to be implemented on components of the wind turbine rotor assembly, likely including the blades and possibly the mechanical pitching system.
- Although the three senior projects for the Cal Poly wind power club overlap, the intent was for our project to work primarily with the club and the relevant leads and not the other senior project groups. The club encourages compartmentalized design procedures.
- Our customer – the operator of our balancing system who is a member of the club should not need to have a background in mechanical vibrations to successfully use the balancing system that we will deliver
- An accompanying graphical user interface (GUI), as a component of the balancing system is wanted, however, the user interface does not need to be extremely aesthetic or maximally accessible – a rougher MATLAB or EES script interface would be acceptable

- Runaway test conditions for the wind turbine rotor assembly roughly correspond to 22 to 25 m/s wind velocity or 4000-5000 RPM for the low speed shaft.
- The desired unit system for this project and all required analysis is the metric system

Meeting with Rotor Dynamics Expert 04/25/2020:

On Saturday, April 25th Caleb and Ethan met with Dr. Xi (Julia) Wu, Cal Poly mechanical engineering department faculty who specializes in rotordynamics. We presented an overview of CPWP's prototype wind turbine as well as our senior project deliverables to Dr. Wu and were then able to ask her several questions regarding balancing methods, modeling techniques/assumptions, and vibrational measurement/analyzer equipment that would potentially be available for use in the Cal Poly vibrations lab. Dr. Wu relayed the several vital considerations, resources, and even questions we had not anticipated that would require more research.

Firstly, Dr. Wu recommended we approach understanding our physical system through modeling instead of building a strong theoretical background due to the complexity and time required to both understand and correctly apply the theory. Next, Dr. Wu recommended we use ADAMS or SOLIDWORKS "COSMOS" to model the wind turbine rotor assembly and balancing system as an overhung rotor with a rigid, lumped mass (disk) at the end—representing the blades and hub, supported by two bearings. Dr. Wu also explained the complexity that is added to the balancing of the wind turbine rotor assembly due to the overhung configuration of the rotor. Even so, she first recommended we try single plane balancing and confer with her again with simulated results from that approach to see if multiplane balancing would be more appropriate. Regarding other modeling techniques and approaches, Dr. Wu advised against FEA unless we could not get the flexible rotor modeling to work in ADAMS or SOLIDWORKS due to its time-intensive nature and need of graduate-level experience. Since our conversation with Dr. Wu, we have decided to switch our modeling software to ABAQUS. We believe this will simplify the modeling process.

Commenting on the feasibility of using the Bently Nevada rotor kit, Dr. Wu felt that the motor would be unable to deliver the torque required to spin the wind turbine rotor assembly at runaway test speeds due to the wind turbine rotor assembly's large size (45 cm in diameter). Besides the size issue, according to Dr. Wu, the probes on the rotor kit were not the correct kind of sensors for our balancing system. While it was unfortunate for our senior project group to hear that using the pre-existing rotor kit would not be feasible, Dr. Wu also mentioned her access to national instruments sensors to measure acceleration and vibration for our balancing system's potential use.

Finally, Dr. Wu resourced us with lecture and lab material from her rotordynamics class, ME 518, several textbooks used in her class, and a grad student, Luke Costello, to reach out to about his thesis on a wind turbine imbalance predicting algorithm.

Meeting with Rotor Dynamics Grad Student 05/01/2020:

The following week on Friday May 1st, we met with Luke Costello, the graduate student recommended to us by Dr. Wu, and consulted him regarding standards for small wind turbine design, more resources on modeling, and the how to go about verifying that our wind turbine has actually been successfully balanced. Luke was happy to share information with us about his current

research and thesis as well as answer our questions. Luke explained that his method, and that taken by many wind turbine designers, is a mechanics of materials approach – regarding tower, shaft, gearbox component – and is primarily fatigue driven. Design constraints from this approach can then be manipulated to get a permissible level of residual imbalances in the turbine. Regarding industry standards, Luke referred us to another grad student working on another component of the Cal Poly wind turbine project, John Cunningham, who supplied us with the IEC 61400-2 for the design of small wind turbines, somewhat like ours. Since these standards do not specify a limit on eccentricity directly, Luke suggested we try to back out the allowable eccentricity from the following equations in annex F Load Case E: Maximum RPM of IEC 61400-2 given to us by John:

$$F_{zB} = m_B R_{cog} (\frac{\pi n_{max}}{30})^2 \quad \text{(F.27)}$$

$$M_{shaft} = m_r g L_{rb} + m_r e_r \Omega_{n,max}^2 R_{cog} \quad \text{(F.28)}$$

Where, for equation F.27, F_{zB} is the blade force due to centripetal acceleration in the z-direction and acting on the blade root, mB is the mass of the blade, R_{cog} is the radius between the blade and rotor centers of gravity, n_{max} is the maximum rotational speed of the wind turbine rotor. For equation F.28 M_{shaft} is the bending moment of the shaft at the bearing at the front of the nacelle, m_r is the mass of the rotating assembly (blades and hub), L_{rb} is the distance between the rotor center and the first bearing in the nacelle, e_r is the eccentricity of the center of mass of the rotating assembly from the axis of rotation, and $\Omega_{n,max}$ is the maximum angular velocity of the rotating assembly.

Status Update and Check-in Meeting with Sponsor 5/04/2020:

On Monday, May 4th, we met with our sponsor, Jess, to review our revised problem statement and ask a few clarifying questions. Jess was satisfied with the problem statement and said it captured the deliverables we were responsible for precisely and accurately. Jess also pointed out that it would be crucial for us to obtain a range of permissible residual imbalance as an engineering target for our balancing system. In addition, Jess also relayed some dimensions and material properties for the components that make up the current turbine prototype to aid our senior project team in the modeling process. There were several other important points of clarification that we received from Jess in this meeting. (1) That our primary focus is mitigating the mass imbalance in the wind turbine rotor assembly—until this point, many of the specifications in our house of quality had been for systems external to our balancing system. (2) If we need information on a system outside of our scope we should immediately reach out to the club for those requirements, specs, etc. (3) The rules for the 2021 CWC competition have not been released yet, only the primer, so we are to record any questions we have regarding the rules/competition tasks and do our best with requirement/specification writing with the information available to us. Finally, (4) our goal is to get the wind turbine rotor assembly sufficiently balanced such that it is not a hazard and does not reduce performance significantly.

Meeting with Dr. Wu and Michael Mullen 5/24/2020:

On Sunday May 24th we met with our modeling advisor Dr. Wu and one of her graduate students, Mike Mullen, who works at PG&E as a rotor balancing engineer, to seek modeling help from Dr. Wu and balancing system instrumentation advice from Mike. Here are the key recommendations from Dr. Wu and Mike.

- **System Characterization and Instrumentation:**
  - Estimate critical speeds of rotating assembly in SolidWorks
  - Use ISO 14964 Industrial Fan Balancing Quality and Vibration Grades to get vibrational limits that are more representative of our physical system with regards to its size, mass, and rotational speed
  - If using a flexible coupling to attach the motor to the competition turbine shaft, validate that its angular misalignment is not exceeded
  - Investigate fatigue life of aluminum pillow blocks as well as the rest of the turbine test bed structure
  - Estimate natural frequency of Nacelle base plate (currently a thin aluminum plate) to ensure system operating speeds do not coincide
  - Consider fatigue strength of Nacelle base plate based on loading from 1X (once per rotation) mass unbalance in the turbine
  - Measure system vibration at bearing housings with accelerometers and integrate back to get vibration displacement and velocity.
  - For single plane balancing only two orthogonal accelerometers are needed plus one shaft speed/angular position measurement (keyphasor or laser tachometer)
  - Currently the vibes lab has several data acquisition (DAQ) systems that support the sensors needed to characterize our system's behavior
  - Mike's masters thesis work was to develop a MATLAB post-processing interface for the Bently Nevada donated 2300 DAQ and it is currently set up to work for a single plane balancing setup. This would be the interface we would use for our senior project.
  - Mike is willing to assist us in DAQ configuration/setup and also willing to lend us his laser tachometer to get the phase data we need.
- **ADAMS Model Recommendations:**
  - First, consider only kinematic behavior of system by just applying a rotational speed as the imposed motion on the model
  - Second, add an applied torque to that imposed rotary motion (both constant at this point) and compare the kinematic results and this rudimentary dynamic model results
  - Third, use ME 518 ADAMS resources to apply a step torque and rotational speed to the ADAMS model of the system
  - Fourth, add in a resistive torque that opposes the applied torque and is about 10 to 20% of the applied torque
  - Fifth, apply imposed torque and rotational speed as first order step responses on the system:

$$T(t) = T_0\left(1 - e^{t/\tau}\right) \qquad \text{Eq. (2.1.1)}$$

$$\omega(t) = \omega_0\left(1 - e^{t/\tau}\right) \qquad \text{Eq. (2.1.2)}$$

  - Sixth, specify a motor and acquire its torque speed curve. Input this torque-speed curve data into your ADAMS model as a motor driving your system. See the motor tutorials in the ADAMS manual.

Michael Mullen's Thesis Defense 5/29/2020:

Per the recommendation of Dr. Wu, the balancing team attended graduate student Michael Mullen's thesis defense presentation. Mr. Mullen has extensive experience in the Cal Poly vibrations lab and has been developing a custom MATLAB program for his thesis. Michael's MATLAB code is a replacement for select ME 318 and ME 518 labs for the current lab interface. Michael's code reads information from the vibrations lab's data acquisition system (DAQ) using the Bentley Nevada rotor kit. It then performs post-processing analysis to present frequency information in the currently implemented rotor systems in a more easy-to-interpret way for students.

Dr. Wu recommended that this code be considered to evaluate the finalized design's efficiency in reducing mass imbalance in a prototype wind turbine rotor system. Mr. Mullen commented that this program may be helpful, but also proposed an alternative. Bentley Nevada recently donated a 2300 Frequency Monitor to the Cal Poly vibrations lab. This machine can also be used to measure the frequency in a rotating system and may simplify the data acquisition and post-processing computation relative to the newly developed MATLAB code. Mr. Mullen also offered his assistance and supplemental equipment, which could ease the data collection process. The CPWP Balancing System senior project will evaluate both options in greater detail once the Cal Poly campus reopens to students and access to the vibrations lab is granted.

Status Update and Check-in Meeting with Sponsor 6/1/2020:

On June 1st Caleb and Ethan met with their project sponsor Jess to update her on our new knowledge of available vibes lab measurement equipment that is designed to be directly applied to our balancing system, discuss the current state of our modeling, and ask for a preliminary design timeline for CPWP during the summer. Jess was pleased to hear that we had access to sensors, data acquisition systems, and software to adequately instrument our system. Jess was also satisfied with the current state of our modeling and recommended that we attend the leads meetings for CPWP over the summer in order to stay up to date with the competition turbine's design progress as well as have the opportunity to make design recommendations based on our modeling and analysis.

Meeting with Sophie Spencer (President of the Cal Poly Wind Power Club) 9/22/2020:

On September 22nd Caleb and Ethan met with their new project sponsor, Sophie Spencer, to discuss the CPWP's position on the need for our senior project for their system given the removal of the runaway test (current CWC 2021 Rules Section 3.2.2). Sophie expressed that our senior project would still be needed. The vibrational analysis and testing that were still within our responsibility to conduct would be included in the now-required analysis submitted to the CWC to prove that the small wind turbine rotor could survive 22 m/s free stream wind speeds.

Mass Imbalance Mitigation Design Considerations Meeting with CPWP 9/29/2020:

A week later, on September 29th, Caleb and Ethan met with several members of the CPWP, including the president, mechanical team lead, mechanical team members, and several members of the turbine senior project (everything past the nacelle). In this meeting, Ethan and Caleb provided design considerations that help mitigate mass imbalance in the wind turbine rotating assembly to the CPWP while also providing clarification on the design considerations that were confusing to the CPWP members in attendance. While Ethan and Caleb hoped that the pitching

and blades senior project teams would be in attendance, neither was able to attend. This meeting was the informal presentation version of the memo Ethan and Caleb had wanted to provide to CPWP and other CPWP senior projects by the middle of the quarter. The notes from the meeting were sent to the blades manufacturing and pitching senior project teams – and are available in Appendix I.

Dr. Wu Office Hours – Balancing Disc Placement 10/06/2020:

In need of clarification on the importance of the placement of the balancing mechanism in proximity to the plane of balancing correction, Ethan and Caleb attended Dr. Wu's office hours. Dr. Wu quickly pointed out that placing another lumped mass (the balancing mechanism) anywhere but fairly close to the plane of the rotor and hub would create a system that would have to be modeled as a multi-degree of freedom (MDOF) system instead of just a single degree of freedom system (SDOF). Dr. Wu explained that this practice of offsetting the balancing mechanism from the plane of correction is never done due to the resulting astronomical increase in complexity of the dynamic balancing as well as balancing equations. Dr. Wu provided our senior project team with a crucial design constrain. Up to this point, several of our designs were located inside the nacelle of the wind turbine while the mass imbalances we hoped to correct were outside in the plane of the rotor.

Phone Call with Michael Mullen Regarding Instrumentation of Wind Turbine 10/06/2020:

On October 6th, recently graduated graduate student and current PG&E rotordynamics engineer, Michael Mullen, called Caleb to discuss the equipment needed to instrument the prototype/competition CPWP wind turbine. Michael informed of several measurement methods using either a single or two accelerometers or two non-contact eddy current proximity probes to get shaft displacement data with a laser tachometer or Bently Nevada Keyphaser ® probe to get the shaft phase data. Michael also suggested the ADRE 208 data acquisition (DAQ) system be employed to collect all of this output data in order to construct the polar plot that would then be used with the ME 318 single plane balancing procedure to balance the CPWP wind turbine. The exact list of equipment and explanation methods is explained in greater detail in section 7.0. Notes regarding the phone call can be found in Appendix J.

CAD Meeting #1 with Pitching Senior Project 10/22/2020:

On Thursday, October 22nd, 2020, our senior project met with the pitching mechanism senior project for the first time to discuss the potential integration of our mechanisms. Since the pitching mechanism occupied the entire region behind the housing, only our single plate balancing mechanism designs would be useable with the pitching team's current design. Pitching provided their current CAD for us to do a mock-up of our selected design so that in the CAD review meetings to come, we could easily catch incompatible portions of our respective designs.

CAD Meeting #2 with Pitching Senior Project 11/17/2020:

On Tuesday, November 17th, 2020 Our senior project team met with the pitching team to discuss our mostly finalized CAD of the balancing mechanism. The Pitching team related their design changes – reducing the size of the rotor housing and increasing the length of the overhung shaft from the end of the nacelle to make room for the pitching mechanism's actuation. Due to the increase in the length of the shaft's overhang, they requested that we make our balancing mechanism as light-weight as possible. Due to our part's complex geometry, our senior project had

already selected 3D printing as our primary manufacturing approach. Our senior project team decided to downsize our grooved plate to match pitching's smaller hub size. Together, our two teams decided to meet again when both of our CAD models had been finalized.

CAD Meeting #3 with Pitching Senior Project 1/12/2021:

On Tuesday, January 12th, 2021, our senior project team met with the pitching senior project team to showcase our finalized design and review it with the pitching team. Our senior project team had decided against downsizing the hub as we had been unable to quantify the imbalance ceiling and were concerned a smaller diameter would impair the ease of adjusting the test masses and impair their effectiveness. The pitching team approved of our design changes once we confirmed that our larger grooved plate would not interfere with the pitching of the blades. Our senior project also gained approval from Jess Dent in parallel with this meeting – our previous sponsor and Aero team lead for the CPWP, for having the grooved plate overlap the wind turbine's blades' roots. Finally, pitching offered to add a boss onto their hub's housing where the grooved plate could mount directly instead of using spacers.

CPWP Balancing Sponsor Meeting 02/05/2021:

On Friday, February 5th, 2021, our senior project team met with project sponsor Sophie Spencer and mechanical team lead Zach Dunkelberger. The meeting specifically discussed the manufacturing timeline for the official 2021 wind turbine, updating both parties on finalized design parameters and the specifics of the virtual testing program being implemented by the WPC to substitute for in-person testing. Our team also sought to establish the exact deliverables desired by the CPWPC, in preparation for the soon delivery of those results. Sophie and Zach clarified that the CPWPC above all, desired tools which can be used in the future to balance the wind turbine. Due to the short timeline left to complete the project, we decided to focus our efforts on a comprehensive memo explaining the theory and practice of wind turbine design, a practical testing procedure which can be used to balance the wind turbine, as well as the tools to complete the incomplete sections of the balancing procedure. Sophie and Zach agreed that these deliverables were acceptable and ideal. Henceforth, the remainder of our project was concentrated on conveying information and tools to the club for future usage. Additionally, our team plans to participate in the formal balancing process during the Spring 2021 quarter directly.

E-Mail Correspondence with CPWPC Advisor Professor Kean (03/19/2021):

In order to obtain vibrations lab access for the Spring 2021 quarter, we reached out to the club advisor for the CPWPC: Professor Kean. Kean has in turn contacted ME faculty in an effort to formalize us as Cal Poly volunteers. By becoming a volunteer, we will be able to access the Cal Poly vibrations lab after graduating and help in the balancing process and in completing the proposed testing procedure. Since we are the most knowledgeable participants of the testing procedure, we hope to be valuable in the balancing effort and in flushing out the technical gaps of the current testing process. By being in the lab during the testing, we will also be able to observe the process and make amendments to the testing procedure as necessary. Kean is continuing to work on officializing us as volunteers, and will remain in contact with us throughout the process. Once the process is complete, we hope to continue to help the WPC by assisting in the first balancing procedure and making recommendations for future improvements as needed.

2.2 Existing Products & Designs

There are currently many accepted industry methods and tools used to balance rotors. While many of these products exceed our allotted budget, examining machine designs and speculating on the adaptivity of existing products for our purposes is worthy of consideration and research. Below in Table 2.2.1 is a list of five balancing mechanisms used in various industries for various applications. Along with their names is a list of specifications needed to balance a rotor and the price of that machine. Please note that some items must receive a quote from the manufacturer before a purchase can be made. While the exact price of these items is not known, we estimate these machines fall in between $1,000 and $10,000, with machines providing less residual imbalance costing more.

Table 2.2.1 Similar product and specifications table.

Product Name	Maximum Rotor Diameter [mm]	Maximum Rotor Weight [kg]	Minimum Residual Imbalance [mm]	Motor Rating [W]	ISO Standards Met	Price [$]
RYQ-3 Turbine Shaft Balancing Machine	350	0.1 - 3.0	$< 5.0 \times 10^{-4}$	90	ISO 12100	3000.00
Pasio 5 Series Rotor Balancing Machine	150	5.0	1.0×10^{-4}	100	ISO 7475	Quote Needed
Ranger RWS-1B Bubble Wheel Balancer	N/A	N/A	2.0	N/A	N/A	155.00
Minibalancer MI 2100	N/A	N/A	0.01	N/A	N/A	Quote Needed
Erbessd EI-30	533	15	2.0×10^{-5}	124	ISO 2953	Quote Needed

See references [1],[2],[3],[4] and [5] for respective information on each product.

The RYQ-3 turbine shaft balancer is the only machine we found which was specifically designed to balance turbine rotors. The machine is specifically made for low-weight turbine rotors for smaller turbines. Additionally, it is one of the few products for which we could ascertain a price and has a user-friendly interface. The RYQ-3 balancing machine is an excellent example of a machine that can balance the CPWP turbine consistently throughout the years. However, with the price as expensive as it is, especially when accounting for our budget of <$500, it becomes clear that the design we invent must meet the standards for small turbine balancing while remaining cheap to manufacture and use.

The Pasio 5 Series rotor balancing machine is a safe and precise machine intended to balance small rotor systems. While the Pasio 5 Series is not seemingly applicable to a wind turbine system—as the wind turbine's hub and blades are too large to be used on the machine—it was the most precise balancing mechanism we were able to find. The Pasio 5 Series also has an intuitive machine

interface. These are great expectations to hold our design to as well, especially since any CPWP member would be able to operate the system effectively.

The Ranger RWS-1B Bubble balancer is intended to balance car wheels. The mechanism is a simple upside-down aluminum alloy cone with a rod protruding from the convergence. The simplicity of the design lends itself to the cheap price tag. A car wheel can be mounted on the rod, and the imbalance of the wheel can be measured via a bubble meter. Theoretically, a similar structure could be used to measure rotor imbalance in the hub and blades by placing the hub into a rod and measuring imbalance due to asymmetrical design. However, this system has no formal method of correcting mass imbalance. While it is possible to correct the visible imbalance with sanding the blades, the precision of the bubble meter and the subjectivity related to sanding the blades are likely not precise enough for our purposes. Additionally, this method provides no dynamic balancing, which will likely be needed in our final design.

The Minibalancer MI 2100 is a field balancing device. This device can measure imbalance, vibration, and rotational speed for a system in the field. It is also very transportable. The key point of interest for this product concerning our project is the ICP sensor it utilizes to measure these qualities. The MI 2100 also boasts of a self-proclaimed reasonable price, which could not be confirmed. However, the price of the sensor is vital to our project, as a vibrational sensor is the most accurate way to determine vibrations in a system. This device's shortcoming includes the lack of a balancing procedure, which is an essential component to our project.

The Erbessed EI-30 balancing machine shares a lot of similarities with the Pasio 5. Both machines are equivalently accurate and are designed to be safe. The Erbessed EI-30, however, is not as intuitive to operate. With nearly no operator interface, the Pasio 5 seems even more simple and easy to use. The Erbessed EI-30 has some strengths over the Pasio 5, as it can handle heavier imbalances and a wider range of rotor diameters. The range exhibited by the Erbessed EI-30 is convenient for multiple systems. Even so, the CPWP's annual wind turbines will likely have a consistently small rotor diameter, so wide ranges are not necessary. Additionally, a more user-friendly interface is nearly necessary, as a series of steps for a specific rotor assembly may limit future design opportunities and limit who can operate the device.

Overall, we came across a few great examples of machines that can balance the CPWP wind turbine. However, many of them are out of the price range offered by the CPWP. While our device may not need to be as precise or heavy-duty as the machines provided in Table 2.2.1, it will need to measure and eliminate rotor imbalance within the turbine to an acceptable amount and at a fraction of the cost. One acknowledgment that came from this research was the spike in precision related to the usage of a sensor. The RYQ-3, Pasio 5, MI 2100, and EI-30 all used specialized sensors to measure the mass imbalance in the rotating assembly, which resulted in much more precision relative to the wheel balancer we considered. Even though it is the least precise sensor, the MI balance sensor may be precise enough for our purposes. Based on our conversation with Michael Mullen, the accelerometers available in the mechanical vibration lab at Cal Poly are sufficient for measuring vibrations in the wind turbine due to mass imbalance. In any case, this research proved helpful for identifying balancing machine elements essential to our vibrations testbed. These elements include physical barriers to protect the user while the machine is operating,

a simple user interface, known eccentricity in the mechanism, and dedicated sensors to measure the imbalance in the rotating assembly.

2.3 Patent Research

Before moving forward with designing a methodology or mechanism to balance the system, we wanted to examine some existing patents that relate to wind turbine balancing. Studying other designs and balancing methods will provide insight on effective, proven balancing methods and can be a helpful contrast to further study which procedures and accessories can be applicable to our design expectations.

Patent US8683688B2 [6] is a wind turbine balancing method which requires measuring a system component that is dependent on the motor workload and calculating rotor imbalance from that measurement. Another calculation is then performed to find the necessary pitch angle modification to eliminate this imbalance. The pitch angle of the blades is then changed to cancel out rotor imbalance in the system. Having a system with a variable input parameter to measure imbalance is convenient and innovative, but seemingly very complicated and would require a large amount of technical analytics, which may be outside the scope of this project.

Patent US8206110B2 [7] is a wind turbine balancing accessory, described as a “threaded ballast,” which can be screwed into holes in the turbine blade to reduce the imbalance. This method presents a few issues. Firstly, there is no measurement of imbalance to base balancing on; the threaded ballasts' usage must be based entirely on intuition and observation and is therefore not likely to be accurate. Furthermore, adding threaded holes to the blades is beyond this project's scope, as we are not responsible for blade design.

Patent US20120183399A1 [8] is a wind turbine balancing method that involves measuring rotor imbalance with a sensor in multiple pitch angle configurations. An algorithm then finds the ideal pitch angle for all blades to minimize imbalance and rotates the blades to the new optimal angle. This method—along with the method presented in US8683688B2—seeks to minimize imbalance by adjusting the pitch angle of the blades. While this is a feasible method to reduce vibrational effects, this solution presents an issue to our design requirements, which will be discussed in greater detail later.

Patent US5140856A [9] is an in-situ wind turbine balancing method that measures the acceleration on critical drive train components. These signals are conditioned and fed into a frequency spectrum analyzer to determine the amplitude and phase of the vibration. This information can then be used to locate and place a counterweight to mitigate the imbalance correctly. Recommendations are also made for fixing the yaw on the turbine such that it cannot yaw during testing as unanticipated yawing skews the measurement.

Patent ES2647816T3 [10] is a wind turbine balancing method that involves parameterizing wind power and turbulence intensity to predict rotor rotational speed changes. The new speed is compared to the threshold operating speed for the generator. If the threshold generator speed is ever met, the generator is shut off.

And finally, patent CN102465830A [11] is a wind turbine balancing accessory which involves mounting masses to the wind turbine pitching mechanism to reduce imbalance. This method seems simple to design, implement, and has the potential to balance the rotor without the addition of a new subsystem. However, it does not include a balancing methodology. Without being able to quantify the imbalance within the system, balancing the system become impossible.

The patents we researched have a couple key similarities. Most patents are balancing methods which measure the system's imbalance directly (via vibration sensors) or calculate the system's imbalance through another parameterized measurement. In addition, most of the patents we found adjust the pitch angles of the blades to reduce or eliminate imbalance.

When taking these patents into account, it seems clear that measuring or analytically calculating the imbalance in the system seems essential to our project's deliverable. This is not a surprise, as calculating imbalance is necessary to correct the imbalance within the system. However, the variation through which the imbalance is calculated is surprising and lends many feasible avenues for our project's design. While direct measurement of the rotor imbalance through a sensor seems like the most convenient and precise method of imbalance measurement, vibrational sensors can be expensive and may exceed our allotted budget.

However, many of the reviewed patent's designs are not in alignment with our design expectations. For instance, patent ES2647816T3 has a shut-off condition. An automatic systemic shut-off would abruptly prevent power collection and impede CPWP's ability to rank highly at the CWC. A shut-off condition may be applied in the future to the turbine as a safety protocol, but that decision will be left up to the club and will not be designed for in the balancing subsystem. Additionally, pitching blades to reduce imbalance will also possibly impede power production. While this balancing procedure is seemingly convenient, common practice, and self-contained within the preexisting systems of the wind turbine, compatibility between the two subsystems may not be possible or optimal for power collection. This realization helped drive our senior project team's decision to add a secondary system to the wind turbine to balance rather than modify preexisting subsystems.

Overall, the patents we have included from our research proved to be an excellent source of ideas for our concept and preliminary design phases.

2.4 Summary of relevant technical literature

Rotor balancing is crucial to ensuring that rotating machinery remains safely operable. In their literature review, Foiles et. al covers the development of analysis and technical underpinnings of the field. [12] In general, an unbalance occurs in a rotor-mass system when the geometric axis of rotation is not concentric with the center of mass of the system [14]. In other words, the rotor is also known as the shaft, and anything that rides on the shaft is considered the mass or lumped mass(es). This eccentricity, often communicated as a mass-radius product, produces a variety of dynamic responses in rotating machinery that are functions of the magnitude of the eccentricity, the speed of rotation of the rotor, the characteristics of the rotor's supports/constraints, the rotor's flexibility or rigidity, the distribution of mass or lumped masses attached to the rotor, and many otherfactors[12][13][14].

Balancing methods can be divided into several subcategories, but in general, they take the form of static and dynamic balancing [15]. Additionally, rotors (shafts) are categorized as rigid or flexible; this classification is typically based on the rotational speed of the rotor with reference to its critical speed – the speed at which deformations of the rotor become especially large and may grow without bound depending on the damping of the rotating system (similar to resonance in a translational system) [13]. Static balancing is typically applied to thin rotors, where all the distributed mass of the modeled lumped mass is assumed to be in a single plane and is achieved when the sum of all forces acting on the rotor is zero [14] [15]. Dynamic balancing accounts for the distribution of the mass of the lumped mass to be in multiple planes and is also referred to as a two-plane or multi-plane balancing [14]. The conditions for Dynamic balancing are both that the forces acting on the rotor sum to zero and the moments induced from an imbalance in different balance planes on the rotor also sum to zero [14]. However, perfect balancing of a rotating piece of machinery is unnecessary given that effective balance leaves a residual unbalance that is inconsequential to the system from an engineering perspective [12].

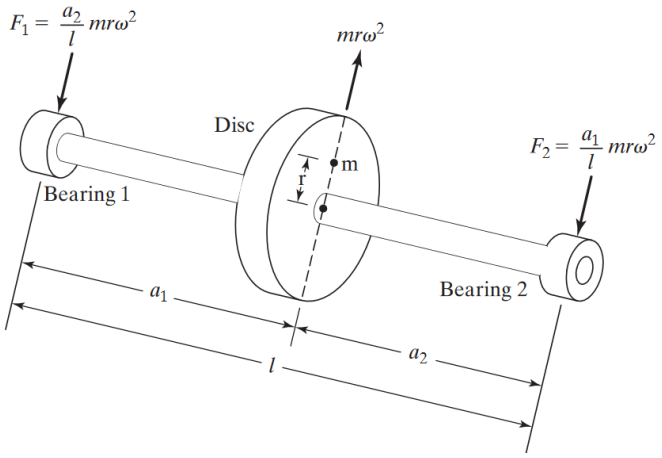

Figure 2.4.1 Single Plane Balancing. [14]

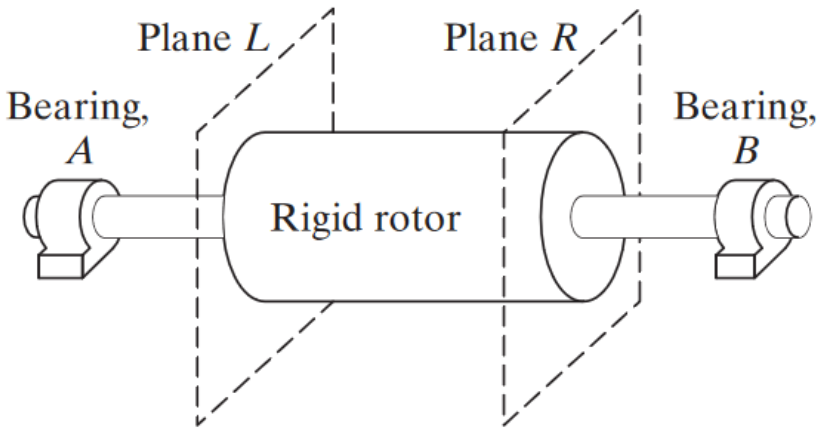

Figure 2.4.2 Two Plane Balancing Schematic [14]

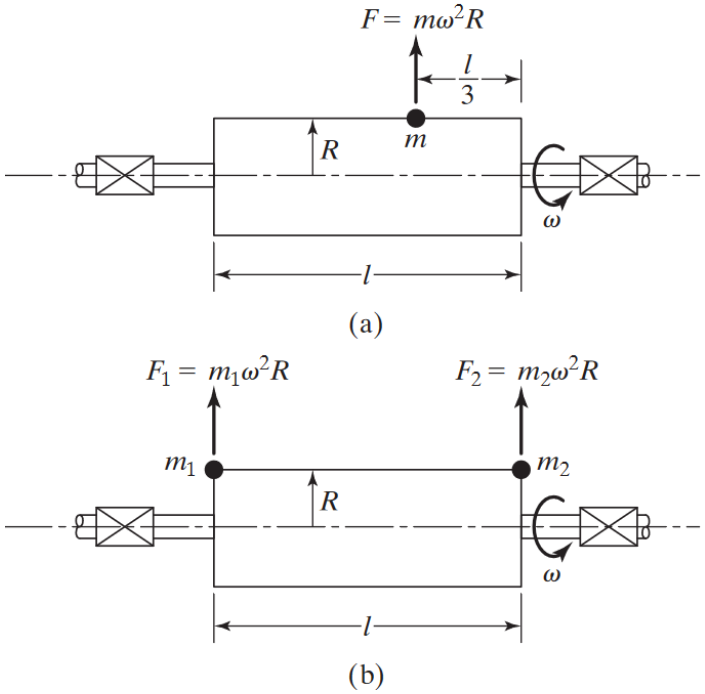

Figure 2.4.3 Two Plane Balancing – expression of equivalent masses for correcting the illustrated mass imbalance of a thick rotor [15].

For our senior project, we are primarily concerned with the balancing of a small-scale wind turbine rotor assembly. In comparison to an industrial balancing machine, the most common approach taken with balancing larger pieces of rotating machinery – like a wind turbine – is field balancing or in situ balancing [16]. The prevalence of this balancing method is due to the difficulty and cost

prohibitive nature of removing a wind turbine rotor to be balanced on a balancing machine as well as the tendency of the rotors to require trim balancing once they have been installed on the wind turbine [16] [17]. In situ balancing is just dynamic balancing via instrumentation of bearings and the rotor on the piece of rotating machinery [16][17]. This instrumentation typically consists of accelerometers, tachometers, and a sensor to monitor the angular displacement of the low-speed shaft to synchronize all the sensor data [13][16]. The collected data can then be processed in several different ways depending on how the balancer has chosen to balance the rotor. However, common to all is the frequency domain analysis of the sensor data, usually a fast Fourier transform (FFT)[16].

Field balancing can be done with or without trial weights [12]. These weights act to characterize the rotating system's response to an added imbalance to then calculate the position of the correction mass(es) [12]. Calibration runs, where no additional weights have been added to the turbine are also used to determine the initial imbalance of the system, which will later help assess how well the system has been balanced [12] These calculation methods include the influence coefficient method (experimental or analytical), the modal balancing method, the least-squares error method, and other iterative approaches to determine both the angular location and amount of correction mass to be placed in each balancing plane [12].

The following summaries of technical papers and journal articles are pertinent to, or present novel solution approaches to our senior project – designing and building a balancing system for a small-scale competition wind turbine.

In their article titled, Mass and Aerodynamic Imbalance Estimates of Wind Turbines, Niebsch, Ramalau, and Nguyen present an algorithm they have collaboratively developed to improve condition monitoring in off-shore wind turbines using only measured vibrational data from the wind turbine. Niebsch et al. constructed a finite element model of an entire Vestas V80-2MW wind turbine accounting for the mass and stiffness of various components. After solving the resulting ordinary differential equation (ODE), the researchers then proceeded to solve the non-linear, inverse version of the problem so that the mass and aerodynamic imbalances theoretically present in the wind turbine model could be computed directly from measured vibration data. The non-linear techniques presented here are too advanced and likely too difficult/time-consuming to implement in our senior project's analysis. However, the state space solving approach of a finite element model of a portion of the wind turbine may prove helpful to verify that our balancing system has successfully balanced CPWP's turbine.

An article published in Wiley Interscience documents the design and usage of a model for a flexible wind turbine and a dampening, passive control system. The project leads first developed an equation of motion (EOM) describing the wind turbine tower, hub, and blades. This EOM was solved then transformed into the frequency domain using the Fourier transform. Their analysis showed that while damping can certainly be used to reduce system vibrations, active control systems are still recommended for high-performance wind turbines. This conclusion was derived from the relative inefficiency of a passive system when compared to an active system, in addition to the fact that passive damping is time-variant and therefore not sufficient for long-term usage.

Another research article also attempted to model an active controls system in a wind turbine and analyze the resulting edgewise vibrations. After modeling the system using the Euler-Lagrangian

approach, the representative equations are transformed into a time-invariant domain using the Coleman transform. The research conducted resulted in a feasible, self-proclaimed "innovative" edgewise vibration controls system. The system involves active, linearly modeled tendons within the blades which can be drawn taut to reduce edgewise vibrations. Using real wind turbine data, researchers predicted a 56% reduction in residual displacements. While this system is interesting and possibly quite effective, attempting to design the blades with the active controls system proposed in this article would be stepping outside our project's scope. Additionally, an active balancing system within the blades could not be applicable to varied, future designs the CPWP may want to pursue.

One group of researchers set out to model flap-wise vibrations in wind turbine blades due to rotation and compare these vibrations to the system's natural frequencies. This vibrational modeling is of interest to our project as the runaway test requires a high rotational speed, which could cause blade vibration. The study concluded that rotational speed affected the natural frequencies of the blades and nacelle. They used a specialized algorithm to calculate the frequency distribution and actively eliminate rotor imbalance. Varying natural frequencies are certainly relevant for our project, as our turbine will be spinning at multiple speeds. Additionally, one imbalanced or vibrating component can affect multiple other components in our system. Thus, we determined that measuring or calculating varying natural frequencies is essential to our project's safety and integrity.

As our senior project team became more well-versed with rotordynamics terminology, we communicated more effectively with Dr. Wu and Michael Mullen – the rotordynamics consultants for our senior project. Dr. Wu and Mr. Mullen's increased understanding of our system's parameters led to the realization that a single plane balancing approach without consideration for flexibility or shaft whirl from the gyroscopic effect would be sufficient for the CPWP wind turbine. Although we were unable to test our system and collect validating test data, the breadth of research we conducted proved to be a fantastic basis for modeling our system and ideating potential problem solutions. Especially as the intricacies of modeling and problem solving came to light, the studies conducted by international researchers also helped develop our balancing procedure and system.

2.5 Applicable Industry Standards

To get a better understanding of helpful industry standards to guide our design, we talked to Cal Poly graduate student Luke Costello. At the time, Luke was working on a wind turbine modeling program for his thesis and had extensive vibrations experience. Luke connected us to an industry professional and friend, John Cunningham. After asking for an industry-standard recommendation for small-scale wind turbines, John recommended IEC 61400-2 [21]. IEC 61400-2—further acknowledged as just IEC—is a modification of IEC 61400-1, intended for small turbines. IEC recommends a series of equations used to model system loads. IEC also recommended using ISO standards in conjunction with its own standards to give a complete list of specifications for design, manufacturing, installation, and maintenance for small wind turbines.

IEC load modeling applies to the CPWP turbine, as it meets the designated IEC requirements: the CPWP turbine is a horizontal axis wind turbine with two or more cantilever blades. IEC load modeling also requires an assumed rigid hub. We reached out to Dr. Wu regarding this

assumption's validity and found that the hub could be reasonably treated as rigid, but the shaft should be modeled as flexible in our analysis. It is important to note IEC analysis is carried out through a mechanics of materials approach. Material property values used in calculations should be estimated within 95% probability with 95% confidence. While the IEC is a fantastic resource for small wind turbine modeling, our models necessitate a vibrations analysis approach instead. However, the IEC standards that John recommended have also been passed along to the CPWP, making it public for the entire club.

Additionally, during our research, we encountered several other ISO standards about the design, safety, testing, and risk assessment of balancing machines. We chose to seek out and utilize such standards due to our team's lack of rotor balancing knowledge. We have provided the following list of ISO standards, accompanied by summaries of their relevance to our project below.

- ISO 1940-1 (1984) Rigid Rotor Balancing Quality Grades [23][24]
    - Gives Balancing Grades and Equations to calculate permissible residual imbalance (imbalance remaining in rotating machinery post balancing).

- ISO 2935-1 (1999) Balancing Machine Testing and Proving [25]
    - Gives Balancing machine proving guidelines and test procedure specific to the type of rotor being balanced –including overhung rotors (the configuration of our balancing system).

- ISO 7475-2002: (2007) Balancing Machine Safety Requirements [26]
    - Gives explicit equations for the calculation of energy absorbed by safety enclosure and other pertinent safety guard design information.
    - Annex A: Class C Enclosure Selection – provides enclosure classification convention as well as methods to calculate the area specific energy the enclosure must absorb to meet this ISO standard—be qualified by a manufacturer as class C.

- ISO 12100-2: Rotating Machinery Risk Assessment Standards [27]
    - An Extensive risk assessment procedure for Balancing machines

- ISO 14694: Industrial Fans – Specifications for Balance Quality and Vibration Levels [28]
    - Gives balancing grades and vibration levels applicable to industrial fans (more representative of our system than large scale wind turbines or large pump impellers as described in ISO 1940)
    - Section 8.3 "Fan vibration limits for test in manufacturer's work-shop" gives specific balance and vibration (BV) grades for different kinds of industrial fans (classified according to ISO 1940-1) in Table 4 (See Appendix M Table M.3).

- ISO 11342: 1998 Mechanical Vibration – Methods and Criteria for the Mechanical Balancing of Flexible Rotors [29]
    - Based off ISO 1940-1 and uses modal balancing correction factors to adjust recommended residual imbalances from ISO 1940-1 as a function of operating speed proximity to system critical speeds.

ISO 1940-1 introduced us to the concept of balancing grades – the allowable amount of mass imbalance remaining in a turbine after balancing. This particular standard is for rigid rotors – shaft and lumped mass assemblies that operate below their natural frequency. However, our team was able to base several useful parametric studies off of this standard (see section 4.2 and appendix D).

ISO 7475-2002 provided the formulas and calculation approach to estimating the guard's enclosure thickness surrounding the rotating wind turbine rotor. Our senior project team determined that an enclosure constructed from ½" plywood would resist penetration from the debris of the 3D-printed turbine blades based on the analysis approach suggested by this standard. However, several definitions of material properties used in the suggested approach were vague, so our calculation – (see appendix M, Table M.4) should be regarded as approximate at best.

ISO 14964 proved to be the most useful to our team in calculating the residual permissible imbalance limits for the CPWP club's miniature wind turbine. Since many fans have narrow rotors (the diameter > rotor thickness by at least a factor of two) and are in an overhung configuration, this standard matched the CPWPC's wind turbine characteristics the best. Table 4 in section 8.3 gives vibration limits as velocities (mm/sec) for balancing an assembled fan. We selected these more stringent balancing vibration limits as the turbine's rotating assembly must be balanced separately from the tower. Despite being lightweight, the miniature wind turbine's relatively high operating speed led us to select balancing grades BV-2 and BV-3 for the upper and lower bounds on residual mass imbalance, respectively. Balancing grade BV-2 corresponds to ISO 1940-1's G16 balancing grade or 16 mm/sec (max) of allowable vibration velocity measured after balancing. Balancing grade BV-3 corresponds to ISO 1940-1's G 6.3 or 6.3 mm/sec (max) of allowable vibration velocity after balancing. Even though BV-1 would technically suffice for this miniature wind turbine, our team selected the subsequent two balancing vibration grades in pursuit of further reducing the likelihood that the turbine will yaw undesirably from mass imbalance during operation.

We retained ISO 11342 in the event that our analysis showed that the rotating assembly would operate above its first natural frequency. However, our analysis showed that the wind turbine rotor and shaft would operate below their composite natural frequency, so our senior project did not use this standard. Since this standard is a simple extension of ISO 1940-1, we decided to mention it in this report for potential future use by the CPWPC.

Our senior project team did not use ISO 12100-2 or 2935-1. We were unable to complete a preliminary design of the vibration testbed for the wind turbine due to time constraints and COVID-19 protocol complications. However, since these standards are especially pertinent to testing safety, we have included them as a recommendation to both the CPWPC and the next senior project assigned to this task.

3.0 Objectives

The 2020-2021 competition year is the first time that the CPWP has considered addressing the problem of imbalance in their rotor system. As a novel consideration for the CPWP club, it is crucial that we thoroughly define the problem and how we plan on solving it. This section will detail our project's scope, designate the specific problem we addressed, and explain the work performed to define the problem adequately.

3.1 Problem Statement

Our senior project team, consisting of Caleb Cross and Ethan Czuppa, shall create and implement (1) a balancing system preliminary design for use with the Cal Poly Wind Power Club wind turbine rotor assembly, (2) balance adjustment mechanisms for the blades, hub, and potentially the pitching mechanism., and (3) an easy-to-use procedure for balancing the assembly. The result of the completion of the three primary objectives will be a balanced wind turbine rotor assembly. Immediately below, we have provided detailed versions of the objectives we outlined above.

(1) This wind turbine rotor assembly balancing system shall be capable of accurate, repeatable, and safe rotating assembly imbalance characterization, providing direction of the user to mitigate this imbalance via the balance adjustment mechanisms to within an acceptable amount of residual imbalance. Additionally, during steady-state operation, the result of balancing on the system should be the elimination of unanticipated wind turbine yawing to help maximize power output. The desired form of this deliverable is a concept design that members of the CPWP club and/or members of this senior project team can use to construct the balancing system.

(2) Similarly, the balance adjustment mechanisms shall not impair the proper functioning of the components that they balance e.g., causing the boundary layer to be tripped on any one of the blades.

(3) Finally, the balancing procedure shall be simple and easy-to-use for the Cal Poly Wind Power Club members that will be employing the balancing system and adjusting the balancing mechanisms implemented on the final wind turbine rotor assembly by this senior project team. This procedure shall be well documented to allow for increased ease of future knowledge transfer/training and not require significant knowledge of mechanical vibrations.

Parameters that directly affect imbalance in the wind turbine system but are not within the scope of work mentioned above have been presented to the CPWP as design recommendations for the wind turbine's features.

3.1.1 Definitions:

- **Wind turbine rotor assembly –** referring to the assembly comprised of the blades, pitching mechanism, hub, and rotor drive shaft.
- **Accurate –** the ability for the completed balancing system and mechanism to correct present mass imbalances within the designed tolerances.
- **Repeatable –** the ability for the balancing system and mechanism to consistently balance a range of wind turbine rotors and shafts comprised of components that are all within the

specifications outlined by the pitching, blade manufacturing, and CPWPC senior project teams.

- **Safe** - insofar as with appropriate risk mitigations taken e.g., safety glasses are worn ANSI z81, appropriate engineering safety controls are implemented such that operation of the balancing system will not damage vibes lab equipment or endanger/cause injury to operator/bystanders

3.2 Boundary Diagram

One way to express the scope of a project is through a boundary diagram. A boundary diagram is a photograph or block diagram connecting system subsystems. Boxes are then superimposed onto the diagram's photo to represent the physical qualities that fall under our team's responsibility. For this project, we decided to do a boundary diagram based on a wind turbine diagram and a block diagram. We have supplied the first boundary diagram immediately below in figure 3.2.1 and the second on the following page.

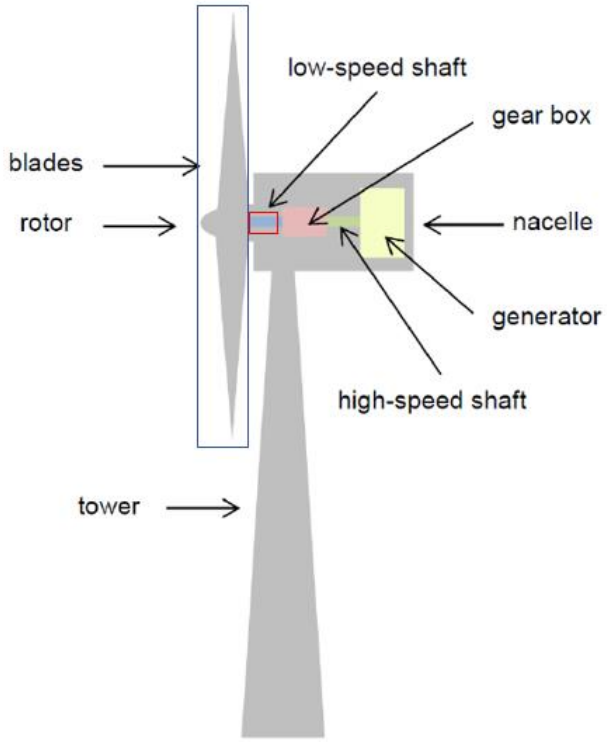

Figure 3.2.1 Boundary diagram for balancing system of a visualized wind turbine.

The above diagram emphasizes two main areas of interest in our project. The first is the connection between the rotor's hub to the low-speed shaft in the wind turbine. It is important to note that since the CPWP is not planning on developing a gearbox, there will be no difference between the low and high-speed shafts. Therefore, both will simply be acknowledged as the shaft moving forward.

The shaft and hub assembly are critical to our project, as shaft vibration due to mass imbalance in the hub is the key component of the imbalance we are trying to eliminate. The hub and blade

assembly will be vulnerable to asymmetrical features and dynamic loading; balancing the rotating shaft is one of—if not the most important—tasks we must achieve with our design.

We initially included the connecting base between the nacelle and the tower in our boundary diagram. However, we later decided to remove it as this segment of the boundary diagram only indicates our system's effectiveness: yawing due to mass imbalance, but it is not directly related to our project's scope or purpose.

While the red box encapsulates the subsystem of the turbine we are directly interested in, the supplementary blue box indicates a close relationship between subsystems. We added this blue box to our boundary diagram to highlight the fact that while the blades, pitching mechanism, and overall turbine hub are not within our project's scope, our project must work closely with both subsystems to make the turbine as balanced as possible. For instance, while we were not directly involved in the wind turbine rotor and shaft design, our senior project team made specific recommendations about wind turbine rotor and shaft designs to minimize the effects of mass imbalance.

To ensure that we understand our project's physical scope, we also made a boundary diagram based on a block diagram representing the entire system. This secondary boundary diagram can be found in Figure 3.2.2 below.

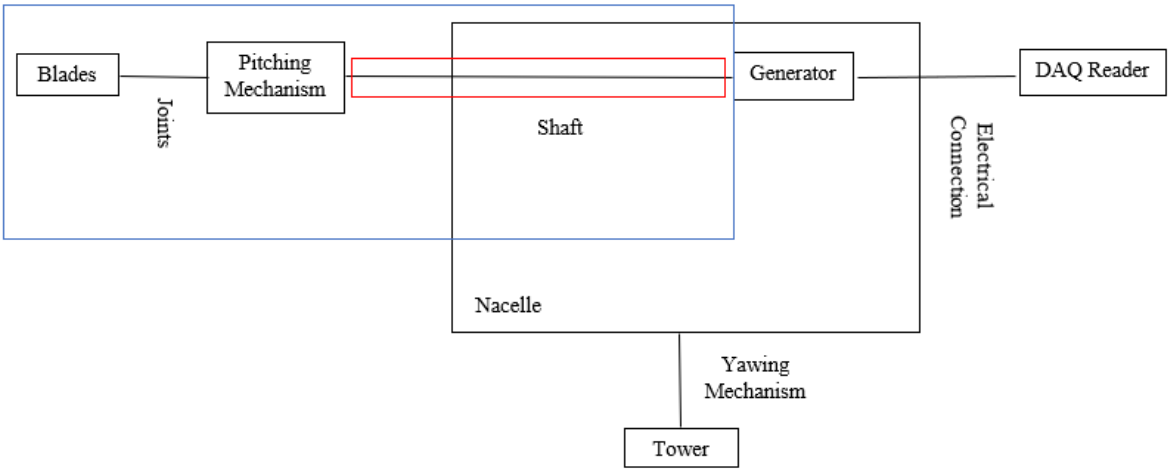

Figure 3.2.2 Boundary diagram for balancing system with block diagram.

The boundary diagram above in Figure 3.2.2 shares a lot of similarities with the block diagram in Figure 3.2.1, with a key change: the low and high-speed shafts have been made one shaft to accurately represent the CPWP turbine design. Aside from this modification, the boundary diagrams are similar and convey a helpful visualization of our project's scope.

3.3 Summary of Customer Needs and Wants

From our meetings with Jess, we determined what deliverables the customer wanted from our senior project team. This list was then divided into wants and needs based on further meetings and exchanges with the customer reviewing our current understanding of the problem with theirs and addressing the feasibility of different deliverables.

Customer Needs:

- A balanced wind turbine rotor assembly
- A balancing system for current and future wind turbine rotor assemblies
- A balancing system that can accurately and repeatably characterize mass imbalance in the wind turbine rotor assembly
- A balancing procedure that is well documented
- Training on the balancing procedure given by the senior project team upon completion of this project and prior to the competition
- A balancing system that meets or is below budget constraints

Customer Wants:

- A balancing procedure that is straight-forward and without the prerequisite of an undergraduate mechanical vibrations class
- A balancing system that is comprised of as much vibrational measurement equipment from the Cal Poly mechanical vibrations lab

3.4 QFD Process & Results

The Quality Function Development or House of Quality tool was employed in parallel with a flow chart approach to arrive at the engineering specifications for our balancing system. Initially, the house of quality was quite difficult for our team to understand—most of the requirements and specifications applied to other subsystems outside the scope of our senior project's work. On the recommendation of our advisor, we developed a sub-system by sub-system breakdown of the competition wind turbine to understand what components our project would interact with as well as have complete control over. This aided the development of our boundary diagram (section 3.2).

A further meeting gave our team the realization that we needed to realign our focus to our project's scope – mitigating the mass imbalance in the CPWP wind turbine rotor assembly. With this new insight and previously created flowchart, Ethan created a list of high-level requirements for the balancing system. He then expanded each requirement until a driving engineering specification could be found (Appendix A). These specifications were then put back into a second house of quality (Appendix B), and the customer requirements were revised from the first house of quality to produce the resulting engineering specifications then. This combined approach of requirement lists and flowcharts with the house of quality tool allowed our senior project team fully specify the problem.

Table 3.4.1 Engineering Specifications Table

Specification #	Parameter or Requirement	Requirement/Target	Tolerance	Risk	Compliance	Notes
1	Required Motor Torque to drive WTRA during Testing [N-m]	0.80	Max	M	T / A	See Note 1
2	Motor Power Requirements [kW]	> 60V / 12.5 A / .750 kW	Max.	M	T / A	See Note 2
3	Operating RPM range for Motor [RPM]	0-3200	Range	M	T / S	See Note 3
4	Bearing Type and Size OD, ID, T [mm]	Front Bearing: 28x12x8 Rear Bearing: 22x8x7	Max.	L	A / I	See Note 4
5	Maximum Allowable Residual Imbalance [g-mm]	5.2 – 6.5 g-mm	Range	M	A / I	See Note 5
6	Maximum Shake Force [N]	< level for infinite life of the testing system	Max.	H	T / A	See Note 6
7	System Critical speeds ratio with System operating speeds [rad/s / rad/s]	$\frac{\omega_{margin}}{\omega_{Critical}} \geq 15\%$	+	H	A	See Note 7
8	Balancing System Cost [$]	$450	Max.	L	A	See Note 8
9	Maximum Rotor diameter [m]	0.45	Max.	L	A	See Note 9
10	Maximum Rotor Weight [kg]	1	Max.	M	A	See Note 10
11	Vibration sensor sensitivity [mV/G]	100-200	Range	L	T / I	See Note 11
12	ISO risk management and balancing machine safety standard compliance (12100-2, 7475, 2953, 1940-1,2)	All safety criteria outlined in the testing procedure are met.	Meets/Does not Meet	H	I / S / A	See Note 12

Note 1: This requirement is based on the motor's ability to maintain a non-stall torque while spinning the CPWPC wind turbine rotor assembly at 3103 RPM (max test speed). We will consider this requirement completed when we test that the motor can spin the rotor up to the max test speed, where this speed is measurable using a tachometer. Additionally, the motor's stall torque must exceed the specified torque, and the no-load speed of the motor must also exceed the desired testing speed. Given the removal of the runaway test we no longer require a motor to spin the rotor at 5000 RPM+, instead 3103 RPM will now be the max rotational speed required with 2500 RPM being the operational speed for the competition wind turbine we will be driving with our specified motor. Our previous estimate was based on a 2.2 kg rotor modeled as a cylindrical disc with a high aspect ratio. Here we calculated the kinetic energy of the rotor at the max test speed, when we thought we had calculated the steady state torque required by the motor to hold it at that speed.

Required motor torque is typically based on the summation of the load torque and acceleration torque multiplied by a safety factor [38][39]. In our case the primary load on the rotor is from aerodynamic loading. The rotational inertia of the rotor is not insignificant – estimated at 1.04E-3 kg-m^2 (see appendix M, Table M.5), but this concerns the acceleration torque not the load torque [38][39]. Additionally, our acceleration torque is small due to the large acceleration time to the max test speed. Dr. Wu recommended we use a ramp rate of 5RPM/sec in our balancing system for safety purposes during vibration measurement and balancing. The CPWPC calculated the load torque vs. pitching angle from incoming wind for us and plotted the result over the range of wind speeds the turbine would see. While we performed our own drag torque element for the turbine operating as a propeller (appendix M, table M.6.1 and 6.2), we decided to use the larger wind torque so that the motor driving our balancing system would be capable of spinning up the assembly with the blades at other pitching angles if needed. Our final motor torque calculation is presented in appendix M tables M.7-M.9.

Note 2: Our motor's power output is ultimately limited by the available power supply. Our senior project checked out a 60V, 12.5A, 750 Watt (Max) adjustable power supply from the Cal Poly ME department as it was the most powerful supply available for student/club checkout.

Note 3: The WTRA currently needs to be tested at two high speeds, but also needs the ability to rotate considerably more slowly than 2500 or 3103 RPM dependent on the imbalance present in the WTRA. Having a large range of rotational speeds allows the balancing to be stopped prematurely if until it is safe to collect data and mitigate the unbalance, at higher speeds. This range was selected based on the median range of our competitors which spans approximately 1 order of magnitude (10^2 – 10^3 RPM).

Note 4: To characterize the imbalance behavior of the wind turbine assembly as accurately as possible, the identical bearing as are used in the competition turbine must be specified to minimize the complex effect of bearing dynamics [7] on the modeling and verification of our balancing system. Analysis to properly size this bearing was completed by the CPWPC.

Note 5: We initially established our residual imbalance limit based on ISO 1940-1 with a selected balancing grade of G 6.3 due to the high operating speed of the rotor and small rotor (referring to the shaft and lumped mass) weight [23]. However, based on Michael Mullen's recommendation,

we used ISO 14694, which handles the balancing vibration limits for small to large industrial fans, to calculate our final residual imbalance limit. Based on the guidance of ISO 14964 and an added conservative factor of safety, we selected BV-2 and BV-3 for our balancing vibration grades. We then back-calculated the imbalance value from the following formula [37]

$$U_{per} = \frac{ma}{\omega^2} \qquad (3.1).$$

Where U_{per} is the residual mass imbalance [g-mm], m is the rotor assembly mass [kg], a is the converted maximum allowable vibration acceleration root mean square (RMS) value measured at the bearings of the fan on the test stand [m/s^2], and omega is the rotational speed of the assembly in [rad/sec]. The vibration velocity measured at the bearings is provided in ISO 14694 Section 8.3 Table 4 "Manufacutrer's Work-Shop Balancing." We converted these velocities to accelerations using a specialized vibration calculator, which relies on the following formula from Annex A of ISO 14964.

$$a_{R.M.S.} = \frac{2\pi f V_{R.M.S.}}{1000} \qquad (3.2)$$

Where V_{rms} is the vibrational velocity in table 4 [mm/sec], and f is the rotational speed of the shaft [Hz]. We chose to use the RMS values for vibrational velocities as the equations mentioned in Annex A hold primarily for the RMS values. Our provided range of U_{per} is for the max test speed (3103 RPM) for the BV-3 and BV-2 balancing vibration grades, as this is the limiting case.

Note 6: To help ensure that the balancing system is safe to operate, a maximum allowable shake force (due to the initial imbalance in the WTRA) must be determined. This limit – from mechanics of material and fatigue analysis – will ensure that the testing system has as long of testing life as possible and does not face the potential for becoming impossible to calibrate due to degradation of components from damaging fatigue cycles. Our senior project recommends using Dunkerly's rule [30] to assess the number of cycles at damaging levels to iterate between levels of damage and the number of cycles until infinite testing system life is reached.

Note 7: Different components in our balancing system will have different natural frequencies and or critical speeds. The shaft presents an important requirement for both the safety and longevity of our proposed balancing system's operation. If either the operating or max test speed of the competition turbine is too close in frequency to the critical speed of the shaft, catastrophic failure of the balancing system could occur resulting in potentially serious injury of the operator and/or significant damage to the balancing system.

Based on design for natural frequency margins from Gunter [33] the ratio of the margin between the operating speed and the critical speed as a fraction of the critical speed (as a percent) should be greater than or equal 15—20 for more conservative design criteria. Current analysis (discussed in section 4) gives critical frequencies as a function of the prototype turbine's geometry. Our

analysis natural frequency estimates of the rotating assembly were updated as the CPWPC's and pitching team designs were finalized. Since the CPWPC's shaft design was not finalized by the end of our senior project, the natural frequency estimates we present in this report do not directly apply to the now-finalized competition shaft. More analysis is needed to ensure this frequency margin is satisfied or that critical speeds can be passed through spin-up or spin-down without turbine damage. Further analysis on the base plate of the nacelle to ensure that none of its natural frequencies fall within the frequency margin for resonant/high amplification factor operation were delegated to the CPWPC.

Note 8: Having received grant money from NREL the CPWPC initially provided our team with a $200 budget, which they then agreed to increase to $450. In addition to the NREL grant funds, the CPWP also recovered club funds from the previous year. While still seeking to minimize the cost of both our balancing system and mechanism, our senior project also made recommendations to the CPWPC for the purchase of a non-contact laser tachometer for vibrations and wind tunnel testing.

Note 9: Our balancing system must be able to operate safely with the current rotor size. This specification drove the sizing of the safety guards outfitted on this balancing system to protect the operator and bystanders in concert with specification 14. While the material for the rotor enclosure has been selected

Note 10: Similarly, our balancing system must be able to safely operate with the current rotor mass. Though this may change some in future years, currently we anticipate that the weight shall deviate from its design value by a small amount. However, for the robustness of the design and longevity of the balancing system the specification of max rotor mass has been set to twice the estimated design mass.

Note 11: This specification is dependent on the maximum permissible imbalance determined by specification 3. As of the completion of our FDR we have determined that the accelerometer from the vibes lab with sensitivities of 100 or 200 mV/G is sufficient for the amount of imbalance we are trying to measure. This decision was based on what was available in the Cal Poly Mechanical Vibrations lab and the consultation of Dr. Wu and Michael Mullen.

Note 12: The ISO standards listed here detail recommended balancing procedures and test practices. The aim of these standards is to ensure safety throughout the balancing process. The details of each ISO are too nuanced to be discussed in detail here. The intent is not to gain or seek certification from ISO on pertinent sections of these balancing machine standards, but instead to meet the requirements of these sections. Our rationale being that these standards are sufficiently rigorous and widely used to maximize the safety and accuracy of our balancing system. However, since our balancing system design remains incomplete, these standards have not been revisited.

4.0 Modeling and Preliminary Analysis

To ensure that we properly balance the wind turbine's rotor assembly, we have decided to emphasize modeling in our concept design approach. This section will discuss the preliminary modeling that we have completed to analyze the overhung, imbalanced, rotating system. We will also describe the limitations of the modeling we have worked on and why modeling an accurate system is relevant to our project. We decided to retain the earlier modeling and simulation results presented in sections 4.2 – 4.4 to illustrate our modeling-focused design process' implementation as discussed in section 4.1. For our most recent modeling results, see section 4.5.

4.1 Modeling Rationale and Approach

Due to the complicated nature of the dynamic behavior of the CPWP wind turbine rotor, as well as our senior project team's lack of experience with rotor dynamics, our senior project team decided to seek a better physical understanding of our system's vibrational behavior by modeling and simulation prior to concept generation and selection. Based on Dr. Wu and Michael Mullen's advice, we utilized several simulation software (ADAMS, SOLIDWORKS, and ABAQUS) to approximate our system's dynamic behavior - specifically estimation of the system's natural frequencies. According to Dr. Wu, it is faster and more efficient to use simplified analytical models whose behavior can be solved by hand in concert with simulated models of the physical system to understand their dynamic behavior instead of trying to grasp and then apply the most complicated and realistic theories that describe such dynamic behavior.

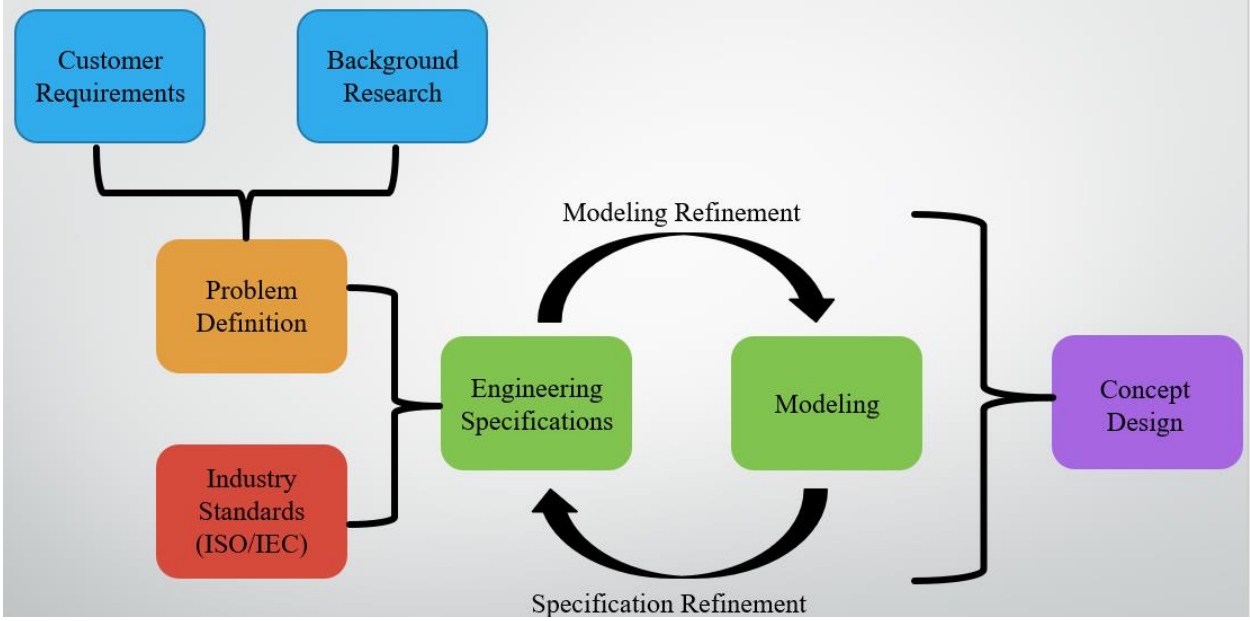

Figure 4.1.1 Design process flowchart – emphasis on modeling to refine engineering specifications. By iteratively progressing through model improvement, our specifications for our deliverables will become more representative of the physical system's characteristics and allow us to arrive at an optimal solution.

While the competition wind turbine will be different from the prototype, the change in dimensions, stiffnesses, masses, damping, and fundamental structure and behavior of the system will be

consistent throughout design iterations. Thus, our modeling approach took the following form. We created incrementally more realistic models of the rotating assembly alongside parametric studies on both standards governing small wind turbine design and balancing procedures. As our system parameters became more consistent due to design finalization, our senior project team to efficiently updated our models and design specifications and gained a better understanding of our physical system along the way. Our current modeling approach is both normal modes and dynamic analysis. This means we are employing modal analysis in SolidWorks to seek the natural frequencies of our current model, while also using ADAMS to simulate the kinematic and dynamic behavior of our system. Normal modes analysis neglects damping and is the free vibration response of an assumed simple harmonic oscillator under base excitation [30].

Identifying our system's critical frequencies is crucial. However, it is also important to characterize the effects of backwards and forwards whirl on our overhung rotor's vibrational behavior. In her paper in the journal of applied mechanical engineering, Wu et al. explains that forward whirl is when the rotor recesses in the same direction as the rotation of the shaft while backward whirl is when the precession direction opposes the spin direction [31]. Wu et al. also explains that forward whirling frequencies grow in displacement while their backward counterparts decrease in displacement with increasing shaft spin speed [31]. Her and her colleagues' suggestion is to conduct a full spectrum analysis on the rotor to diagnose component damage most accurately or locate sources of unbalance/excess vibration [31].

Our preliminary research and calculations have provided a basic understanding of a wind turbine rotor's vibrational behavior. In the subsections following this introduction to our modeling-focused design process, we have provided the results of our modeling and parametric studies along with our initial interpretations of them. Our completed preliminary modeling efforts have provided new and narrower lines of investigation for our next stages of modeling.

4.2 Rigid Shaft Parametric Study

While Dr. Wu recommended that we model our rotor system as dynamic and flexible, we saw value in modeling a rigid shaft rotor system as well. We wanted to model a rigid shaft rotor system to calculate preliminary results for rotor behavior which can later be validated through flexible models. Additionally, ISO 1940-1 outlines a maximum allowable residual imbalance for rigid rotor assemblies. Allowable imbalance in the CPWPC wind turbine is likely something that we will have to determine through flexible shaft modeling; however, baseline values provided by a rigid shaft study can certainly be helpful in guiding our calculations and verifying our results.

Using the ISO 1940-1 standard for rotor systems and IEC 61400-2 for small-scale wind turbines, we were able to perform a comprehensive parametric study for a rigid shaft system. To ensure that our model reflected realistic values, we used the CPWP's 2020 wind turbine dimensioned CAD model as a reference.

The first part of our rigid shaft parametric study calculated the allowable maximum residual imbalance for variable rotor assembly dimensions. ISO 1940 recommends a maximum residual imbalance based from the parameters labeled b, c and d labeled in Figure 4.2.1 below.

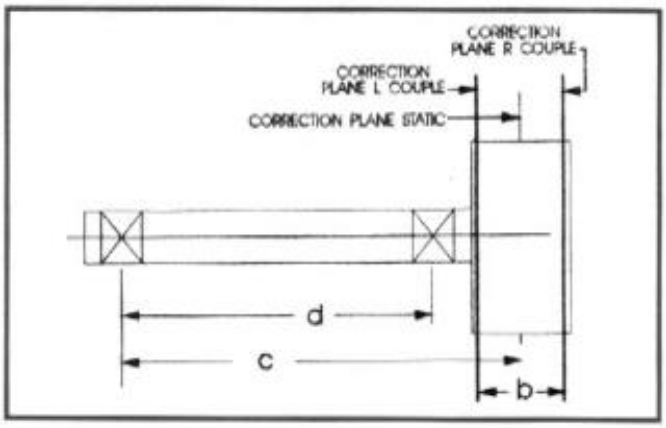

Figure 4.2.1 ISO 1940 overhung rotor dimensioned diagram for residual imbalance parameters.

Using reference values from the CPWP 2020 wind turbine CAD model, we performed a parametric study for variable rotational speeds and measurements for each parameter to examine how these values affected the maximum allowable residual imbalance for the system. Since the rotational speed of the shaft has yet to be designed by the 2021 wind turbine team, we wanted to use rotational speeds ranging from 0 RPM to the highest proposed rotational speed of 5300 RPM. While this is subject to change, for the purposes of this study, 5300 RPM is an acceptable maximum rotational speed. Figure 4.2.2 below displays the effect of rotational speed on allowable residual vibrations for the dimensions of the 2020 CPWP wind turbine. Appendix D contains tabulated data for the computation of allowable imbalance as a function of rotational speed.

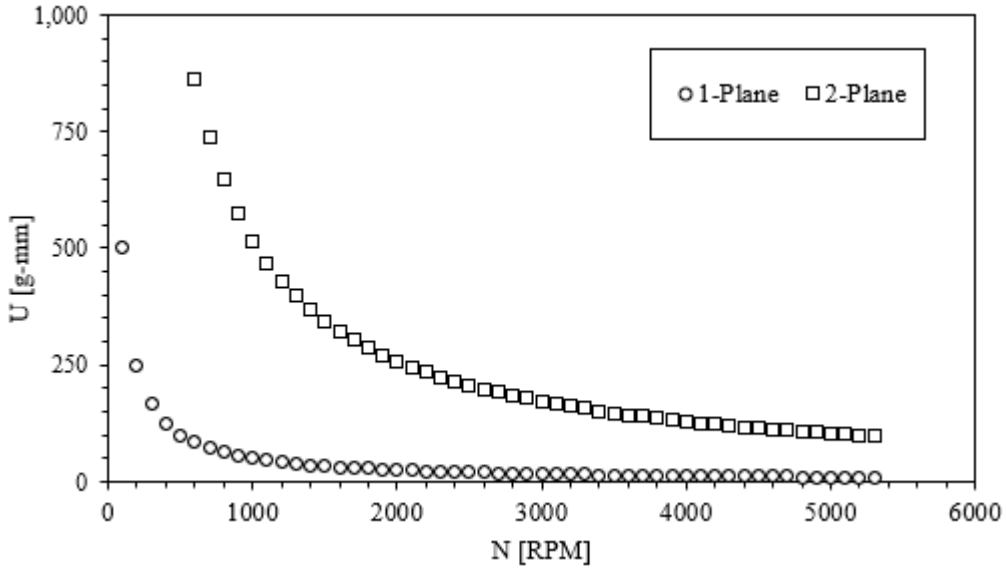

Figure 4.2.2 ISO 1940 recommended residual imbalance for single and double plane balancing for variable rotational speeds.

While unintuitive, it is ideal to maximize allowable residual imbalance. A small allowable imbalance implies a highly precise system, which is difficult and expensive to manufacture. Therefore, a higher residual imbalance is desired. As rotational speed increases, allowable

imbalance decreases, which aligns with expectations for the system behavior. An imbalance in a system will become more dangerous and damaging at higher rotational speeds. Lastly, we wanted to examine both single plane and double plane balancing recommended maximum imbalance. Flexible modeling will later reveal whether a single-plane or double-plane balancing system is necessary for our system; for the time being, both options will be considered. Although not encapsulated in Figure 4.2.2, the allowable imbalance for two-plane balancing reaches values as high as 5000 g-mm. However, since the wind turbine will not be operating as such a low RPM, the top of the curve was excluded for a clearer visualization of the rest of the system behavior.

Rotational speed is only one parameter which affects allowable vibrations in the system. For the next portion of our study, we examined how variance in the measurements in Figure 4.2.1 affect the system. Figure 4.2.3 below details how rotor plane thickness (b) affects allowable imbalance. Appendix D contains tabulated data for the computation of allowable imbalance as a function of rotor plane thickness.

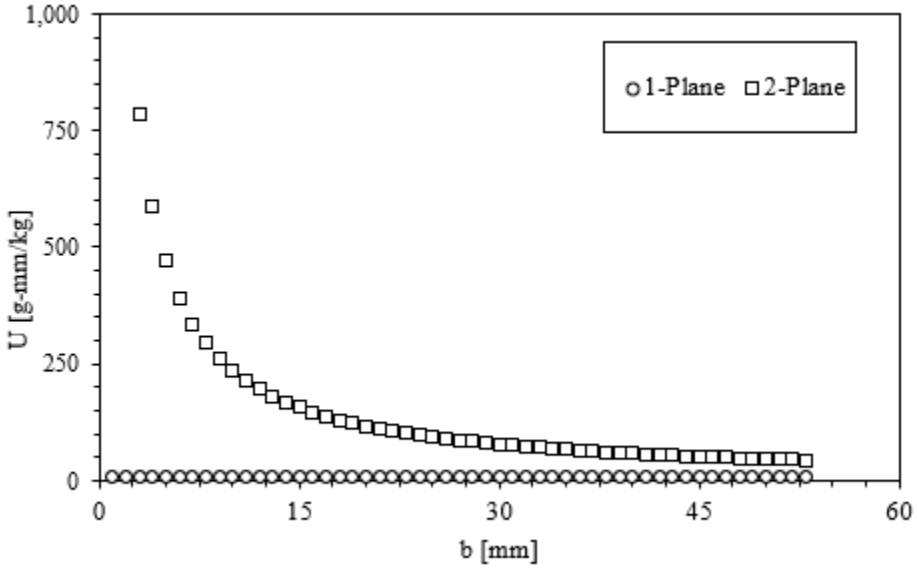

Figure 4.2.3 ISO 1940 recommended residual imbalance for single and double plane balancing for variable rotor plane thickness (b).

For single-plane balancing, allowable residual imbalance is not affected. However, double-plane balancing resembles as asymptotic behavior, similar to Figure 4.2.2. The curve used to model our system's residual imbalance will depend on whether flexible modeling indicates whether one-plane or two-plane balancing is necessary. Figure 4.2.4 below displays the trend resulting from variable shaft length (c). Appendix D contains tabulated data for the computation of allowable imbalance as a function of shaft length.

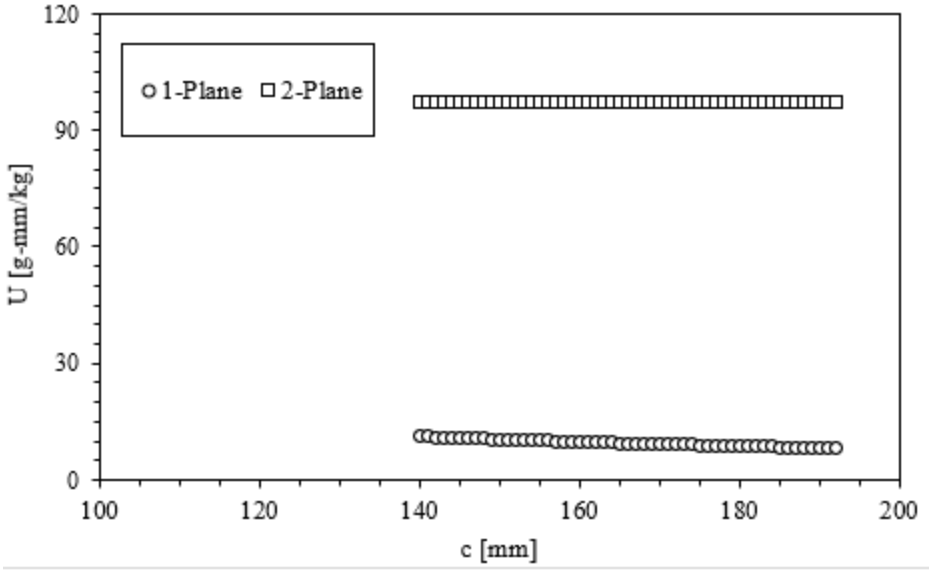

Figure 4.2.4 ISO 1940 recommended residual imbalance for single and double plane balancing for variable shaft length (c).

Our parametric study showed that shaft length is not a primary contribution to residual imbalance, and has a negligible effect on two-plane balancing vibrations. Figure 4.2.5 below displays the trend resulting from variable distances between shaft bearings (d). Appendix D contains tabulated data for the computation of allowable imbalance as a function of bearing spacing.

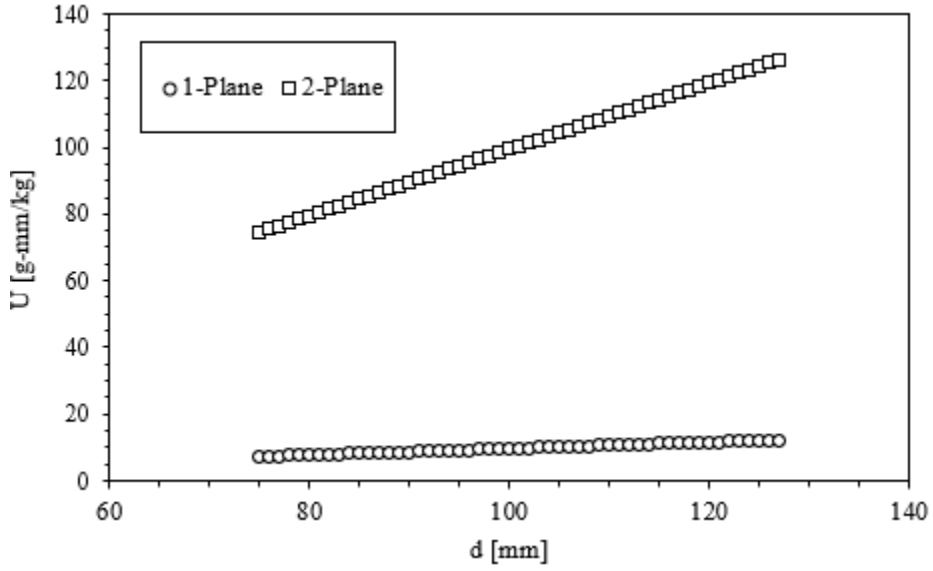

Figure 4.2.5 ISO 1940 recommended residual imbalance for single and double plane balancing for variable distance between shaft bearings (d).

The effects of bearing placement influence both one-plane and two-plane balancing in a linear fashion. Two-plane balancing is more severely affected by this parameter.

The second part of our parametric study focused on understanding how the center of (COM) of a point mass and rigid link model of a wind turbine rotor varies with translational and angular displacement of the point masses relative to each other as well as unequal point-mass mass.

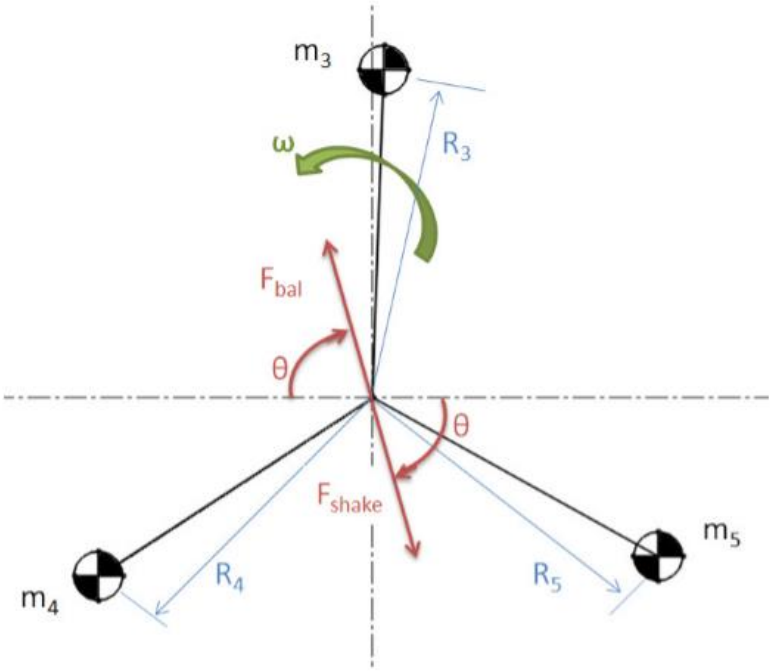

Figure 4.2.6 Rigid link and point mass model of 3 blade wind turbine rotor [32]. This is the same model presented by Simon in his thesis on the static balancing of the Cal Poly wind turbine.

Two outputs were calculated for this second portion of the rigid parametric study, the magnitude of the radial location of the center of mass and the mass required balance the rotor – in this case locate the center of mass coincident with the axis of rotation of the rotor. From this portion of the parametric study we noticed that all variance in rigid link length, point-mass mass, or angular position of the 'blades' relative to each other as well a steady frame of reference resulted in a proportional relationship with increasing rotor COM eccentricity and mass required to balance (for single plane balancing only). We did not investigate two plane balancing, as single plane balancing is a more realistic and simple solution which can be realistically implemented.

The derivation for these outputs is available in Appendix G. Additionally, an arbitrary balance radius of 15 mm was selected to allow the required balance mass to be solved for. The point masses represent the center of mass locations of the blades and the rigid links serve to connect these lumped masses to the axis of rotation. We assumed that the hub mass was concentric with the axis of rotation and thus neglected its effect on COM eccentricity and required balancing mass. Additionally, since the focus of this first model was single plane balancing the mass distribution of the shaft as well as the location of its supports were not accounted for or in the scope of this analysis.

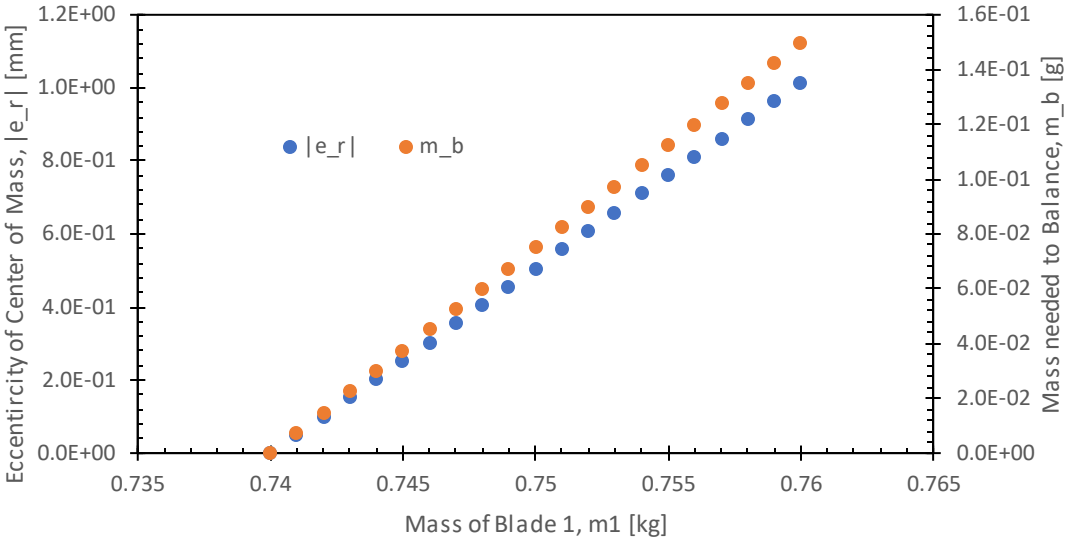

Figure 4.2.7 COM eccentricity and balance mass required as a function of blade 1 mass. Without varying the system mass, the mass of blade one was increased by 20 grams [g] while the other two point masses where decreased by half. Notice that the maximum eccentricity of the rotor is only 1 mm and the mass imbalance is 0.14g. These values are much smaller even when combined as a mass radius product than the residual unbalance limits

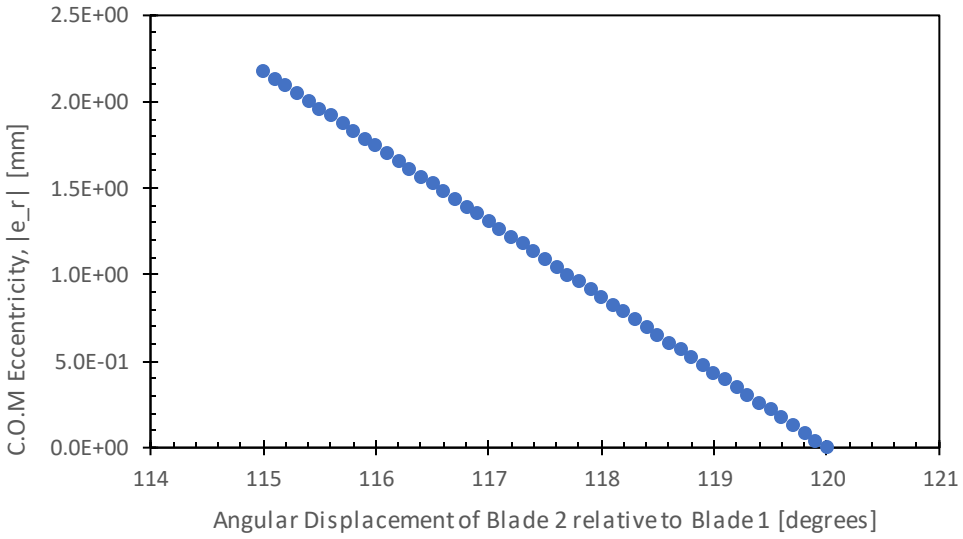

Figure 4.2.8 COM eccentricity as a function of angular displacement of blade 2. After 5 degrees of angular misalignment with the other two blades still only about 2.25mm of eccentricity were realized.

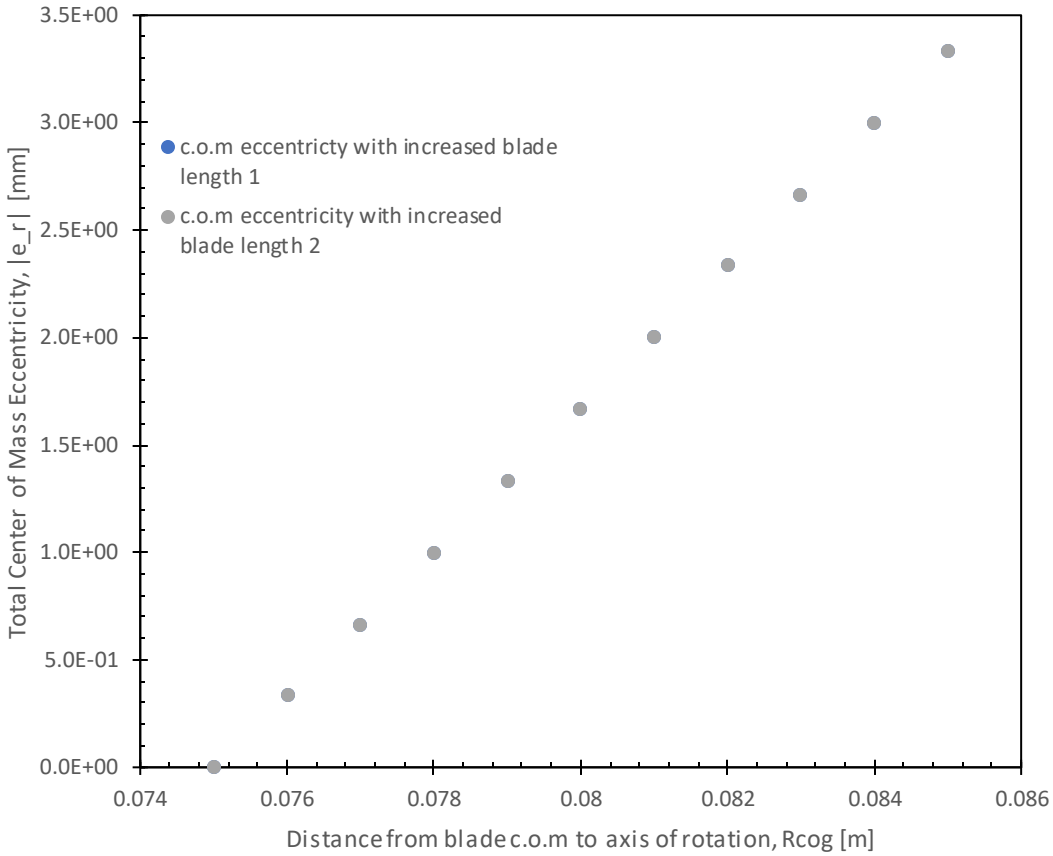

Figure 4.2.9 COM Eccentricity as a function of blade elongation. An increase of 10 mm gave only about a 3.5mm center of mass eccentricity. Perhaps there is some tolerance for center of mass alignment in our system. The blade lengths changed were done for a blade located on the steady state axis and one displaced from it. Here the change in center of mass is indistinguishable.

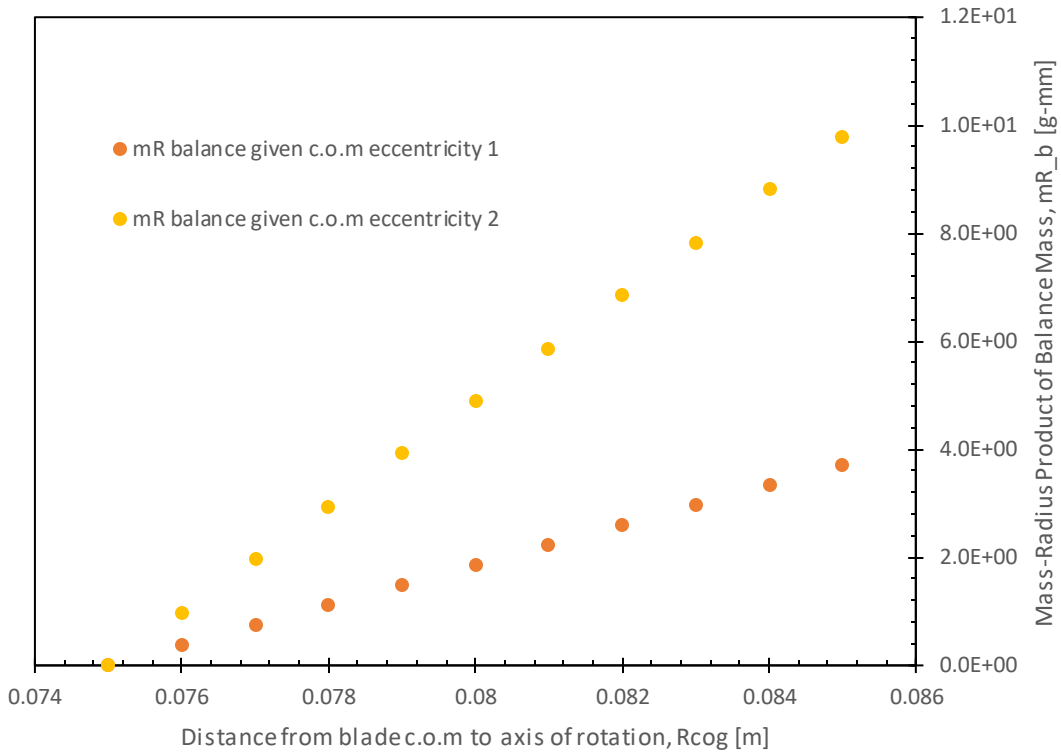

Figure 4.2.10 Mass required to balance rotor model as a function of blade elongation. While the required mass to balance this rotor remains small despite the noticeable change in center of mass position, the required mass radius balance product for blade 2 increases at approximately twice the rate of blade 1. This may be the result of choosing to locate blade 1 on the steady frame of references axis, but it remains unclear as to why the model is behaving this way.

Combining the insights from each of these plots we have the following recommendations to reduce the inherent imbalance in the system prior to balancing:

- Verify the mass properties of the blades – primarily center of mass location and total mass in this case – to ensure the most similar set of blades are used in a turbine rotor
- Verify the equal spacing between the center of mas of each blade
- Minimize or eliminate blade mounting issues, including angular and translational displacement relative to other blades in the rotor

By creating a simple model of our wind turbine rotor to then perform a single plane balance on it allowed our senior project team to gain confidence in modeling our system. This also built our senior project team's engineering intuition for single-plane balancing.

For the third part of our rigid parametric study, we began to analyze the effect of the eccentric rotor mass-radius product and rotation speed on the resulting dynamic forces. Only preliminary analysis was completed here, but the IEC 61400-2 equations F.27 and 28 were not parametrically studied as without the selection of a safety factor and several other supporting fatigue strength calculations, a meaningful residual imbalance threshold could not be backed out.

Our initial results confirmed the linear relationship between dynamic force generated (the apparent centrifugal force) [15] and COM eccentricity as well as eccentric mass. We first treated the entire mass of the rotor as if it were all lumped at a variable eccentricity from the rotor. This model is unrealistic because it amplifies the effect of the eccentric mass with respect to the mass of the rotor that is not eccentric. The second model took the maximum center of mass eccentricity obtained from the second portion of the rigid parametric study and varied the amount of eccentric mass present. For both 4.2.11 and 12 the runaway test speed is 5300 RPM and the operating speed is 3000 RPM.

The dynamic force (apparent centrifugal force) is given by:

$$F_{dyn} = m_e e_r \omega^2 \qquad \text{(Eqn 4.2.1)}$$

Where m_e is the eccentric mass in [kg], e_r is the eccentric radius in [m] and omega is the rotational speed of the spinning body in [rad/sec], giving a force in [N].

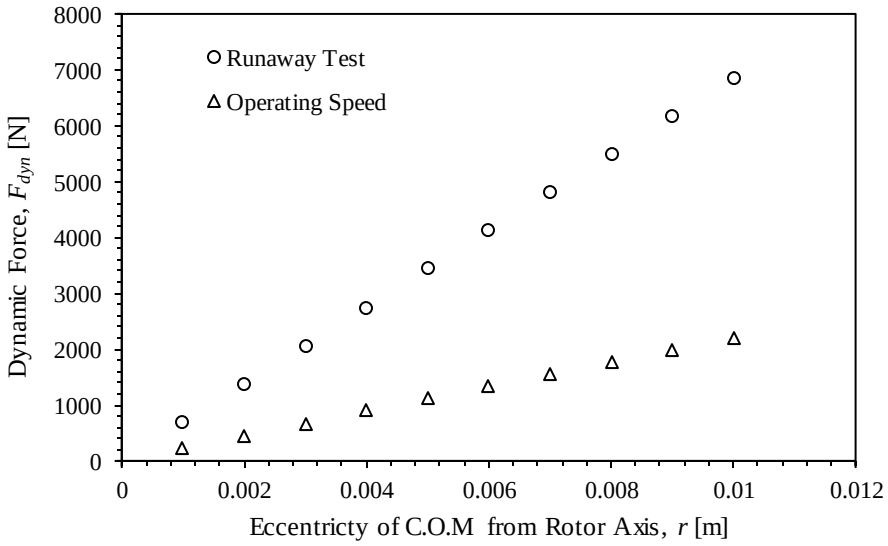

Figure 4.2.11 Generated dynamic force as a function of eccentricity of lumped mass.

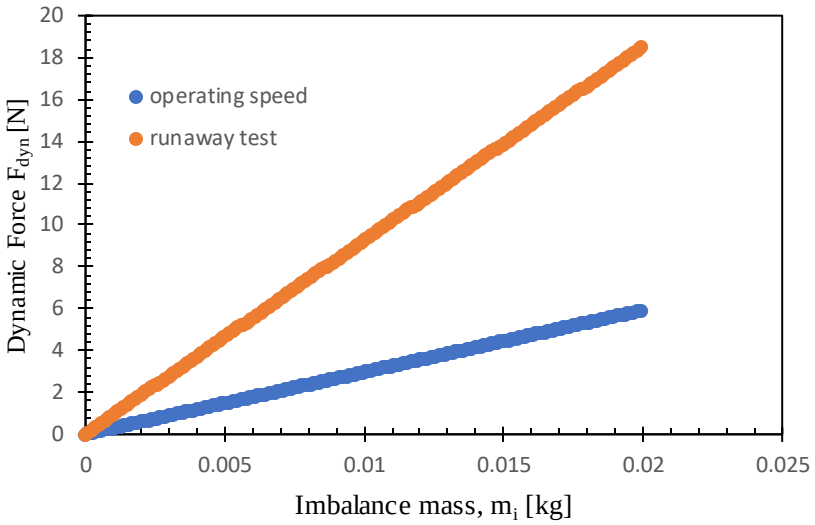

Figure 4.2.12 Generated dynamic force as a function of imbalance mass at a 3 mm eccentricity.

It is apparent that lumping all rotor mass at some eccentric location from the axis of rotation creates disproportionately large dynamic forces. For Figure 4.2.11 we used a maximum eccentricity based on locating the point mass of the blade at its tip instead of approximately a third of its length. This higher eccentricity value also contributed to the creation of unreasonably high dynamic forces. For the second model, we used the maximum eccentricity generated from the rigid link point mass model where the point mass locations coincided with the approximate location of the actual blade centers of mass, not at the tip! A 20-gram imbalance is needed to generate a maximum of about 19 N at the maximum runaway speed instead of a 2.22kg imbalance at 8 mm eccentric generating upwards of 7000 N. Currently, we recognize that these two plots bound the dynamic force, and more investigation is needed to identify an amount of dynamic force that is significant to fatigue life of the turbine and/or balancing system.

Concluding our parametric study, we realized that the scope of our project ought to be adjusted. Many of the parameters which dictate the magnitude of mass imbalance in the rotor system are not within the scope of our project. For example: the length of overhang between the wind turbine nacelle and the rotor plane heavily affects the allowable maximum residual vibration within the system. This parameter will be designed by the CPWP 2021 wind turbine team and is therefore something we cannot govern. In turn, we have decided to include a series of recommendations as part of our senior project deliverables. These design suggestions are based on the results of this parametric study as well as the compiled advice from several meetings with Dr. Wu and Michael Mullen. Ultimately, our system will adequately be described as rigid due to the scale of the rotor assembly. Hence, these rigid parametric studies have become the groundwork for our recommendations to the CPWP.

4.3 Preliminary ADAMS Model

To model the wind turbine rotor assembly as a flexible system, Dr. Wu recommended that we use a dynamic modeling software called ADAMS. ADAMS can compute a wide variety of system

variables, and is readily accessible through the Cal Poly servers. After gaining remote access to Cal Poly computers, we were able to begin our flexible shaft model.

We transferred the CPWP's 2020 wind turbine CAD model from SolidWorks into ADAMS. With a corrected resolution, the full wind turbine rotor assembly became fully applicable in ADAMS. To model rotation, a motor needed to be applied to the rotating shaft. Following equations 2.1.1 and 2.1.2, the simulated motor acts as a realistic motor with appropriate ramping speeds. Another suggestion from Dr. Wu to legitimize our model includes a resistant torque. This torque is a representative friction torque, resulting from the mass moment of inertia of the shaft and the speed at which the shaft is rotating.

Unfortunately, our model was never completed, due to over-complications with the ADAMS interface, and the unnecessary modeling of our system as overtly flexible. A picture of the incomplete ADAMS rotor assembly model can be found in Figure 4.3.1 and 4.3.2 below. Visible in these pictures is the imbalanced rotor, rotating joint connecting to the shaft and the representative motor torque.

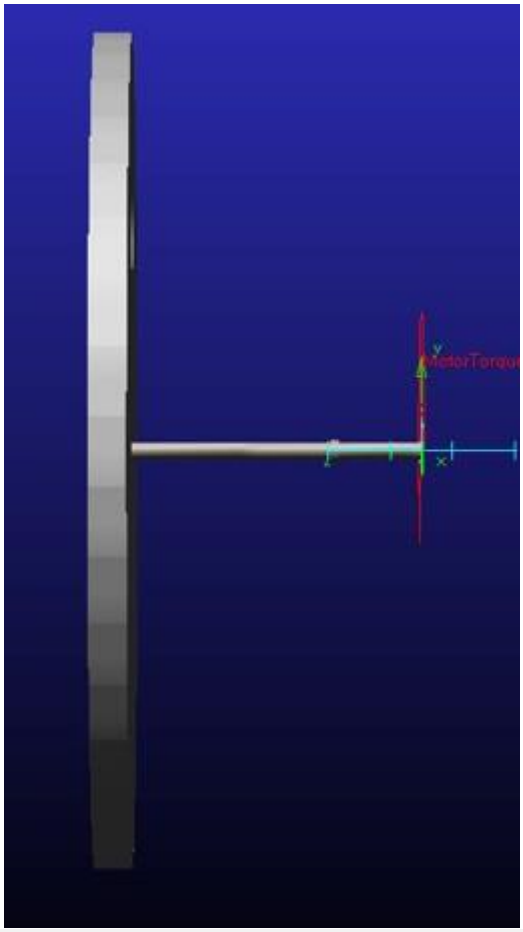

Figure 4.3.1 Orthogonal view of preliminary ADAMS model.

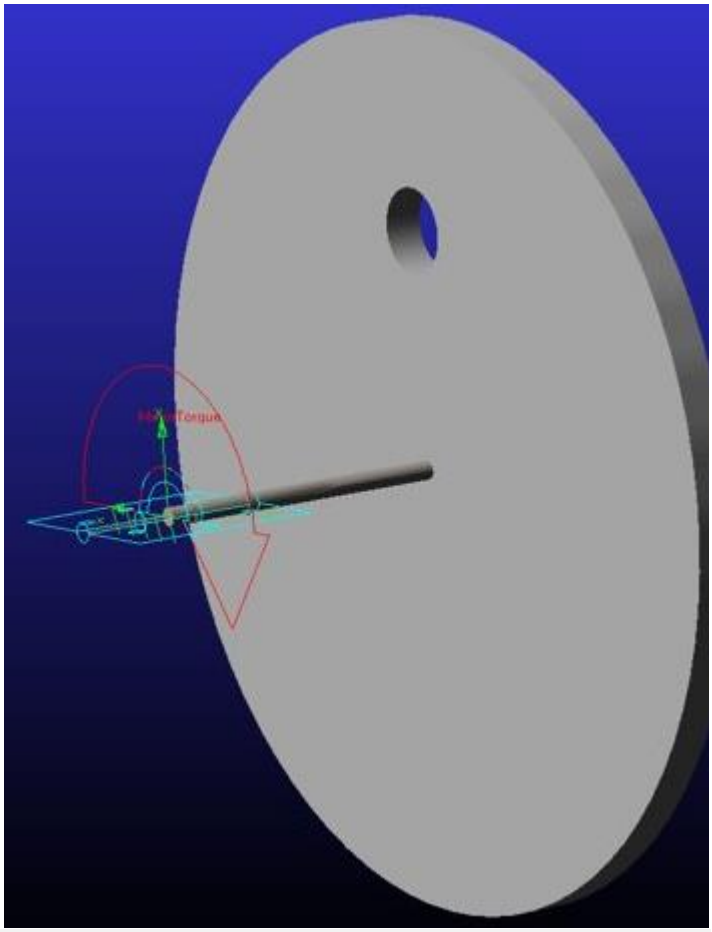

Figure 4.3.2 Isometric view of preliminary ADAMS model.

While the rotor assembly and applied motor are finished, there are still a few essential modifications that need to be made in order for this to be a complete model. The resisting torque would need to be applied and customized to be a function of the rotational speed from the motor. In addition, the bearings in the current model should be reapplied with valid stiffness and damping values. Since these parameters can vary in each system and from company-to-company, finding accurate values for our simulation became an issue. The CPWP has yet to select a specific bearing for each support, so any bearing and stiffness values we find will likely vary between our model and the soon-to-be-designed wind turbine. To ascertain valid stiffness and damping values for each bearing, our advisor recommended reaching out to an established bearing company. Most bearing companies keep specific bearing values private. Nevertheless, some bearing companies can simulate a described system with the desired bearing(s) and provide accurate stiffness and damping values. However, since we decided to move away from the dynamic ADAMS model was scrapped in favor of a rigid model, we found no need to reach out to obtain these exact values.

Since our work on ADAMS, we have decided to shift over to ABAQUS as our primary modeling software. This decision was driven by the difficulty associated with learning and ascertaining data from the ADAMS software. Furthermore, ABAQUS is capable of performing natural frequency estimation and dynamic analysis like ADAMS but is considerably more user-friendly. Due to this project's limited time frame, the time required for a team to learn and adequately use simulation software was a decisive factor in selecting ABQUS over ADAMS. A detailed process for our plans to model the wind turbine's rotor system in ABAQUS can be found in Appendix K.

4.4 SolidWorks Frequency Analysis – Critical Speeds

Before this senior project, none of our senior project team members had ever completed a frequency simulation or normal modes analysis in SOLIDWORKS. To help ensure that our results would be somewhat valid and to expedite modeling, we sought training in using this simulation feature of SOLIDWORKS appropriately. We found a Linked In Learning course by Toney Abney, FEA expert, and consultant, on the subject. Abney's recommendations on mesh refinement as well as the mesh elements to apply to simulated components were used heavily in this attempt to get initial estimates of our system's critical speed.

To ascertain approximate critical speeds for the CPWP wind turbine rotor we ran several SOLIDWORKS frequency Simulations on an idealized model of our system. As mentioned previously, our initial model consisted of the CPWP's 2020 prototype wind turbine shaft and a rigid disc. The rigid disc has the same diameter and thickness as the blade and hub assembly. We created a hole feature in the rigid disc to induce an imbalance in the system by redistributing the disc's mass. Both the hole diameter and density of the disc were configured to produce a 5, 10, 15, and 20-gram imbalance while maintaining the same rotor mass. Our model also made use of bearing fixtures at the same locations on our model as the prototype.

Initially, we investigated the effect of a varied imbalance on the critical frequencies but quickly found that there was no significant variation (~1%). From this point on, we focused on refining the mesh to ensure that the mesh being applied to the rigid disc and shaft were sufficiently fine to accurately characterize our system's mode shapes. Relatively early on, we caught a meshing mistake in our frequency study. We were treating the rotating shaft as a shell element when it

should have been comprised of 3D solid or beam elements. This resulted in critical frequencies from our frequency study being skewed higher as this effectively made the shaft stiffer. From this point on, we used a curvature-based 3D solid mesh (as recommended by SOLIDWORKS) to discretize both the shaft and rigid disc. After performing a mesh convergence study, we found that the first six natural frequencies did not vary significantly (< 2%) with the coarseness/fineness of the mesh (see Appendix E).

The figure we have provided below shows the idealized turbine model in SOLIDWORKS and immediately following it are the approximate natural frequencies of the CPWP's prototype turbine rotor in units of Hz, radians/sec, and RPM.

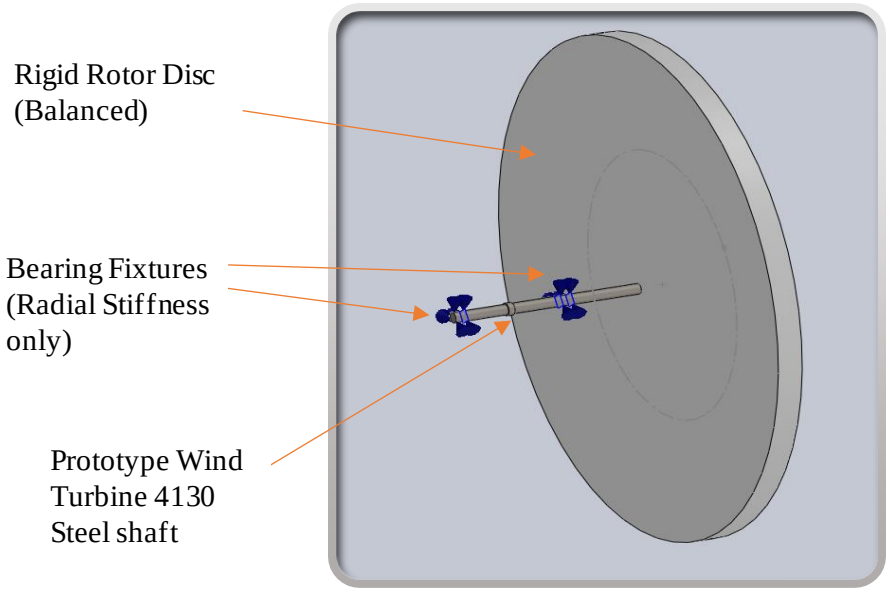

Figure 4.4.1 Preliminary Wind Turbine Rotor Model used in SOLIDWORKS Frequency Study.

When solving for the mode shapes and critical frequencies, the damping and detailed stiffness characteristics of the bearings can be ignored. Instead, we used an approximate estimate for the prototype turbine's nacelle bearings radial stiffness and neglected the axial stiffness of the bearings as any axial loads would be taken by the coupling that attaches the wind turbine rotor shaft to the generator. This design choice is from the CPWPC, which, at the time of this analysis, had decided to press the bearings into their nacelle pillow blocks but a running clearance with the wind turbine rotor shaft.

Table 4.4.1 Preliminary Wind Turbine Rotor Model Critical Frequencies

Mode No.	Average Natural Frequency		
[-]	[rad/sec]	[Hz]	[RPM]
1	0.000837	0.000133	0.00799
2	0.942	0.150	9.00
3	2.10E+02	33.5	2.01E+03
4	2.19E+02	34.8	2.09E+03
5	1.04E+03	1.65E+02	9.90E+03
6	1.06E+03	1.69E+02	1.01E+04

Provided with the CPWP's tip speed ratio of 5.0, we can assume that operating speed will be about 2500 – 3000 RPM. The runaway test—which we still plan to design for—has a range of 3900 – 5300 RPM operating speed. At this point, none of our estimated critical frequencies are cause for concern. Additionally, not all the frequencies/speeds listed in the table above are as likely to be as potentially damaging to our wind turbine rotor system as others. In our case, even though the 3rd and 4th modes are somewhat close to the lower bound of operating speeds, SOLIDWORKS gives an indication of which modes are the most significant via the mass participation factor [30]. A mass participation factor more than 70% is typically cause for considering that mode significant [30]. Specifically, the modes with the highest mass participation factor, also known as modal effective mass, in any direction are the modes most likely to be excited by external loading or base excitation of the system [33]. Frequency analysis will be performed once the CPWP finalized their CAD for the wind turbine.

In Table 4.4.2 we have provided the mass participation factors from the SOLIDWORKS frequency study. Modes 5 and 6, which occur at and above 10,000 RPM both have mass participation factors greater than 80%, while modes 3 and 4, which our system will travel through, both have mass participation factors <10%. Thus, the most damaging vibrational modes are at speeds that far exceed the upper bound on maximum rotational speed for our system.

Table 4.4.2 Mass Participation Factors for Preliminary Wind Turbine Model in SOLIDWORKS

Mode No.	Frequency	X direction	Y direction	Z direction
[-]	[Rad/sec]	[Decimal %]	[Decimal %]	[Decimal %]
1	0.000798	1.44E-10	4.18E-19	1.18E-20
2	0.942	1.43E-23	2.98E-24	~~0.99999~~
3	210.5	1.85E-07	0.0493	1.03E-23
4	218.7	0.0547	1.37E-07	4.89E-23
5	1,037	1.14E-05	0.884	1.32E-24
6	1,061	0.87837	1.15E-05	5.54E-24
		Sum X = 0.93	**Sum Y = 0.93**	~~Sum Z = 0.99999~~

We have ignored the Z-direction as due to some error in the bearing fixtures, this was a rigid body mode of translation back and forth along the Z-axis. In addition to refining our bearing stiffness estimate we will also ensure that the model is constrained such that the study will not return any rigid body mode results.

Besides the mass participation factor, we also examined the frequency ratio and frequency margin for each bound on rotational speed for the turbine relative to the six critical frequencies (modes) identified. The frequency ratio is a direct comparison of the systems input frequency to its critical frequencies [34]. However, this ratio does not as effectively convey how close any one system operating speed is to one of its own critical frequencies as the frequency margin. The frequency margin is the absolute value of the difference between the operating speed of interest and the critical frequency normalized by the critical frequency [34]:

$$Frequency\ Ratio = \frac{\omega_{input}}{\omega_{Critical}} \quad \text{(Eqn 4.4.1)}$$

$$\omega_{margin} = |\omega_{operating\ -} \omega_{ciritcal}| \quad \text{(Eqn 4.4.2)}$$

$$\frac{\omega_{margin}}{\omega_{Critical}} * 100\ \geq 15\% \quad \text{(Eqn 4.4.3)}$$

As expressed in equation 4.4.3 it is desired that the frequency margin exceeds 15% for any operating speed and system critical speed [34].

Immediately below we have provided the frequency ratios for our systems operating speed ranges with respect to its critical speeds. For the first four modes our operating speeds are sufficiently above the critical speeds to produce frequency ratios >1.15. However, due to the approximate nature of these estimations we have decided that frequency ratios less than 1.5 are in danger falling below 1.5 if the mass, stiffness, or geometry of the competition wind turbine system differs significantly from that of CPWP's prototype turbine. In modes 5 and 6 our system's operating speed is well below the critical speed so all the frequency ratios are less than 1.

Table 4.4.3 Frequency ratio for upper and lower bounds on turbine model rotational speeds

		Frequency Ratio (Ω_{in}/ Ω_N) [dimensionless frequency]					
		Mode 1 (RPM)	Mode 2 (RPM)	Mode 3 (RPM)	Mode 4 (RPM)	Mode 5 (RPM)	Mode 6 (RPM)
		7.99E-03	9.00	2.01E+03	2.09E+03	9.90E+03	1.01E+04
LB	Operating Speed (2500 RPM)	3.13E+05	278	1.25	1.20	0.253	0.247
UB	Operating Speed (3000 RPM)	3.75E+05	333	1.49	1.44	0.303	0.296
LB	Runaway speed (3900 RPM)	4.88E+05	433	1.94	1.87	0.394	0.385
UB	Runaway speed (5300 RPM)	6.63E+05	589	2.64	2.54	0.535	0.523

Unlike the frequency ratio, the frequency margin gives the proximity to the critical speed as a positive percentage whether the operating speed is above or below the critical speed. This makes it easier to quickly assess whether an operating frequency needs to be adjusted to meet or exceed the 15% frequency margin. In Table 4.4.4 all the frequency margins currently exceed 15%. As a

result we have initially concluded that runaway speed range will not be a concern for any of the current critical frequencies of this wind turbine rotor system, but that we will need to pay close attention to the turbine's oscillation amplitude as it ramps up from its cut in speed to its operating speed. If the tip speed ratio is lowered, shifting all the speed ranges down closer to the 3rd and 4th modes the stiffness of the system should be increased or the mass of the system should be decreased to raise modes 3 and 4 above turbine operating speeds but also to keep modes 5 and 6 sufficiently above the runaway test speed range.

Table 4.4.4 Frequency margin for upper and lower bounds on turbine model rotational speeds

			Frequency Margin (%)					
Turbine Rotational Speed			F1	F2	F3	F4	F5	F6
[Descriptor]	[RPM]	[rad/sec]	[%]	[%]	[%]	[%]	[%]	[%]
Operating LB	2500	261.7994	3.13E+07	2.77E+04	24.5	19.8	74.7	75.3
Operating UB	3000	314.1593	3.75E+07	3.32E+04	49.4	43.7	69.7	70.4
Runaway LB	3900	408.407	4.88E+07	4.32E+04	94.2	86.8	60.6	61.5
Runaway UB	5300	555.0147	6.63E+07	5.88E+04	164	154	46.5	47.7

Finally, the last metric we employed to interpret the results from the SOLIDWORKS frequency study is the transmissibility also known as the transfer function operator or the amplification factor. For our undamped system, this amplification factor is expressed as [33]:

$$H(\omega) = \frac{1}{\left|1 - \left(\frac{\omega_{in}}{\omega_{cr}}\right)^2\right|} \qquad \text{Eqn. 4.4.4}$$

it gives the maximum amplitude of vibration excitation possible for an applied force, forced at a frequency. Infinite amplification is predicted for a frequency ratio of 1, but if the ratio is greater than 1.15 the amplification factor asymptotically approaches zero. In table 4.4.5 we have concerning amplification factors for the modes 3 and 4 only and acceptable ones for modes 5 and 6. Optimally, the amplification factor would be one or below for a properly damped system, but factors less than or equal to 8 are acceptable (e.g. not critically damaging) according to Gunter [33].

Table 4.4.5 Amplification factor for upper and lower bounds on turbine model rotational speeds

		Resonance Transmissibility Envelope – Undamped $\{1/\lvert 1-(\Omega_{in}/\Omega_N)^2\rvert\}$					
		Mode 1 (RPM)	Mode 2 (RPM)	Mode 3 (RPM)	Mode 4 (RPM)	Mode 5 (RPM)	Mode 6 (RPM)
		7.99E-03	9.00	2.01E+03	2.09E+03	9.90E+03	1.01E+04
LB	Operating Speed (2500 RPM)	1.02E-11	1.30E-05	1.82	2.30	1.07	1.06
UB	Operating Speed (3000 RPM)	7.10E-12	9.00E-06	0.81	0.94	1.10	1.10
LB	Runaway speed (3900 RPM)	4.20E-12	5.32E-06	0.361	0.401	1.18	1.17
UB	Runaway speed (5300 RPM)	2.27E-12	2.88E-06	0.168	0.184	1.40	1.38

Finally, we have provided visuals of the natural modes with their easily excited and not so easily excited counterparts. The figures below show the deflected shape normalized to a maximum unit deflection [30]. These are only shapes and need the appropriate force scaling factors applied to produce accurate deflections [30].

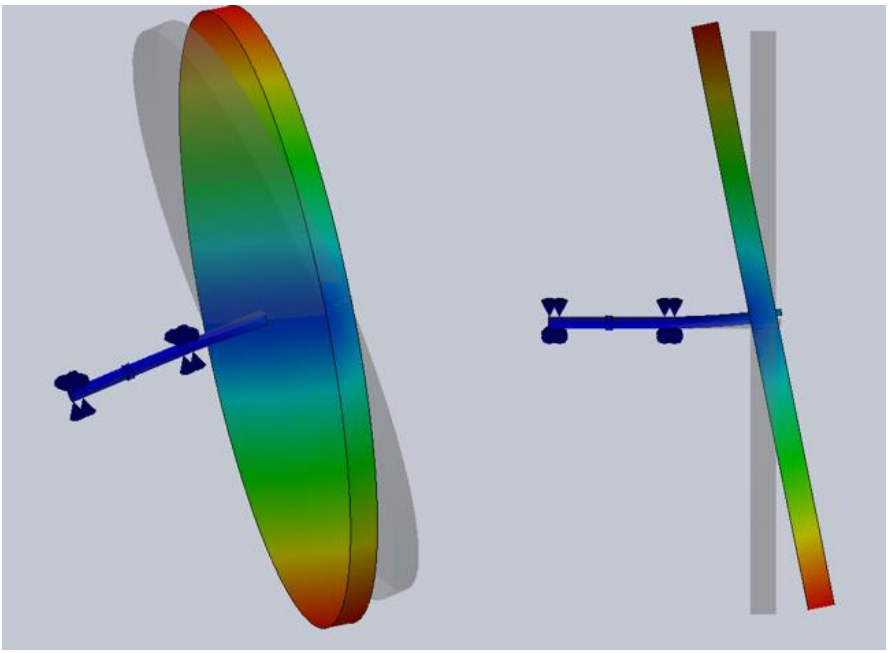

Figure 4.4.2 SOLIDWORKS Frequency Study Mode 3 (Y-Bending 1st) Vibration visualization

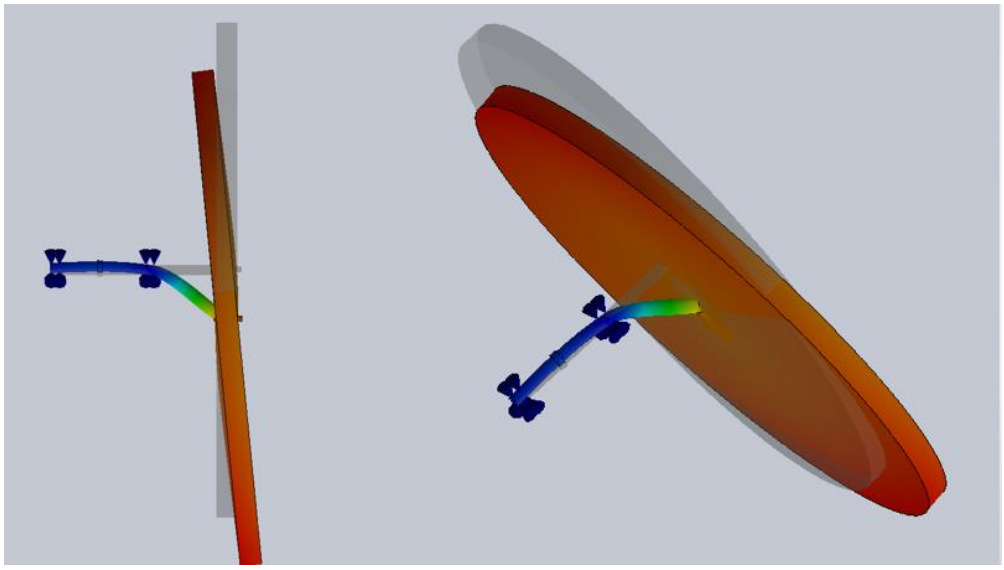

Figure 4.4.3 SOLIDWORKS Frequency Study Mode 5 (Y-Bending 2nd) Vibration visualization. The undeflected shape is shown in translucent gray and is superposed on the colored deflected result. The color scheme ranges from cool colors to hot colors indicating low to high deflection, respectively.

Note that this analysis was performed using the CPWPC's CAD model for their 2020 wind turbine. Once the 2021 wind turbine is finalized in SOLIDWORKS, we will recommend that the club uses this procedure to ensure that their system is not at risk of failure due to its critical frequencies.

Our Preliminary SOLIDWORKS frequency study allowed our senior project team to approximate the natural frequencies of the CPWPC's miniature wind turbine while gaining crucial knowledge and understanding of the simulation process. Despite the approximate nature of our results, this experience provided a helpful foundation in normal modes analysis that we leveraged in our ABAQUS modeling on the competition shaft geometry's first iteration (presented in the following section).

4.5 ABAQUS Linear Static and Linear Dynamic Modeling of Rotor Shaft System

Here we present our most recent modeling results. Our ABAQUS modeling results should be considered as similarly approximate with the results of our SOLIDWORKS frequency study, as they were based on non-finalized competition shaft geometry and the estimated mass of the pitching assembly. The summary of results that we have provided here was taken from our full report on our ABAQUS modeling, attached in appendix L.

Similar to our previous SOLIDWORKS modeling efforts, we simplified the wind turbine rotor down to a thin cylinder with matching diameter, mass, and thickness. Additionally, we modeled the bearing boundary conditions with rigid and flexible versions of a 3D pin and roller joint. We completed the flexible modeling with the spring elements in ABAQUS, adding one in each direction that was initially constrained by the rigid 3D joints with their approximated stiffnesses. We used Gargulio's method [34] to model the bearings' radial and axial stiffness instead of contacting SKF or another bearing supplier for more exact results since the final bearings for the turbine had not been selected by the CPWPC. Below, in figure 4.5.1, we have provided the rendering from ABAQUS of our simplified rotor model constructed of beam elements.

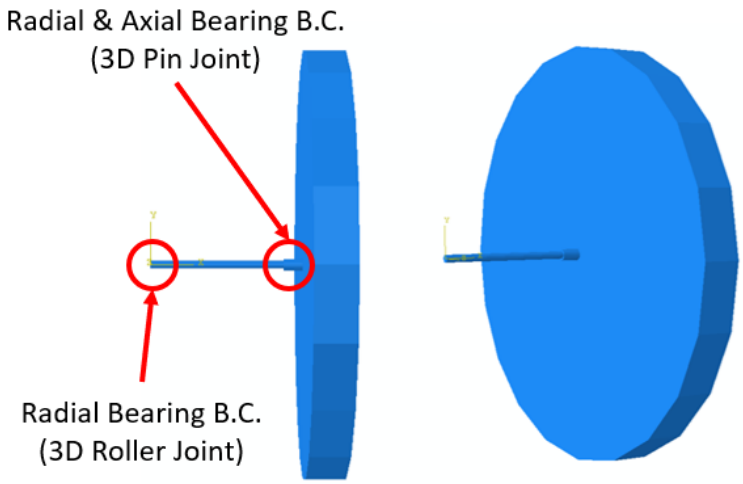

Figure 4.5.1. Simplified rotor + shaft ABAQUS model with annotated boundary conditions.

We chose to simplify the rotor assembly as the assembly's complexity made completing mesh convergence within the timeline of this FEA project impossible. Note the annotated boundary

conditions (B.C.'s). The first bearing takes radial and axial loads from the incoming wind and was located on the smaller shaft step (8 mm diameter) flush against the overhung, larger 12 mm diameter shaft step. The second bearing only took radial loads and was located at the leftmost end of the 8 mm section.

First, we validated the mesh for a simple, linear static load case (see appendix L, figure L.5). Once the static load case mesh converged with the flexible boundary conditions, we proceeded to linear dynamic modeling. Here we carried out the natural frequency estimation analysis, which neglects the damping of the assembly, and sought the first 30 modes (frequencies) to ensure that the solver captured all the vibratory mode(s) (in/about each coordinate direction) where the unconstrained mass of the model exhibits significant participation. These particular modes are the most important and can be the most damaging; thus, we took extra care to make sure they were extracted [30][32][33]. We have provided our tabulation of the 10 unique modes from our ABAQUS natural frequency extraction analysis below in table 4.5.1.

Table 4.5.1. Unique, non-rigid body modes for simplified shaft + rotor model

Mode No.	**Frequency**	**Frequency**	**Rotational Speed**
(#)	**(rad/sec)**	**(Hz)**	**(RPM)**
2	651.33	103.66	6219.6
5	6633.4	1055.7	63342
7	11343	1805.3	108318
9	22715	3615.1	216906
12	41851	6660.8	399648
15	63176	10055	603300
17	88154	14030	841800
20	118528	18864	1131840
22	154577	24602	1476120
24	157536	25073	1504380

Though the first mode listed in the table was the second mode found by the solver, the first mode identified was a rigid body mode, an artifact of improper model constraints we were unable to eliminate. The modes that we excluded in Table 4.5.1 are identical to those listed except in the direction of oscillation. With an operating speed of 2500 RPM and a maximum test speed of 3103 RPM, we determined that the CPWPC wind turbine operates well below its first natural frequency and can reasonably be classified as rigid. For all testing speeds, our natural frequency estimate suggests that a resonance condition is extremely unlikely. Since the frequency margin for the runaway test wind speed (22 m/sec) is just over 15% above the first critical frequency, the rotating assembly is technically rated for this speed. However, since the CPWPC updated the turbine shaft geometry and specified the final bearings after completing this analysis, this analysis must be repeated to confirm all previously mentioned results.

5.0 Concept Design

In this section we have provided a comprehensive account of our ideation and process through controlled convergence to select a concept design from the 19 we had initially ideated. After conducting our research and in parallel with our modeling, we brainstormed several concept designs for our balancing mechanism and system. To select the concept that best coincided with our project's scope, we started with a Go-No-Go down-selection, then proceeded to Pugh matrix down-selection, and finally weighted decision matrix down selection. This process reduced our options to four potential designs. Consultation with the other CPWP senior project teams regarding compatibility allowed us to select a final design from these options (See section 6.0 Final Design).

5.1 Initial Ideation & Concept Block Diagram

This section will discuss the preliminary brainstorming that was performed to identify an elegant solution to the issue of mass imbalance in a small-scale wind turbine.

Our ideation session was broken down into a couple of subcategories. We allowed each other to design anything that could eliminate imbalances in the rotating plane(s) and bending along the length of the shaft. From our ideation session we developed a few interesting designs. One design is a grooved disc attached to shaft with sliding masses in radial grooves. A software would measure mass imbalance in the system, then advise specific radial locations for each of the sliding masses to eliminate the rotor imbalances. A rudimentary schematic of this proposed design can be found in Figure 5.1.1 below.

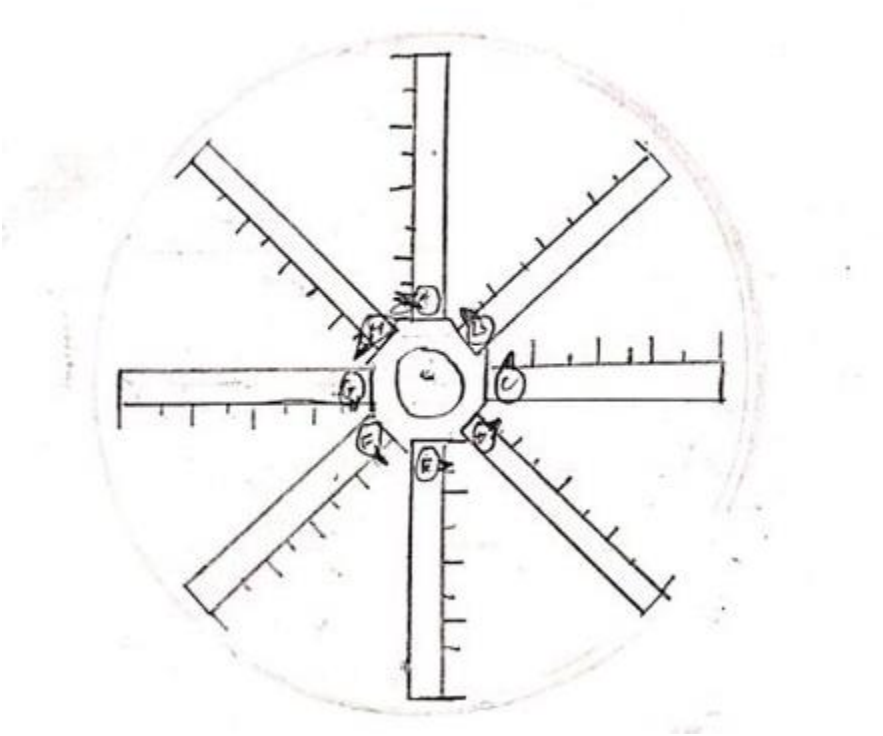

Figure 5.1.1 Grooved disc brainstormed design.

Similar to the grooved disc, a common industry rotor balancer includes a simple plate attached to the shaft with threaded holes in a radial pattern. Bolts of variable mass can be placed into these slots to also eliminate mass imbalances. Figure 5.1.2 below displays a sketch of the proposed design.

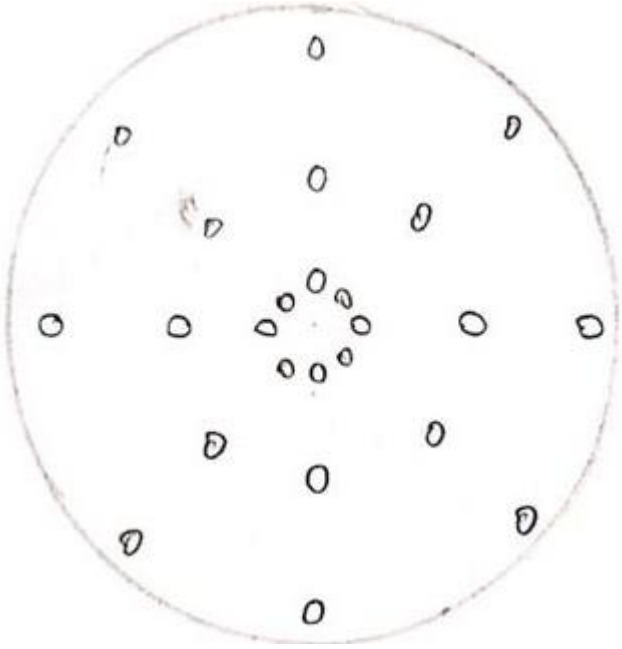

Figure 5.1.2 Threaded disc brainstormed design.

Another possible design involved a suspended tube through which the shaft would enter. The tube would be attached to three or more dampers, connecting to the interior of the nacelle. Figure 5.1.3 below shows a rudimentary drawing of the proposed solution.

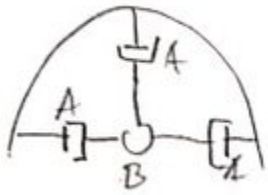

Figure 5.1.3 Suspended damping system (A designates a damper, B designates the rotating shaft).

This ideation session yielded a few interesting conclusions. One conclusion being that if mass imbalance in the rotating system is eliminated through a counteracting moment, either the distance or mass can be varied. We have agreed that variable masses can become costly and implementation can be difficult. Therefore, if our design utilizes a moment to cancel vibrations, distance will be varied rather than mass. For example: the design specified in Figure 5.1.2 would not use variable mass bolts, as those can add to project expenses and the same level of precision may be achieved with the addition of more threaded holes.

Another conclusion from our ideation session enforced something we have already discovered: some parameters that reduce mass imbalance are not within our scope. For example, vibrational bending along the shaft can best be limited by additional shaft supports, adjusting the rotational speed, or a thicker shaft. None of these design changes are within our senior project authority to make. This conclusion emphasizes the importance of design recommendations that can be used by future CPWP teams to reduce and help to cancel out mass imbalances.

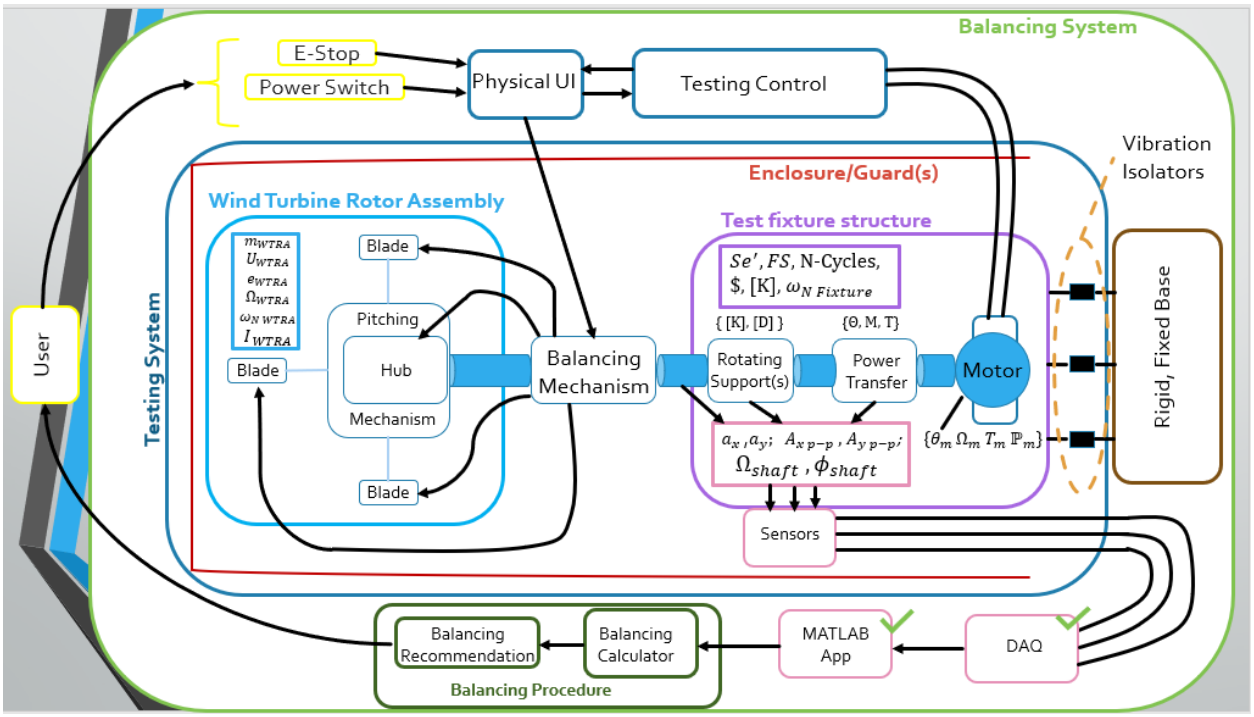

Figure 5.1.4 Concept design block diagram.

This block diagram provides a visual representation of all the elements that we know are essential to our balancing system, procedure and mechanism. Additionally, we have listed specific parameters that characterize dynamic behavior or that we believe will govern design decisions in the future. A larger version of this is available in Appendix F – Figure F.1 While this block diagram is busy and perhaps overwhelming to some, it was helpful to our senior project team as it allowed us to map the effects of different components on one another and compile our knowledge (at the time) of the critical parameters to the balancing system and mechanism.

5.2. Go-No-Go Down Selection

From our Preliminary Design Review, we defined 19 potential designs. Appendix F contains hand drawings for all 19 designs. We decided to perform a broad down selection process that expressed the cost and complexity of each possible design selection. From this process, we wanted to identify consistencies in strong designs and inconsistencies in weak designs. To thoroughly articulate each design aspect, cost and complexity were designated with subcategories which were rated on a scale of 1-3. Table 5.2.1 below details each component of "cost" and "complexity," along with a description of each subset.

Table 5.2.1 Cost and complexity down selection definitions.

Cost	Complexity
Time (1-3). The time needed to manufacture, analyze, simulate and implement the part.	Manufacturing (1-3). The difficulty of making the part.
Price (1-3). The monetary cost of manufacturing, analyzing, simulating and implenting the part.	Analysis (1-3). The hand calculations needed to make the part.
	Simulation (1-3). The difficulty of simulating the part.
	Implementation (1-3). The difficulty of implementing the part in the wind tubine assembly.

Note that a lower score indicates a simpler design, and a higher score indicates a more complicated design. Cost and complexity were then normalized and plotted in Figure 5.1.1. All analytical work and numerical assignments that were conducted for this down selection process can be found in Appendix H.

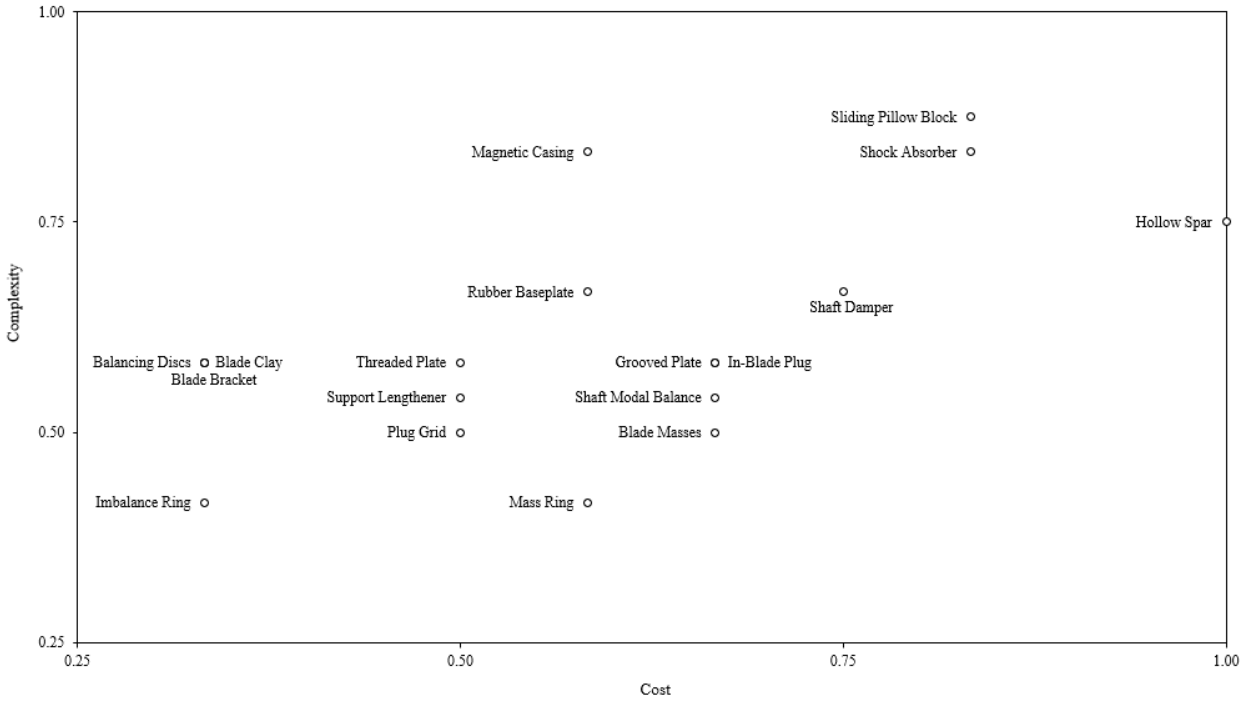

Figure 5.2.1 Normalized cost and complexity for 19 potential designs.

Our philosophy denoted that designs that rank too highly or lowly on this spectrum are not ideal designs to pursue. Higher ranking designs are going to be extraordinarily time-intensive and expensive. On the other hand, low-ranking designs may not acknowledge our problem statement. Therefore, we decided to focus our attention on the designs that ranked in the middle. These designs would not be overly complicated but would also provide enough complexity to properly balance the system on a reasonable budget.

To help in the go-no-go down-selection process, we decided to evaluate our potential designs using another criterion: effectiveness and scope. Effectiveness refers to the ability for the potential design to directly eliminate the mass imbalance in the system. Scope refers to whether the potential design addresses each component of our problem statement. These criteria were also ranked on a scale of 1-3, similar to each component of cost and complexity. The evaluation and normalization of these criteria can be found in Appendix H. The plotted results for scope and effectiveness can be found in Figure 5.2.2 below.

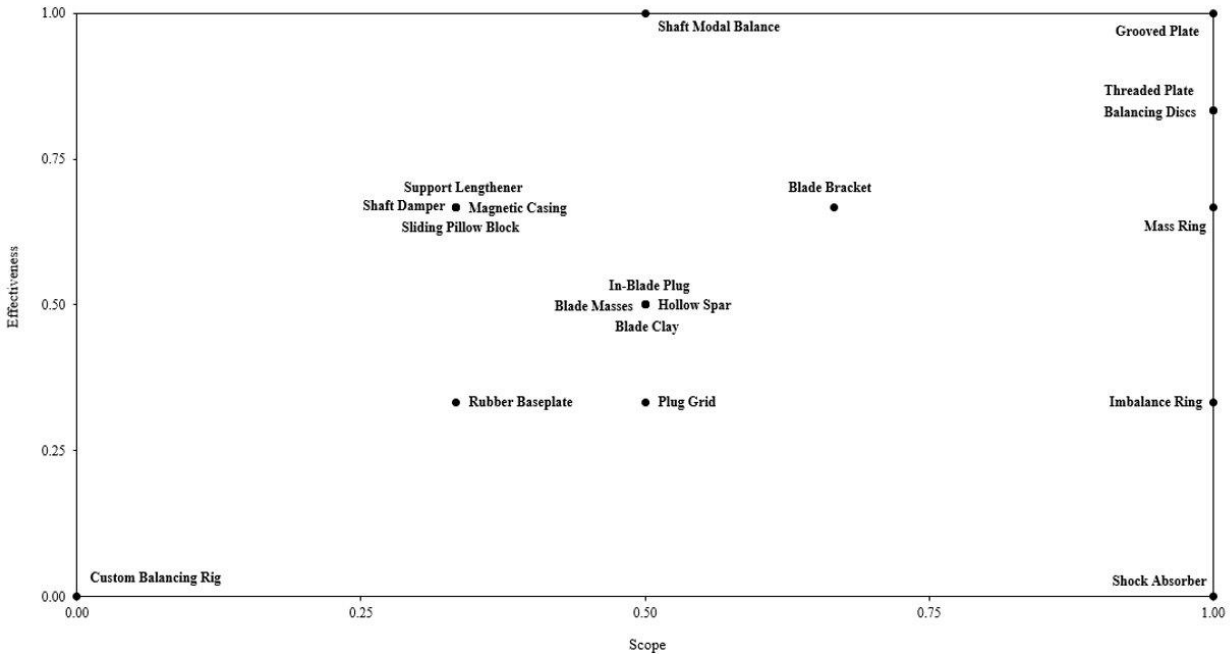

Figure 5.2.2 Normalized effectiveness and scope for 19 potential designs.

Note that this scale praises designs that rank highly in both scope and effectiveness. Oppose to the cost and complexity index, a high score for both scope and effectiveness is preferred. From both Figure 5.1.1 and Figure 5.1.2, we were able to formally eliminate 11 potential designs. These designs were eliminated because they did not directly address the issue of mass imbalance in the rotating system, they were too complicated or because they were no longer feasible to implement in the wind turbine assembly.

5.3 Pugh Matrices Down Selection

After filtering our 19 generated concept designs through our cost-complexity index, gauging the design's perceived effectiveness and scope, evaluating each design's alignment with our problem statement, we were left with 8 potential designs. We have provided the sketches of these 8 designs below as a primer to our Pugh matrices and weighted decision matrix which do not have pictures of these designs.

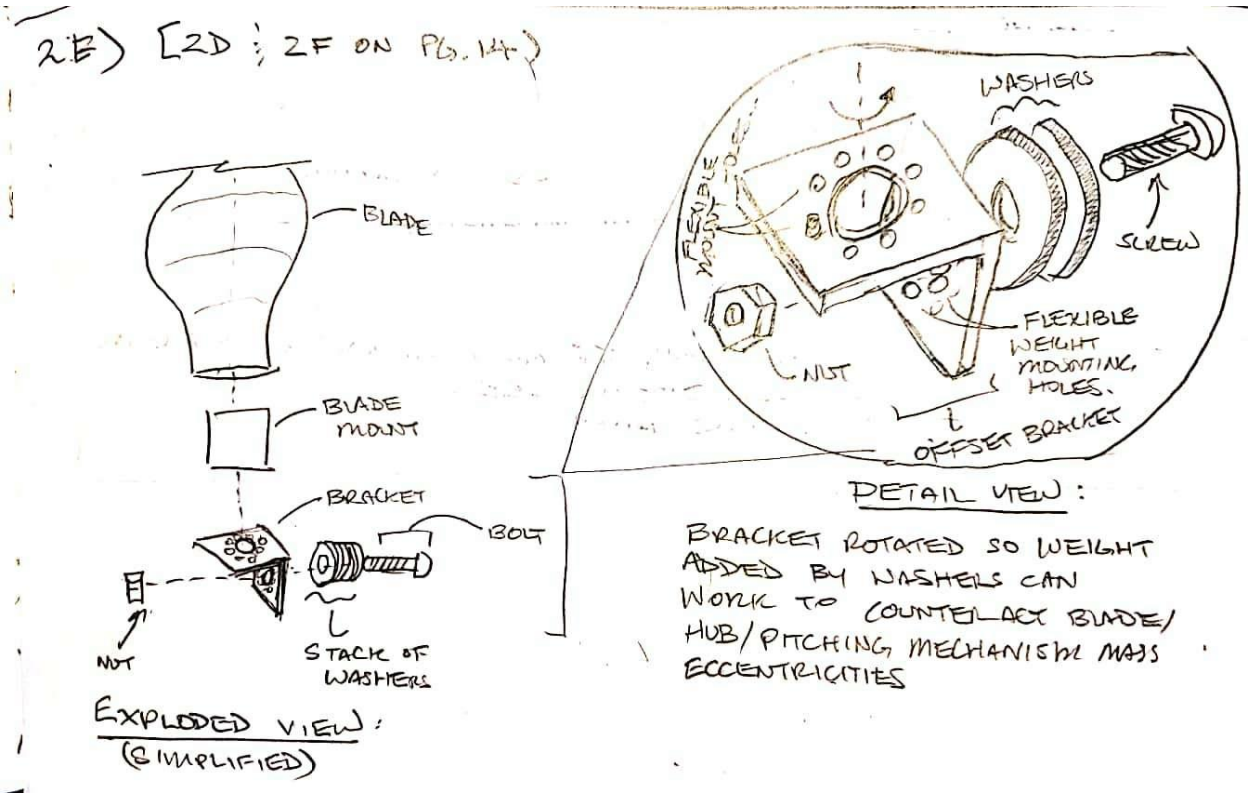

Figure 5.3.1 Blade bracket balancing mechanism concept sketch.

Our blade bracket design (see Figure 5.2.1) consists of a L-shaped bracket with a bolt circle and enlarged center hole for alignment to the blade as well as grid of blind tapped holes which short button head screws with washers thread into as correction masses. Our team would mount this bracket with correction masses directly to the hub such that it would not rotate with the pitching mechanism but instead be repositioned about the hub with screws and washers added as needed to correct the mass imbalance in the rotating assembly.

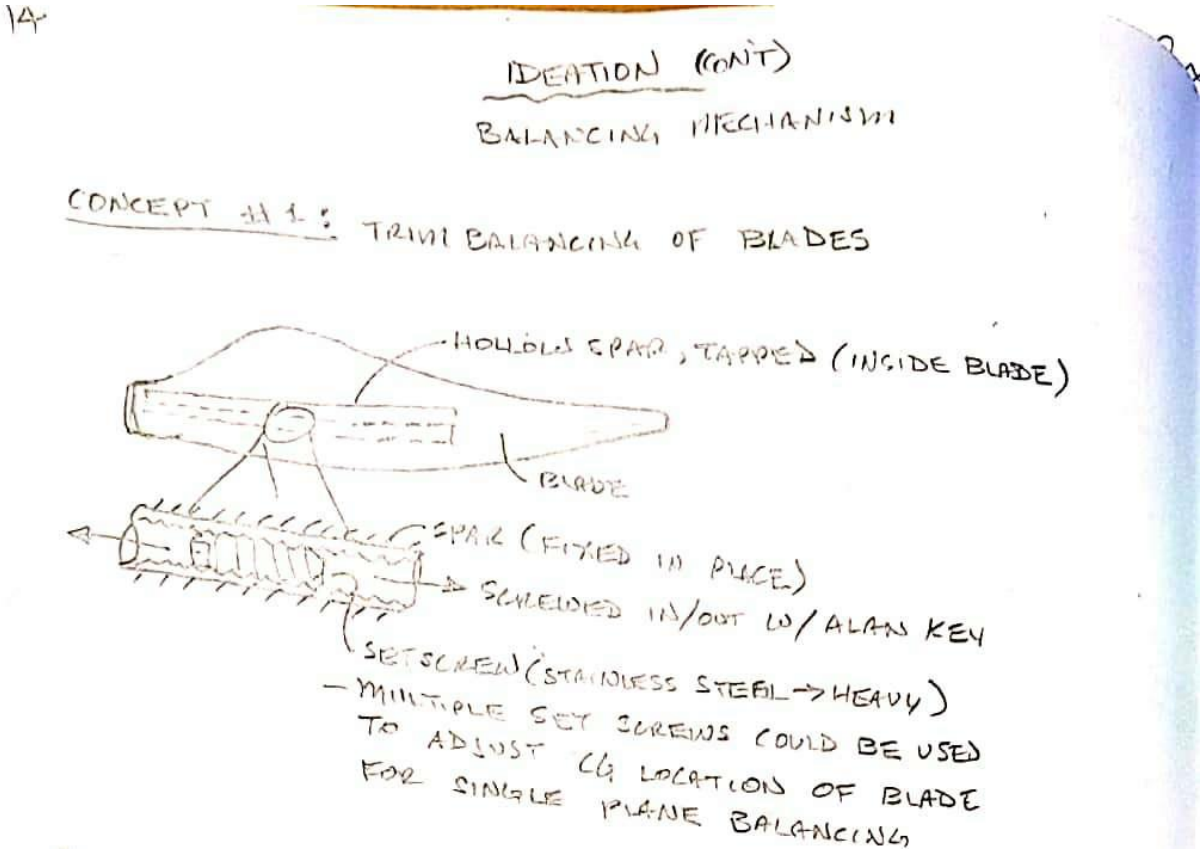

Figure 5.3.2 Hollow spar balancing mechanism concept sketch.

Our hollow spar design (see Figure 5.3.2) makes use of a hollow recess inside of the competition wind turbine blades where a cylindrical threaded insert would be located such that threaded rods and/or set screws could be inserted to shift the center of mass of the blade along its axis. Adjusting the center of mass of the blade with our hollow spar design would consist of repositioning the set screws/threaded rod and would require us to remove the blades from the pitching assembly each time. Additionally, the hollow spar design assumes that most of the mass imbalance to be corrected exists in just the wind turbine blades.

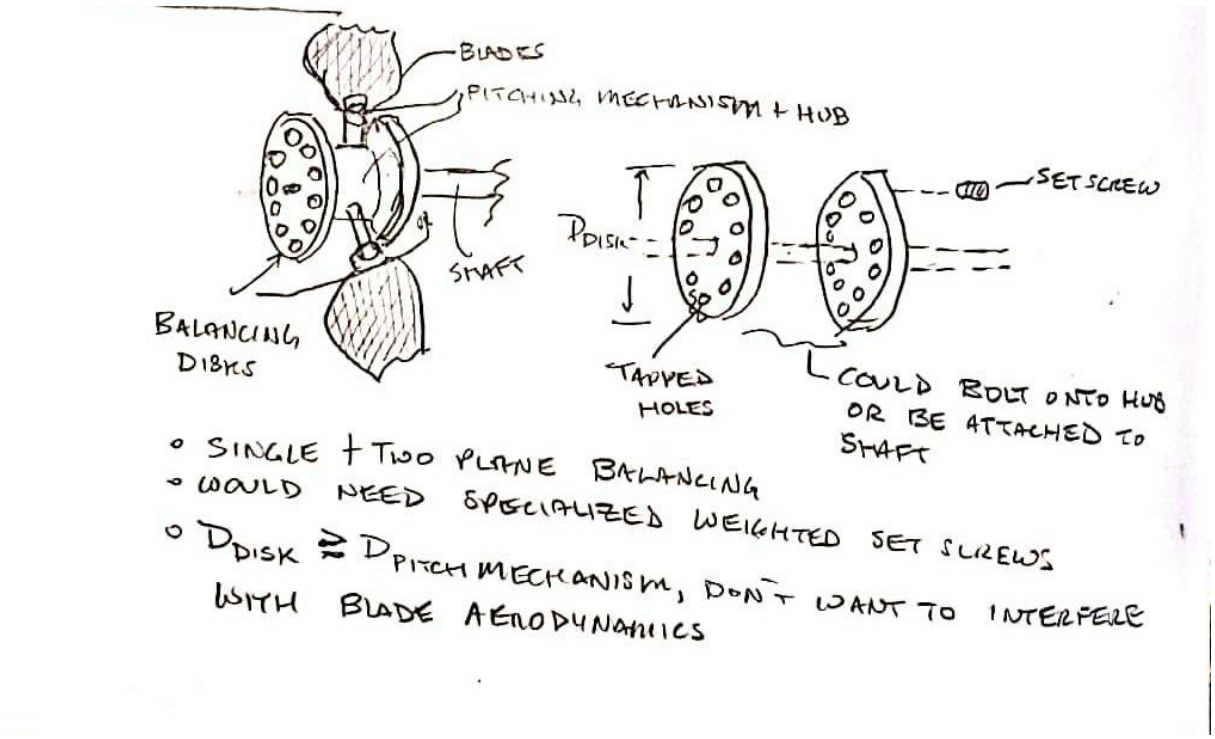

Figure 5.3.3 Balancing discs balancing mechanism concept sketch.

Our balancing discs design (see figure 5.3.3) makes use of two threaded plates which have tapped through holes where setscrews (the correction masses) are inserted to minimize the characterized mass imbalance. Unlike the rest of our designs, the balancing discs have the capability to do both single and two plane balancing – more accurately it can simulate single plane balancing. Our design simulates single plane balancing by having the user place 2 set screws in tapped holes diagonal from each other to ensure that the moment contributions are automatically canceled out. Conversely, when the balancing disc design is being used in two-plane balancing mode, the set screws can be placed in either diagonal or matching tapped holes on the two discs.

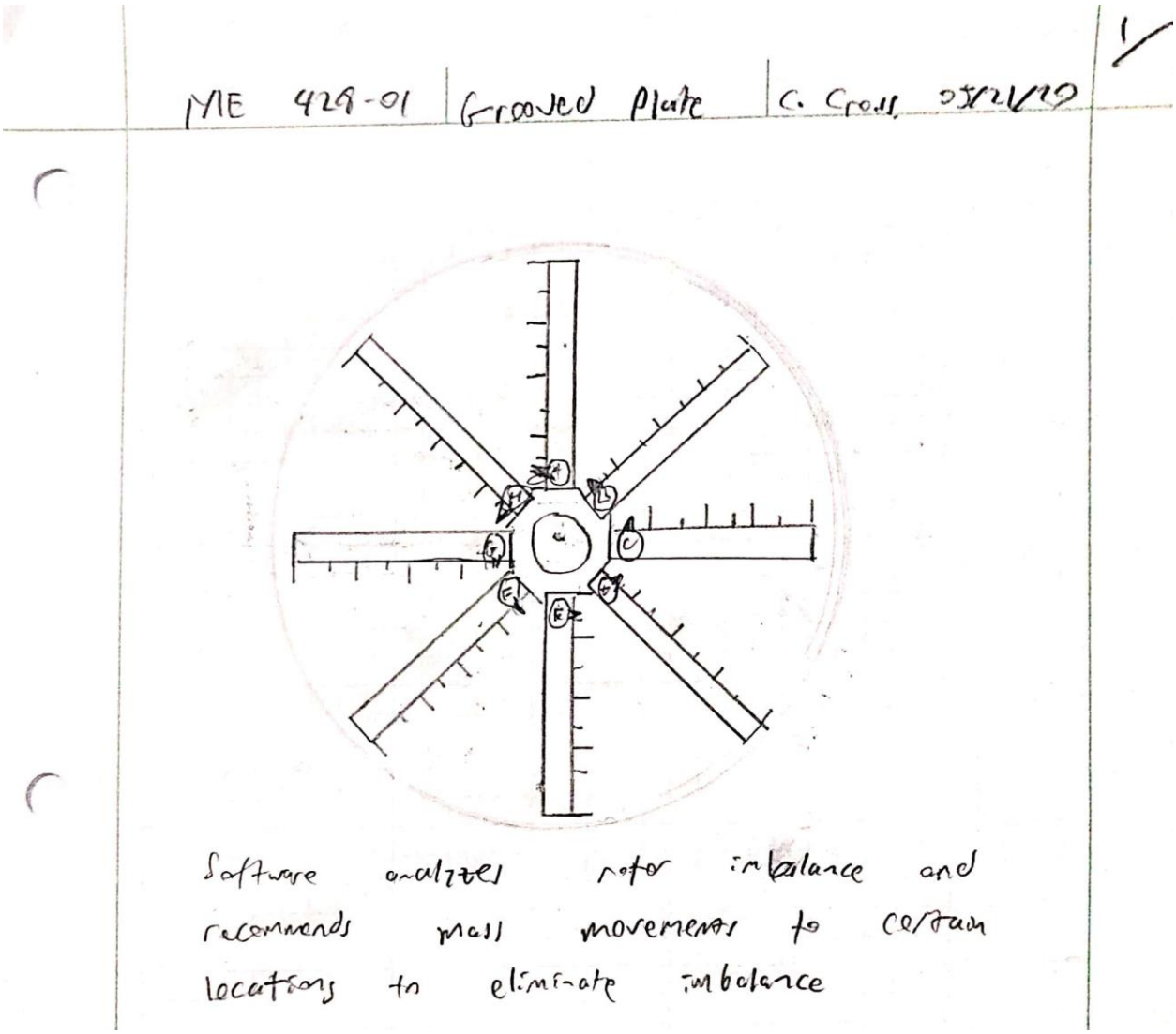

Figure 5.3.4 Grooved plate balancing mechanism concept sketch.

The grooved plate design (see Figure 5.3.4) consists of 9 radial slots in a plate which each hold a sliding mass. This plate—along with our other designs which use a plate or disc—will need to be mounted at the hub of the turbine and at the base of the blades. This is because mass imbalance must be corrected in the plane of imbalance. The sliding masses can be positioned at variable distances from the center to precisely counteract mass imbalances in the rotating system. A weakness of this design is the potential human error that is introduced by sliding the masses to their correct locations.

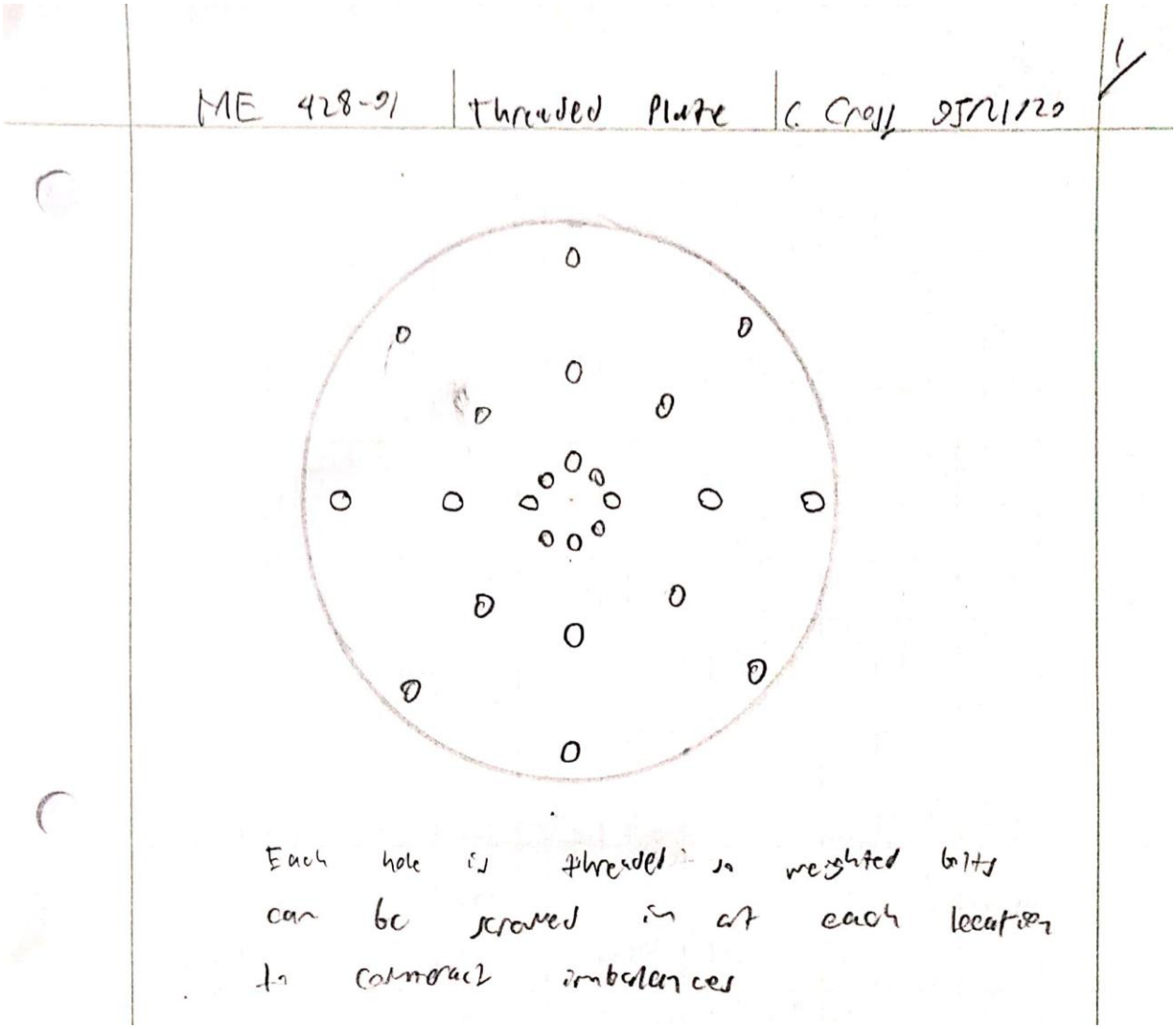

Figure 5.3.5 Threaded plate balancing mechanism concept sketch.

The threaded plate (see Figure 5.3.5) is a widely used solution in the rotor balancing industry. This design includes 9 radial lines of threaded holes. Set screws can be placed into these holes to counteract mass imbalance in the system. While simple to manufacture, this design is not precise. Depending on the weight of the rotating assembly, a more precise design may be required. A multitude of differently weighed set screws may be used for more precise calibrations. However, this will drive up the requires cost to make the part.

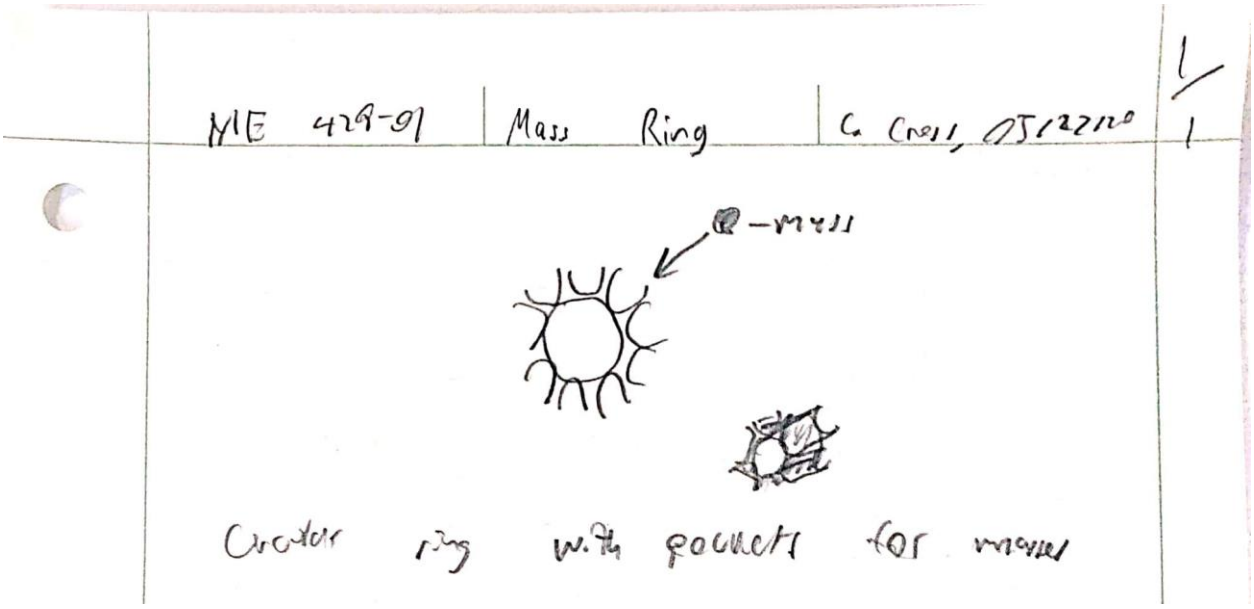

Figure 5.3.6 Mass ring balancing mechanism concept sketch.

The mass ring (see Figure 5.3.6) is a cylindrical attachment that connects to the shaft of the wind turbine. On the outside of the cylinder are 9 axisymmetric clips intended to hold variable masses. These masses would be calibrated to account for the mass imbalance in the rotating plane. This design requires a variety of precise masses which can be inserted and removed from the mass ring. Purchasing variable masses in the range of weight that is needed for precise calibration may prove difficult and expensive. Simple design refinement however may make the part easy to manufacture via 3D printing.

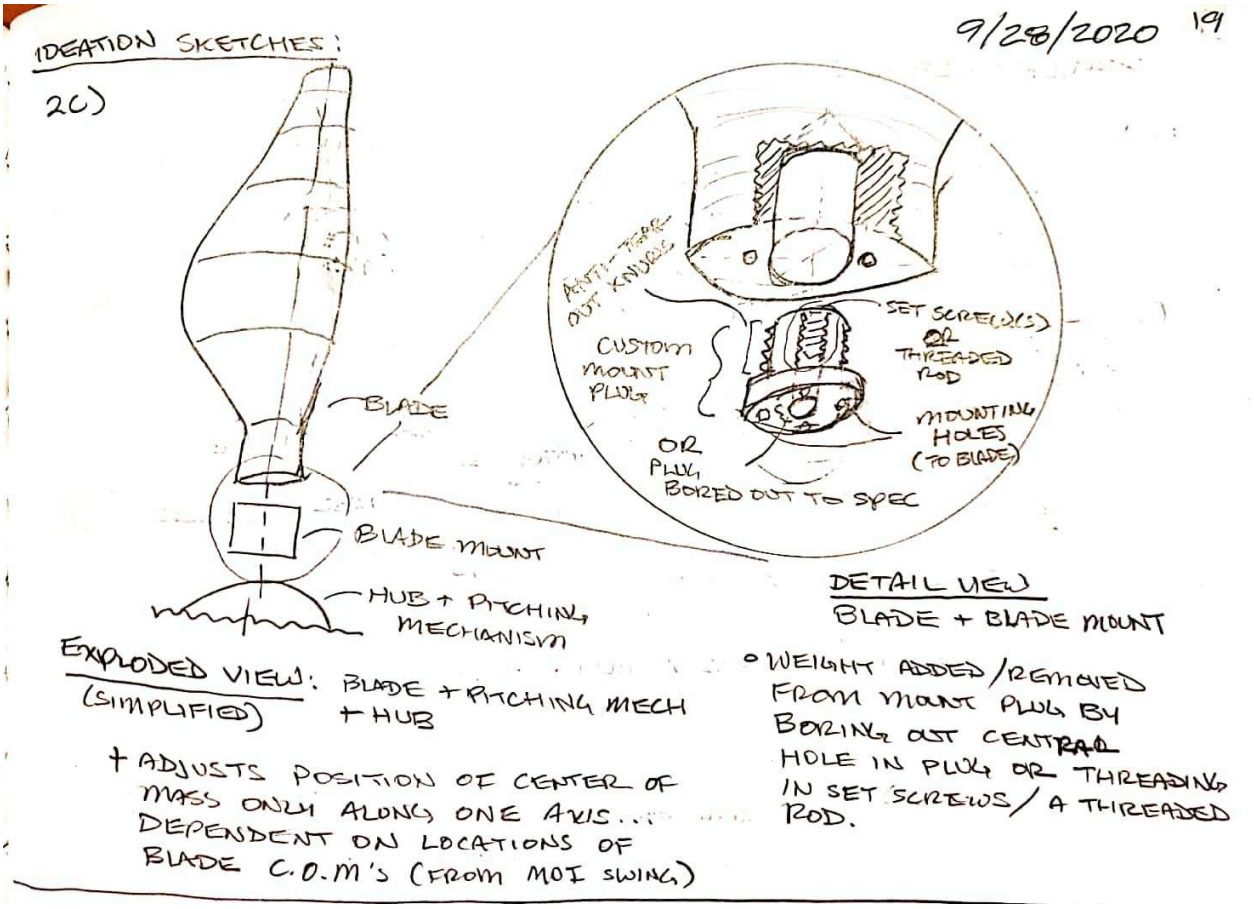

Figure 5.3.7 Blade plug balancing mechanism concept sketch.

Our blade plug design (see Figure 5.3.7) would act like a threaded insert (helicoil or brass inserts melted into 3D prints) and allow for adjustment of the center of mass of the blade through the insertion of threaded rods or set screws into the bore of the blade plug. The blade plug would be mounted inside each of the 3 competition wind turbine blades and would act as the interface between the blade and blade mount. To adjust the center of mass of each blade the wind turbine blade we would have to be removed from the rest of the rotor assembly. Similar to the hollow spar, our blade plug design assumes that the majority of the imbalance to be corrected exists solely in the blades.

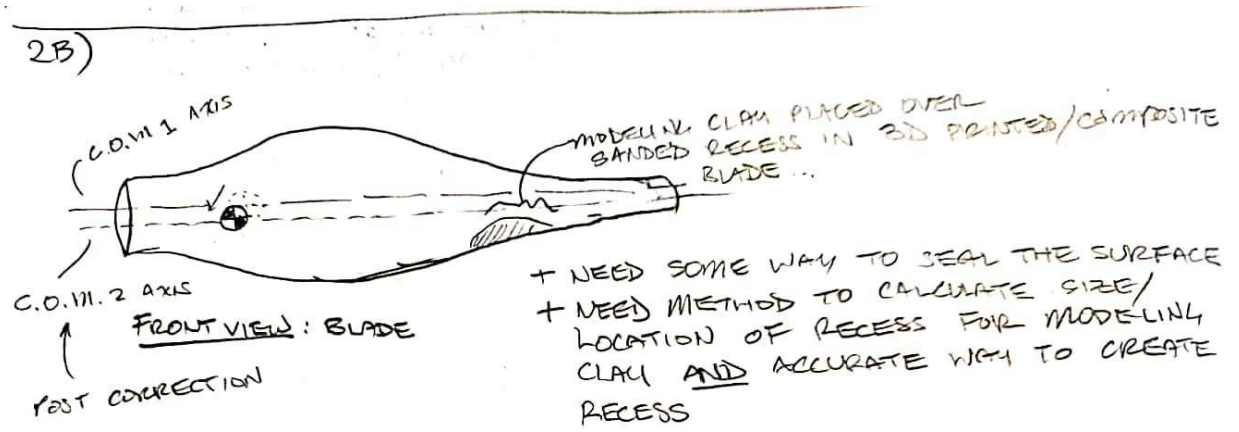

Figure 5.3.8 Blade clay balancing mechanism concept sketch.

Our blade clay design (see Figure 5.3.8) leverages the pliable nature of modeling clay to fine-tune the position of the center of mass. First, we would create a recess in a portion of the blade for the clay to be added such that the center of mass of this blade would closely match its nominal location. Then, we would add the clay and refinish the surface of the blade, likely with epoxy to ensure the surface, especially where the clay was added, would not induce turbulence thereby reducing the power output of the turbine rotor. Besides assuming that the majority of mass imbalance to be corrected exists in the blades of the wind turbine rotor our blade clay balancing mechanism design would only really be feasible for fine tuning and may not be up to the task of actually minimizing the mass imbalance in the wind turbine's rotating assembly.

With 8 potential final designs, we proceeded to more concentrated down selection techniques. We decided to evaluate our designs using the Pugh matrix method. To use a Pugh matrix, we needed to identify the relevant criteria for our design. Each criterion we decided to consider is detailed below, along with a brief description of each.

- **Easy to use**. The ease of adjustment and prior knowledge needed to operate the design.
- **Precision**. The minimal possible adjustment that can be made to the part.
- **Correction capacity**. A speculative observation concerning the amount of imbalance each design can correct.
- **Safe to operate**. The design can be operated and handled with minimal risk to the user or the assembly.
- **Adjustability**. The part can be re-calibrated if necessary.
- **Easy to implement**. A speculative observation concerning the difficulty of synergizing the design with the pre-existing wind turbine system.
- **Cost to manufacture**. The design requires a small portion of our budget.
- **Easy to manufacture**. The design is simple to make.

Using the industry standard "in-situ" balancing technique as a datum, we were able to express whether our designs performed better, worse or the same relative to the industry standard for each

criterion we defined. In-situ balancing is the process of measuring mass imbalance in a rotating assembly, then adding weights to individual components of that assembly to eliminate the mass imbalance. Our first Pugh matrix iteration can be found in Table 5.3.1 below.

Table 5.3.1 Pugh matrix (I) with in-situ balancing datum.

Design / Criterion	Industry Standard (In-situ)	Blade Bracket	Hollow Spar	Balancing Discs	Grooved Plate	Threaded Plate	Mass Ring	Blade Plug	Blade Clay
Easy to use	0	0	-1	0	0	0	0	-1	-1
Precision	0	0	0	0	1	0	0	0	-1
Correction capacity	0	0	0	0	0	0	0	0	0
Safe to operate	0	0	0	0	0	0	-1	0	-1
Adjustability	0	0	-1	0	1	0	0	0	1
Easy to implement	0	0	-1	0	0	0	0	-1	1
Cost to manufacture	0	1	0	0	0	0	0	-1	1
Easy to manufacture	0	1	-1	1	0	1	-1	0	1
Total	0	2	-4	1	2	1	-2	-3	1

The performance of each design in the Pugh matrix can be evaluated using two standards: final score and consistency. The score each design receives roughly articulates how the design compares relative to the datum. The consistency of each design refers to the number of positive and negative evaluations each design is allocated. Consistent designs have only positive or negative scores which directly contribute to its final score.

From our first Pugh matrix, we noted two poorly performing designs: the hollow spar and the blade plug. Since each design did not outperform the in-situ balancing procedure for any criteria, these designs were eliminated from future considerations.

Moving forward, we wanted to use more Pugh matrices to compare our potential designs against each other. Our second Pugh matrix used the blade bracket design as a datum, and the process was repeated; each design was ranked either better, worse, or equivalent to the blade bracket for each criterion. This Pugh matrix can be found in Table 5.3.2 below.

Table 5.3.2 Pugh matrix (II) with blade bracket datum.

Design / Criterion	Blade Bracket	Balancing Discs	Grooved Plate	Threaded Plate	Mass Ring	Blade Clay
Easy to use	0	0	1	0	-1	-1
Precision	0	0	1	0	0	-1
Correction capacity	0	0	0	0	0	0
Safe to operate	0	0	0	0	0	0
Adjustability	0	0	0	0	0	-1
Easy to implement	0	0	0	0	0	1
Cost to manufacture	0	-1	-1	-1	-1	0
Easy to manufacture	0	0	-1	0	0	0
Total	0	-1	0	-1	-2	-2

No designs were able to rank higher than the selected datum. While the grooved plate design scored similarly to the datum, it was also more inconsistently scored. These results brought into question how important the manufacturing process is relative to the other aspects of the design. This will be discussed in detail with regards to the weighted decision matrix.

After evaluating the results from our second Pugh matrix, we decided not to eliminate any potential designs. Before doing so, we wanted to make one more Pugh matrix, this time using the grooved plate as a datum. Table 5.3.3 below details our third Pugh matrix, using the grooved plate design as a datum.

Table 5.3.3 Pugh matrix (III) with grooved plate datum.

Design / Criterion	Grooved Plate	Balancing Discs	Blade Bracket	Threaded Plate	Mass Ring	Blade Clay
Easy to use	0	-1	0	0	0	-1
Precision	0	-1	-1	-1	-1	-1
Correction capacity	0	0	0	0	0	0
Safe to operate	0	0	0	0	0	0
Adjustability	0	0	0	0	0	-1
Easy to implement	0	0	0	0	0	1
Cost to manufacture	0	1	1	1	0	1
Easy to manufacture	0	1	0	1	0	0
Total	0	0	0	1	-1	-1

This Pugh matrix yielded some interesting results. Firstly, compared to our second decision matrix (see Table 5.3.2), the scores in this matrix are more varied. This is to be expected with a new datum. After our third Pugh matrix, we decided to eliminate blade clay as a design consideration. Our reasoning for this elimination was that the process of applying blade clay was irreversible and imprecise. Although blade clay may later be considered as a fine-tuning procedure—along with appropriate sanding—the lack of numerical analysis and the potential human error associated with the design made it not ideal for our primary balancing procedure.

5.4 Weighted Decision Matrix Down Selection

After eliminating the hollow spar, the blade plug, and mass ring concept designs we moved on to the final phase of our qualitative down selection – a weighted decision matrix.

We chose to expand our grading criteria from the eight used before in the Pugh matrices. We decided to include repeatability as a new consideration. We defined repeatability as the consistency of the mass imbalance correction achieved by each design. As we were entering into a more granular phase of our down selection with just 5 designs instead of the original 19 we decided it was time to include this additional criterion that we had purposefully omitted in the earlier rounds of our down selection process. Additionally, the repeatability criterion was better expressed in the context of the original eight criteria after all our criterion had been assigned a weight.

To quantify the weight for each criterion, we ranked each criterion from most important to least important. From there, we assigned weights in 0.005 increments, with important criterion receiving higher weights and vice versa. We rated each criterion on a scale of 1-5, where the 1-5 scale maps to fulfillment of the design criterion – 1 being unfulfilled and 5 being fulfilled as specified. We then multiplied the rating in all the design criterion for each design by the weight of each criteria, the sum of which is the design's normalized score out of 5.

5.4.1 Weighted Decision Matrix Weight Justification

Our most important criteria is safety as the mechanisms we are working with and the interactions between our balancing mechanism and the wind turbine's drive train, etc. have the potential to create a resonance condition that damages the turbine and could injure bystanders. This motivated the runaway test, and in turn, motivated our project in the first place. Therefore, first and foremost, our design must consider safety a top priority.

We chose correction capacity to be our second most important design selection criterion as the ability of the balancing mechanism to balance the turbine when implemented is at the crux of our senior project's problem statement.

Our team reached the consensus that both the precision of the balancing mechanism and the ease of implementation were equally important criterion. Precision deals with our balancing mechanism having sufficient resolution to incrementally correct for the mass imbalance present in the wind turbine without over/under correcting for it. If our mechanism is too imprecise to be able to deal with present mass imbalance accurately and effectively in the wind turbine rotating assembly, then the entire system may be placed in jeopardy.

Additionally, we were concerned with the difficulty of putting our balancing mechanism design into practice due to how it would need to be integrated with the blades or pitching mechanism. This implementation criteria captures both the logistical difficulty of working closely on the design with another or multiple senior project teams as well as how difficult of a design problem it is to integrate the two designs.

Repeatability of the balancing mechanism's balance was our 4th most important criterion. After being safe to use and capable of correcting the imbalance, it is crucial that our adjusting of the correction masses in the same manner on the balancing mechanism yield reasonably consistent results. Additionally, we desire that our mechanism be able to tolerate being removed from the turbine or having other drivetrain components disassembled to replace components. When reassembled, our system should be able to balance the system again without error. Finally, the third aspect of repeatability regarding our design is that over time the effect of an adjustment on the balancing mechanism does not drift significantly – barring shaft plastic deformation from whirling or other unforeseen complications that fundamentally change the systems' behavior.

After repeatability, we selected ease of use and adjustability as the 5th most important design criterion. Making a balancing mechanism and procedure that is user-friendly is essential to allow anyone in the CPWP club to balance the wind turbine. If however, it is the case that our sponsor is willing to compromise on the user interface in return for a more effective, small form factor

mechanism accompanied by a detailed procedure (see section 3.1 and section 2.2 sponsor meetings), then we may be able to justifiably re-weight this criterion.

While it would be ideal that the final product, we produce from this senior project be applicable to all future wind turbine designs, this expectation is unrealistic. Yet, it is important that this design not be so highly specified to this year's turbine that it would be impossible to transfer even core design choices to a similar system for next year's turbine. Thus, we also included the adjustability criteria as a check to ensure our balancing mechanism design, or at minimum its basis could be easily modified and applied to future turbines.

Our lowest ranking design criterion were ease of manufacturing and the cost of manufacturing, respectively. We differentiated between the two as a function of how much spending a little more money could save on time in the shop making custom components. As a two person senior project team, it is imperative that we pay close attention to the amount of work we are assigning to ourselves and constantly check if it is feasible for the two of us to accomplish what we have said we will do. While these criteria are the lowest importance for our weighted decision matrix, they are nonetheless essential as they help to ground the design judging process in the reality of making a physical mechanism from our detailed design.

5.4.2 Weighted Decision Matrix Rating Dissection

As our senior project team filled out the decision matrix, we ran into difficulty in establishing appropriate weights for each design criterion. Specifically, we ran into difficulties with the following criteria: safe to operate, correction capacity, and ease of implementation.

Other mechanisms that will be employed during the instrumentation and testing processes of the competition turbine contribute to the overall safety of the selected balancing mechanism. Because of this, we chose to limit the maximum rating to 4 in operational safety category to make room for unaccounted safety issues that could arise from external systems (e.g. the mechatronic system that runs the motor to drive the wind turbine, the instrumentation, etc.). Finally, with regards to the ease of implementation we chose to limit the maximum rating to 3 (the middle ground between fulfilled and unfulfilled) as we had little or no knowledge regarding how easy it would be to modify the blade's or pitching mechanism's design to suit the needs our balancing mechanism. In this case, 3 was considered workable and any rating below that was indicative of significant redesign for either our balancing mechanism or the blades and pitching mechanism senior projects.

Before we present our decision matrix results, we would also like to clarify the case where all our designs were rated as fulfilling the adjustability requirement. In the case of adjustability, none of our mechanisms would make irreparable changes to the competition turbine while in the pursuit of balancing it. Any design which had necessitated irreversible changes had already been eliminated by this point in the down selection process. Also, all balancing mechanism designs judged in our weighted decision matrix use very similar balancing methods whose core concepts are readily transferable between future competition turbine designs.

5.4.3 Weighted Decision Matrix Results

Here we have provided the results of our weighted decision matrix, in Table 5.4.1 shown below. Although it was not our lowest scoring design, we decided to eliminate the mass ring balancing

mechanism as it would require a wide range of highly specified correction masses, in the form of metal bars that could be slid into the 9 cylindrical pockets in the hub, to achieve the effectiveness we desired for it. Thus, we were left with 4 finalist design concepts: grooved plate, balancing discs, blade bracket, and threaded plate, where threaded plate scored the highest, followed by grooved plate, then balancing discs, and finally blade bracket. Our final design selection is still pending and is contingent upon the constraints arising from the pitching mechanism's senior project selected design. This is because our system must be implemented in the plane of imbalance, and therefore, immediately in the plane of the blades and pitching mechanism.

Table 5.4.1 Weighted Decision Matrix.

Design / Criterion	Weights	Grooved Plate	Balancing Discs	Blade Bracket	Threaded Plate	Mass Ring
Easy to use	0.075	4	3	2	5	4
Precision	0.150	5	4	4	4	4
Correction capacity	0.175	4	4	3	4	4
Safe to operate	0.200	4	4	4	4	3
Repeatability	0.100	4	5	5	5	5
Adjustability	0.075	5	5	5	5	5
Easy to implement	0.150	3	2	2	3	3
Cost to manufacture	0.025	3	3	5	4	2
Easy to manufacture	0.050	3	4	5	5	4
Total	1.000	4.000	3.775	3.625	4.150	3.775

Our most robust design was the threaded plate. Not only is it an exact copy of an industry standard method of correcting imbalances on larger rotating shafts, it is also by far the simplest of our designs to manufacture. Our threaded plate design did well across the board (taking into consideration the artificial limits we placed on the ratings for some of the criterion). Similarly, our grooved plate design scored very similarly to the threaded plate design only losing out the threaded plate in manufacturing cost, ease of manufacturing and repeatability. However, the grooved plate has the potential for having the highest resolution in adjustment of the correction mass positions and thereby likely the highest precision of any of our designs. Even so, the method of adjustment of our grooved plate design leaves room for potentially significant human error, while the setscrew holes in the remaining designs are primarily subject to the positional tolerances we set for them – making them more repeatable.

Scoring noticeably lower than our grooved plate design, the balancing discs design suffered in implementation, ease of use, and cost to manufacture. While the cost of making what amounts to two threaded plates is only marginally more than making a single one, doubling the number of holes to be tapped would require more taps to be purchased as a precautionary measure to prevent the scrapping of unnecessary parts. More time will also be needed to tap all the necessary holes.

More importantly, the single plane and two plane adjustment modes could prove to be confusing to the user and if misapplied could even lead to an unintended resonance condition potentially doing permanent damage to the turbine. More concerning is how feasible it would be to both sandwich the hub with two threaded plates while not interfering with the pitching mechanism and simultaneously still having sufficient room to access the balancing discs for balancing adjustment.

The lowest scoring of our finalist concept designs, our blade bracket design raised concerns with regards to its correction capacity, ease of use, and ease of implementation. Although the blade bracket design scored lower than the mass ring design, the blade bracket was kept because it was the cheapest and easiest design to manufacture, as well as to source components for. Since our blade bracket design uses short button head screws (likely #6, #8, or M3) and stacks of washers as the correction masses instead of set screws or two-piece sliding masses, the time required to build up a correction mass assembly could prove difficult to implement and use. Since the weights of the washers and screws making up the correction masses are not tightly controlled, it could make the system more difficult to use. Similarity between three unique parts must also be considered, as variance may introduce more imbalance to the system. This design almost certainly proposes interference with the pitching mechanism. To counteract this interference, we could invert the mounting position of the bracket such that the correction masses are closer to the axis of rotation of the hub. But this would require heavier correction weights to make up for the reduced distance from the axis of rotation. If we were to mount the blade brackets in this inverted position, it raises the question of if this balancing mechanism design would even have the needed correction capacity without resorting to 1 to 1.5 in long screws to hold the required number of washers.

5.5 Selected Balancing Mechanism Finalist Design Descriptions

Having discussed the rationale behind our selection of the 4 final balancing mechanism designs we will now present a more detailed look at each of these designs. Each of our designs will be presented with selected views of the preliminary CAD models to ease visualization as well as table of the strengths and weaknesses of the design (qualitatively assessed) for the purpose of further dissecting the design's score from the decision matrix.

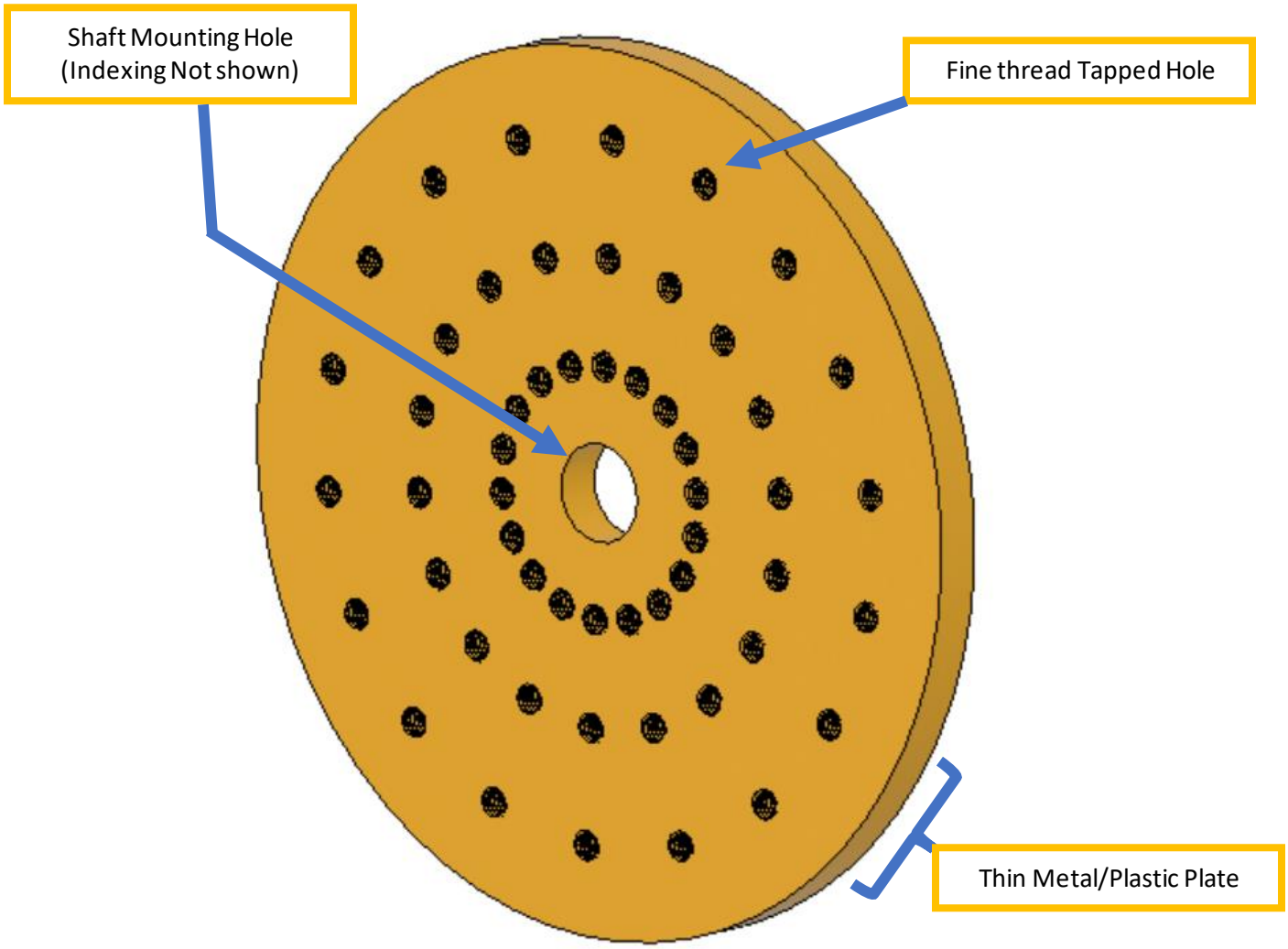

Figure 5.5.1 Threaded plate balancing mechanism detail view of CAD model

Table 5.5.1 Threaded plate design pro/con comparison.

Balancing mechanism design: Threaded Plate	
Design strengths	Design weaknesses/Concerns
• Extremely easy to use – once the position of the correction mass (the set screw) is known, the user just needs to insert it. • As safe to operate as the remaining finalist designs given our preliminary FMEA • Several rows of multiple tapped holes facilitate needed correction capacity while balancing fine-tuning adjustments with repeatability of adjustments • Except for tapping all the holes, very easy to manufacture (cf. the M60 waterjet) • Given our knowledge of the pitching mechanism at CDR at minimum workable to integrate into their design or find space for.	• Threaded plate retains required strength and stiffness after having 54+ holes drilled and tapped in it – especially for holes spaced close together nearest to where the threaded plate mounts to the shaft • Deviation of set screw masses inducing unintended eccentricities • Positional tolerance placed on concentric rows of drilled and tapped holes to prevent the introduction of unintended eccentricities • Diameter envelope for controlling size of plate to allow for sufficient correction capacity while also not interfering with the pitching mechanism • Vibration amplitude/frequency required for set screws to back themselves out from the holes they are threaded into

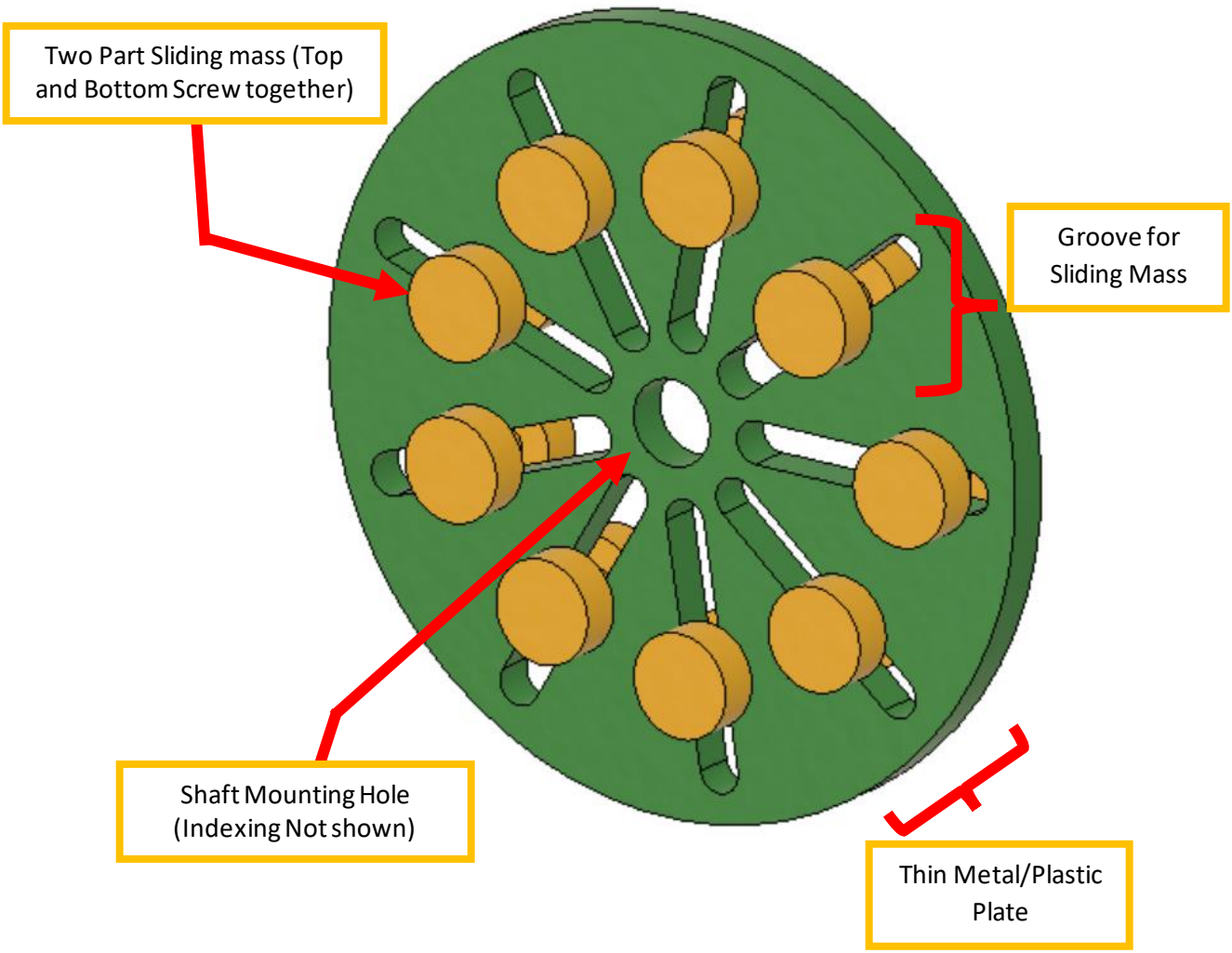

Figure 5.5.2 Grooved plate balancing mechanism detail view of CAD model

Table 5.5.2 Grooved plate design pro/con comparison.

Balancing mechanism design: Grooved Plate	
Design strengths	Design weaknesses
• Maximum range of adjustability facilitated by continuous adjustment of fixed-mass correction mass in grooves. • 9 grooves, 3 per each blade ease splitting of adjustments of fixed-mass correction masses when imbalance lies between blades • Continuous range of adjustment within confines of grooves allows for maximum level of precision adjustments of any of our final concept designs • Given current knowledge of the pitching team's senior project at minimum, this design is workable to integrate. • Majority of failure modes that are dangerous or damaging to the turbine are catastrophic failures of either the grooved plate body or the threads that hold the fixed-mass correction masses together and therefore quite unlikely to occur.	• Human error is introduced due to continuous adjustment, requires measurement of correction masses to ensure they are placed in desired location instead of just placing them in a single, fixed position. • Requires precise fits between correction masses while sliding in grooves, smooth running fit with minimal slop required to prevent introduction of unintended eccentricity • Requires sufficiently similar mass fixed-mass correction masses, which decreases the tolerance window for these parts • Clamping force of fixed-mass correction masses must be sufficient to prevent sliding from desired position during operation • Clamping force of fixed-mass correction masses must be able to be repeatably attained • Diameter envelop for controlling size of plate to allow for sufficient correction capacity while also not interfering with the pitching mechanism

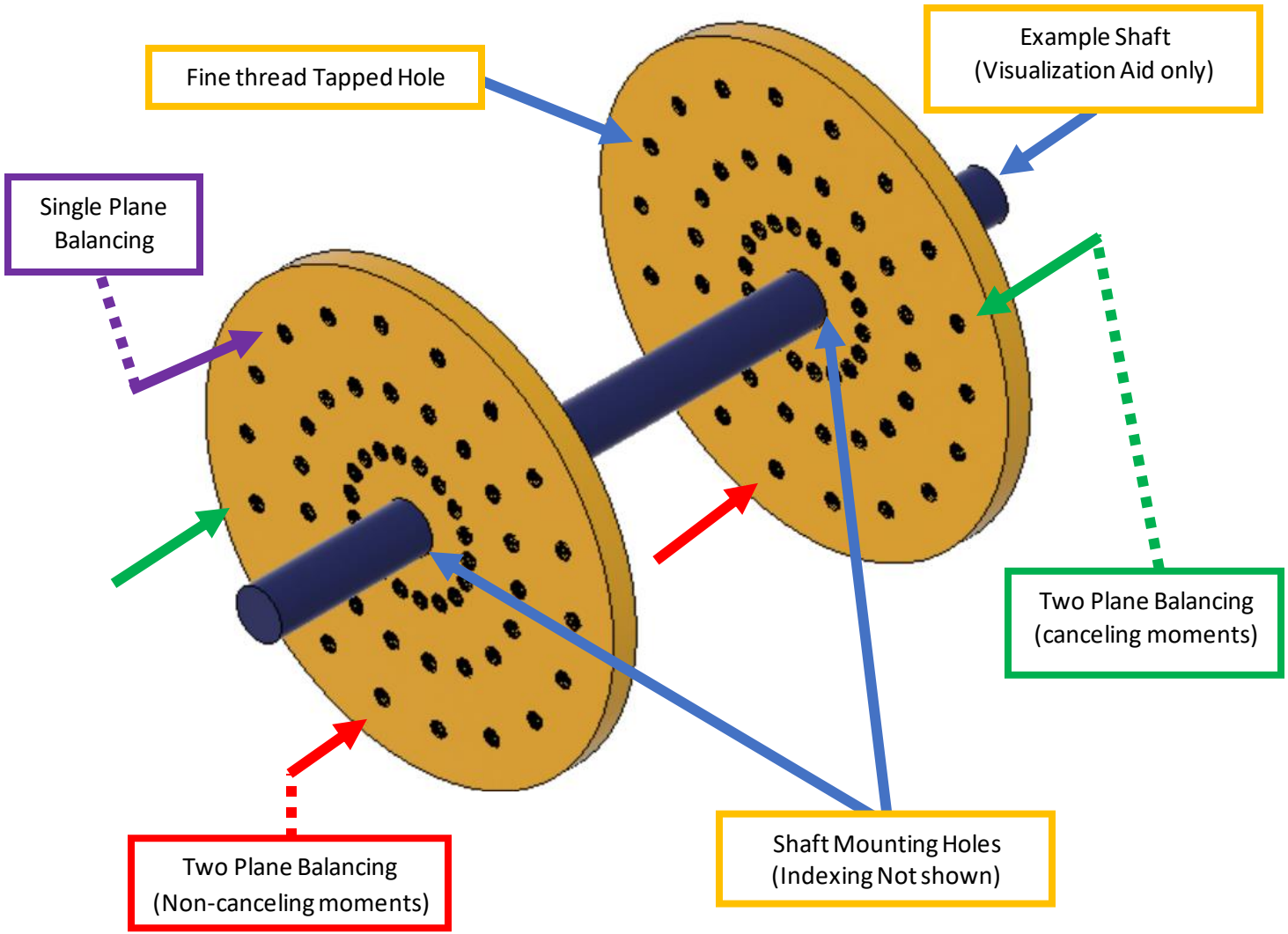

Figure 5.5.3 Balancing discs balancing mechanism detail view of CAD model

Table 5.5.3 Balancing discs design pro/con comparison.

Balancing mechanism design: Balancing Discs	
Design strengths	Design weaknesses
• Essentially two threaded plates, so ease of manufacturing remains high • Comparable precision to threaded plate in having an identical number of tapped holes for set screws to be placed in • Augmented correction capacity given the ability to leverage one or both of the discs to perform dynamic balancing • Very repeatable adjustments that are simple to make (placement of one or multiple set screw(s) into fixed positions).	• Requires access to front and back faces of hub in order to straddle plane of the rotor – high probability of interfering with pitching mechanism • Single and two plane balancing modes make adjustment more complicated for an inexperienced user • Increased complexity of balancing adjustment increases chances of an adjustment being incorrect and possibly damaging to the turbine • More material required for manufacturing than just the threaded plate – likely increasing cost • More parts to manufacture than the threaded plate • Vibration amplitude/frequency required for set screws to back themselves out from the holes they are threaded into is unknown.

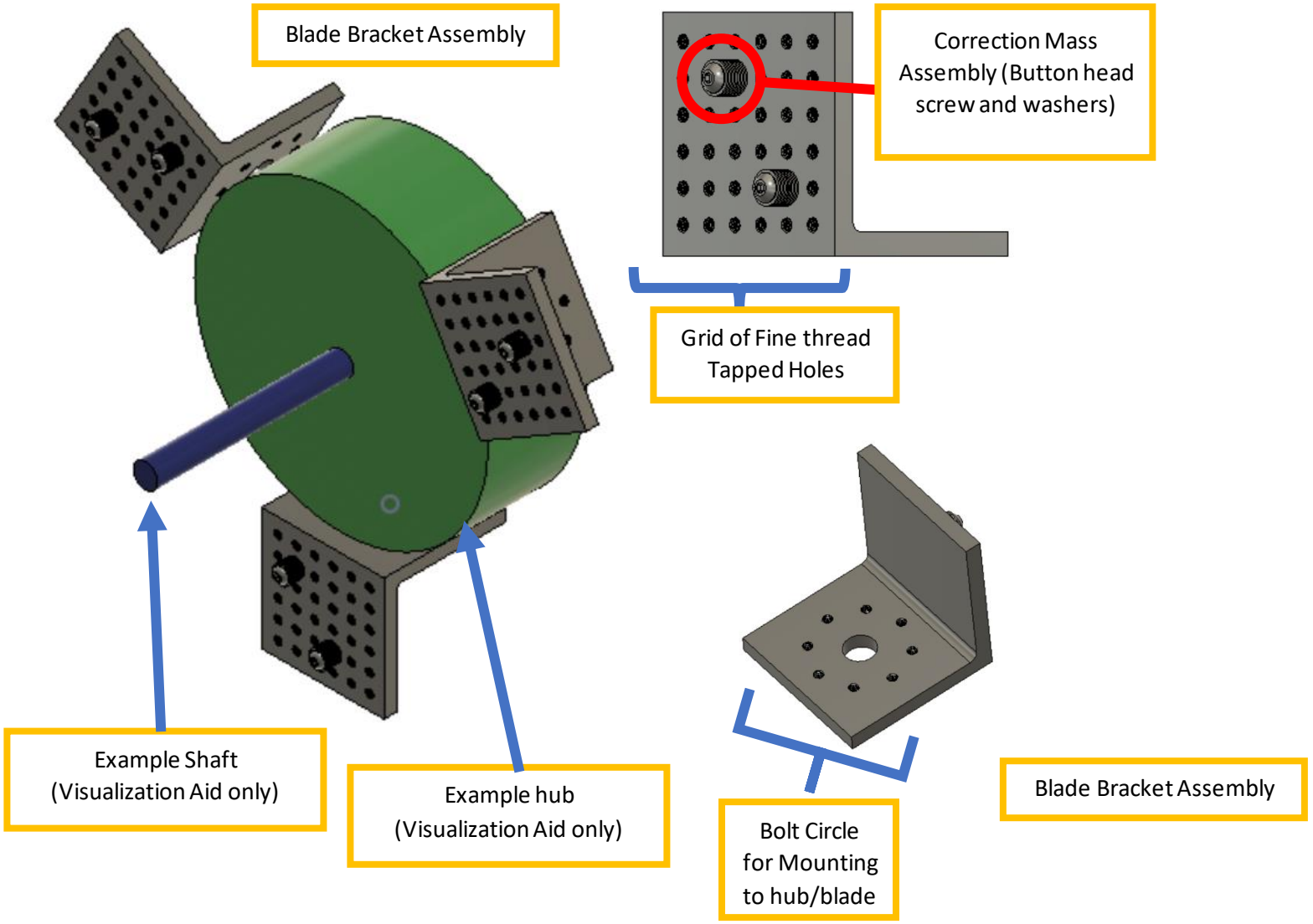

Figure 5.5.4 Blade bracket balancing mechanism detail view of CAD model

Table 5.5.4 Blade bracket design pro/con comparison.

Balancing mechanism design: Blade Bracket	
Design strengths	Design weaknesses
• Fixed position of holes in a grid on the front face of blade bracket eliminate the potential for human error in measurement to position the screw-washer correction masses when compared with the grooved plate • Constructed entirely of readily available and inexpensive commercial off-the-shelf (COTS) products – aluminum angle, small screws and washers. • Manufacturing costs minimized • Manufacturing schedule is maximally flexible for this mechanism as it can be made through multiple workflows to mitigate limited shared access to the shops	• Lots of small parts to keep track of – not as user friendly as desired • Mounting in its current configuration of the blade bracket could make it impossible to integrate into or even attach to the pitching mechanism • Correction mass assemblies must be carefully constructed to ensure they are of sufficiently similar mass to prevent the introduction unintended eccentricities • Positional tolerances on grid of tapped holes may prove to be unachievable on a manual mill and require the use of a CNC mill • Altering of mounting of blade brackets may significantly reduce the radius from the axis of rotation of the shaft the correction masses act at lowering the correction capacity of this design beneath what is needed to balance the wind turbine rotating assembly • Vibrational amplitude/frequency required to cause screw and washer assemblies to unthread themselves from the shallow, blind tapped holes unknown. • Rotation of the bracket about the axis of the blade will likely interfere with the pitching mechanism reducing the out-of-rotor-plane portion of this design's mass imbalance correction capacity.

5.6 Final Balancing Mechanism Design Selection

Since most of our selected final designs ranked similarly with variable weaknesses and strengths, the final design was finalized based off integration feasibility with the wind turbine's pitching mechanism. We have provided a summary of the detailed discussion in section 6.0 to clarify the following section on the development of our test mass positioning tool since the grooved plate requires such a tool to be effective.

From our meetings with the pitching senior project team (see section 2.2), our senior project team determined that a separate rather than integrated balancing mechanism mounted on the front of the rotor housing would be the optimal overall wind turbine design. This locational requirement eliminated the balancing discs and blade bracket designs, as their mounting requirements interfered with the pitching mechanism's structural integrity and actuation. A diagram of the finalized pitching mechanism design can be found in Figure 5.6.1 below.

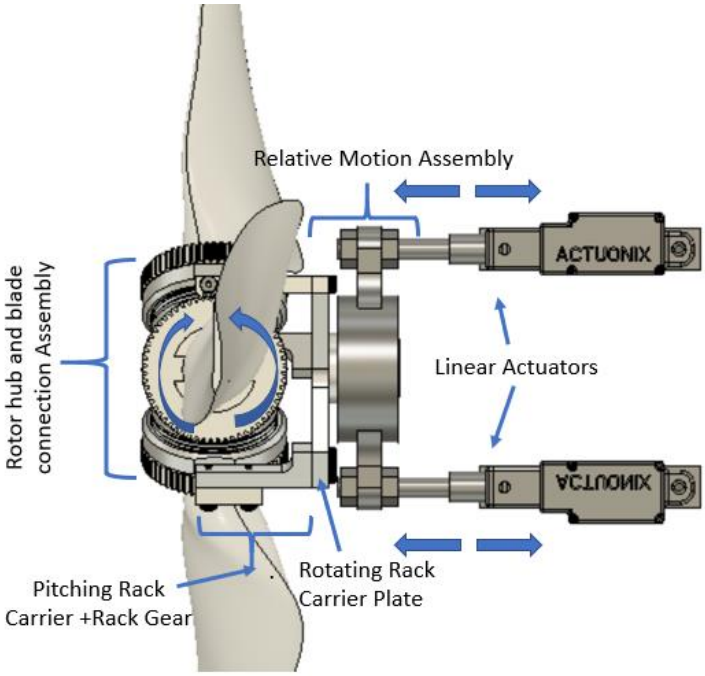

Figure 5.6.1 Pitching mechanism actuation assembly diagram.

To pitch the blades through the entire amount of their rotation, the pitching rack gear carriers and plate are advanced along the shaft (not shown) by the linear actuators via the relative motion assembly. The motion shown by the arrows in Figure 5.6.1 demonstrates the mechanical relationship between the motion of the actuators and the pitching of the blades. This diagram also illustrates the limited amount of space for mounting our senior project's balancing mechanism. Our senior project team and the pitching senior project team considered integrating tapped holes for balancing masses into the rotor housing and rotating rack carrier plate. However, the movement of the plate and the thin walls of the rotor hub did not allow for the mounting of the test multiple masses in their required locations.

After eliminating these design options, we were left with the grooved and threaded plate balancing mechanisms. Since we did not know the amount of mass imbalance our balancing mechanism would need to correct, we selected the grooved plate design as it is had a wider range of mass imbalance capacity than the threaded plate. Because of this, we selected the grooved plate as our final design.

5.7 Grooved Plate Final Concept Design

Here we have briefly outlined our selected concept design – the grooved plate. We will detail our refined grooved plate concept design, which was modified to optimize mass imbalance elimination and positioning on the wind turbine hub.

As we refined our grooved design from the simplified CAD model presented in section 5.5 we selected simplified test mass designs. We decided to contract the test masses our of basic carriage bolts and hex nuts. By utilizing square slots with tight tolerances, we were able to fit carriage bolts snugly into each slot, preventing unprovoked movements. By tightening the bolt and nut onto the grooved plate body after positioning the test mass where we desired, we could prevent the test mass from moving during testing and match the functionality of our proposed concept design in section 5.5. The thickness of the plate was driven by the size of the bolt head and the bolt's square drive. Additionally, the number of slots was reduced from 9 to 6 in order to fit onto the small disc, while still offering mass correction at all angles. Our finalized concept design CAD is provided below in Figure 5.7.1.

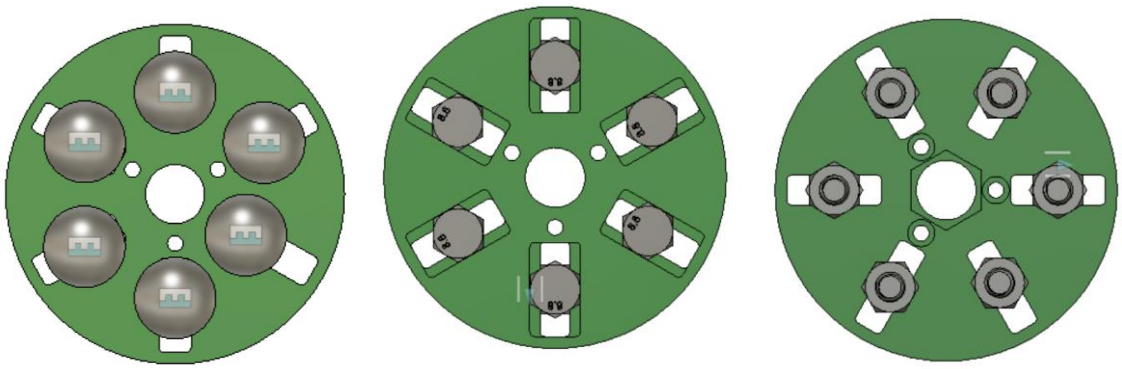

Figure 5.7.1 Grooved Plate hex bolt and carriage bolt final concept design

From left to right, the carriage bolt variant of the grooved plate, hex bolt variant, and front of the grooved plate where hex jam nuts were tightened onto split lock washers to simultaneously prevent overtightening and sliding of test masses during rotor rotation. We realized that the large heads of the carriage bolts would interfere with the mounting bolts by obscuring the mounting holes when moved to the end of their travel. Because of this, we transitioned to standard hex head bolts to avoid this issue.

In this configuration the user would measure from the flat on the hexagonal datum feature to outer diameter of the test mass bolt to set the position of the test mass. This feature is located in the rightmost photo in Figure 5.7.1. The appropriate offsets between this measured distance and the desired center-to-center distance would need to be factored in ahead of time to ensure the desired

distance was precisely met. We decided to use modified calipers in order to set this distance. Calipers were the initial design mock-up we presented to the pitching senior project. However, the pitching mechanism senior project team suggested that we create a gauge to help us set the distance between the test masses and the center of the turbine shaft. grooved plate bore. Our positioner design, which was delayed until the finalizing of our grooved plate design, is discussed in the following section.

5.8 Concept Design of Test Mass Positioner

After we selected the grooved plate as our final design, we began work on a precise measurement mechanism which we could use to position each mass. We needed this tool to pick up locating features related to or on the test masses and center bore of the grooved plate to allow the user's desired displacement to be set by the user. Our senior project team considered using the test masses' outer diameters, center drilling holes on the ends of the test mass bolts, and using the center drilled hole on the end of the turbine shaft. In the figures that follow, we have provided our brainstormed concept designs which are also available in Appendix F.

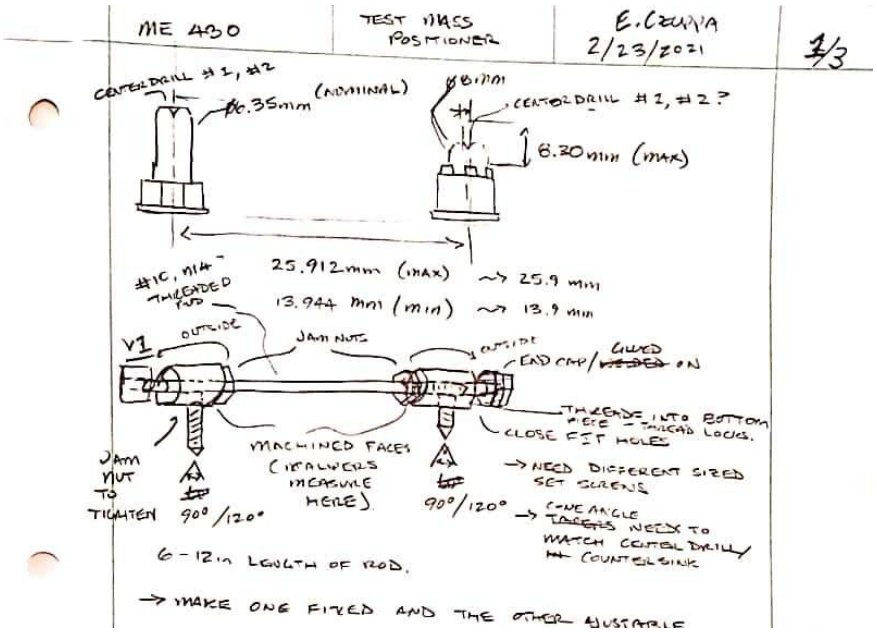

Figure 5.8.1 Version 1 of the bar compass-like test mass positioner.

The first iteration of our positioner design used cone-point setscrews threaded into cylindrical bar stock sections that had been drilled to slide along a fully-threaded bolt. One end would remain fixed between a jam nut and the bolt head while the other would be adjusted by two jam nuts. The distance between the two set screws is the center-to-center distance, but the measured distance would have to be adjusted by the offsets from the set screws to the edges of the bar stock. This design did not allow for the adjustment of the set screw heights to handle the difference in height between the ends of the test masses and the end of the shaft protruding from the grooved plate body.

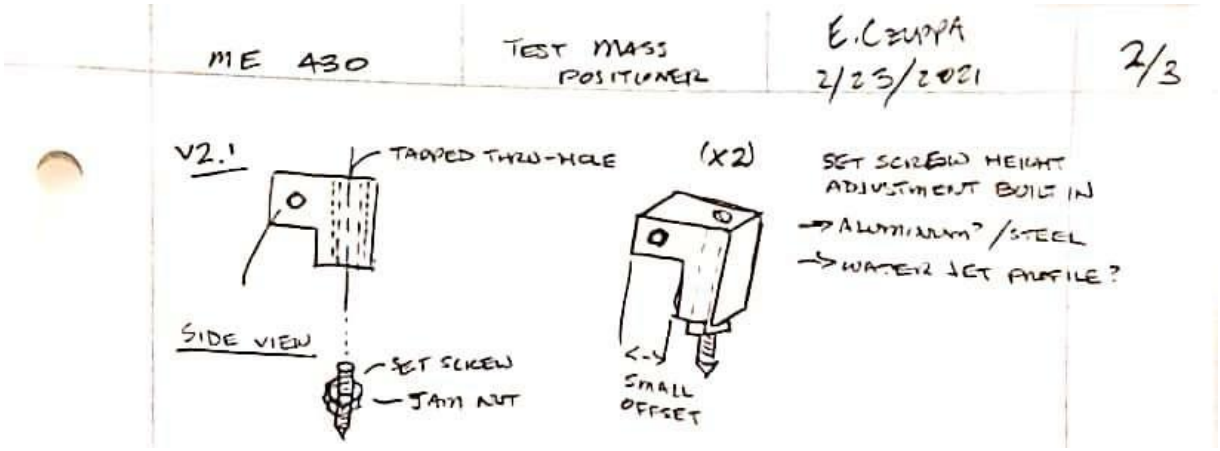

Figure 5.8.2 Verion 2 of the positioner "anvil" for the version 1 positioner design.

The second positioner "anvil" design – the component that carried the set screw – allowed for height adjustment to help ensure that the positioner was measuring the horizontal distance between the test mass and the bore and not being skewed by cosine error. The measurement distance as set by calipers would not match the distance between the set screw points, so a known, measured offset would also be needed with this design. With this design the outside or inside legs of the calipers could be used to indirectly set the test mass distance.

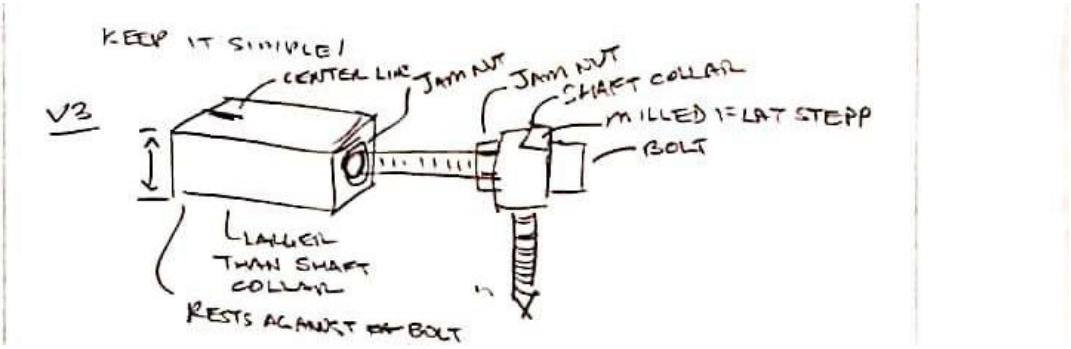

Figure 5.8.3 Version 3 of the test mass positioner

Our third iteration attempted to use more commercially available hardware instead of custom machined components to save manufacturing time. Here a shaft collar would hold the cone point set screw such that it would locate off the center drilled hole on the turbine shaft. A machined block with a threaded blind hole and center mark on each face would be rotated about the fully-threaded bolt to adjust the distance between the test mass' outer diameter and the center of the shaft to match the distance set by the outside legs of the dial/digital calipers.

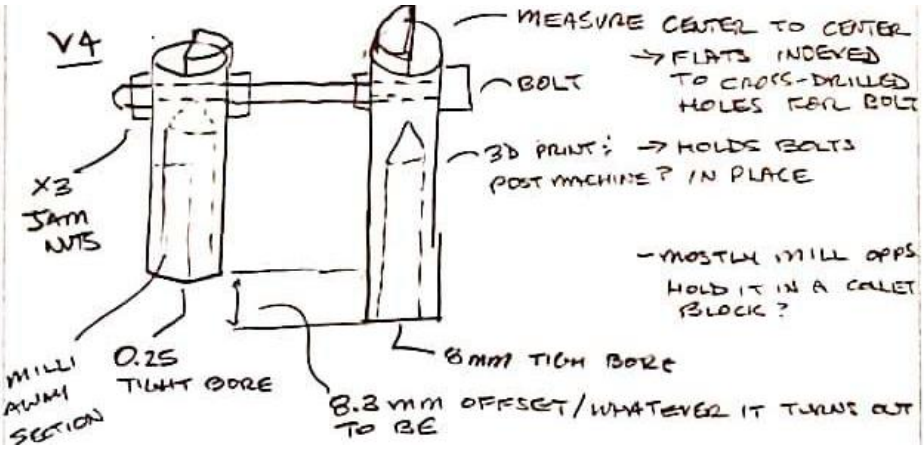

Figure 5.8.4 Version 4 of the test mass positioner.

In contrast to the previous three iterations, this version would use the test mass and turbine shaft's outer diameters to set the center-to-center distance. The milled or printed locating features were designed to accept the outside caliper legs, which would be measured to determine what adjustments would need to be made to the specified distance to account for manufacturing errors. However, the fits between the bores and the shaft and bolt outer diameters would directly affect the positioner's accuracy. If the fits were too tight, using this positioner while the balancing mechanism was mounted on the turbine would be even more difficult. Another problem that came to light with this design was the annoyance of using jam nuts to lock the moving "anvil" in place as this would require both the user's hands and multiple wrenches, not to mention the rotation of the moving "anvil" out of planar alignment with the fixed one. In the finalized design iteration, the cotter pin would cover up the turbine shaft outer diameter protruding from the castle nut, so we updated the fourth revision of our positioner design to account for this change.

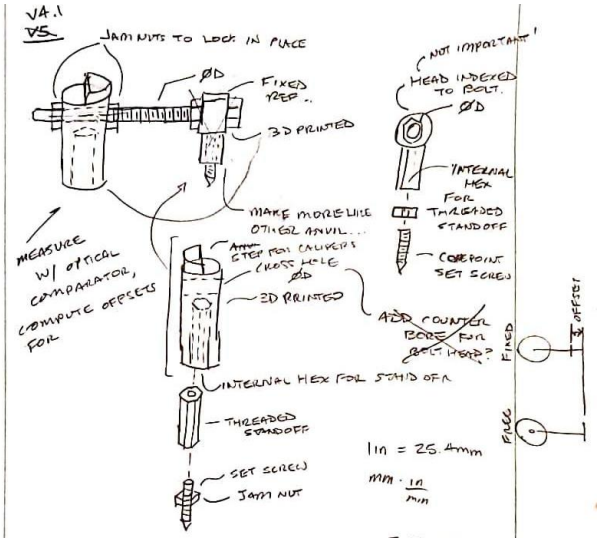

Figure 5.8.5 Minor design adjustment to 4th version of the positioner.

Instead of two cylindrical anvils with precise bores, a single fixed anvil would be able to locate the center drilled hole in the shaft, providing the necessary datum. The adjustable anvil would

locate the centerline of the test mass from its outer diameter. Our senior project team addressed the height offset issue between the test mass' bolt end and the center drilled face of the turbine shaft in this iteration. The problematic jam nuts were also retained in this design iteration. Overall, we had become stuck in a rut with our positioner concept designs.

We realized that our positioner design was not user-friendly, and relied on too many measured offsets for accurate test mass positioning from these four iterations. As a result, we changed our design approach from designing a custom tool to looking for a pre-existing one we could adapt to work with our system. As an accessory to the grooved plate, we needed the most straightforward design to conserve our limited manufacturing time from our prolonged design process. This led to our final positioner design which is shown in Figure 5.8.6 below.

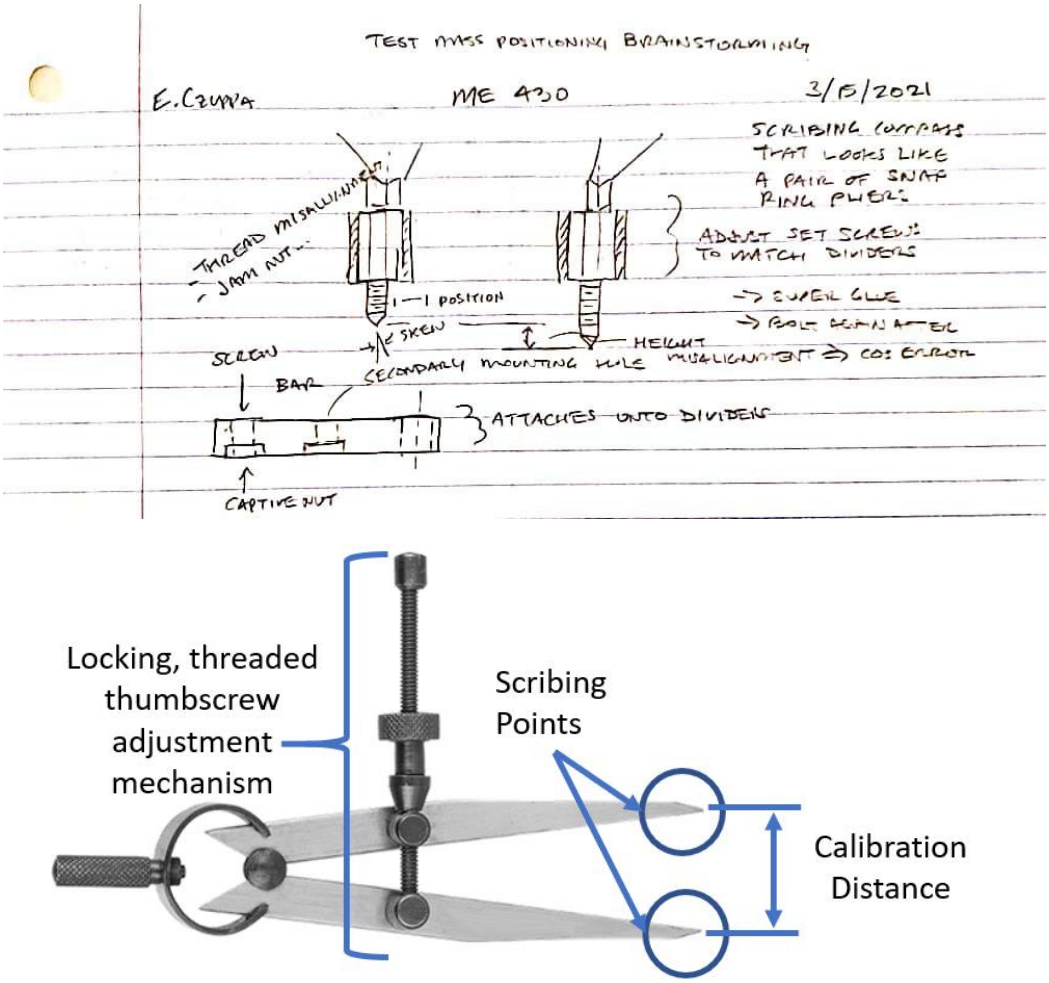

Figure 5.8.6 Test Mass positioner preliminary design and annotated scribing compass.

We selected a small scribing compass as the base for our measurement tool. The compass' scribing points are setup so that they touch each other when the compass is fully closed, which allows us to reliably trust the thumbscrew-driven threaded adjustment mechanism on the scribing compass. By attaching two 3D printed “arms” that carry cone-point setscrews to the scribing compass' underside at a single pivot point, we created a positioner that addressed all our previous design

issues and could be calibrated with ease. Once calibrated, the distance set with the inside caliper legs on the compass's scribing points would correspond almost exactly with the point-to-point distance between the set screws – no special measured offsets needed. Our 5th and final iteration took inspiration from our updated fourth iteration positioner design to address the height offset problem. We opted to use set screws to locate both the test mass' and turbine shaft's centerlines as we could control and account for these center-drilled holes' positioning more closely than we could with the outer diameter of the test mass bolts.

5.9 Balancing System Concept Design

In addition to a balancing mechanism and its accessories, our senior project's objectives also included a balancing procedure and balancing system. Here we have outlined our concept design for the balancing system and present our proposed preliminary design in section 6.0.

Due to the vibrations analysis' complexity, our senior project desired to minimize the differences between the competition turbine and the balancing testbed. For testing, we wanted to use the same rotor assembly, shaft, bearings, base plate, and coupler to be used on both the balancing testbed and the competition turbine. In doing so, we could help ensure that the balancing results we achieved on the testbed would transfer over to the competition turbine without unexpected changes in the operational behavior of the turbine. Since we could not use the current WPC generator for fear of damage during balancing, we would have to control for the runout present in the output shaft of the drive motor. Most of all our balancing system was intended to balance the turbine as a fan since we had already established that mass imbalance could be treated similarly between the two configurations

We combined the balancing machine product research we had previously conducted and our familiarity with the rotor balancing lab apparatus utilized in the ME 318 laboratory at Cal Poly for our balancing system design. Additionally, we also had the wants and needs of the WPC to consider, especially the use of pre-existing vibrations measurement equipment in the mechanical vibrations lab instead of purchasing our own equipment. Thus, our concept design utilized a direct drive motor, instrumentation near the bearings, guards to surround the rotating assembly, a speed controller interface, and a data acquisition system. We captured this concept for a balancing system at the outset of our ideation and brainstorming process and have provided it on the next page in figure 5.9.1.

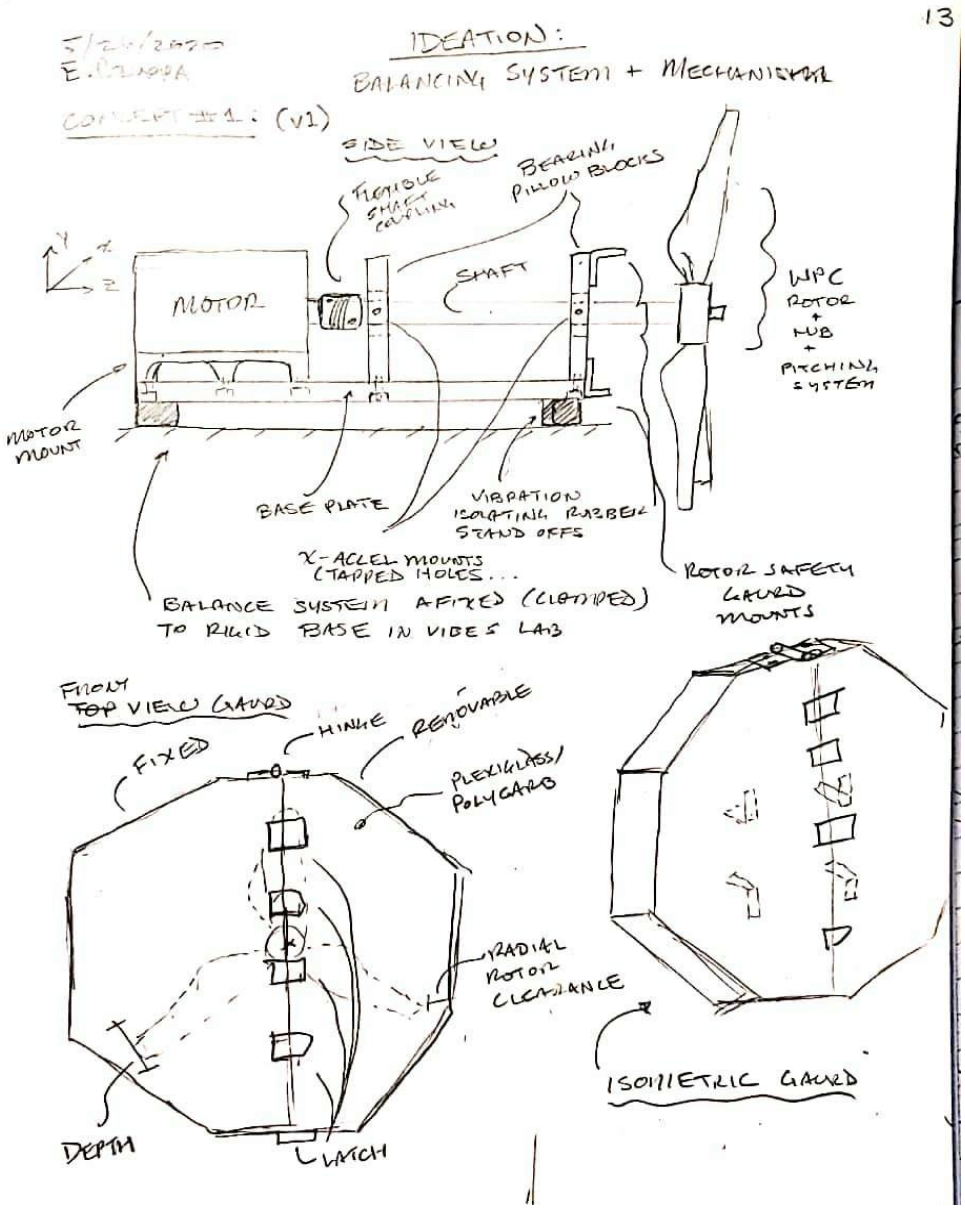

Figure 5.9.1 Balancing System Concept Design.

A motor mounted to the nacelle base plate in place of the generator drives the competition shaft through a vibration damping and misalignment correcting shaft coupling. The competition shaft is supported by identical bearings and bearing housings used in the nacelle assembly of the competition turbine. The bearing housings are instrumented with the appropriate vibration sensors, e.g., accelerometers or proximity probes just outboard of the housings, to capture the vibration of the turbine shaft. During the operation of our proposed balancing system, the partially 3D printed rotor assembly spins inside of an enclosure that splits in two and mounts to the balancing testbed frame. We did not include the tower assembly in our balancing system design as we determined that the uncontrolled yaw degree of freedom of the assembly could prove dangerous if the present mass imbalance was sufficient to cause the turbine to yaw noticeably. Additionally, the tower of the wind turbine is one of its few features that is not within our designated project scope. The

ungoverned yaw added oscillation could cause critical wiring connections to come loose resulting in loss of control system function and a potentially out of control turbine.

Besides the mechanical portion of the balancing system, we also had to consider the electrical and software portions. Due to Ethan's mechatronics background and familiarity with micropython and the Nucleo L476RG microcontroller, these were selected to form the basis of the control system. The electrical subsystem design of the balancing system was also initially driven by Ethan's mechatronics experience from his concentration coursework.

To mimic the behavior of the vibrations rotor balancing apparatus as well as other balancing machines researched in our concept design, a closed-loop velocity control scheme would be applied to the drive motor. The calculated shaft speed, measured by a quadrature encoder mounted to the motor output shaft, would be fed into a proportional integral (PI) loop that would output the appropriate drive motor duty cycle. After consulting with Dr. Wu regarding our concept balancing mechanism we realized we would also need to limit the rate at which the shaft speed increased. Dr. Wu recommended we use a ramp rate of 5 RPM/sec.

With regards to safety features, our senior project team decided that an emergency stop or similar circuit breaker, a current limiting fuse for the motor, and the ability to command the system remotely via a personal computer connected to the microcontroller (MCU) were all necessary features for maximizing the safety of the operator during testing. Our simplified electrical subsystem diagram for our concept balancing mechanism is provided below in Figure 5.9.2.

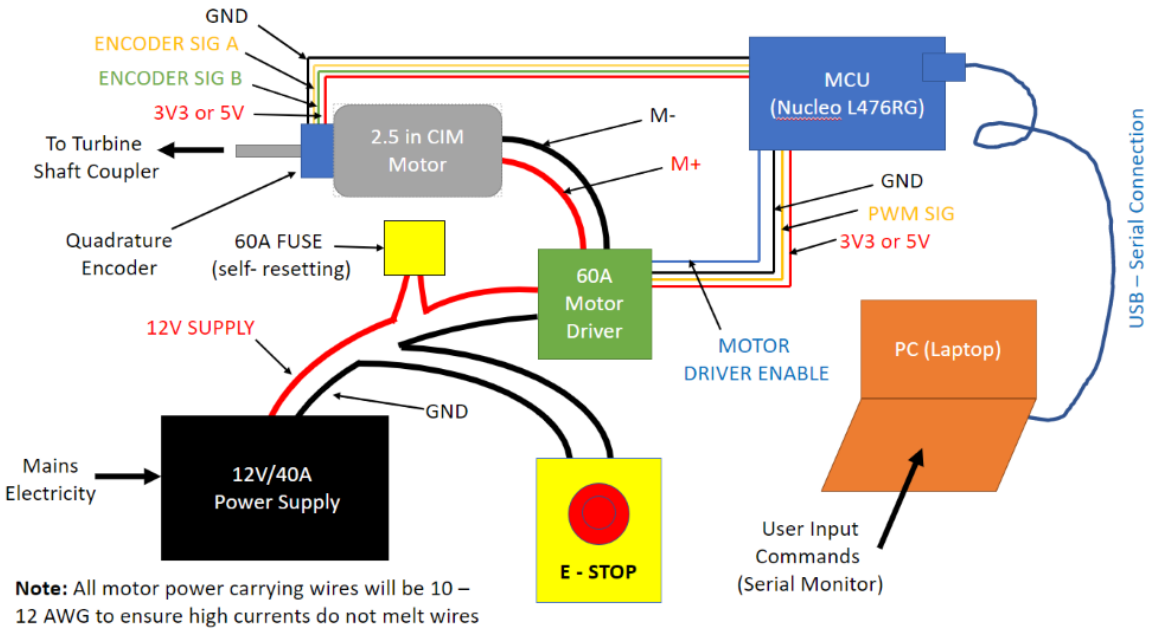

Figure 5.9.2 Simplified wiring diagram for concept balancing system.

The 2.5 CIM motor was initially selected by Ethan as a possible drive motor due to his experience with it from high school FIRST robotics. This motor could be purchased with a corresponding encoder and motor driver from AndyMark.com, a FIRST robotics supplier. The self-resetting fuse

was intended to protect the motor from overheating but was accidentally placed on the wrong side of the motor driver module. The intended input to the motor driver was a pulse-width modulated (PWM) signal from the Nucleo microcontroller (MCU). If the user needed to shut down the system manually, for any reason, the emergency stop switch would cut power to the motor driver preventing the motor from continuing to spin accelerate in a potentially dangerous state. The laptop serial connection to the MCU was also intended to allow the user to control the stages of balancing data acquisition, including stopping the test by disabling the motor driver – a sort of software emergency stop. Since the software is the most likely to fail, a physical switch, as mentioned earlier, rated for the supply current power was also included as part of our concept design.

Continuing our senior project's practice of meeting with experts in residence to review our designs and confirm our understanding of the problem, Ethan Czuppa met with Dr. John Ridgely – a Cal Poly Mechanical Engineering professor who specializes in mechatronics – to go over the concept design. Dr. Ridgely was concerned by the high current requirements of the circuit and recommended that a motor that could run on higher voltage and lower current (direct current, DC) would be preferable for the safety of our senior project team and the club members that would use the system after us.

At this point, our senior project team had approximated the required motor torque with an energy method approach (See appendix M). Since we did not know the final mass properties of the turbine shaft and rotor or the difference in torque from drag when operating the turbine as a propeller during balancing, this was the best we could do at the time.

Reference block diagram

- Requirements
    - Mostly vibes lab equipment
    - Safety
        - Enclosed rotor with penetration proof material/thickness
        - Electrical Safety (overcurrent protection, Emergency stop,
        - Motor torque and speed
        - Control motor RPM and ramp (rate of increase of RPM) for vibration measurement
        - No yawing of assembly- tower assembly and slew bearing removed
    - Measurement – instrumentation (accelerometers/proximity probes + laser tachometer/keyphaser© probe
        - Get unbalance data
    - Adaptable for future testing years
    - Identical to nacelle assembly (save aerodynamic cover) for similarity of results to actual turbine
    - Direct drive electric motor to reduce complexity of analysis and added sources of vibration and imabalnce from gearbox
- Initial sketches
- Initial components tried (12V motor, motor driver,

- Down selection -

- Section 6.0 somewhere
    - Proposed balancing system design
    - Cartoon CAD
    - Wiring diagram
    - Control system state machine diagram
    - Rough iBOM

6.0 Final Design

From our four finalist designs – the blade bracket, balancing discs, threaded plate, and grooved plate, we selected the grooved plate for the final balancing mechanism design. There were several factors that contributed to this decision. However, the most significant proved to be the range of adjustability of the test masses and the mass of the test masses that could be accommodated by the grooved plate. Here we will discuss the supporting calculations, final design decisions, evaluation of our specifications, and briefly outline the safety and maintenance considerations for the grooved plate.

Our test mass positioner is also discussed, however, because this was such a last-minute addition, the current documentation constitutes a rough prototype that was put into CAD from a conversation. The vibrations test bed design is not discussed here because it is both incomplete, and outside the scope of this project (as it is nearly a second senior project's worth of work to complete).

6.1 Selected Design – Balancing Mechanism & Test Mass Positioner

The grooved plate balancing mechanism consists of a 12mm thick, 68 mm diameter disc with 6 ¼" slots spaced evenly about the diameter. On the rear face, which mates to the matching boss on the rotor housing, 6 rectangular cut-outs centered on each slot capture the square heads of the ¼" x 20 bolts that serve as the test mass assembly with the ¼"x20 flanged Nylock lock nuts. On the front face of the plate 3x M3 clearance holes counterbored to allow the heads of the mounting socket head cap screws to sit flush with plate are indexed to the two three slots each spaced 120 degrees from each other. At the center of the plate is an 8mm bore intended to be the datum feature for the plate as well as what provides the accurate location of the plate on the turbine shaft. The M3 mounting bolts are intended to provide the indexing to the blades, hence the clearance holes. To supplement this written description, we have provided annotated assembled and exploded views of the grooved plate immediately below.

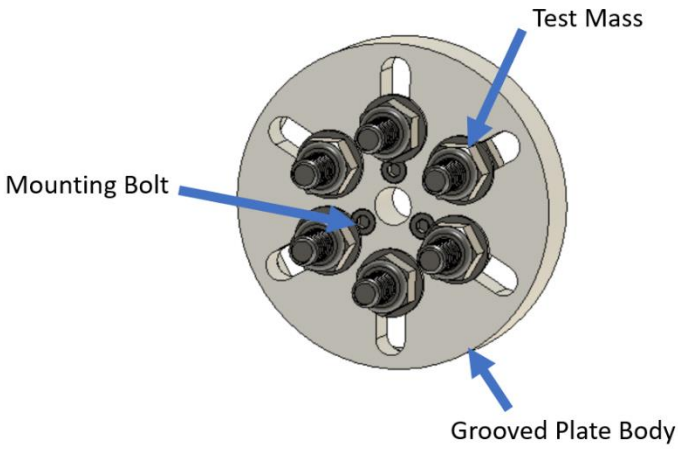

Figure 6.1.1. Annotated assembled grooved plate balancing mechanism.

They are not shown here, but all test masses will have center drilled and 90 degree countersunk spot holes to accommodate for test mass positioning.

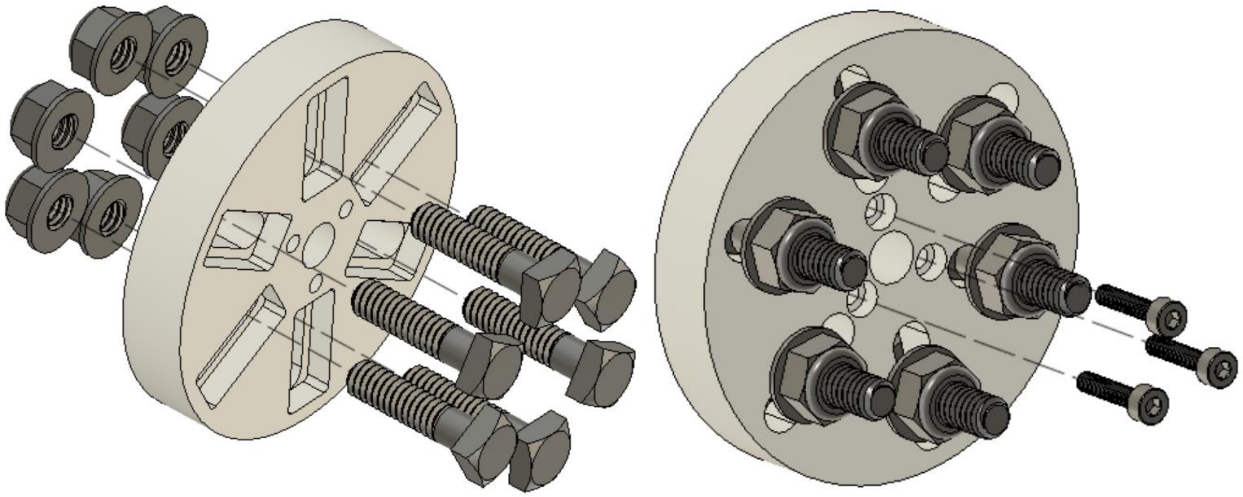

Figure 6.1.2. Exploded views of grooved plate balancing mechanism.

The six test mass sub assemblies are assembled onto the grooved plate body and then the M3 mounting bolts are screwed into the rotor housing boss (not shown). Since the castle nut (not shown) that installs on the end of the competition shaft (not shown), covers the heads of all three M3 mounting bolts and prevents them from coming lose. Additionally, after printing, the slots are numbered 1-6 in correspondence with the MATLAB script that performs the balancing calculation based on the measured vibrational data. After measuring an imbalance (see "8.0 Testing" and the Testing Procedure in appendix), the adjustments are outputted and made with the test mass positioner.

The test mass positioner consists of a scribing compass modified to accommodate two cone point set screws situated on swinging arms. The arms are adjusted so that the center-to-center distance between the set screws cone points matches the distance between the edges of the scribing compass. In this way, the pre-existing, semi-trustworthy locating features on the scribing compass can be used to calibrate the position of the swing arms. On the following page we have provided isometric exploded and assembled views of the test mass positioner, to clarify the preceding written description.

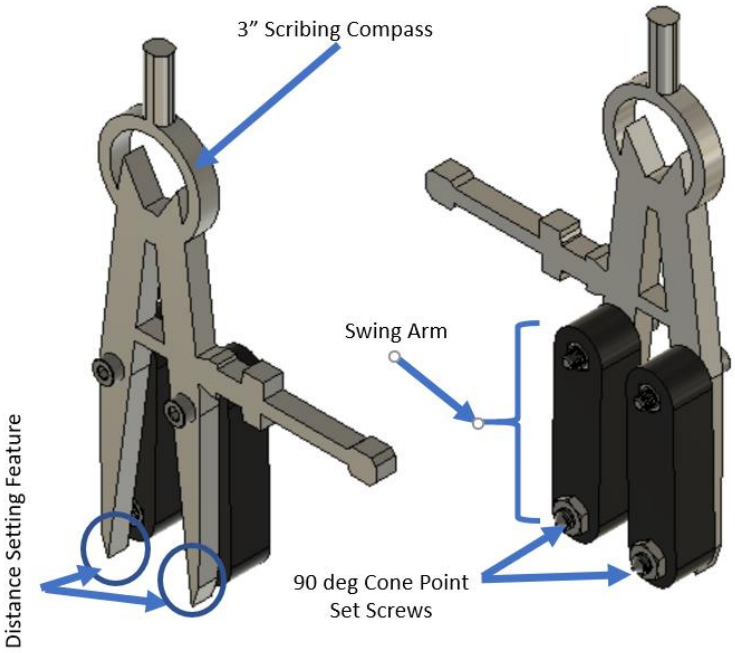

Figure 6.1.3. Annotated assembled view of test mass positioner.

By placing a pair of calipers (dial or digital) inside measurement legs in contact with the surfaces of the inside edges, the desired distance can be measured and set using the scribing compass as one normally would. The distance between the set screws in whatever default position is then measured on an optical comparator to adjust the swing arms until the measurements match, within the resolution of the comparator. Once the calibration is complete, the M3 mounting bolts are fully tightened to secure the arms in their calibrated position. Now, whenever the distance between the scribing compass' legs is set with the inside legs of dial/digital calipers, the center-to-center distance of the set screws will be in good correspondence with the measurement on the calipers. The locking mechanism on the scribing compass is then used to hold the set distance while positioning the test masses. This process involves loosening a test mass with a 7/16 in. combination wrench, setting the distance of the positioner with inside calipers, and then sliding the selected test mass in its slot with one of the set screw arms until the other arm's set screw rests in the matching center-drilled and countersunk hole on the competition shaft.

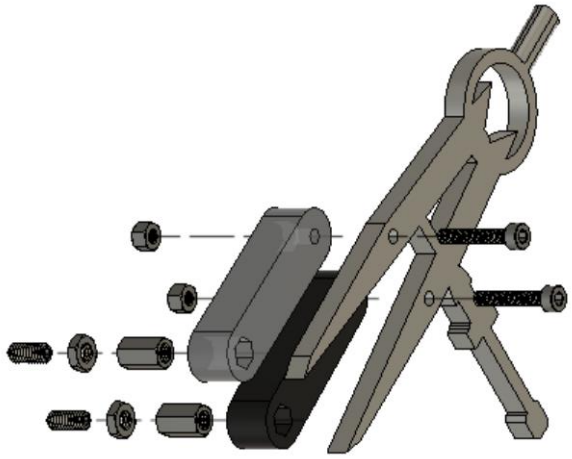

Figure 6.1.4. Exploded view of test mass positioner.

The swing arm bodies will also be 3D printed in PETG as they are under no appreciable loads and would require multiple traditionally machining operations to complete. To secure the swing arms in place after calibration, the M3 mounting bolts are tightened into captive nylon insert lock nuts. The set screw heights are also adjustable as each set screw threads into a tapped standoff. A thin hex jam nut tightens against the standoff and locks the set screw in place. This adjustment in height is important as it accounts for the difference in height between the locating hole on each test mass and the locating hole on the competition shaft.

Here are the intended bills of materials for the grooved plate balancing mechanism and test mass positioner in table format.

Table 6.1.1a. Grooved plate balancing mechanism iBOM.

Assembly Level	Part Number	Level					Cost in Sold Quantities			
							Qty.	Cost	Total Cost	Package of
		lvl 0	lvl 1	lvl 2	lvl 3	lvl 4	(#)	($)	($)	(#)
0	1000	Final Asm								
1	1100		Balancing Mechanism				1			
2	1110			Grooved Plate Body			1	22.99	22.99	1.75mm 1kg roll of PETG
2	1120			Test Mass Sub Asm			6			
3	1121				1/4"x20x1" Squarehead bolt		1	5.11	5.11	25
3	1122				1/4"X20 Flanged Nylock nut		1	7.48	7.48	100
2	1130			Mounting Sub Asm			3			
3	1131				M3 x 15mm x 0.5mm Socket Head Cap Screws		1	10.00	10.00	50
							16	45.58	45.58	175

Table 6.1.1b. Test mass positioner iBOM.

Assembly Level	Part Number	Level					Cost in Sold Quantities			
							Qty.	Cost	Total Cost	Package of
		lvl 0	lvl 1	lvl 2	lvl 3	lvl 4	(#)	($)	($)	(#)
0	2000	Final Asm								
1	2100		3" Scribing Compass				1	18.32	18.32	1
1	2200		Positioner Asm				2			
2	2210			Set Screw Arm			1	22.99	22.99	1.75 mm 1kg roll of PETG
2	2220			Set Screw Sub Asm			1			
3	2221				M4x0.7x10 90 deg cone point set screw		1	8.19	8.19	50
3	2222				M4X0.7x10 standoff		1	3.15	12.6	4
3	2223				M4X0.7 hex jam nut		1	2.26	2.26	100
2	2230			Mounting Sub Asm			1			
3	2231				M3x0.5X18 SHCS		1	11.45	11.45	50
3	2232				M3X0.5 Nylock hex nut		1	3.57	3.57	100
							13	69.93	79.38	-

6.2 Grooved Plate Design Justifications

We selected ¼”x20x1” square head bolts and ¼”x20 Nylock© lock nuts to comprise the test mass assemblies as metric square-headed bolts are not readily available. Previously, we had desired to use carriage bolts. Though the square drive below the domed head of the bolt would allow for adjustment with only one wrench, the large heads interfered with each other, further limiting their adjustment range, as well as required a larger offset from the rotor housing boss. Square head bolts eliminate this issue as the head sits flush with the rear surface of the plate (in the context of assembly) and is prevented from rotating by the corresponding rectangular slot it sits in. To aid in adjustment of the balancing mechanism, the rectangular slots were sized to be a tight sliding fit with the bolt heads which prevents the test mass from shifting drastically from its initial position when the flanged lock nut is loosened. Due to the need to reposition the test masses during turbine balancing, locking mechanisms that marred the surface of the 3D print or distorted the thread of the test mass were out of the question. Instead, a lock nut with a large surface area that could be used multiple times was needed. The only locking nut that satisfied all these requirements was a flanged lock nut with a nylon insert. The flange provides necessary surface area to prevent yielding of the material when tightening and helps to hold the test mass securely in position despite the centripetal accelerations acting on it during operation.

Per the recommendation of graduate student Michael Mullen, we designed our balancing mechanism so that each correcting mass’ dynamic force (from centripetal acceleration) is ~40% of the static weight of the rotating assembly. While this rule of thumb is typically set to be 10%, Mullen pointed out that our small diameter and limited adjustment range warranted more massive correction masses to ensure that our grooved plate would have the capacity to sufficiently correct the imbalance in the wind turbine. The calculation confirming that our final design assembly meets this criterion can be found in Appendix N. Altogether, our test mass assemblies have a nominal mass of 13.1g. This is triple the required mass from our calculation in Appendix M, however, smaller square head bolts are not commercially available. We plan to mitigate the hazards from larger than necessary test masses by reducing the mass of the bolts as needed (reducing the length, drilling a hole through the center of the bolt from end to end, etc,) as well as splitting the test mass adjustments between opposing slots.

The Diameter was set to 68 mm as this was the largest diameter the rotor housing could accommodate without the grooved plate interfering with the pitching mechanism or the aerodynamics of the blades. Additionally, this diameter proved to be the limit for fitting the six test mass slots, indexing holes, and locating bore on the grooved plate while maintaining at least 1mm wall thicknesses between the mounting holes, bore, and corners of the rectangular slots. Since the amount of mass unbalance present in the rotor is still unknown, we decided to maximize our range of adjustment for each test mass. Given the diameter size constraint, 11 mm of travel (center to center of initial and final test mass positions) proved to be the maximum possible while still satisfying wall thickness constraints. This thickness constraint was primarily aesthetic and for the purpose of easing concern of those examining the grooved plate balancing mechanism for the first time.

Our original concept for this plate had 12 slots, however, since there are only three blades on the turbines having two slots to account for mass imbalance along each blade gives six evenly spaced slots. While this does require more vector splitting of the test masses for imbalances that do not lie on or between the blades, we plan to automate these calculations with a MATLAB script. However, the largest determinant for the number of slots was a number that would easily index with the blades. Six 0.25" slots proved to be the easiest to index to a three-bladed turbine.

After meeting with the pitching team following the Critical Design Review, we determined that it would be ideal if we could 3D print our grooved plate to help reduce the weight of the overhanging rotor assembly. Since this entire assembly would be spinning at a maximum speed of ~3000 RPM materials with brittle failure modes could pose a significant risk of shrapnel and jagged debris that could injure observers or damage the wind tunnel. While PLA is the easiest material to work with for 3D printing, PETG was selected instead due to its comparable strength, similar ease of printing, and vastly superior ductility. Additionally, layer delamination is not a significant concern in this design as the entire assembly is under compression from the castle nut on the end of the shaft which captures the entire rotor assembly on the turbine shaft as well as the clamping force resulting from the bolt tension in the tightened test mass assemblies.

6.3 Design Verification Calculations for Grooved Plate

Unlike the test masses, the geometry of the grooved plate body was iteratively determined by engineering judgement on 3D printed parts and packaging CAD to meet the overall geometric constraint (a diameter no larger than 68 mm). When we were confident with our final geometry in CAD we determined loading cases to perform simple stress analyses that would confirm the capacity of the final material geometry to not yield. While more in-depth analysis could have been done, since the part is a 3D print and non-isotropic even at 100% infill, our team decided that the more conservative, simplified analysis would suffice.

The load cases we considered were the shaft torque and the rated clamping force the grooved plate body could sustain. In all these cases, we were primarily concerned with member yield. Thus, with the guidance of Juvinall and Markesh's recommendations for safety factors [37], we selected a safety factor of 3.

From the shaft torque load case analysis (see appendix M) we found the factor of safety of material yield given the current geometry (see drawing package in appendix N) to be 6.7 between the rated torque of 4 N-m and the shaft torque (specification given by CPWPC) of 0.6 N-m, and 3.3 between the drive motor torque.

Before a design is finalized, some concerns must be addressed. One of these concerns is the risk of the test mass bolts flying off the part during testing. To evaluate whether this is indeed a threat, we performed a static calculation analyzing the forces on the bolt to calculate the clamping force required to safely secure the bolt. This calculation can be found in Appendix M. The results dictated that only about 4 lbf at a torque arm of 15mm (<1in) were needed to properly tighten the bolt with no risk of flying off at the fastest testing speed. Since most humans can exert their body weight as a force, we, in turn, concluded that the sliding masses were not at risk of coming off the

balancing mechanism so long as they are tightened correctly. Our testing procedure will help ensure proper tightening.

From the clamping force load case we determined that we had a safety factor of material yield from the bolt tension due to applied torque given the current geometry (see drawing package appendix N) to be 3 between the rated load of 544 N and the rated load of 177 N.

FEA in ABAQUS would have been the next step to confirming these hand calculations. However, due to time constraints and scope issues, this FEA was not completed. Destructive testing would also be easy to implement here, however due to the current pandemic access protocols and time constraints, sample testing of 3D printed tensile specimens was not completed. Though we still have not determined the mass imbalance ceiling for the rotating assembly we were able to calculate a residual imbalance – or acceptable mass imbalance following balancing – using ISO 14694. From the balancing grade table (See appendix M) and assuming the rigidly mounted configuration, as our testing apparatus will be clamped rigidly to a table, we determined that the residual imbalance limit for the BV-2 grade at the maximum test speed of 3101 RPM to be ~8 g-mm. This gives our MATLAB balancing program (see section 8.3 of Testing and appendix P) an approximate target for reducing the mass imbalance two for a given set of adjustments.

6.4 Proposed Balancing System Design

Our proposed preliminary design for the balancing system is detailed in this section. Our design is only preliminary and incomplete as this corresponds to the terms of our senior project that we adjusted with the CPWPC's permission due to unforeseen obstacles stemming from COVID-19 protocol changes. In figure 6.4.1 we have illustrated the simplified mechanical system of our proposed balancing system design.

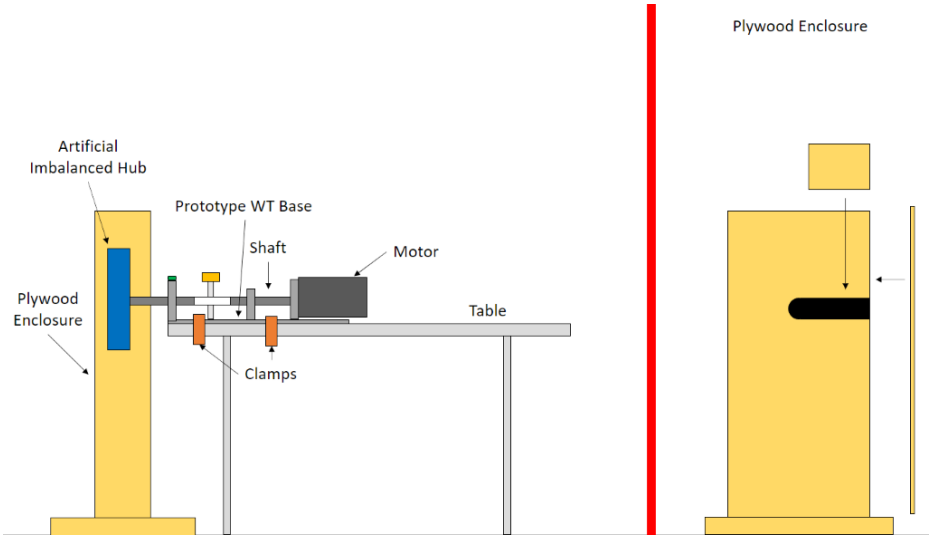

Figure 6.4.1 Schematic diagrams of balancing mechanical subsystem and rotor enclosure.

In figure 6.4.1, on the preceding page, the side view of the testbed shows the nacelle assembly plus the drive motor and motor mount clamped to a standard sized table with c-clamps while the artificial hub (for proving of the balancing system) or the competition rotor assembly (including

the pitching mechanism) are surrounded by a ½" thick plywood enclosure (see appendix M, table M.4 for the corresponding design calculation based on ISO 7475). Since the drive motor used with the competition nacelle assembly is considerably larger than the generator, the drive motor is aligned with the shaft coupler via an adapter mount (not shown). Our mechanical design is incomplete at this time as it is built around the CPWPC wind turbine nacelle assembly and selected electrical components which are still not yet finalized.

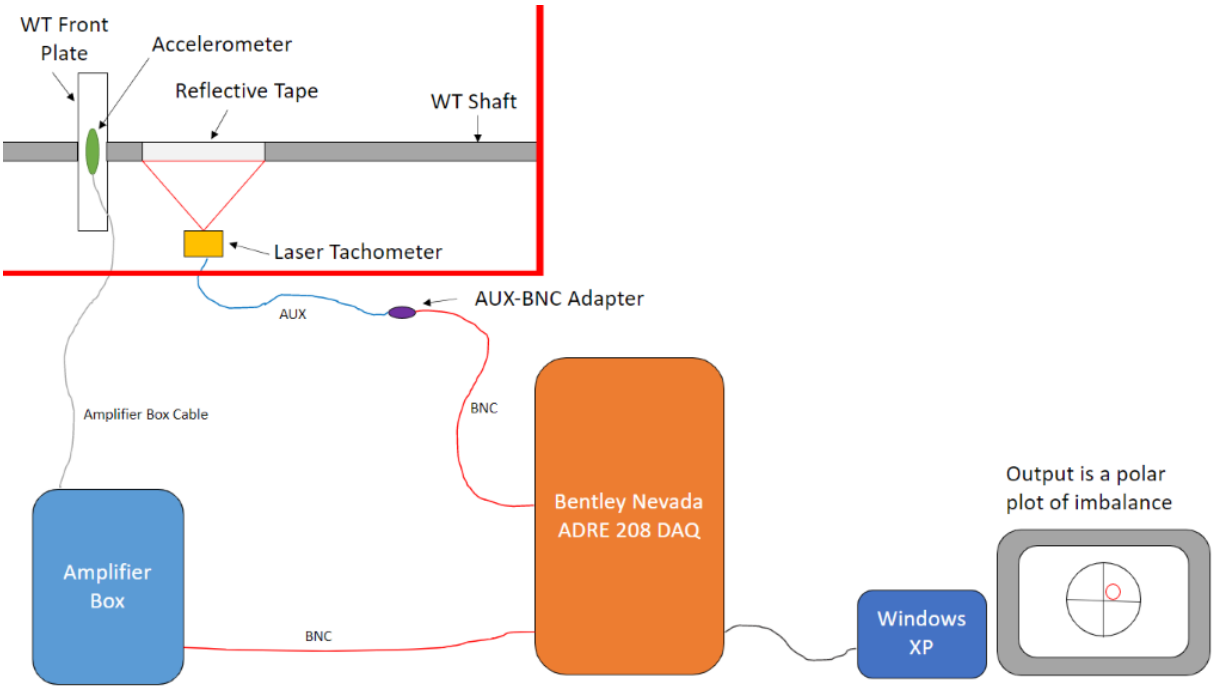

Figure 6.4.2 Simplified instrumentation diagram for balancing system.

The accelerometer on the front bearing measures the vibration accelerations of the shaft due to the mass imbalance in the overhung assembly. Although the quality of this measurement is improved by ensuring the vibration sensor is as close to the portion of interest of the rotating assembly as possible, the placement of the pitching mechanism's actuation assembly prevents a proximity probe from being trained on the shaft immediately behind the rotor hub. As a result, the front bearing housing is the closest to the source of vibration and where the accelerometer is located in our design. To collect shaft speed and phase data our design utilizes a laser tachometer. The tachometer is positioned with a camera tripod or 3D printed mount so that the laser beam is trained on the T-5 reflective tape and the tachometer is held at the proper distance from the shaft. The signal from the accelerometer is amplified and processed by the amplifier box (from the Cal Poly Mechanical Vibrations lab) and then sent to the ADRE Data Acquisition system (DAQ). In figure 6.4.2 the 208 DAQ is pictured, however, Dr. Wu prefers that we use the 408 DAQ if possible since the 208 DAQs are difficult to move and used for the ME 318 lab. Finally, the data from the DAQ is processed by the ADRE for Windows software, which outputs a polar plot of the shaft's eccentricity vs. rotational speed that the imbalance present in the rotor can be calculated from.

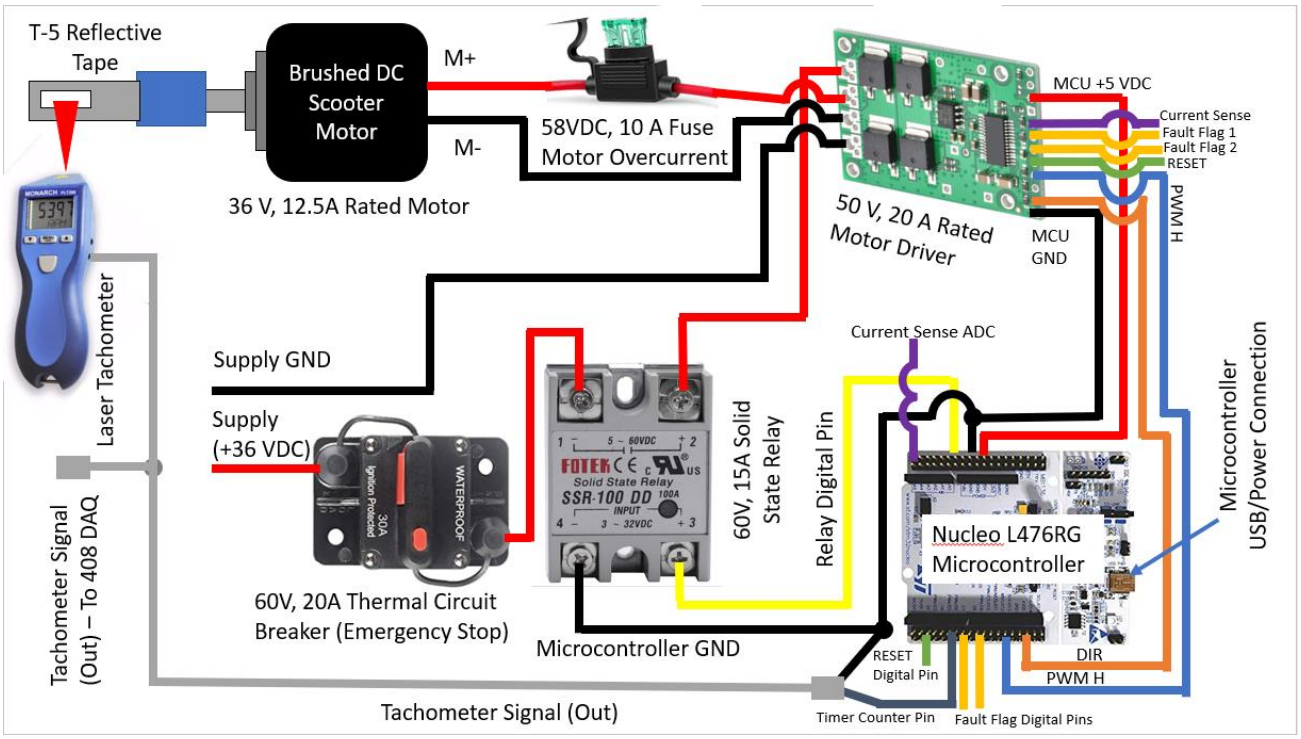

Figure 6.4.3 Simplified wiring diagram for proposed balancing system.

In its current configuration, our balancing system's electrical subsystem includes the previously mentioned emergency stop and overcurrent protection fuse for the motor. We also added a rated solid-state relay to allow the control system to switch the supply power to the circuit on or off instead of just disabling the motor driver. Unlike our previous design, the shaft position (and calculated speed) sensor data is provided by the transistor-transistor logic signal (TTL) output from the laser tachometer rather than a quadrature encoder. Additionally, in this proposed subsystem design we have also corrected the location error of the current limiting fuse so that the totally enclosed non-ventilated (TENV) drive motor does not overheat and destroy itself.

The principles of operation for our electrical subsystem of the balancing system remain the same. However, we have updated our proposed implementation with specified components based on Dr. Ridgely's recommendations, the power supply available, and the power requirements of the drive motor we have currently specified. All components were selected such that their voltage ratings were as close to the power supply maximum rated voltage (60 VDC) as possible to allow for the usage of a more powerful drive motor that our currently specified one (see appendix M, tables M.6 -M.9 for motor specification) if needed.

The high-power dual H-bridge single motor driver was also selected because of its safety features and current sensing capabilities. This driver board can protect itself from short circuiting of the motor outputs as well as well as provide approximate indication of board state through the fault flags. Most importantly, the on-board current sensor can be utilized to prevent a stall condition and board burnout by monitoring the current draw of the motor and having the microcontroller turn off the solid-state relay if the 20A continuous rating of the board is exceeded.

The motor that we have currently selected for our proposed balancing system is the MY1016 36V 350W brushed DC electric scooter motor. Finding a motor that could provide the required torque without any assistance from a reduction proved to be quite difficult. The motor we are currently proposing is rated for continuous operation with an output torque of 1.2 N-m at 2800 RPM (see appendix M, Table M.7), is rated for 12.5 A. We calculated the required torque of the motor with a safety factor of 2 to be 0.80 N-m (See appendix M, Tables M.5-M.9 for details). At the max test speed, 3103 RPM, our selected motor can deliver 0.72 N-m of torque (see appendix M, table M.9). This is technically insufficient, but only because of our selected safety factor. Our motor is over specified for our proposed balancing system. However, this conservative selection provides for longer motor life, better motor performance, and could allow for balancing at pitching angles other than zero degrees if, for example, aerodynamic and mass imbalance needed to be measured together.

The proposed components are not yet ready to be purchased as further review of the electrical subsystem is still needed. This review is for the purpose of confirming desired functionality, reducing component cost, and reducing shipping cost by sourcing from as few suppliers as possible.

Finally, since our control system design is incomplete, we have instead prevented the outline of our control system and the approximate requirements it will need to meet. Mechatronic system design rule of thumb for software architecture is to have one task per hardware component. The task diagram and finite state machine software design approach that would be applied for the completion of our control system design is outlined in Dr. Ridgely's handout for the ME 405 and 507 courses [44].

Proposed control system general requirements:

- Operate 10x faster than physical system's time constant (at least) [44]
- Avoid aliasing on sensor inputs by sampling and filtering properly
- Implement stable velocity control of balancing system
- Safety features
    - Software emergency stop
    - Stall detection and prevention with motor current sensing
        - Protection of motor driver board
        - Protection of drive motor

Proposed tasks for control system software:

- Tachometer signal processing task
    - Filters the tachometer signal data for velocity input into PI control loop on motor speed
- User interface task
    - Takes in terminal commands and stores multiple for processing by the motor control task

- Relay operation task
    - Switches the solid-state relay on/off in response to the testing task
- Motor control task
    - Takes in shaft velocity data from the tachometer signal processing task
    - Runs the control loop on the motor
    - Receives interpreted commands from the user (final test speed, test state)
    - Calculates next setpoint based on required ramp rate (5 RPM/sec)
    - Responds to faults detected by the safety task and delegates to other tasks as needed.
- Motor PWM task
    - Sets the pulse-width modulated (PWM) signal sent to the motor driver board based on the motor control task's command
    - Interfaces with motor driver
- Current sensing signal processing task
    - Filters current data from motor driver current sensor captured by the microcontroller's onboard analog to digital converters
- Safety task
    - Monitors filtered current to detect a stall condition of the motor and instruct the relay task to turn the relay off.
    - Monitors fault flag pins on motor driver and responds accordingly
    - Communicates with motor control task
    - Handles resetting fault flags

6.5 Maintenance and Safety Concerns

Since the grooved plate body and set screw arms for the positioner are 3D printed parts, they will wear out unpredictably. To account for this, we have decided to print multiple grooved plate bodies and sets of set screw. (See Manufacturing 7.3). However, even though the grooved plate will fail in non-brittle mode, the PLA blades on the turbine will not. So, an enclosure to surround the entire rotor assembly is needed. Preliminary calculations were completed to determine the thickness of this enclosure, but they have not been verified, and they are listed in Appendix M in Table M.4.

Besides the grooved plate, the nylock lock nuts are only rated to be reused two to three times. Even though they are not securing a bolted joint, the loosening and tightening them over and over wears out the nylon insert causing the nut to eventually lose its hold (from consultation with Prof. Fabijanic). Since we have not been able to test in the vibrations lab, we are unsure of the effects of wear in the lock nut on the overall proper-functioning of the balancing mechanism (e.g. positioning error in test masses). Maintaining the positioning gauge's calibration will require gentle handling and routine checks of calibration accuracy, optimally, before use in balancing the turbine. Again, due to a lack of testing experience, we are unsure how repeatable and accurate the test mass positioner is.

Additionally, sensitivity analysis to the positioning error in the test masses has not yet been conducted – due to time constraints. Though we attempt to account for the manufacturing error in

the grooved plate and positioning gauge through measurement and calibration, we still need to quantify an acceptable error limit such that a dangerous amount of imbalance to correct for the inherent imbalance in the rotating assembly is never inadvertently introduced.

Many of the electrical components that we selected are sensitive to static electricity and pose the risk of becoming too hot to touch (but not overheated for functional purposes) during operation. A heat sink is sold with the solid-state relay, however, no cooling solution for the high-power motor driver board has been determined. Additionally, during the development of the software for the controls system it is possible that the microcontroller could be destroyed from improper wiring or static discharge.

The programming development tools to make changes to the control system software and run the microcontroller from a personal computer during testing must be transferred to the computer/laptop of the CPWPC member(s) designated to take charge of the control system during testing. As a result, they must be trained how to operate the microcontroller and programming tools if they do not already have experience with MicroPython. Additionally, changes to the control system code should be tested in a controlled manner and reviewed by a mechatronics professor (Dr. Murray, Dr. Ridgely, or Professor Refvem) prior to testing.

7.0 Manufacturing

Our final design consists almost entirely of 3D printed components and commercial off the shelf hardware. Here we have provided the slicer and corresponding settings used to complete the printing of the grooved plate body and positioner prototype. Cura © 4.7.1 was used for all slicing of .STL files into G-Code for printing on Ethan Czuppa's Ender 3 fused deposition modeling (FDM) printer. Due to COVID restrictions and access to a 3D printer, Ethan undertook the manufacturing entirely and consulted with Caleb as needed.

7.1 Manufacturing Set-Up

The exact slicer settings are tabulated in appendix W, but in general the print settings between hobby 3D printers varies noticeably. We recommend that a test print is completed and inspected prior to final printing of the components to allow for tuning of feature warpage (shrinkage/growth/taper/deformation). In general, the nozzle of the printer was kept standard at 0.4mm, the layer height was also kept standard at 0.2 mm, the extruder was heated to 225 C while the bed was heated to 80 C for printing PETG filament, and the print was conducted when the inside temperature was greater than 64 F as this printer is not enclosed.

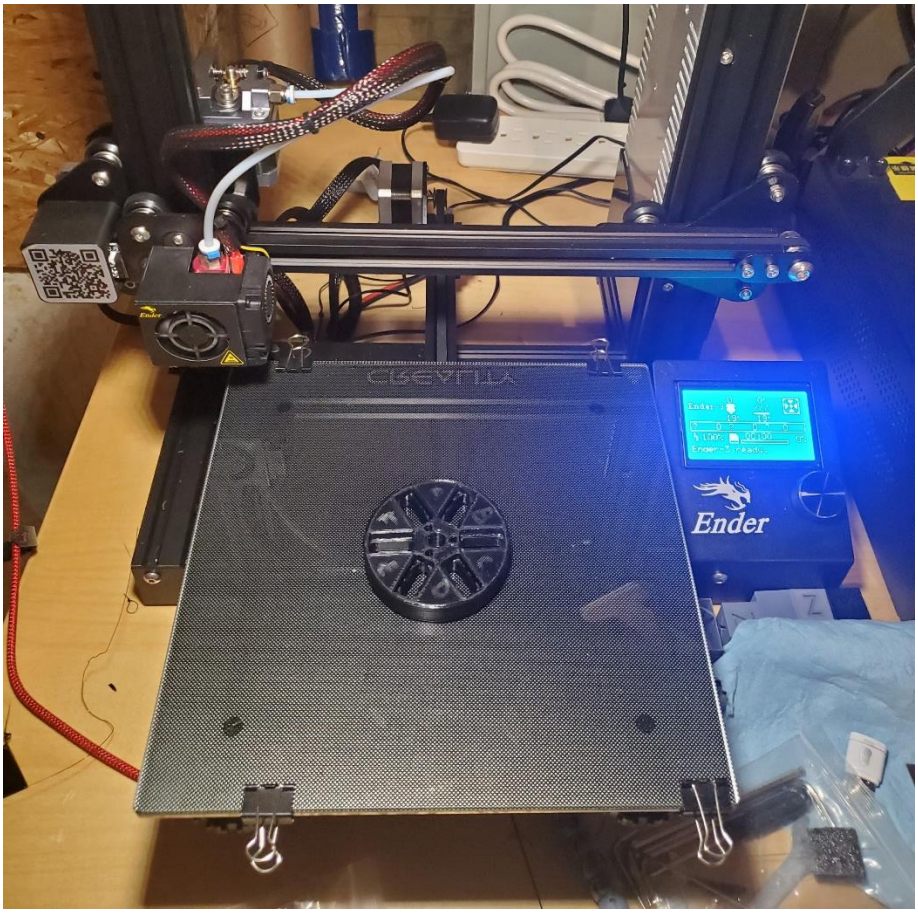

Figure 7.1.1. Manufacturing set up in Ethan Czuppa's Garage on Ender-3 3D printer.

All prints were conducted on the smooth side of the glass bed plate for maximum bed adhesion. At these settings, no issues with adhesion occurred. A skirt (concentric rings surrounding the

part) was printed around the part to help ensure the molten filament flow was as smooth as possible for layer-by-layer extrusion of the grooved plate body (not shown).

7.2 Post-Print Inspection

Following printing and removal from the build plate, I allowed the part to come down to room temperature (until it was cool to the touch) and then used digital calipers – zeroed with the outside caliper legs just clamped together – to measure the features of the grooved plate body. Additionally, sample hardware was obtained from Miner's ACE in SLO to perform fit testing and assist in the tuning of the prints.

As mentioned previously, I adjusted the dimensions of features expected to shrink by approximately 0.25 mm and then corrected this adjustment after inspecting each of the individual features. The full inspection list is provided in appendix O. To speed up the tuning process, the infill % was reduced from the intended 80-100% range to 20% so that each print would be about 2.75 hrs.

Due to time constraints the final grooved plate body's features have not been measured with respect to each other as this would require the use of the optical comparator in Mustang 60, at a minimum.

7.3 Manufacturing Considerations

The PETG filament is commonly known for its affinity to absorb moisture and produce print defects [35][36]. So, while multiple grooved plate bodies may be printed all at once, the filament should be stored in at minimum a resealable plastic bag with some sort of packages desiccant agent – one is typically supplied with each roll of 3D printer filament.

Wear from sliding masses and repeated clamping cycles has not been accounted for to establish the end of life of one of these 3D printed grooved plate bodies. To account for this, we are printing multiple final grooved plate bodies to ensure the CPWPC has extra in case one begins to deteriorate. However, since we have not yet been able to conduct final integration testing or even access the vibrations lab we do not have any empirical data on how well our grooved plate body will hold up to the abuses of testing. Additionally, statistically analysis on the dimensional variation of the features of the grooved plate has not been completed due to the small sample size of prints (3 as of the end of this project, though the remainder will be printed in fulfillment of our team's agreement with the CPWPC). So I cannot say for certain how well my printer holds tolerances, however, based on the preliminary inspection results, the printer is doing a good job.

3D printing is especially well suited to this complicated geometry. Traditional methods would require several set ups, tool changes, and operations to complete this part, for example machining the grooved plate out of a comparable thermoplastic to PETG on CNC mill. Additionally, since hobby level 3D printers are ubiquitous and relatively inexpensive (<$200 on sale) the ease of manufacturing is considerably increased for members of the CPWPC.

8.0 Proposed Testing

In this section, we will discuss the preliminary work we performed to verify our design through testing. Although we unfortunately were not able to officially test the wind turbine in-lab and properly balance the rotor assembly before the end of the project, we did make significant efforts towards cementing a consistent balancing procedure which the CPWP can use in the future to balance their wind turbines.

8.1 Proposed Instrumentation and Measurements to Characterize Mass Imbalance

To ensure that our part can balance the CPWP's 2021 wind turbine, we need to test our balancing mechanism. These tests will ensure that our design functions as intended and can correctly minimize eccentricity for a variety of potential mass imbalances. The Cal Poly vibrations lab will be used to test our procedure and verify our balancing mechanism's functionality.

Thanks in large part to Cal Poly graduate student Michael Mullen, we have a detailed testing procedure which documents how to measure mass imbalance in a rotor assembly. The proposed testing procedure will combine shaft speed and phase data with position and velocity data from either the proximity probes or accelerometers placed on the competition turbine to yield a polar plot, indicating where the mass imbalance is located. A MATLAB code will be used to quantify the results from the test and output a recommended calibration setting for the balancing mechanism which will effectively counteract present imbalances.

Figure 8.1.1 displays all our possible measurement methods for characterizing the mass imbalance initially present and after balancing in the wind turbine rotating assembly. Our three measurement methods are detailed in Appendix J. As a primer to the instrumentation description (Figure 8.1.1) here is a brief description of the placement of each of the sensors, important considerations that will help us select a single measurement method, and finally what data we will be collecting in order to produce our desired output. Firstly, both the proximity probes and accelerometers (if using two) must be placed 90 degrees apart. This is done to ensure sufficient separation between the sensors to accurately capture the shaft vibrational displacement and velocity. This perpendicular separation allows for measurement of the horizontal and vertical vibrations in the system.

Unlike the accelerometers–which can be mounted with wax relatively far away from the actual bearing in the front of the nacelle–the proximity probes require outboard mounting from the nacelle plate and an unobstructed view of the shaft. The proximity probes measure shaft vibrational displacements allowing for both imbalance measurement and approximate indication of shaft whirl. Shaft whirl is important to quantify because it can detail the stability of the system [33] [34].

Finally, both the shaft speed and phase (angular displacement from a reference mark) are needed to construct the polar plot. We plan on acquiring the shaft phase and speed data with either the Bently Nevada keyphaser® probe assembly or with a laser tachometer in concert with a special piece of reflective tape mounted on an exposed section of the shaft.

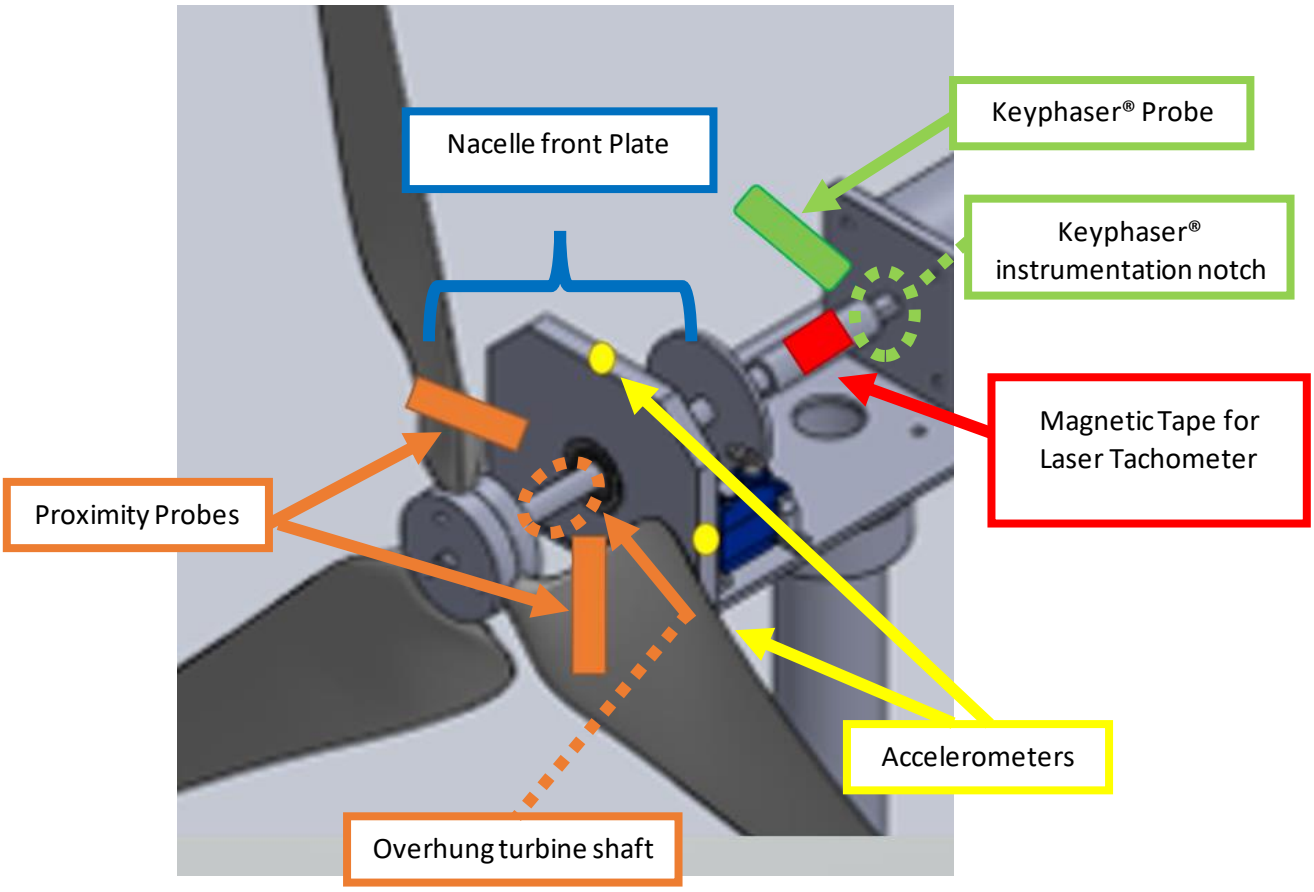

Figure 8.1.1 Diagram of testing setup overlaid on prototype wind turbine CAD model. Accelerometers, proximity probes, laser tachometer, Keyphaser ® probe

This test will yield a polar plot describing the rotor's imbalance. The resulting polar plot will be analyzed by a custom MATLAB code, which will output a recommended calibration setting or our design to appropriately minimize imbalance. All steps and both potential measurement methods are detailed in Table 8.1.1 on the next page.

Table 8.1.1 Testing procedure guide and required equipment.

	Vibration Measurement 1	Vibration Measurement 2	Shaft Speed Measurement 1	Shaft Speed Measurement 2
Procedure	1) Place accelerometers 2) Connect accelerometers to amplifier box 3) Connect amplifier box to 208 DAQ 4) Configure Windows XP software to read accelerometer 5) Use Windows XP program to generate polar plot.	1) Instrument notch in shaft 2) Insert proximity probe into notch 3) Connect proximity probe to proximiter assembly 4) Connect proximiter assembly to 2ADRE 08 DAQ 5) Use Windows XP program to generate polar plot.	1) Place reflective tape on shaft 2) Connect laser tachometer to ADRE 208 DAQ	1) instrument a second notch in shaft 2) Mount Bently Nevada Keyphaser® probe so it has a clear view of the notch 3) Connect keyphaser® probe to ADRE 208 DAQ
Equipment	Accelerometer (100 [mV/G]) (x2) Amplifier box (x1) Bentley Nevada ADRE 208 DAQ (x1) Windows XP desktop (x1) BNC cable (x2) White accelerometer wires (x2) Wax	Bentley Nevada proximity probes (x2) Bentley Vevada proximiter assembly (x1)	Laser tachometer (x1) BNC-AUX cable (x1)	Keyphaser Probe (x1) BNC cable (x1)

Vibration measurement 1 measures the vibration of the shaft via two accelerometers are 90˚ apart to capture the horizontal and vertical acceleration of the rotor assembly. The accelerometers will be mounted with lightweight wax and be as lightweight as possible to minimize the effect of the instrumentation's mass on the resulting vibrational data. From the accelerations at the bearing, we can backout the shafts position (transverse deflection), and in turn the vibration of the shaft.

Vibration measurement 2 measures deflection of the shaft directly with two Bently Nevada proximity probes. The proximity probes—alongside the proximiter assembly—are specifically designed by Bentley Nevada to measure the vibrational behavior of a rotating system and output a polar plot. Thus, this vibration measurement option must make use of the Keyphaser® probe (which is what the ADRE 208 DAQ expects to be used with the proximiter probes).

Shaft speed and phase measurement option 1 requires reflective tape to be mounted to the shaft. As the shaft rotates, a laser tachometer measures the phase and speed of the shaft. While the Cal Poly vibrations lab does not provide a laser tachometer, Michael Mullen has volunteered his time and his personal laser tachometer for testing. Combining the data from both measurements, a polar plot representing the imbalance in the system can be generated.

Shaft speed and phaser measurement option 2 makes use of the Keyphaser® probe and an instrumented notch in the rotating shaft provided by a keyway or external component from Bently Nevada applied to the shaft which is designed to work specifically with the Keyphaser® probe.

Per the guidance provided by graduate student Michael Mullen, we recommend utilizing a laser tachometer and an accelerometer to measure vibrations. This is recommended because it is the simplest method and requires the least design considerations to adequately use. Note however that a proximiter probe and a Keyphaser® can both be used as an alternative to the accelerometer and laser tachometer respectively. Some wind turbine designs may facilitate or necessitate usage of one of these alternate measurement methods. Our proposed testing procedure can be found in Appendix U.

8.2 Testing Procedure

To properly balance the wind turbine, we will treat the system as a fan. By analyzing the system as a fan, we are able to balance the wind turbine using industry standard methods for fans. This has helped us concentrate our testing procedure and officialize the balancing process.

Through consultation with graduate student Michael Mullen, we have cultivated a detailed testing procedure which utilizes the Cal Poly vibrations lab. This procedure details how to measure the present imbalances in the system, along with the relevant safety precautions taken to ensure the safety of all testers. To measure mass imbalance in the wind turbine, we utilize an accelerometer to collect vibration magnitude and a laser tachometer to measure vibration phase.

However, this testing procedure is lacking some essential nuances. Certain elements of the process, such as exact port locations, equipment plug-ins, and general interface details still need to be added once access to the vibrations lab is approved. We plan to help the parent Cal Poly Wind Power club in flushing out this testing procedure during the Spring 2021 academic quarter. The incomplete testing procedure can be found in Appendix U.

8.3 Calibration MATLAB Code

We have outlined our detailed testing plan for measuring imbalance in the wind turbine. However, once the imbalance is quantified, our balancing mechanism must be properly calibrated in order to counteract any existing imbalances. To calibrate our mechanism, we have authored a MATLAB code capable of taking a mass imbalance readout from the DAQ provided in the vibrations lab and outputting a position for each sliding mass on the grooved plate. The resulting calibration will be able to effectively eliminate any mass imbalances in the system. Appendix P contains the MATLAB calibration code.

The code was designed to keep four of the six sliding masses stationary. Since each mass has enough weight to eliminate any present unbalances alone, two masses are all that is needed to correct for an imbalance at any angle between the six radial slots. The code firstly sections the grooved plate into different angle ranges. The code then identifies the angular location of the imbalance, and selects the two nearest radial slots which will be used to correct the imbalance. From there, simple matrix division is used to calculate the necessary distance to calibrate each mass.

Unfortunately, this code has not been verified through testing. This code should be further tested, refined and optimized before official in-lab testing and balancing.

To move each mass to their respective locations with precision, we plan on utilizing a precision tool. This precision tool will be made out of a modified divider with 3D printed attachments which will sit in the countersunk tops of each of our test masses. Baseline measuring from the central castle nut of the balancing mechanism, the precision tool should be able to deliver accurate calibration results. This precision tool will need to be manufactured before in-lab testing.

9.0 Proposed Design Verification

This section discusses how the wind turbine will need to be verified as functional and safe. Normally we would provide our verification plan and testing results, however, our senior project was unable to complete these due to lab access issues. Since our design verification process for the completed balancing mechanism and system has yet to be completed, the contents of this section will outline the preliminary precautions that can be taken to ensure safety during testing, as well as the next steps which need to be taken to verify the current system's design. It is our intention to complete what we have outlined here during the 2021 spring quarter.

9.1 Update Simulation in ABAQUS

Our simplified turbine shaft and rotor model linear dynamic analysis confirmed that the estimated natural frequencies of the assembly are sufficiently faster than the operating speeds to ensure (even in the theoretical 22 m/s wind speed resulting shaft speed) that a resonance condition is never introduced. The frequency margin for each mode detected from the natural frequency estimation exceeds a frequency margin of 15% (above) and is considered safe for balancing [33][34] (See Section 4.5 in 4.0 Modeling). There are still many limitations to this model, but perhaps the most significant is that the shaft geometry has been revised since the completion of this modeling to rendering the results less useful. The most noticeable difference between the current and previous shaft is the increase of overhung length from the front nacelle bearing. Thus, this simplified analysis will need to be completed again to adjust for the new shaft geometry. Thankfully, many of the analysis tools and files for this analysis were developed with alteration of parameters in mind, so redoing this analysis will not be a significant undertaking. However, due to time constraints and a lack of finalized shaft geometry from the CPWPC (we are a quarter ahead of their senior project, this is acceptable and expected), this analysis remains incomplete.

9.2 Proposed Testing and Verification Plans

As mentioned, our final design has yet to be formally verified. Instead of presenting our verification results here, we have provided the steps necessary to complete our design verification process. The majority of the verification will occur when the balancing mechanism and the associated balancing procedure are tested in the Cal Poly vibrations lab. This section specifically outlines the necessary steps which will need to be completed before the balancing operation is dependable. In response to our senior project's request, Dr. Kean, Dr. Widmann, and Mr. Bob Crockett were able to create a protocol to allow our senior project team to continue working with CPWPC after graduating and access the vibrations lab as volunteers. Our point of contact will be Christine Haas of the Mechanical Engineering department. This special method of access was necessary for our senior project in order to continue helping the CPWPC as after graduating in winter of 2021, neither Ethan nor Caleb are considered students at Cal Poly SLO. However, this specialized access protocol is not needed for currently enrolled students.

Firstly, access to the vibrations lab must be granted. To initiate this, the senior project team that wants to conduct the testing should contact the CPWPC management and faculty advisor for approval. One or more member(s) of the CPWPC must be delegated as points of contact and testers for in-lab testing. Once the CPWPC's participant(s) are selected, access must be granted by the Cal Poly vibrations lab coordinator(s) and the ME department chair. Additionally, an eligible Cal

Poly graduate student must be selected to assist in testing. The graduate student should be familiar with vibrations lab equipment and must be familiarized with the proposed testing procedure. A graduate student will likely not be needed for his/her technical skills beyond the design verification testing, however, a graduate student may be required to supervise CPWPC balancers in the future; check with the Cal Poly vibrations lab coordinators and the ME department chair for details on what is needed for future testing. We recommend that whatever equipment is needed for testing and the testing procedure are mostly complete before reaching out to the lab coordinator(s). Finally, other guidance for lab access should be sought from the Student Success Guide. All points of contact mentioned in this paragraph are provided immediately below and are current as of Spring quarter 2021.

Contacts:

- Dr. Widmann – jwidmann@calpoly.edu Mechanical Engineering Department Chair
- Dr. Kean – akean@calpoly.edu Cal Poly Wind Power Club Faculty Advisor
- Sophie Spencer – saspence@calpoly.edu Cal Poly Wind Power Club President
- Dr. Wu – xwu@calpoly.edu Mechanical Vibrations Lab Head Coordinator
- Dr. H.P. -- hporumam@calpoly.edu Mechanical Vibrations Lab Coordinator

After our updated ABAQUS model verifies that the system is not at risk of failure—due to its natural frequencies—we will proceed to the testing phase. The results of our testing process will include a polar plot describing the rotor's imbalance. Ideally, we would compare the polar plot received from experimental testing and the polar plot received from Abaqus simulation to verify our simulation – however this is a stretch goal for our continued balancing work outside of the our senior project.

Having established our access to the vibrations lab for all testing participants, our current senior project members would then perform a dry-run through our testing procedure under the supervision of Dr. Wu to fill and gaps and correct errors in our procedure. Permission to complete turbine balancing will require the review and approval of our finalized testing procedure by the vibrations lab coordinators.

With permission to test secured, the preliminary subsystems must be completed and implemented. These subsystems include the mechanical subsystem, electrical subsystem, and the control system (software). The plywood rotor enclosure design must also be completed and constructed. Once these systems are completed and functioning properly, they may be verified by completing the inspections outlined by our engineering specifications for this senior project (section 3.0). At this point the MATLAB balancing code's output from generated or empirical imbalance data as a polar plot would need to match the result of the single-plane influence vector balancing procedure as outlined in the Rotor balancing lab section of the ME 318 Lab manual [43]. The controls system must appropriately regulate the motor speed, allowing a ramp speed of 5 RPM/s. The system must also be compatible with the borrowed power supply that will be used in testing. The plywood enclosure must entirely enclose the wind turbine's rotor, while offering safe clearances to ensure

that no issues develop during testing. Lastly, the MATLAB calibration code must be tested to ensure functionality, and may be optimized as necessary.

Following our testing updated procedure from what is currently outlined in the Appendix U, we will measure the system's imbalance and articulate it using a polar plot. This can be done using the Windows XP software available in the Cal Poly vibrations lab. Then, using our MATLAB balancing code, we will input the experimental polar plot and receive a recommended calibration setting for the given unbalance. After we calibrate our part, we will rerun the test and measure the remaining imbalance in the system.

If the remaining imbalance falls beneath the maximum allowable imbalance for the system, our design, MATLAB code, and testing procedure will be verified as and considered to be working as intended. If imbalance in the system remains above the maximum allowable imbalance, we will proceed by isolating the problem and identifying which system the issue stems from. After diagnosing the problem and the subsystem that is at fault, we will proceed to refine that system or adjust the testing method as needed until the process yields the results we are looking for.

Although we are graduating in the Winter 2021 quarter, we both plan to assist in the formal testing verification process as Cal Poly volunteers. This process is currently underway, and has yet to be officialized. However, we are confident that with our knowledge of the testing procedure and systems, we will be able to ease the balancing process and provide a more fluid transfer of responsibilities to the CPWPC.

10.0 Project Management

We have detailed the goal of this project and specified how others have managed to balance similar systems. We have also delved into our own brainstorming and down-selection process. We have discussed testing plans and detailed our final design. And finally, we have detailed plans moving forward to assist in the testing and balancing process, as well as flush out our currently incomplete procedure. Now we will discuss how we aim to complete these tasks and why we managed our project in the way we did.

Moving forward, we plan to work as a part of the CPWPC research team. As a part of their research team, we will be able to access the vibrations lab during the Spring 2021 quarter, assist in completing the balancing procedure and help in officially balancing the completed wind turbine. This plan is currently in the process of being approved by Dr. Widmman, Dr. Kean, and the CENG Dean, Dr. Fleischer, but no formal word has been issued at this point.

Initially, our management process consisted of weekly meetings and consistent work times. Unfortunately, due to scheduling conflicts, this quarter was not as organized as previous quarters. By being put into separate lab sections, our schedules did not align, and consistent, unified work times became scarce. Going forward, cementing a weekly schedule to meet and work will be helpful in working towards project milestones.

From the beginning, we established a very open line of communication. Since this is a two-person senior project, clear communication is required to work efficiently and quickly. This worked fantastically, and allowed us to complete as much work as we did. By communicating clearly and consistently, we have been able to stay on top of tasks and manage tasks efficiently. In the future, we will be sure to establish clear, consistent lines of communication with points of contact for each project.

Much of our work has been handled through premeditated delegations- namely weekly meetings with an agenda, WSR, and meeting minutes. This system has helped us stay accountable for our work and meet deadlines. We also made it clear that if needed, we can ask for assistance to ensure that deadlines are met and that all work is up to standard. This certainly strengthened our work practice. Delegating work is an essential component of project-based work, as it is important for everyone to bring their own, unique ideas to the table while also working in a group of other people. Unfortunately, our practice of using this system diminished significantly in the final quarter of quarter of our senior project. While we had developed better work-planning habits as a team, we fell short of being able to consistently implement them at the level required to even come close to completing out lofty goals.

One thing that would have aided our work would have been working in an actively preemptive way. By approaching problems and tasks farther ahead of time, we may have been able to overcome some of the steep list of deliverables, or at least make more progress towards balancing the competed wind turbine. Yet, the underlying issue was really one of scope (see section 11.0 Conclusion) and the accruing fatigue from online learning, an arduous approval process for accessing the vibes lab, and as mentioned earlier significant scheduling conflicts.

11.0 Conclusion

The goal of this project is to design a rotor balancing system for the Cal Poly Wind Power club. The balancing system should minimize residual mass imbalance within the wind turbine, ensure that the wind turbine is safe to operate and ideally be applicable to future CPWP designs. Any features of the wind turbine that may reduce imbalance but are not within our scope will be included as a design recommendation to the CPWP and other senior projects. According to the preliminary research we have conducted, we will need both a method to measure imbalance, and a device to minimize imbalance. Our project must meet these requirements while remaining within the allotted CPWP budget.

We began designing a solution to this problem by modeling the wind turbine rotor assembly. The initial rigid shaft parametric study—while not necessarily realistic—will serve as a useful tool for design suggestions and be an essential reference for allowable residual imbalances in the rotor assembly. The flexible shaft ADAMS model has proven to be too complicated to simulate and refine. Instead, we will be modeling the rotor system in Abaqus. Lastly, our SolidWorks frequency study provided us with preliminary data for sensitive system frequencies. This modeling method can be used by the CPWP in the future to ensure that their final design models are not subject to damage or failure due to the system's critical frequencies.

After modeling, we proceeded to ideation and concept design. The down selection process is nearly complete, but our final design choice will be officialized after consultation with the CPWP Pitching team. Once a final design is selected, we will appropriately dimension the part and refine the design as needed to allow easy implementation into the existing wind turbine assembly design.

Proceeding design selection and refinement, we began manufacturing process. A MATLAB code used to calibrate the balancing mechanism has also been developed. Finally, our part will be tested in the Cal Poly vibrations lab by the WPC in the Spring 2021 quarter. If the testing process yields a valid, balanced rotor system, we will thoroughly document our procedure and present our design and testing protocol to the CPWP.

Although our project aimed to completely balance the 2021 WPC wind turbine, we did not complete the balancing process or the testing necessary to validate our design. We were unfortunately unable to complete all of our outlined, desired deliverables. The WPC is aware of and nonetheless content with our progress. Notwithstanding, we were not able to test our balancing procedure and mechanism, verify our design, nor verify our MATLAB calibration code. Additionally, we were unable to manufacture the plywood testing enclosure, the electrical controls system, or the calibration gage used to properly distance correction masses. The calibration gage designed drawing can be found in Appendix N.

There are a few key reasons for our unmet goals. Firstly, we were divided into two separate lab sections this quarter. The reduced collaborative work time and inconsistent scheduling lead to a schism, which hindered productivity and organization. With the addition of less meetings with our project advisor—now once every two weeks—lead to decreased organization.

Another cause for the reduced work output would be the fact that this is a two-person senior project. As an initially undefined project, this project was not something that would seem to need

more people. However, the work required to research the effects of mass imbalance on a small-scale, overhung rotating assemblies certainly hindered our first quarter of work to thoroughly define the problem. Due to the complexity of the subject matter concerning our project, it took longer than most other projects for our senior project team to get a solid footing. A third project contributor would have certainly bolstered our work progress and help us catch up to our expected deliverables.

Probably the most crippling cause of our incomplete project is the logistical issues of working with the WPC on a different timeline. Specifically, our project was made in hopes to appropriately balance the 2021 wind turbine, which was being designed and manufactured three months behind our schedule. With that in mind, we were supposed to have a completed, dimensioned design selected before the wind turbine itself was designed. This was unrealistic, and lead to our senior project operating nearly one quarter ahead of schedule of the WPC, but one quarter behind our senior project schedule. In turn, complications were inevitable.

Yet another reason for this delay was due to the complications associated with obtaining access to the Cal Poly vibrations lab under the COVID-19 pandemic. The procedure of gaining access was modified continually throughout the last few months. Initially, a completed testing procedure needed to be submitted and approved by the Cal Poly vibrations lab coordinator. After that, our safety precautions would have to be verified by Eric Pulse, the lab safety coordinator. After this process was completed, we were advised to pursue access through the ME department chair, and finally through the WPC itself. The inconsistency of criteria for lab access certainly delayed our project and complicated access to the vibrations lab.

Upon review, we would have preferred to maintain the rigorous template for senior project provided during the Spring 2020 quarter. By meeting weekly with our advisor and providing a detailed agenda and summary of that week's accomplishments, we were able to meet consistently and more thoroughly plan out our project and anticipated timeline. Although this would not have changed the complications that arose with our project, this would have helped us adapt to those changes in a more timely and calculated manner.

Additionally, we would have liked to keep in closer contact with the WPC and its sub-teams. Much of our design and down selection process was impeded by unclear and inconsistent communication with other senior project teams. More thorough, adamant communication channels would have bolstered our project's success and given us more time to work on other, more demanding tasks.

11.1 Next Steps

There are still some tasks which need to be completed for complete wind turbine balancing to be achieved. The first step in completing the balancing process is to acquire reliable access to the Cal Poly vibrations lab. Access should be granted to the testers, as well as a knowledgeable graduate student from Cal Poly who can assist in the technical procedure of wind turbine balancing. Since lab access can require time to finalize, we recommend starting this process as soon as possible.

After approval for lab access is established, we recommend finalizing the preparatory work required for in-lab testing and balancing to commence. This means manufacturing the testing enclosure, the calibration gage (Appendix N) used to set the displacements for each test mass, as well as the complete controls system.

Before in-lab testing can begin the MATLAB calibration code must also be verified. The code is currently designed to work in cartesian coordinates. However, if this is evaluated to be too imprecise for the testing system, then the code can be amended to work in a radial coordinate system. Additionally, the designed controls system must be manufactured and implemented. The MATLAB code should be able to efficiently run for a realistic imbalance measurement before in-lab testing commences.

After these steps completed, follow the WPC Wind Turbine Balancing Procedure document provided to balance the wind turbine in the Cal Poly vibrations lab. A Cal Poly graduate student is required for the first in-lab balancing process, as the technicalities of many equipment interfaces have not yet been specified in the procedure. The Cal Poly graduate student will certainly help complete the process in a timely and competent manner. As the balancing process is being completed, the test procedure can be completed in tandem. After all the specifics of the procedure are determined, the test procedure can be completely documented for future usage.

Any remaining tasks would pertain to optimizing the system(s) or troubleshooting errors that arose during testing. All other procedures have been completed. If any assistance is needed to complete the balancing process, we can be reached for consultation or guidance.

Finally, supporting documentation listed in this report will be provided to the CPWPC in more accessible file formats for (final CAD as converted SOLIDWORKS part files, dimensioned drawings as .pdf, Cura slicer profile as .3mf file, MATLAB balancing script as an .m file, and so on). These will be complied into a zip archive and uploaded to the folder on the shared Google drive specified by the CPWPC.

Thank you for your time and support. All the best.

Works Cited

[1] Alibaba RYQ-3 Turbine Shaft Balancing Machine Datasheet
[2] Schenck Pasio 5 Series Datasheet
[3] Ranger RWS-1B Bubble Wheel Balancer Datasheet
[4] Hofmann Minibalancer MI 2100 Datasheet
[5] Erbessd EI-30 Datasheet
[6] Foiles, W. C., P. E. Allaire, and E. J. Gunter. "Rotor balancing." Shock and Vibration 5.5-6 (1998): 325-336.
[7] Axelsson, Ulf, Mikael Bjork, and Christian Haag. "Method for balancing a wind turbine." U.S. Patent No. 8,683,688. 1 Apr. 2014.
[8] Vettese, Sharolyn. "Horizontal wind turbine blade balancing accessory." U.S. Patent No. 8,206,110. 26 Jun. 2012.
[9] Perkinson, Robert H. "Method and apparatus for balancing wind turbines." U.S. Patent Application No. 13/009,402.
[10] Larsen, Orla W. "In situ balancing of wind turbines." U.S. Patent No. 5,140,856. 25 Aug. 1992.
[11] Barace, Alberto Garcia, et al. "Wind turbine control." U.S. Patent No. 8,380,357. 19 Feb. 2013.
[12] Grabau, Peter, Michael Friedrich, and Carsten Bendix Sorensen. "Pitch system balancing." U.S. Patent Application No. 13/299,489.
[13] Cakmak, Onur, and Kenan Y. Sanliturk. "A Dynamic Model of an Overhung Rotor with Deep-Groove Ball Bearings." Proc. of The First Joint Int. Conf. on Multibody System Dynamics. 2010.
[14] Gunter, Edgar J., and Charles Jackson. "Balancing of rigid and flexible rotors." Fredric F. Ehrich, Krieger Publishing Company, Malabar, Florida (1999): 3-1.
[15] Norton, Robert L. *Design of machinery: an introduction to the synthesis and analysis of mechanisms and machines*. "Chapter 12: Balancing." pp.570-79. Boston: McGraw-Hill Higher Education, 2004.
[16] Rao, Singgiresu S. *Mechanical Vibrations*. "Chapter 9: Vibration Control." pp. 776-98. 5th ed. New Upper Saddle River: Prentice Hall, 2011.
[17] Larsen, Orla W. "In situ balancing of wind turbines." U.S. Patent No. 5,140,856. 25 Aug. 1992.
[18] Niebsch, Jenny, Ronny Ramlau, and Thien T. Nguyen. "Mass and aerodynamic imbalance estimates of wind turbines." *Energies* 3.4 (2010): 696-710.
[19] Graabak, Ingeborg, and Magnus Korpås. "Balancing of variable wind and solar production in continental europe with nordic hydropower–a review of simulation studies." *Energy Procedia* 87.1876 (2016): 91-99.
[20] Staino, A., B. Basu, and Søren RK Nielsen. "Actuator control of edgewise vibrations in wind turbine blades." *Journal of Sound and Vibration* 331.6 (2012): 1233-1256.
[21] Arrigan, John, et al. "Control of flapwise vibrations in wind turbine blades using semi-active tuned mass dampers." *Structural Control and Health Monitoring* 18.8 (2011): 840-851.
[22] IEC 61400-2 International Standard, Wind Turbines – Part 2: Design requirements for small

wind turbines, 2nd Edition 2006-03.
[23] Balancing, I. R. D. "Balance quality requirements of rigid rotors: the practical application of ISO 1940/1." (2001).
[24] International Organization of Standards. ISO 1940-1: "Mechanical Vibration-Balance Quality Requirements of Rigid Rotors." *Part I: Determination of Permissible Residual Unbalance,* (1998).
[25] International Organization of Standards. ISO 7475-2002: *"Mechanical Vibration – Balancing Machines. Enclosures and Other Protective Measures for the Measuring Station."* (2002). Bureau of Indian Standards.
[26] International Organization of Standards. ISO 2953-1999: "Mechanical Vibration – Balancing Machines – Description and Evaluation. (2007). Bureau of Indian Standards
[27] ISO, EN. "12100-1: 2003/prA1: 2008." *Safety of machinery—Basic concepts, general principles for design—Part 1: Basic terminology, methodology—Amendment 1 (ISO 12100-1: 2003/DAM* 1 (2008).
[28] International Orgnaization of Standards. "ISO 14694:2003" *Industrial Fans – Specifications for Balance Quality and Vibration Levels.* (2003). British Standard.
[29] Flexible Rotor Balancing ISO standard
[29] Budynas, Richard G., and J. Keith Nisbett. *Shigley's mechanical engineering design*. McGraw-Hill Education, 2020.
[30] Abney, T. "SOLIDWORKS Simulation: Dynamic Analysis." video recording. LinkedIn Learning (2018). Viewed 27 May, 2020. [Online]. https://www.linkedin.com/learning/solidworks-simulation-dynamic-analysis/mass-participation-background?u=2121556
[31] Wu, X., C. Naugle, and J. Meagher. "A full spectrum analysis methodology applied to an anisotropic overhung rotor." *J Appl Mech Eng* 5 (2016): 232. [Online].
[32] Simon, Derek. "Static Balancing of the Cal Poly Wind Turbine Rotor." (2012).
[33]E.J. Gunter. "Introduction to Rotor Dynamics - Critical Speed and Unbalance Response Analysis." (2001). *Dyrobes Rotordynamics Software* ©. [Online]. https://dyrobes.com/wp-content/uploads/2016/04/Introduction-to-Rotor-Dynamics-Critical-Speed-and-Unbalance-Response-Analysis-E.-J.-Gunter_linked.pdf
[34] Wijker, J. J. "Modal Effective Mass." *Spacecraft Structures* (2008): 247-263. [Online] doi: 10.1007/978-3-540-75553-1_16
[35] Greenburg, J. The Perfect Ender 3 PETG Settings. ALL3DP. [Online]. https://all3dp.com/2/ender-3-petg-settings-profile/
[36] Kivela, L. PETG vs. PLA: The Differences – Simply Explained. ALL3DP. [Online] https://all3dp.com/2/petg-vs-pla-3d-printing-filaments-compared/ https://all3dp.com/2/petg-vs-pla-3d-printing-filaments-compared/
[37] Juvinall & Markesh, Safety Factor Considerations, CH 6 Failure Theoreis, Safety Factors, and Reliability. [Online]. https://polylearn.calpoly.edu/AY_2018-2019/pluginfile.php/507251/mod_resource/content/0/Juvinall-Marshek-Factor%20of%20Safety.pdf
[38] "Rotary Device Sizing Tool." (2020). Oriental Motor Corp USA. [Online]. https://www.orientalmotor.com/motor-sizing/rotaryDevice-sizing.html#QuickReport

[39] "Motor Sizing Calculations." Oriental Motor Corp USA. [Online]. https://www.orientalmotor.com/products/pdfs/F_TecRef/TecMtrSiz.pdf
[40] Tang, J. (2020). "Motor Sizing Basics Part 1: Load Torque." *Engineering Notes.* Oriental Motor Corp USA. [Online]. https://blog.orientalmotor.com/motor-sizing-basics-part-1-load-torque?hsCtaTracking=758b58b5-92d0-44f3-9d18-a9421f30bf73%7Cc3fbe5ce-14d4-4b84-81b9-96fefa8e849a
[41] Tang, J. (2020). "Motor Sizing Basics Part 2: Load Inertia." *Engineering Notes.* Oriental Motor Corp USA. [Online]. https://blog.orientalmotor.com/motor-sizing-basics-part-2-load-inertia?hsCtaTracking=95e3b5c5-570b-4403-9b54-aa346abde034%7C773a672a-9bbb-411d-ae39-0276910ef191
[42] Tang, J. (2020). "Motor Sizing Basics Part 3: Acceleration Torque (and RMS Torque)." *Engineering Notes.* Oriental Motor Corp USA. [Online]. https://blog.orientalmotor.com/motor-sizing-basics-part-3-acceleration-torque-and-rms-torque
[43] Meagher, J., Ridgely, J., Garner, E., Iannce, M., Porumamilla, H., Cooper, M. (2015). Handbook and Reference for the ME 318 Laboratory. California Polytechnic State University San Luis Obispo.
[44] Ridgely, J., R. (2017). "Using Tasks and Finite State Machines in Python: ME 405/MicroPython Edition." Cal Poly Mechanical Engineering.

Appendices:

[A] Preliminary Design Flowchart
[B] House of Quality
[C] Gantt Chart for CPWP Balance System
[D] Rigid Shaft Parametric Study
[E] SolidWorks Frequency Study Post-Processing
[F] Initial Concept Block Diagram & Ideation
[G] Mass Eccentricity Derivation
[H] Go-No-Go Down Selection
[I] Notes on Imbalance Determinants
[J] Notes on Michael Mullen's Recommended Testing Procedure
[K] ABAQUS Simulation Plan
[L] ABAQUS Modeling Study
[M] Grooved Plate & Vibrations Test Bed Design Calculations
[N] Drawing Package
[O] Manufacturing Inspection Log
[P] MATLAB Calibration Code
[Q] Product Literature
[R] Final Project Budget
[S] Failure Modes & Effects Analysis + Risk Assessment (designsafe Report)
[T] Design Hazards Checklist
[U] Testing Procedure
[V] The Theory and Practice of Small-Scale Wind Turbines
[W] Cura© Slicer Profile

Appendix A - Preliminary Design Flowchart

WTRA Balancing System:

- High Level Requirement(s):
  - 1) Measure and Detect Mass Imbalance in WTRA
  - 2) Correct Mass Imbalance in WTRA
- Measure and Detect Mass Imbalance in WTRA
  - Maximum allowable residual imbalance in WTRA (mR product g-mm, kg-m, oz-in, etc.)
  - Specify sensors with appropriate resolution/sensitivity
    - Be able to accurately measure vibrational amplitude or accelerations at bearing supports of overhung mass on flexible rotor...
      - Sensor DC gain
      - Sensor smallest level of vibration measurable with good correspondence
      - Sensor natural frequency/frequency response characteristics
    - Required Sensor Data:
      - Accelerations at Bearing Supports (mV/g)
        - Typically use soft bearing supports
      - Vibration Amplitude/Force Measurement (mV/N, mV/lbf)
        - Typically use hard bearing supports
      - Shaft Phase – rotational timing of measured characteristic (referring to either the accelerations or the vibrational amplitude)
        - Keyphasor ® probe/Tachometer/IR LED Sensor/Optical Encoder
          - Required sample rate based on max rotational frequency
  - Replicate Conditions of constant RPM turbine operation
    - Specify a motor suitable to drive the rotor
      - Required Motor torque (N-m)
      - Motor Power Requirements (Watts, I_stall, V_nom)
      - (NEED) Max Thrust generated by driven WTRA
    - Specify an identical flexible shaft coupling to the motor
      - Type (metric to metric vs. Standard to standard)
      - Size
    - Turbine rotor Parameters
      - Turbine rotor diameter
      - Turbine rotor Weight
    - Specify an Identical bearing to support flexible rotor and overhung mass in balancing system as is used by competition turbine (?)
  - Calibrate out or account for on-the-fly balancing system inherent imbalance

        - Characterize the imbalance of the system prior to running tests with WTRA
        - Use the slow roll approach to correct for shaft eccentricity, sensor signal noise (?)
        - Appropriately filter acceleration data collected at bearing interfaces (?)
    - Process Sensor Data
        - Fast Fourier Transform
        - Filtering
        - Coherence Measurement
        - ...
    - Report Detected Imbalance to User through some graphical display/interface
    - System Safety

Juvinal Factor of Safety selection (good resource) … how much of a driver is blade mass in these equations, for parametric study…

Fab's personal recommendations – really interested in us becoming specialists in this problem in the system so that when we are designing the rig we know why we are doing what we doing, but also giving a well-reasoned, things to watch out for procedure for the senior project team…getting the bigger picture is important, to get the best, high performance…still not getting very close to what does a balancing machine looks like…

Appendix B - House of Quality

QFD: House of Quality
Project: CPWP Balance - Balancing System

Rigid Shaft

Revision: 0.1
Date: 5/7/2020

Correlations	
Positive	+
Negative	−
No Correlation	

Relationships	
Strong	●
Moderate	○
Weak	▽

Direction of Improvement	
Maximize	▲
Target	◇
Minimize	▼

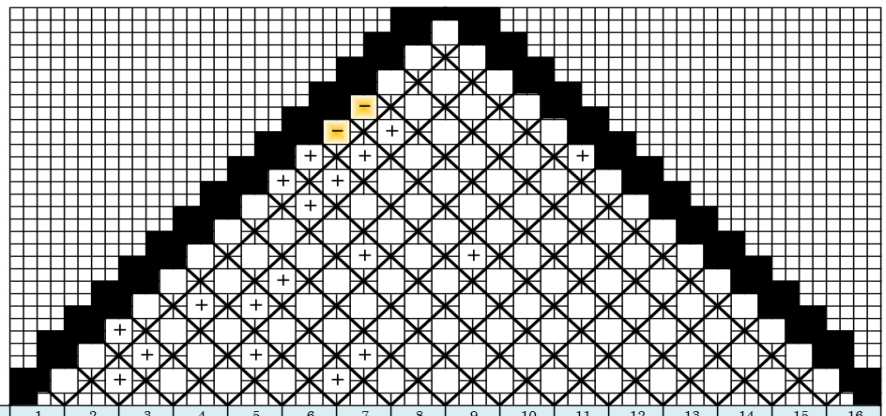

Row #	Weight Chart	Relative Weight	WPC Members (Operator)	Vibrations Lab Operator(s)	CWC Judges		Maximum Relationship	WHO: Customers / HOW: Engineering Specifications — WHAT: Customer Requirements (explicit & implicit)	1 Required Motor Torque to drive WTRA during Rotor Strength Test (N-m)	2 Bearing Type and Size	3 Maximum allowable residual imbalance [g-mm/kg]	4 Motor Power Requirements (kW)	5 ~~Shaft Bow and Deflection Inspection~~	6 Maximum Shake Force (N)	7 Maximum Allowable Blade to Blade static missalignement (mm)	8 Non-Rotating Static Balancing of WTRA allowable residual imbalance (mR tolerance)	9 Ratio of system operating speeds to crtical speeds [rad/s / rad/s]	10 Balancing System Cost ($) - components not sourceable from the vibes lab	11 Operating RPM range for Motor (RPM)	12 Maximum Rotor diameter (m)	13 Maximum Rotor "Weight" (kg)	14 Vibration sensor/Accelerometer Sensitivity (mV/g, mV/N)	15 ISO risk management and balancing machine safety standard compliance (12100-2 7475 2953 1940-1 2)	16 Allowable Balancing System Tare (mR tolerance)	NOW: Current Product Assesment - Customer Requirements: Our Current Product	*Erbessd Instruments EI-30* Rotor Balancing Machine	Pasieo 5 Schneck Universal Balancing Machine	MI 2100 Field Balancer and Instrumentation Kit	RYQ-3 Turbo Charger Balancer	Ranger RWS 1B Field Bubble Wheel Balancer	Row #
Column #									1	2	3	4	5	6	7	8	9	10	11	12	13	14	15	16							
Direction of Improvement									◇	◇	▼	◇	◇	◇	◇	▼	◇	▼	◇	▲	▲	◇	◇							
1		8%	4	5	1		9	Balancing Procedure time required	▽	○	○	▽		▽	○	●			▽				▽	○		4	5	4	4	1	1
2		6%	4	2	1		9	Balancing procedure # of steps	▽	○	▽	▽		▽	○	●			▽				○	▽		4	4	3	4	3	2
3		15%	5	5	5		9	Wind Turbine is Adequately Balanced after application of system and procedure	▽	●	●	▽		●	●	○	●	○		▽	○	○	●	●		4	4	3	5	2	3
4		9%	5	5	1		9	Repeatability of rotor balancing (on the same rotor or with a some components replaced)	▽	●	●	▽		○	●	●	○	○				●	●	●		4	4	3	3	3	4
5		5%	5	1	1		9	Balancing System is able to work with future rotor configurations	○	●	●	○		○	○	○	○	○	○	○	○	○		○		5	4	5	4	3	5
6		8%	5	4	1		9	imbalance measurement components on balancing system correctly characterize WTRA imbalance	○	●	●	○		○	○		▽	●	▽	▽	○	●		○		5	5	5	5	1	6
7		8%	5	4	1		9	Balancing System is can be calibrated/re-calibrated.	▽	●	●	▽		▽	○		○	○	▽			○	●	●		4	3	4	4	3	7
8		15%	5	5	5		9	Balanacing System is safe to operate	●	○	○	○		●	○		●	●	●	●	●		●	○		3	5	4	3	4	8
9		4%	3	1	1		9	~~Want: Balancing system can also serve as run-away test-bed.~~	●	●	▽	●		●	▽		●	●	●	●	●	▽		▽		1	1	1	1	1	9
10		7%	5	3	1		3	The Balancing procedure does not require extensive mechanical vibrations background knowledge to complete			▽				▽	▽		○					○	▽		4	4	4	4	3	10
11		9%	5	5	1		9	Balancing System has an accesible user interface (MATLAB/EES)															●			4	5	5	5	3	11
12		8%	5	1	3		9	Balancing System is within budget constraints										●	●	○	○	●	○			1	1	1	1	5	12
13		0%																												13
14		0%																												14
15		0%																												15
16		0%																												16
								HOW MUCH: Target	Max Non-Stall Motor Torque: 1.1 E04 N-m		Allowable Residual Imbalance: < 10g-mm															
								Max Relationship	9	9	9	9		9	9	9	9	9	9	9	9	9	9							
								Technical Importance Rating	252.1	517	480	164.4	0	386.2	366.3	265.1	372.7	442.7	288.5	231.9	276.6	308.8	557.1	401.7							
								Relative Weight	5%	10%	9%	3%	0%	7%	7%	5%	7%	8%	5%	4%	5%	6%	10%	8%							
								Weight Chart																							
Current Product Assesment - Engineering Specifications								Our Product		TBD	TBD	TBD						500	550-5000	0.45	TBD	TBD	TBD							
								Competitor #1: Erbessd Instruments EI-30 Rotor Balancing Machine		Soft Bearin	2E-5 mm	0.124						N/A	?	0.533	15	N/A	97%							
								Competitor #2: Pasio 5 Schneck Universal Balancing Machine		Soft Bearin	1E-4 mm	0.1						N/A	?	0.15	5	N/A	C							
								Competitor #3: MI 2100 Field Balancer		N/A	0.01 mm	N/A						N/A	180-60000	N/A	N/A	120 mV/g	?							
								Competitor #4: RYQ-3 Turbo Charger Balancer		Soft Bearin	5E-4 mm	0.09						3000	100-10000	0.35	3	N/A	100%							
								Competitor #5: Ranger RWS-1B Bubble Wheel Balancer		N/A	2.0 mm	N/A						155	N/A	N/A	N/A	N/A	N/A							

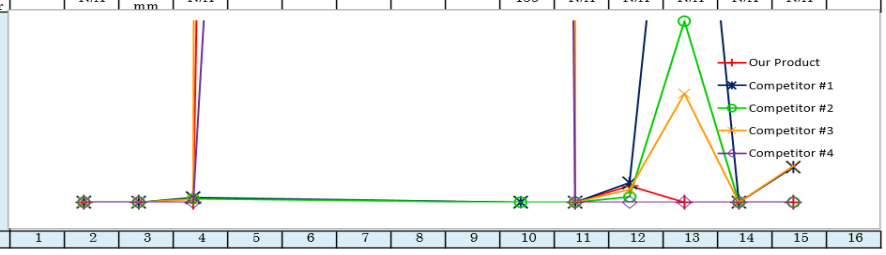

Template Revision: 0.9 Date: 4/23/2010
Christopher Battles

Appendix C - Gantt Chart for CPWP Balance

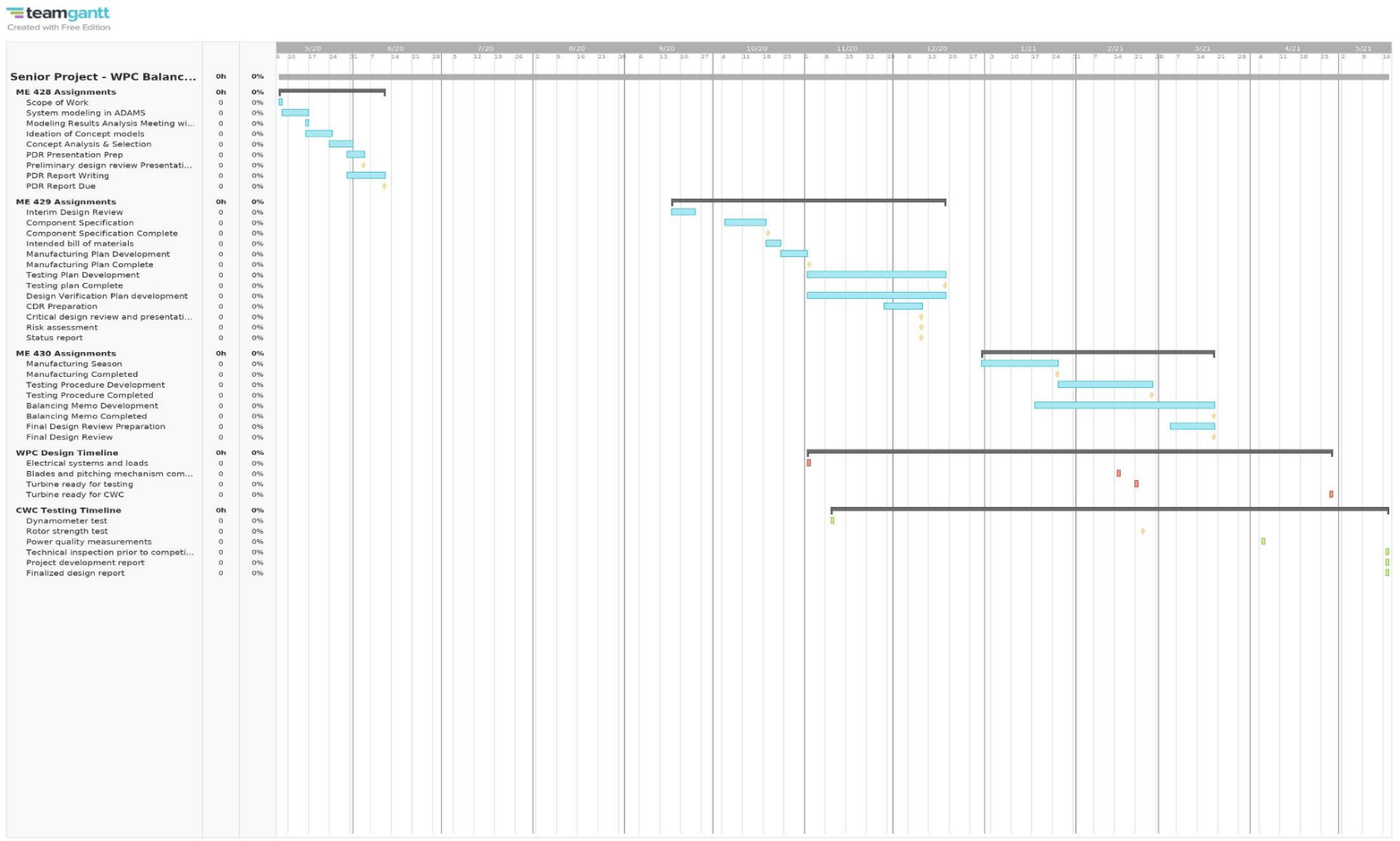

Appendix D – Rigid Shaft Parametric Study

Table D.1 Maximum allowable residual imbalance for variable rotational speeds.

Balancing grade quality, G [mm/s]	Weight of rotor, W [kg]	Rotational speed, N [rpm]	Residual imbalance U [g-mm]	Max. residual imbalance (1-plane) U_{stat} [g-mm]	Max. residual imbalance (2-plane) U_{couple} [g-mm]
16	2.22	100	3391.80	501.98	5167.83
16	2.22	200	1695.90	250.99	2583.91
16	2.22	300	1130.60	167.33	1722.61
16	2.22	400	847.95	125.50	1291.96
16	2.22	500	678.36	100.40	1033.57
16	2.22	600	565.30	83.66	861.30
16	2.22	700	484.54	71.71	738.26
16	2.22	800	423.98	62.75	645.98
16	2.22	900	376.87	55.78	574.20
16	2.22	1000	339.18	50.20	516.78
16	2.22	1100	308.35	45.63	469.80
16	2.22	1200	282.65	41.83	430.65
16	2.22	1300	260.91	38.61	397.53
16	2.22	1400	242.27	35.86	369.13
16	2.22	1500	226.12	33.47	344.52
16	2.22	1600	211.99	31.37	322.99
16	2.22	1700	199.52	29.53	303.99
16	2.22	1800	188.43	27.89	287.10
16	2.22	1900	178.52	26.42	271.99
16	2.22	2000	169.59	25.10	258.39
16	2.22	2100	161.51	23.90	246.09
16	2.22	2200	154.17	22.82	234.90
16	2.22	2300	147.47	21.83	224.69
16	2.22	2400	141.33	20.92	215.33
16	2.22	2500	135.67	20.08	206.71
16	2.22	2600	130.45	19.31	198.76
16	2.22	2700	125.62	18.59	191.40
16	2.22	2800	121.14	17.93	184.57
16	2.22	2900	116.96	17.31	178.20
16	2.22	3000	113.06	16.73	172.26
16	2.22	3100	109.41	16.19	166.70
16	2.22	3200	105.99	15.69	161.49
16	2.22	3300	102.78	15.21	156.60
16	2.22	3400	99.76	14.76	151.99
16	2.22	3500	96.91	14.34	147.65
16	2.22	3600	94.22	13.94	143.55
16	2.22	3700	91.67	13.57	139.67
16	2.22	3800	89.26	13.21	136.00
16	2.22	3900	86.97	12.87	132.51
16	2.22	4000	84.80	12.55	129.20
16	2.22	4100	82.73	12.24	126.04
16	2.22	4200	80.76	11.95	123.04
16	2.22	4300	78.88	11.67	120.18
16	2.22	4400	77.09	11.41	117.45
16	2.22	4500	75.37	11.16	114.84
16	2.22	4600	73.73	10.91	112.34
16	2.22	4700	72.17	10.68	109.95
16	2.22	4800	70.66	10.46	107.66
16	2.22	4900	69.22	10.24	105.47
16	2.22	5000	67.84	10.04	103.36
16	2.22	5100	66.51	9.84	101.33
16	2.22	5200	65.23	9.65	99.38
16	2.22	5300	64.00	9.47	97.51

Table D.2 Maximum allowable residual imbalance for variable rotor plane thickness.

Balancing grade quality, G [mm/s]	Weight of rotor, W [kg]	Rotational speed, N [rpm]	Residual imbalance U [g-mm]	Rotor plane width, b [mm]	Distance from rear bearing to rotor plane, c [mm]	Distance between bearings, d [mm]	Max. residual imbalance (1-plane) U_{stat} [g-mm]	Max. residual imbalance (2-plane) U_{couple} [g-mm]
16	2.22	5300	64.0	1	165.61	98.04	9.47	2352.82
16	2.22	5300	64.0	2	165.61	98.04	9.47	1176.41
16	2.22	5300	64.0	3	165.61	98.04	9.47	784.27
16	2.22	5300	64.0	4	165.61	98.04	9.47	588.21
16	2.22	5300	64.0	5	165.61	98.04	9.47	470.56
16	2.22	5300	64.0	6	165.61	98.04	9.47	392.14
16	2.22	5300	64.0	7	165.61	98.04	9.47	336.12
16	2.22	5300	64.0	8	165.61	98.04	9.47	294.10
16	2.22	5300	64.0	9	165.61	98.04	9.47	261.42
16	2.22	5300	64.0	10	165.61	98.04	9.47	235.28
16	2.22	5300	64.0	11	165.61	98.04	9.47	213.89
16	2.22	5300	64.0	12	165.61	98.04	9.47	196.07
16	2.22	5300	64.0	13	165.61	98.04	9.47	180.99
16	2.22	5300	64.0	14	165.61	98.04	9.47	168.06
16	2.22	5300	64.0	15	165.61	98.04	9.47	156.85
16	2.22	5300	64.0	16	165.61	98.04	9.47	147.05
16	2.22	5300	64.0	17	165.61	98.04	9.47	138.40
16	2.22	5300	64.0	18	165.61	98.04	9.47	130.71
16	2.22	5300	64.0	19	165.61	98.04	9.47	123.83
16	2.22	5300	64.0	20	165.61	98.04	9.47	117.64
16	2.22	5300	64.0	21	165.61	98.04	9.47	112.04
16	2.22	5300	64.0	22	165.61	98.04	9.47	106.95
16	2.22	5300	64.0	23	165.61	98.04	9.47	102.30
16	2.22	5300	64.0	24	165.61	98.04	9.47	98.03
16	2.22	5300	64.0	25	165.61	98.04	9.47	94.11
16	2.22	5300	64.0	26	165.61	98.04	9.47	90.49
16	2.22	5300	64.0	27	165.61	98.04	9.47	87.14
16	2.22	5300	64.0	28	165.61	98.04	9.47	84.03
16	2.22	5300	64.0	29	165.61	98.04	9.47	81.13
16	2.22	5300	64.0	30	165.61	98.04	9.47	78.43
16	2.22	5300	64.0	31	165.61	98.04	9.47	75.90
16	2.22	5300	64.0	32	165.61	98.04	9.47	73.53
16	2.22	5300	64.0	33	165.61	98.04	9.47	71.30
16	2.22	5300	64.0	34	165.61	98.04	9.47	69.20
16	2.22	5300	64.0	35	165.61	98.04	9.47	67.22
16	2.22	5300	64.0	36	165.61	98.04	9.47	65.36
16	2.22	5300	64.0	37	165.61	98.04	9.47	63.59
16	2.22	5300	64.0	38	165.61	98.04	9.47	61.92
16	2.22	5300	64.0	39	165.61	98.04	9.47	60.33
16	2.22	5300	64.0	40	165.61	98.04	9.47	58.82
16	2.22	5300	64.0	41	165.61	98.04	9.47	57.39
16	2.22	5300	64.0	42	165.61	98.04	9.47	56.02
16	2.22	5300	64.0	43	165.61	98.04	9.47	54.72
16	2.22	5300	64.0	44	165.61	98.04	9.47	53.47
16	2.22	5300	64.0	45	165.61	98.04	9.47	52.28
16	2.22	5300	64.0	46	165.61	98.04	9.47	51.15
16	2.22	5300	64.0	47	165.61	98.04	9.47	50.06
16	2.22	5300	64.0	48	165.61	98.04	9.47	49.02
16	2.22	5300	64.0	49	165.61	98.04	9.47	48.02
16	2.22	5300	64.0	50	165.61	98.04	9.47	47.06
16	2.22	5300	64.0	51	165.61	98.04	9.47	46.13
16	2.22	5300	64.0	52	165.61	98.04	9.47	45.25
16	2.22	5300	64.0	53	165.61	98.04	9.47	44.39

Table D.3 Maximum allowable residual imbalance for variable shaft length.

Balancing grade quality, G [mm/s]	Weight of rotor, W [kg]	Rotational speed, N [rpm]	Residual mbalance U [g-mm]	Rotor plane width, b [mm]	Distance from rear bearing to rotor plane, c [mm]	Distance between bearings, d [mm]	Max. residual imbalance (1-plane) U_{max} [g-mm]	Ucoup [g-mm]
16	2.22	5300	64.00	24.13	140	98.04	11.20	97.51
16	2.22	5300	64.00	24.13	141	98.04	11.12	97.51
16	2.22	5300	64.00	24.13	142	98.04	11.05	97.51
16	2.22	5300	64.00	24.13	143	98.04	10.97	97.51
16	2.22	5300	64.00	24.13	144	98.04	10.89	97.51
16	2.22	5300	64.00	24.13	145	98.04	10.82	97.51
16	2.22	5300	64.00	24.13	146	98.04	10.74	97.51
16	2.22	5300	64.00	24.13	147	98.04	10.67	97.51
16	2.22	5300	64.00	24.13	148	98.04	10.60	97.51
16	2.22	5300	64.00	24.13	149	98.04	10.53	97.51
16	2.22	5300	64.00	24.13	150	98.04	10.46	97.51
16	2.22	5300	64.00	24.13	151	98.04	10.39	97.51
16	2.22	5300	64.00	24.13	152	98.04	10.32	97.51
16	2.22	5300	64.00	24.13	153	98.04	10.25	97.51
16	2.22	5300	64.00	24.13	154	98.04	10.19	97.51
16	2.22	5300	64.00	24.13	155	98.04	10.12	97.51
16	2.22	5300	64.00	24.13	156	98.04	10.05	97.51
16	2.22	5300	64.00	24.13	157	98.04	9.99	97.51
16	2.22	5300	64.00	24.13	158	98.04	9.93	97.51
16	2.22	5300	64.00	24.13	159	98.04	9.87	97.51
16	2.22	5300	64.00	24.13	160	98.04	9.80	97.51
16	2.22	5300	64.00	24.13	161	98.04	9.74	97.51
16	2.22	5300	64.00	24.13	162	98.04	9.68	97.51
16	2.22	5300	64.00	24.13	163	98.04	9.62	97.51
16	2.22	5300	64.00	24.13	164	98.04	9.56	97.51
16	2.22	5300	64.00	24.13	165	98.04	9.51	97.51
16	2.22	5300	64.00	24.13	166	98.04	9.45	97.51
16	2.22	5300	64.00	24.13	167	98.04	9.39	97.51
16	2.22	5300	64.00	24.13	168	98.04	9.34	97.51
16	2.22	5300	64.00	24.13	169	98.04	9.28	97.51
16	2.22	5300	64.00	24.13	170	98.04	9.23	97.51
16	2.22	5300	64.00	24.13	171	98.04	9.17	97.51
16	2.22	5300	64.00	24.13	172	98.04	9.12	97.51
16	2.22	5300	64.00	24.13	173	98.04	9.07	97.51
16	2.22	5300	64.00	24.13	174	98.04	9.01	97.51
16	2.22	5300	64.00	24.13	175	98.04	8.96	97.51
16	2.22	5300	64.00	24.13	176	98.04	8.91	97.51
16	2.22	5300	64.00	24.13	177	98.04	8.86	97.51
16	2.22	5300	64.00	24.13	178	98.04	8.81	97.51
16	2.22	5300	64.00	24.13	179	98.04	8.76	97.51
16	2.22	5300	64.00	24.13	180	98.04	8.71	97.51
16	2.22	5300	64.00	24.13	181	98.04	8.67	97.51
16	2.22	5300	64.00	24.13	182	98.04	8.62	97.51
16	2.22	5300	64.00	24.13	183	98.04	8.57	97.51
16	2.22	5300	64.00	24.13	184	98.04	8.52	97.51
16	2.22	5300	64.00	24.13	185	98.04	8.48	97.51
16	2.22	5300	64.00	24.13	186	98.04	8.43	97.51
16	2.22	5300	64.00	24.13	187	98.04	8.39	97.51
16	2.22	5300	64.00	24.13	188	98.04	8.34	97.51
16	2.22	5300	64.00	24.13	189	98.04	8.30	97.51
16	2.22	5300	64.00	24.13	190	98.04	8.26	97.51
16	2.22	5300	64.00	24.13	191	98.04	8.21	97.51
16	2.22	5300	64.00	24.13	192	98.04	8.17	97.51

Table D.4 Maximum allowable residual imbalance for variable bearing spacing.

Balancing grade quality, G [mm/s]	Weight of rotor, W [kg]	Rotational speed, N [rpm]	Residual imbalance U [g-mm]	Rotor plane width, b [mm]	Distance from rear bearing to rotor plane, c [mm]	Distance between bearings, d [mm]	Max. residual imbalance (1-plane) U_{max} [g-mm]	Ucoup [g-mm]
16	2.22	5300	64.00	24.13	165.61	75	7.25	74.59
16	2.22	5300	64.00	24.13	165.61	76	7.34	75.59
16	2.22	5300	64.00	24.13	165.61	77	7.44	76.58
16	2.22	5300	64.00	24.13	165.61	78	7.54	77.58
16	2.22	5300	64.00	24.13	165.61	79	7.63	78.57
16	2.22	5300	64.00	24.13	165.61	80	7.73	79.56
16	2.22	5300	64.00	24.13	165.61	81	7.83	80.56
16	2.22	5300	64.00	24.13	165.61	82	7.92	81.55
16	2.22	5300	64.00	24.13	165.61	83	8.02	82.55
16	2.22	5300	64.00	24.13	165.61	84	8.11	83.54
16	2.22	5300	64.00	24.13	165.61	85	8.21	84.54
16	2.22	5300	64.00	24.13	165.61	86	8.31	85.53
16	2.22	5300	64.00	24.13	165.61	87	8.40	86.53
16	2.22	5300	64.00	24.13	165.61	88	8.50	87.52
16	2.22	5300	64.00	24.13	165.61	89	8.60	88.52
16	2.22	5300	64.00	24.13	165.61	90	8.69	89.51
16	2.22	5300	64.00	24.13	165.61	91	8.79	90.50
16	2.22	5300	64.00	24.13	165.61	92	8.89	91.50
16	2.22	5300	64.00	24.13	165.61	93	8.98	92.49
16	2.22	5300	64.00	24.13	165.61	94	9.08	93.49
16	2.22	5300	64.00	24.13	165.61	95	9.18	94.48
16	2.22	5300	64.00	24.13	165.61	96	9.27	95.48
16	2.22	5300	64.00	24.13	165.61	97	9.37	96.47
16	2.22	5300	64.00	24.13	165.61	98	9.47	97.47
16	2.22	5300	64.00	24.13	165.61	99	9.56	98.46
16	2.22	5300	64.00	24.13	165.61	100	9.66	99.46
16	2.22	5300	64.00	24.13	165.61	101	9.76	100.45
16	2.22	5300	64.00	24.13	165.61	102	9.85	101.44
16	2.22	5300	64.00	24.13	165.61	103	9.95	102.44
16	2.22	5300	64.00	24.13	165.61	104	10.05	103.43
16	2.22	5300	64.00	24.13	165.61	105	10.14	104.43
16	2.22	5300	64.00	24.13	165.61	106	10.24	105.42
16	2.22	5300	64.00	24.13	165.61	107	10.34	106.42
16	2.22	5300	64.00	24.13	165.61	108	10.43	107.41
16	2.22	5300	64.00	24.13	165.61	109	10.53	108.41
16	2.22	5300	64.00	24.13	165.61	110	10.63	109.40
16	2.22	5300	64.00	24.13	165.61	111	10.72	110.40
16	2.22	5300	64.00	24.13	165.61	112	10.82	111.39
16	2.22	5300	64.00	24.13	165.61	113	10.92	112.38
16	2.22	5300	64.00	24.13	165.61	114	11.01	113.38
16	2.22	5300	64.00	24.13	165.61	115	11.11	114.37
16	2.22	5300	64.00	24.13	165.61	116	11.21	115.37
16	2.22	5300	64.00	24.13	165.61	117	11.30	116.36
16	2.22	5300	64.00	24.13	165.61	118	11.40	117.36
16	2.22	5300	64.00	24.13	165.61	119	11.50	118.35
16	2.22	5300	64.00	24.13	165.61	120	11.59	119.35
16	2.22	5300	64.00	24.13	165.61	121	11.69	120.34
16	2.22	5300	64.00	24.13	165.61	122	11.79	121.34
16	2.22	5300	64.00	24.13	165.61	123	11.88	122.33
16	2.22	5300	64.00	24.13	165.61	124	11.98	123.32
16	2.22	5300	64.00	24.13	165.61	125	12.08	124.32
16	2.22	5300	64.00	24.13	165.61	126	12.17	125.31
16	2.22	5300	64.00	24.13	165.61	127	12.27	126.31

Table D.5 Dynamic force at variable rotational speeds.

m [kg]	r [m]	omega [RPM]	omega [rad/sec]	F_dyn [N]
2.22	0.008	100	10.47198	1.947602
2.22	0.008	200	20.94395	7.790408
2.22	0.008	300	31.41593	17.52842
2.22	0.008	400	41.8879	31.16163
2.22	0.008	500	52.35988	48.69005
2.22	0.008	600	62.83185	70.11367
2.22	0.008	700	73.30383	95.43249
2.22	0.008	800	83.7758	124.6465
2.22	0.008	900	94.24778	157.7558
2.22	0.008	1000	104.7198	194.7602
2.22	0.008	1100	115.1917	235.6598
2.22	0.008	1200	125.6637	280.4547
2.22	0.008	1300	136.1357	329.1447
2.22	0.008	1400	146.6077	381.73
2.22	0.008	1500	157.0796	438.2104
2.22	0.008	1600	167.5516	498.5861
2.22	0.008	1700	178.0236	562.857
2.22	0.008	1800	188.4956	631.023
2.22	0.008	1900	198.9675	703.0843
2.22	0.008	2000	209.4395	779.0408
2.22	0.008	2100	219.9115	858.8925
2.22	0.008	2200	230.3835	942.6393
2.22	0.008	2300	240.8554	1030.281
2.22	0.008	2400	251.3274	1121.819
2.22	0.008	2500	261.7994	1217.251
2.22	0.008	2600	272.2714	1316.579
2.22	0.008	2700	282.7433	1419.802
2.22	0.008	2800	293.2153	1526.92
2.22	0.008	2900	303.6873	1637.933
2.22	0.008	3000	314.1593	1752.842
2.22	0.008	3100	324.6312	1871.645
2.22	0.008	3200	335.1032	1994.344
2.22	0.008	3300	345.5752	2120.939
2.22	0.008	3400	356.0472	2251.428
2.22	0.008	3500	366.5191	2385.812
2.22	0.008	3600	376.9911	2524.092
2.22	0.008	3700	387.4631	2666.267
2.22	0.008	3800	397.9351	2812.337
2.22	0.008	3900	408.407	2962.303
2.22	0.008	4000	418.879	3116.163
2.22	0.008	4100	429.351	3273.919
2.22	0.008	4200	439.823	3435.57
2.22	0.008	4300	450.2949	3601.116
2.22	0.008	4400	460.7669	3770.557
2.22	0.008	4500	471.2389	3943.894
2.22	0.008	4600	481.7109	4121.126
2.22	0.008	4700	492.1828	4302.253
2.22	0.008	4800	502.6548	4487.275
2.22	0.008	4900	513.1268	4676.192
2.22	0.008	5000	523.5988	4869.005
2.22	0.008	5100	534.0708	5065.713
2.22	0.008	5200	544.5427	5266.316
2.22	0.008	5300	555.0147	5470.814

Table D.6 Dynamic force at operating speed and variable eccentricity.

m [kg]	r [m]	omega [RPM]	omega [rad/sec]	F_dyn [N]
2.22	0.001	3000	314.1593	219.1052
2.22	0.002	3000	314.1593	438.2104
2.22	0.003	3000	314.1593	657.3157
2.22	0.004	3000	314.1593	876.4209
2.22	0.005	3000	314.1593	1095.526
2.22	0.006	3000	314.1593	1314.631
2.22	0.007	3000	314.1593	1533.737
2.22	0.008	3000	314.1593	1752.842
2.22	0.009	3000	314.1593	1971.947
2.22	0.01	3000	314.1593	2191.052

Table D.7 Dynamic force at runaway test speed and variable eccentricity.

m [kg]	r [m]	omega [RPM]	omega [rad/sec]	F_dyn [N]
2.22	0.001	5300	555.0147	683.8517
2.22	0.002	5300	555.0147	1367.703
2.22	0.003	5300	555.0147	2051.555
2.22	0.004	5300	555.0147	2735.407
2.22	0.005	5300	555.0147	3419.259
2.22	0.006	5300	555.0147	4103.11
2.22	0.007	5300	555.0147	4786.962
2.22	0.008	5300	555.0147	5470.814
2.22	0.009	5300	555.0147	6154.666
2.22	0.01	5300	555.0147	6838.517

Table D.8 Variable wind turbine blade masses and respective eccentricity.

m1 [kg]	m2 [kg]	m3 [kg]	R1 [m]	R2 [m]	R3 [m]	theta_12 [deg]	theta_23 [deg]	theta_31 [deg]	delta_1 [deg]	delta_2 [deg]	delta_3 [deg]	e_x [mm]	e_y [mm]	|e_t| [mm]	Balance Radius [mm]	mb*Rb_x [kg-mm]	mb*Rb_y [kg-mm]	m_b [g]	mR_b [g-mm]
0.74	0.74	0.74	0.075	0.075	0.075	120	120	120	0	30	30	0.0E+00	3.1E-15	3.1E-15	1.5E+01	0.0E+00	0.0E+00	0.0E+00	0.0E+00
0.741	0.7395	0.7395	0.075	0.075	0.075	120	120	120	0	30	30	0.0E+00	5.1E-02	5.1E-02	1.5E+01	0.0E+00	-1.1E-04	7.5E-03	1.1E-01
0.742	0.739	0.739	0.075	0.075	0.075	120	120	120	0	30	30	0.0E+00	1.0E-01	1.0E-01	1.5E+01	0.0E+00	-2.2E-04	1.5E-02	2.2E-01
0.743	0.7385	0.7385	0.075	0.075	0.075	120	120	120	0	30	30	0.0E+00	1.5E-01	1.5E-01	1.5E+01	0.0E+00	-3.4E-04	2.2E-02	3.4E-01
0.744	0.738	0.738	0.075	0.075	0.075	120	120	120	0	30	30	0.0E+00	2.0E-01	2.0E-01	1.5E+01	0.0E+00	-4.5E-04	3.0E-02	4.5E-01
0.745	0.7375	0.7375	0.075	0.075	0.075	120	120	120	0	30	30	0.0E+00	2.5E-01	2.5E-01	1.5E+01	0.0E+00	-5.6E-04	3.7E-02	5.6E-01
0.746	0.737	0.737	0.075	0.075	0.075	120	120	120	0	30	30	0.0E+00	3.0E-01	3.0E-01	1.5E+01	0.0E+00	-6.7E-04	4.5E-02	6.7E-01
0.747	0.7365	0.7365	0.075	0.075	0.075	120	120	120	0	30	30	0.0E+00	3.5E-01	3.5E-01	1.5E+01	0.0E+00	-7.9E-04	5.2E-02	7.9E-01
0.748	0.736	0.736	0.075	0.075	0.075	120	120	120	0	30	30	0.0E+00	4.1E-01	4.1E-01	1.5E+01	0.0E+00	-9.0E-04	6.0E-02	9.0E-01
0.749	0.7355	0.7355	0.075	0.075	0.075	120	120	120	0	30	30	0.0E+00	4.6E-01	4.6E-01	1.5E+01	0.0E+00	-1.0E-03	6.7E-02	1.0E+00
0.75	0.735	0.735	0.075	0.075	0.075	120	120	120	0	30	30	0.0E+00	5.1E-01	5.1E-01	1.5E+01	0.0E+00	-1.1E-03	7.5E-02	1.1E+00
0.751	0.7345	0.7345	0.075	0.075	0.075	120	120	120	0	30	30	0.0E+00	5.6E-01	5.6E-01	1.5E+01	0.0E+00	-1.2E-03	8.2E-02	1.2E+00
0.752	0.734	0.734	0.075	0.075	0.075	120	120	120	0	30	30	0.0E+00	6.1E-01	6.1E-01	1.5E+01	0.0E+00	-1.3E-03	9.0E-02	1.3E+00
0.753	0.7335	0.7335	0.075	0.075	0.075	120	120	120	0	30	30	0.0E+00	6.6E-01	6.6E-01	1.5E+01	0.0E+00	-1.5E-03	9.7E-02	1.5E+00
0.754	0.733	0.733	0.075	0.075	0.075	120	120	120	0	30	30	0.0E+00	7.1E-01	7.1E-01	1.5E+01	0.0E+00	-1.6E-03	1.0E-01	1.6E+00
0.755	0.7325	0.7325	0.075	0.075	0.075	120	120	120	0	30	30	0.0E+00	7.6E-01	7.6E-01	1.5E+01	0.0E+00	-1.7E-03	1.1E-01	1.7E+00
0.756	0.732	0.732	0.075	0.075	0.075	120	120	120	0	30	30	0.0E+00	8.1E-01	8.1E-01	1.5E+01	0.0E+00	-1.8E-03	1.2E-01	1.8E+00
0.757	0.7315	0.7315	0.075	0.075	0.075	120	120	120	0	30	30	0.0E+00	8.6E-01	8.6E-01	1.5E+01	0.0E+00	-1.9E-03	1.3E-01	1.9E+00
0.758	0.731	0.731	0.075	0.075	0.075	120	120	120	0	30	30	0.0E+00	9.1E-01	9.1E-01	1.5E+01	0.0E+00	-2.0E-03	1.3E-01	2.0E+00
0.759	0.7305	0.7305	0.075	0.075	0.075	120	120	120	0	30	30	0.0E+00	9.6E-01	9.6E-01	1.5E+01	0.0E+00	-2.1E-03	1.4E-01	2.1E+00
0.76	0.73	0.73	0.075	0.075	0.075	120	120	120	0	30	30	0.0E+00	1.0E+00	1.0E+00	1.5E+01	0.0E+00	-2.2E-03	1.5E-01	2.2E+00

Table D.9 Variable wind turbine blade alignment and respective eccentricity.

m1 [kg]	m2 [kg]	m3 [kg]	R1 [m]	R2 [m]	R3 [m]	theta_12 [deg]	theta_23 [deg]	theta_31 [deg]	delat_1 [deg]	delta_2 [deg]	delta_3 [deg]	e_x [mm]	e_y [mm]	|e_t| [mm]	Balance Radius [mm]	mb*Rb_x [kg-mm]	mb*Rb_y [kg-mm]	m_b [g]	mR_b [g-mm]
0.74	0.74	0.74	0.075	0.075	0.075	120	120	120	0	30	30	0.0E+00	3.1E-15	3.1E-15	1.5E+01	0.0E+00	0.0E+00	0.0E+00	0.0E+00
0.74	0.74	0.74	0.075	0.075	0.075	120	119.9	120	0	29.9	30	2.2E-02	3.8E-02	4.4E-02	1.5E+01	4.8E-05	-8.4E-05	6.5E-03	9.7E-02
0.74	0.74	0.74	0.075	0.075	0.075	120	119.8	120	0	29.8	30	4.4E-02	7.6E-02	8.7E-02	1.5E+01	9.7E-05	-1.7E-04	1.3E-02	1.9E-01
0.74	0.74	0.74	0.075	0.075	0.075	120	119.7	120	0	29.7	30	6.5E-02	1.1E-01	1.3E-01	1.5E+01	1.4E-04	-2.5E-04	1.9E-02	2.9E-01
0.74	0.74	0.74	0.075	0.075	0.075	120	119.6	120	0	29.6	30	8.7E-02	1.5E-01	1.7E-01	1.5E+01	1.9E-04	-3.4E-04	2.6E-02	3.9E-01
0.74	0.74	0.74	0.075	0.075	0.075	120	119.5	120	0	29.5	30	1.1E-01	1.9E-01	2.2E-01	1.5E+01	2.4E-04	-4.2E-04	3.2E-02	4.8E-01
0.74	0.74	0.74	0.075	0.075	0.075	120	119.4	120	0	29.4	30	1.3E-01	2.3E-01	2.6E-01	1.5E+01	2.9E-04	-5.0E-04	3.9E-02	5.8E-01
0.74	0.74	0.74	0.075	0.075	0.075	120	119.3	120	0	29.3	30	1.5E-01	2.7E-01	3.1E-01	1.5E+01	3.4E-04	-5.9E-04	4.5E-02	6.8E-01
0.74	0.74	0.74	0.075	0.075	0.075	120	119.2	120	0	29.2	30	1.7E-01	3.0E-01	3.5E-01	1.5E+01	3.8E-04	-6.7E-04	5.2E-02	7.7E-01
0.74	0.74	0.74	0.075	0.075	0.075	120	119.1	120	0	29.1	30	1.9E-01	3.4E-01	3.9E-01	1.5E+01	4.3E-04	-7.6E-04	5.8E-02	8.7E-01
0.74	0.74	0.74	0.075	0.075	0.075	120	119	120	0	29	30	2.1E-01	3.8E-01	4.4E-01	1.5E+01	4.8E-04	-8.4E-04	6.5E-02	9.7E-01
0.74	0.74	0.74	0.075	0.075	0.075	120	118.9	120	0	28.9	30	2.4E-01	4.2E-01	4.8E-01	1.5E+01	5.2E-04	-9.3E-04	7.1E-02	1.1E+00
0.74	0.74	0.74	0.075	0.075	0.075	120	118.8	120	0	28.8	30	2.6E-01	4.6E-01	5.2E-01	1.5E+01	5.7E-04	-1.0E-03	7.7E-02	1.2E+00
0.74	0.74	0.74	0.075	0.075	0.075	120	118.7	120	0	28.7	30	2.8E-01	4.9E-01	5.7E-01	1.5E+01	6.2E-04	-1.1E-03	8.4E-02	1.3E+00
0.74	0.74	0.74	0.075	0.075	0.075	120	118.6	120	0	28.6	30	3.0E-01	5.3E-01	6.1E-01	1.5E+01	6.6E-04	-1.2E-03	9.0E-02	1.4E+00
0.74	0.74	0.74	0.075	0.075	0.075	120	118.5	120	0	28.5	30	3.2E-01	5.7E-01	6.5E-01	1.5E+01	7.1E-04	-1.3E-03	9.7E-02	1.5E+00
0.74	0.74	0.74	0.075	0.075	0.075	120	118.4	120	0	28.4	30	3.4E-01	6.1E-01	7.0E-01	1.5E+01	7.6E-04	-1.4E-03	1.0E-01	1.5E+00
0.74	0.74	0.74	0.075	0.075	0.075	120	118.3	120	0	28.3	30	3.6E-01	6.5E-01	7.4E-01	1.5E+01	8.0E-04	-1.4E-03	1.1E-01	1.6E+00
0.74	0.74	0.74	0.075	0.075	0.075	120	118.2	120	0	28.2	30	3.8E-01	6.9E-01	7.9E-01	1.5E+01	8.5E-04	-1.5E-03	1.2E-01	1.7E+00
0.74	0.74	0.74	0.075	0.075	0.075	120	118.1	120	0	28.1	30	4.0E-01	7.2E-01	8.3E-01	1.5E+01	8.9E-04	-1.6E-03	1.2E-01	1.8E+00
0.74	0.74	0.74	0.075	0.075	0.075	120	118	120	0	28	30	4.2E-01	7.6E-01	8.7E-01	1.5E+01	9.4E-04	-1.7E-03	1.3E-01	1.9E+00
0.74	0.74	0.74	0.075	0.075	0.075	120	117.9	120	0	27.9	30	4.4E-01	8.0E-01	9.2E-01	1.5E+01	9.8E-04	-1.8E-03	1.4E-01	2.0E+00
0.74	0.74	0.74	0.075	0.075	0.075	120	117.8	120	0	27.8	30	4.6E-01	8.4E-01	9.6E-01	1.5E+01	1.0E-03	-1.9E-03	1.4E-01	2.1E+00
0.74	0.74	0.74	0.075	0.075	0.075	120	117.7	120	0	27.7	30	4.8E-01	8.8E-01	1.0E+00	1.5E+01	1.1E-03	-2.0E-03	1.5E-01	2.2E+00
0.74	0.74	0.74	0.075	0.075	0.075	120	117.6	120	0	27.6	30	5.0E-01	9.2E-01	1.0E+00	1.5E+01	1.1E-03	-2.0E-03	1.5E-01	2.3E+00
0.74	0.74	0.74	0.075	0.075	0.075	120	117.5	120	0	27.5	30	5.2E-01	9.6E-01	1.1E+00	1.5E+01	1.2E-03	-2.1E-03	1.6E-01	2.4E+00
0.74	0.74	0.74	0.075	0.075	0.075	120	117.4	120	0	27.4	30	5.4E-01	1.0E+00	1.1E+00	1.5E+01	1.2E-03	-2.2E-03	1.7E-01	2.5E+00
0.74	0.74	0.74	0.075	0.075	0.075	120	117.3	120	0	27.3	30	5.6E-01	1.0E+00	1.2E+00	1.5E+01	1.3E-03	-2.3E-03	1.7E-01	2.6E+00
0.74	0.74	0.74	0.075	0.075	0.075	120	117.2	120	0	27.2	30	5.8E-01	1.1E+00	1.2E+00	1.5E+01	1.3E-03	-2.4E-03	1.8E-01	2.7E+00
0.74	0.74	0.74	0.075	0.075	0.075	120	117.1	120	0	27.1	30	6.0E-01	1.1E+00	1.3E+00	1.5E+01	1.3E-03	-2.5E-03	1.9E-01	2.8E+00
0.74	0.74	0.74	0.075	0.075	0.075	120	117	120	0	27	30	6.2E-01	1.2E+00	1.3E+00	1.5E+01	1.4E-03	-2.6E-03	1.9E-01	2.9E+00
0.74	0.74	0.74	0.075	0.075	0.075	120	116.9	120	0	26.9	30	6.4E-01	1.2E+00	1.4E+00	1.5E+01	1.4E-03	-2.6E-03	2.0E-01	3.0E+00
0.74	0.74	0.74	0.075	0.075	0.075	120	116.8	120	0	26.8	30	6.6E-01	1.2E+00	1.4E+00	1.5E+01	1.5E-03	-2.7E-03	2.1E-01	3.1E+00
0.74	0.74	0.74	0.075	0.075	0.075	120	116.7	120	0	26.7	30	6.8E-01	1.3E+00	1.4E+00	1.5E+01	1.5E-03	-2.8E-03	2.1E-01	3.2E+00
0.74	0.74	0.74	0.075	0.075	0.075	120	116.6	120	0	26.6	30	7.0E-01	1.3E+00	1.5E+00	1.5E+01	1.6E-03	-2.9E-03	2.2E-01	3.3E+00
0.74	0.74	0.74	0.075	0.075	0.075	120	116.5	120	0	26.5	30	7.2E-01	1.3E+00	1.5E+00	1.5E+01	1.6E-03	-3.0E-03	2.3E-01	3.4E+00
0.74	0.74	0.74	0.075	0.075	0.075	120	116.4	120	0	26.4	30	7.4E-01	1.4E+00	1.6E+00	1.5E+01	1.6E-03	-3.1E-03	2.3E-01	3.5E+00
0.74	0.74	0.74	0.075	0.075	0.075	120	116.3	120	0	26.3	30	7.6E-01	1.4E+00	1.6E+00	1.5E+01	1.7E-03	-3.2E-03	2.4E-01	3.6E+00
0.74	0.74	0.74	0.075	0.075	0.075	120	116.2	120	0	26.2	30	7.8E-01	1.5E+00	1.7E+00	1.5E+01	1.7E-03	-3.2E-03	2.5E-01	3.7E+00
0.74	0.74	0.74	0.075	0.075	0.075	120	116.1	120	0	26.1	30	8.0E-01	1.5E+00	1.7E+00	1.5E+01	1.8E-03	-3.3E-03	2.5E-01	3.8E+00
0.74	0.74	0.74	0.075	0.075	0.075	120	116	120	0	26	30	8.2E-01	1.5E+00	1.7E+00	1.5E+01	1.8E-03	-3.4E-03	2.6E-01	3.9E+00
0.74	0.74	0.74	0.075	0.075	0.075	120	115.9	120	0	25.9	30	8.4E-01	1.6E+00	1.8E+00	1.5E+01	1.9E-03	-3.5E-03	2.6E-01	4.0E+00
0.74	0.74	0.74	0.075	0.075	0.075	120	115.8	120	0	25.8	30	8.6E-01	1.6E+00	1.8E+00	1.5E+01	1.9E-03	-3.6E-03	2.7E-01	4.1E+00
0.74	0.74	0.74	0.075	0.075	0.075	120	115.7	120	0	25.7	30	8.8E-01	1.7E+00	1.9E+00	1.5E+01	1.9E-03	-3.7E-03	2.8E-01	4.2E+00
0.74	0.74	0.74	0.075	0.075	0.075	120	115.6	120	0	25.6	30	9.0E-01	1.7E+00	1.9E+00	1.5E+01	2.0E-03	-3.8E-03	2.8E-01	4.3E+00
0.74	0.74	0.74	0.075	0.075	0.075	120	115.5	120	0	25.5	30	9.1E-01	1.7E+00	2.0E+00	1.5E+01	2.0E-03	-3.9E-03	2.9E-01	4.4E+00
0.74	0.74	0.74	0.075	0.075	0.075	120	115.4	120	0	25.4	30	9.3E-01	1.8E+00	2.0E+00	1.5E+01	2.1E-03	-3.9E-03	3.0E-01	4.5E+00
0.74	0.74	0.74	0.075	0.075	0.075	120	115.3	120	0	25.3	30	9.5E-01	1.8E+00	2.1E+00	1.5E+01	2.1E-03	-4.0E-03	3.0E-01	4.6E+00
0.74	0.74	0.74	0.075	0.075	0.075	120	115.2	120	0	25.2	30	9.7E-01	1.9E+00	2.1E+00	1.5E+01	2.2E-03	-4.1E-03	3.1E-01	4.6E+00
0.74	0.74	0.74	0.075	0.075	0.075	120	115.1	120	0	25.1	30	9.9E-01	1.9E+00	2.1E+00	1.5E+01	2.2E-03	-4.2E-03	3.2E-01	4.7E+00
0.74	0.74	0.74	0.075	0.075	0.075	120	115	120	0	25	30	1.0E+00	1.9E+00	2.2E+00	1.5E+01	2.2E-03	-4.3E-03	3.2E-01	4.8E+00

Table D.10 Variable eccentricity between center of rotation and center of mass.

m1 [kg]	m2 [kg]	m3 [kg]	R1 [m]	R2 [m]	R3 [m]	theta_12 [deg]	theta_23 [deg]	theta_31 [deg]	delat_1 [deg]	delta_2 [deg]	delta_3 [deg]	e_x [mm]	e_y [mm]	|e_t| [mm]	Balance Radius [mm]	mb*Rb_x [kg-mm]	mb*Rb_y [kg-mm]	m_b [g]	mR_b [g-mm]
0.74	0.74	0.74	0.075	0.075	0.075	120	120	120	0	30	30	0.0E+00	3.1E-15	3.1E-15	1.5E+01	0.0E+00	0.0E+00	0.0E+00	0.0E+00
0.74	0.74	0.74	0.075	0.076	0.075	120	120	120	0	30	30	2.9E-01	1.7E-01	3.3E-01	1.5E+01	-6.4E-04	-7.4E-04	6.5E-02	9.8E-01
0.74	0.74	0.74	0.075	0.077	0.075	120	120	120	0	30	30	5.8E-01	3.3E-01	6.7E-01	1.5E+01	-1.3E-03	-1.5E-03	1.3E-01	2.0E+00
0.74	0.74	0.74	0.075	0.078	0.075	120	120	120	0	30	30	8.7E-01	5.0E-01	1.0E+00	1.5E+01	-1.9E-03	-2.2E-03	2.0E-01	2.9E+00
0.74	0.74	0.74	0.075	0.079	0.075	120	120	120	0	30	30	1.2E+00	6.7E-01	1.3E+00	1.5E+01	-2.6E-03	-3.0E-03	2.6E-01	3.9E+00
0.74	0.74	0.74	0.075	0.08	0.075	120	120	120	0	30	30	1.4E+00	8.3E-01	1.7E+00	1.5E+01	-3.2E-03	-3.7E-03	3.3E-01	4.9E+00
0.74	0.74	0.74	0.075	0.081	0.075	120	120	120	0	30	30	1.7E+00	1.0E+00	2.0E+00	1.5E+01	-3.8E-03	-4.4E-03	3.9E-01	5.9E+00
0.74	0.74	0.74	0.075	0.082	0.075	120	120	120	0	30	30	2.0E+00	1.2E+00	2.3E+00	1.5E+01	-4.5E-03	-5.2E-03	4.6E-01	6.9E+00
0.74	0.74	0.74	0.075	0.083	0.075	120	120	120	0	30	30	2.3E+00	1.3E+00	2.7E+00	1.5E+01	-5.1E-03	-5.9E-03	5.2E-01	7.8E+00
0.74	0.74	0.74	0.075	0.084	0.075	120	120	120	0	30	30	2.6E+00	1.5E+00	3.0E+00	1.5E+01	-5.8E-03	-6.7E-03	5.9E-01	8.8E+00
0.74	0.74	0.74	0.075	0.085	0.075	120	120	120	0	30	30	2.9E+00	1.7E+00	3.3E+00	1.5E+01	-6.4E-03	-7.4E-03	6.5E-01	9.8E+00

Appendix E – SolidWorks Frequency Analysis Results

Table E.1.a Frequency ratio calculations over increasing system operating speeds

Sytem Speeds [RPM]	System Frequencies (rad/sec)	Frequency ratio 1 (omega_in / omega_n)	Frequency ratio 2 (omega_in / omega_n)	Frequency ratio 3 (omega_in / omega_n)	Frequency ratio 4 (omega_in / omega_n)	Frequency ratio 5 (omega_in / omega_n)	Frequency ratio 6 (omega_in / omega_n)
0	0	0	0	0	0	0	0
100	1.05E+01	1.25E+04	1.11E+01	4.98E-02	4.79E-02	1.01E-02	9.87E-03
200	2.09E+01	2.50E+04	2.22E+01	9.96E-02	9.58E-02	2.02E-02	1.97E-02
300	3.14E+01	3.75E+04	3.33E+01	1.49E-01	1.44E-01	3.03E-02	2.96E-02
400	4.19E+01	5.00E+04	4.45E+01	1.99E-01	1.92E-01	4.04E-02	3.95E-02
500	5.24E+01	6.26E+04	5.56E+01	2.49E-01	2.40E-01	5.05E-02	4.94E-02
600	6.28E+01	7.51E+04	6.67E+01	2.99E-01	2.87E-01	6.06E-02	5.92E-02
700	7.33E+01	8.76E+04	7.78E+01	3.49E-01	3.35E-01	7.07E-02	6.91E-02
800	8.38E+01	1.00E+05	8.89E+01	3.98E-01	3.83E-01	8.08E-02	7.90E-02
900	9.42E+01	1.13E+05	1.00E+02	4.48E-01	4.31E-01	9.09E-02	8.88E-02
1000	1.05E+02	1.25E+05	1.11E+02	4.98E-01	4.79E-01	1.01E-01	9.87E-02
1100	1.15E+02	1.38E+05	1.22E+02	5.48E-01	5.27E-01	1.11E-01	1.09E-01
1200	1.26E+02	1.50E+05	1.33E+02	5.98E-01	5.75E-01	1.21E-01	1.18E-01
1300	1.36E+02	1.63E+05	1.44E+02	6.47E-01	6.23E-01	1.31E-01	1.28E-01
1400	1.47E+02	1.75E+05	1.56E+02	6.97E-01	6.71E-01	1.41E-01	1.38E-01
1500	1.57E+02	1.88E+05	1.67E+02	7.47E-01	7.19E-01	1.52E-01	1.48E-01
1600	1.68E+02	2.00E+05	1.78E+02	7.97E-01	7.67E-01	1.62E-01	1.58E-01
1700	1.78E+02	2.13E+05	1.89E+02	8.47E-01	8.14E-01	1.72E-01	1.68E-01
1800	1.88E+02	2.25E+05	2.00E+02	8.96E-01	8.62E-01	1.82E-01	1.78E-01
1900	1.99E+02	2.38E+05	2.11E+02	9.46E-01	9.10E-01	1.92E-01	1.88E-01
2000	2.09E+02	2.50E+05	2.22E+02	9.96E-01	9.58E-01	2.02E-01	1.97E-01
2100	2.20E+02	2.63E+05	2.33E+02	1.05E+00	1.01E+00	2.12E-01	2.07E-01
2200	2.30E+02	2.75E+05	2.44E+02	1.10E+00	1.05E+00	2.22E-01	2.17E-01
2300	2.41E+02	2.88E+05	2.56E+02	1.15E+00	1.10E+00	2.32E-01	2.27E-01
2400	2.51E+02	3.00E+05	2.67E+02	1.20E+00	1.15E+00	2.42E-01	2.37E-01
2500	2.62E+02	3.13E+05	2.78E+02	1.25E+00	1.20E+00	2.53E-01	2.47E-01
2600	2.72E+02	3.25E+05	2.89E+02	1.29E+00	1.25E+00	2.63E-01	2.57E-01
2700	2.83E+02	3.38E+05	3.00E+02	1.34E+00	1.29E+00	2.73E-01	2.67E-01
2800	2.93E+02	3.50E+05	3.11E+02	1.39E+00	1.34E+00	2.83E-01	2.76E-01
2900	3.04E+02	3.63E+05	3.22E+02	1.44E+00	1.39E+00	2.93E-01	2.86E-01
3000	3.14E+02	3.75E+05	3.33E+02	1.49E+00	1.44E+00	3.03E-01	2.96E-01
3100	3.25E+02	3.88E+05	3.44E+02	1.54E+00	1.49E+00	3.13E-01	3.06E-01
3200	3.35E+02	4.00E+05	3.56E+02	1.59E+00	1.53E+00	3.23E-01	3.16E-01
3300	3.46E+02	4.13E+05	3.67E+02	1.64E+00	1.58E+00	3.33E-01	3.26E-01
3400	3.56E+02	4.25E+05	3.78E+02	1.69E+00	1.63E+00	3.44E-01	3.36E-01
3500	3.67E+02	4.38E+05	3.89E+02	1.74E+00	1.68E+00	3.54E-01	3.45E-01
3600	3.77E+02	4.50E+05	4.00E+02	1.79E+00	1.72E+00	3.64E-01	3.55E-01
3700	3.87E+02	4.63E+05	4.11E+02	1.84E+00	1.77E+00	3.74E-01	3.65E-01
3800	3.98E+02	4.75E+05	4.22E+02	1.89E+00	1.82E+00	3.84E-01	3.75E-01
3900	4.08E+02	4.88E+05	4.33E+02	1.94E+00	1.87E+00	3.94E-01	3.85E-01
4000	4.19E+02	5.00E+05	4.45E+02	1.99E+00	1.92E+00	4.04E-01	3.95E-01
4100	4.29E+02	5.13E+05	4.56E+02	2.04E+00	1.96E+00	4.14E-01	4.05E-01
4200	4.40E+02	5.26E+05	4.67E+02	2.09E+00	2.01E+00	4.24E-01	4.15E-01
4300	4.50E+02	5.38E+05	4.78E+02	2.14E+00	2.06E+00	4.34E-01	4.24E-01
4400	4.61E+02	5.51E+05	4.89E+02	2.19E+00	2.11E+00	4.45E-01	4.34E-01
4500	4.71E+02	5.63E+05	5.00E+02	2.24E+00	2.16E+00	4.55E-01	4.44E-01
4600	4.82E+02	5.76E+05	5.11E+02	2.29E+00	2.20E+00	4.65E-01	4.54E-01
4700	4.92E+02	5.88E+05	5.22E+02	2.34E+00	2.25E+00	4.75E-01	4.64E-01
4800	5.03E+02	6.01E+05	5.33E+02	2.39E+00	2.30E+00	4.85E-01	4.74E-01
4900	5.13E+02	6.13E+05	5.45E+02	2.44E+00	2.35E+00	4.95E-01	4.84E-01
5000	5.24E+02	6.26E+05	5.56E+02	2.49E+00	2.40E+00	5.05E-01	4.94E-01
5100	5.34E+02	6.38E+05	5.67E+02	2.54E+00	2.44E+00	5.15E-01	5.03E-01
5200	5.45E+02	6.51E+05	5.78E+02	2.59E+00	2.49E+00	5.25E-01	5.13E-01
5300	5.55E+02	6.63E+05	5.89E+02	2.64E+00	2.54E+00	5.35E-01	5.23E-01
5400	5.65E+02	6.76E+05	6.00E+02	2.69E+00	2.59E+00	5.46E-01	5.33E-01
5500	5.76E+02	6.88E+05	6.11E+02	2.74E+00	2.63E+00	5.56E-01	5.43E-01
5600	5.86E+02	7.01E+05	6.22E+02	2.79E+00	2.68E+00	5.66E-01	5.53E-01
5700	5.97E+02	7.13E+05	6.33E+02	2.84E+00	2.73E+00	5.76E-01	5.63E-01
5800	6.07E+02	7.26E+05	6.45E+02	2.89E+00	2.78E+00	5.86E-01	5.73E-01

Table E.1.b Transmissibility - undamped calculations over increasing system operating speeds

Transmissibilty 1	Transmissibilty 2	Transmissibilty 3	Transmissibilty 4	Transmissibilty 5	Transmissibilty 6
|G(omega_in)|	|G(omega_in)|	|G(omega_in)|	|G(omega_in)|	|G(omega_in)|	|G(omega_in)|
1	1	1	1	1	1
6.39E-09	8.16E-03	1.00E+00	1.00E+00	1.00E+00	1.00E+00
1.60E-09	2.03E-03	1.01E+00	1.01E+00	1.00E+00	1.00E+00
7.10E-10	9.01E-04	1.02E+00	1.02E+00	1.00E+00	1.00E+00
3.99E-10	5.06E-04	1.04E+00	1.04E+00	1.00E+00	1.00E+00
2.55E-10	3.24E-04	1.07E+00	1.06E+00	1.00E+00	1.00E+00
1.77E-10	2.25E-04	1.10E+00	1.09E+00	1.00E+00	1.00E+00
1.30E-10	1.65E-04	1.14E+00	1.13E+00	1.01E+00	1.00E+00
9.98E-11	1.27E-04	1.19E+00	1.17E+00	1.01E+00	1.01E+00
7.89E-11	1.00E-04	1.25E+00	1.23E+00	1.01E+00	1.01E+00
6.39E-11	8.10E-05	1.33E+00	1.30E+00	1.01E+00	1.01E+00
5.28E-11	6.69E-05	1.43E+00	1.38E+00	1.01E+00	1.01E+00
4.44E-11	5.62E-05	1.56E+00	1.49E+00	1.01E+00	1.01E+00
3.78E-11	4.79E-05	1.72E+00	1.63E+00	1.02E+00	1.02E+00
3.26E-11	4.13E-05	1.95E+00	1.82E+00	1.02E+00	1.02E+00
2.84E-11	3.60E-05	2.26E+00	2.07E+00	1.02E+00	1.02E+00
2.50E-11	3.16E-05	2.74E+00	2.42E+00	1.03E+00	1.03E+00
2.21E-11	2.80E-05	3.53E+00	2.97E+00	1.03E+00	1.03E+00
1.97E-11	2.50E-05	5.09E+00	3.90E+00	1.03E+00	1.03E+00
1.77E-11	2.24E-05	9.56E+00	5.83E+00	1.04E+00	1.04E+00
1.60E-11	2.02E-05	1.27E+02	1.22E+01	1.04E+00	1.04E+00
1.45E-11	1.84E-05	1.07E+01	8.26E+01	1.05E+00	1.04E+00
1.32E-11	1.67E-05	4.99E+00	9.03E+00	1.05E+00	1.05E+00
1.21E-11	1.53E-05	3.20E+00	4.67E+00	1.06E+00	1.05E+00
1.11E-11	1.41E-05	2.33E+00	3.11E+00	1.06E+00	1.06E+00
1.02E-11	1.30E-05	1.82E+00	2.30E+00	1.07E+00	1.06E+00
9.45E-12	1.20E-05	1.48E+00	1.81E+00	1.07E+00	1.07E+00
8.76E-12	1.11E-05	1.24E+00	1.49E+00	1.08E+00	1.08E+00
8.15E-12	1.03E-05	1.06E+00	1.25E+00	1.09E+00	1.08E+00
7.60E-12	9.63E-06	9.21E-01	1.08E+00	1.09E+00	1.09E+00
7.10E-12	9.00E-06	8.11E-01	9.39E-01	1.10E+00	1.10E+00
6.65E-12	8.43E-06	7.23E-01	8.30E-01	1.11E+00	1.10E+00
6.24E-12	7.91E-06	6.49E-01	7.41E-01	1.12E+00	1.11E+00
5.87E-12	7.44E-06	5.88E-01	6.67E-01	1.13E+00	1.12E+00
5.53E-12	7.01E-06	5.36E-01	6.05E-01	1.13E+00	1.13E+00
5.21E-12	6.61E-06	4.91E-01	5.52E-01	1.14E+00	1.14E+00
4.93E-12	6.25E-06	4.52E-01	5.06E-01	1.15E+00	1.14E+00
4.67E-12	5.92E-06	4.17E-01	4.67E-01	1.16E+00	1.15E+00
4.42E-12	5.61E-06	3.87E-01	4.32E-01	1.17E+00	1.16E+00
4.20E-12	5.32E-06	3.61E-01	4.01E-01	1.18E+00	1.17E+00
3.99E-12	5.06E-06	3.37E-01	3.74E-01	1.20E+00	1.18E+00
3.80E-12	4.82E-06	3.16E-01	3.50E-01	1.21E+00	1.20E+00
3.62E-12	4.59E-06	2.96E-01	3.28E-01	1.22E+00	1.21E+00
3.45E-12	4.38E-06	2.79E-01	3.08E-01	1.23E+00	1.22E+00
3.30E-12	4.18E-06	2.63E-01	2.90E-01	1.25E+00	1.23E+00
3.15E-12	4.00E-06	2.49E-01	2.74E-01	1.26E+00	1.25E+00
3.02E-12	3.83E-06	2.35E-01	2.59E-01	1.28E+00	1.26E+00
2.89E-12	3.67E-06	2.23E-01	2.46E-01	1.29E+00	1.27E+00
2.77E-12	3.51E-06	2.12E-01	2.33E-01	1.31E+00	1.29E+00
2.66E-12	3.37E-06	2.02E-01	2.22E-01	1.32E+00	1.31E+00
2.55E-12	3.24E-06	1.92E-01	2.11E-01	1.34E+00	1.32E+00
2.46E-12	3.11E-06	1.83E-01	2.01E-01	1.36E+00	1.34E+00
2.36E-12	2.99E-06	1.75E-01	1.92E-01	1.38E+00	1.36E+00
2.27E-12	2.88E-06	1.68E-01	1.84E-01	1.40E+00	1.38E+00
2.19E-12	2.78E-06	1.60E-01	1.76E-01	1.42E+00	1.40E+00
2.11E-12	2.68E-06	1.54E-01	1.68E-01	1.45E+00	1.42E+00
2.04E-12	2.58E-06	1.48E-01	1.61E-01	1.47E+00	1.44E+00
1.97E-12	2.49E-06	1.42E-01	1.55E-01	1.50E+00	1.46E+00
1.90E-12	2.41E-06	1.36E-01	1.49E-01	1.52E+00	1.49E+00

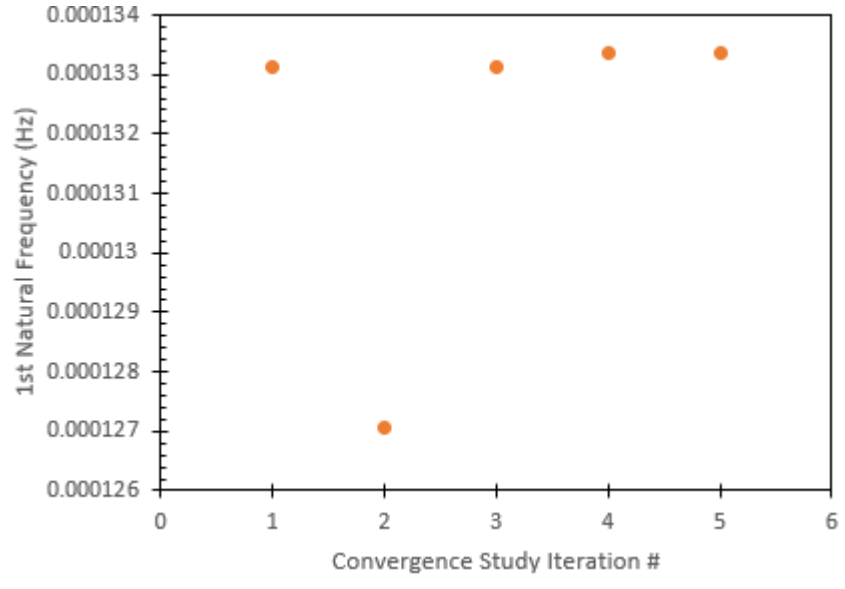

Figure E.2 1st Modal Frequency Mesh Convergence.

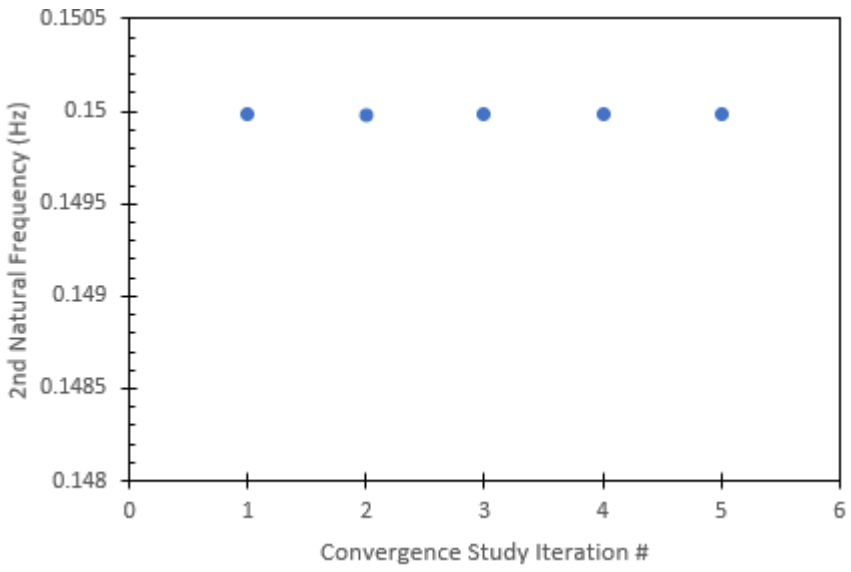

Figure E.3 2nd Modal Frequency Mesh Convergence.

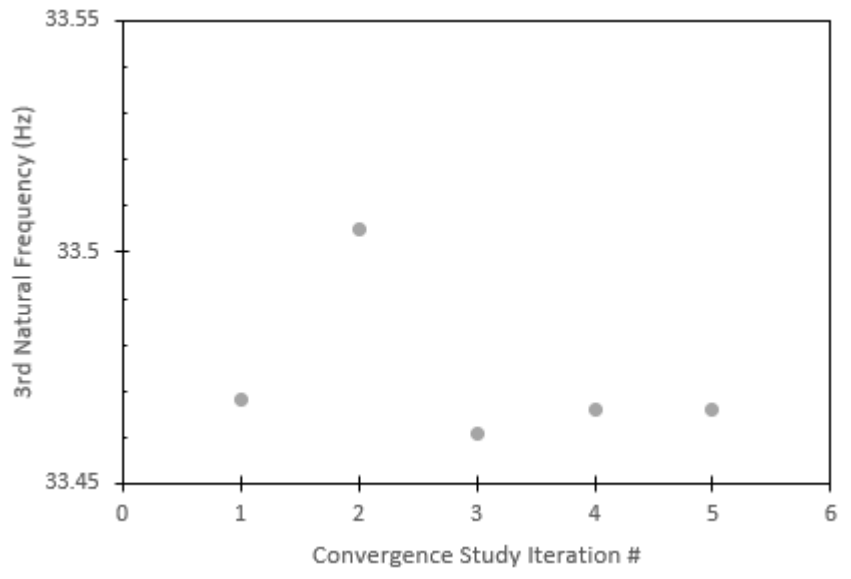

Figure E.4 3rd Modal Frequency Mesh Convergence.

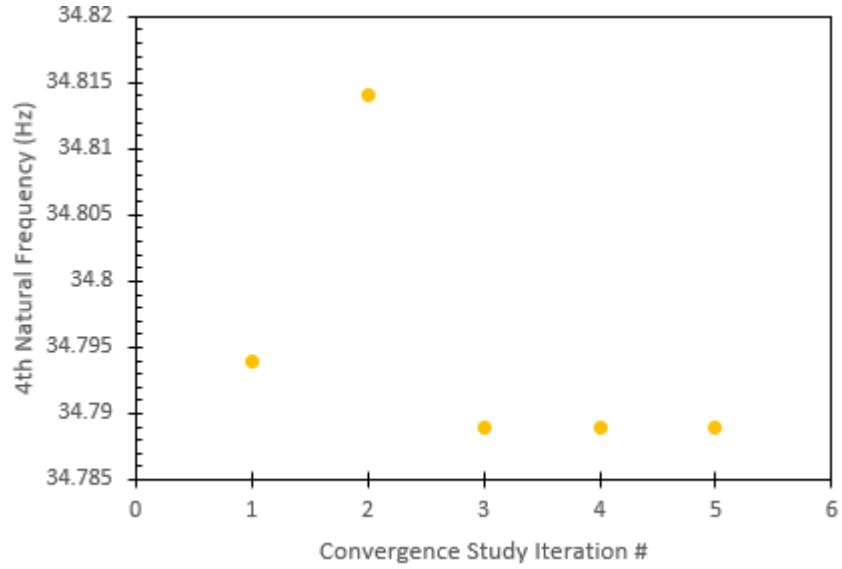

Figure E.5 4th Modal Frequency Mesh Convergence.

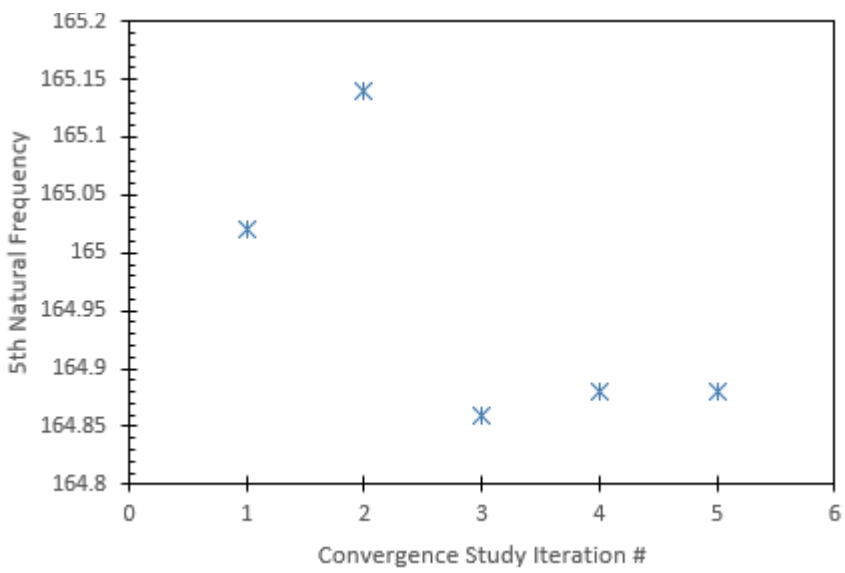

Figure E.6 5th Modal Frequency Mesh Convergence.

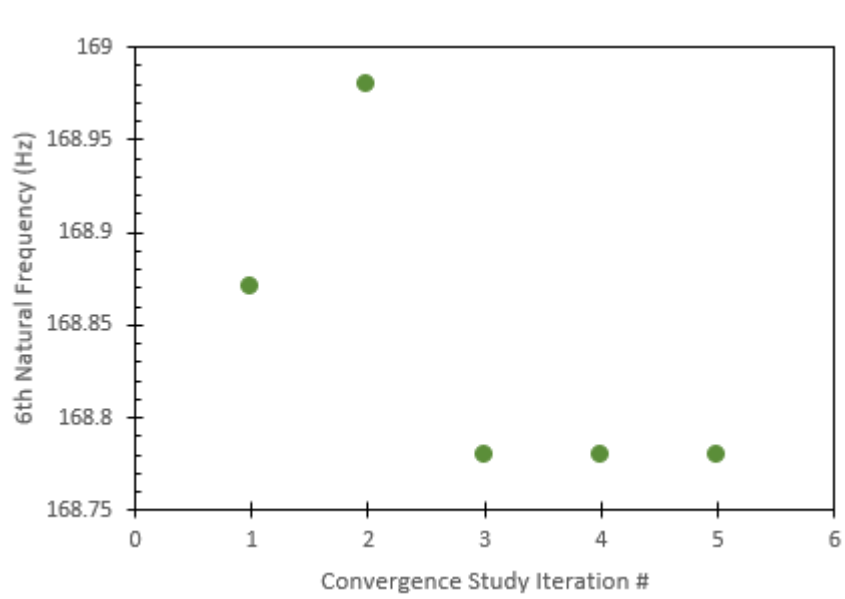

Figure E.7 6th Modal Frequency Mesh Convergence.

Table E.8 Mesh Convergence Study with Each Natural Frequency (Hz)

		Global Element Size Max / Minimum Element Size [mm]				
		14/2.9	29/4	25/5	35/7	40/8.5
Mode #	1	0.00013314	0.000127	0.000133	0.000133	0.000133
	2	0.14998	0.14998	0.14998	0.14998	0.14998
	3	33.468	33.505	33.461	33.466	33.466
	4	34.794	34.814	34.789	34.789	34.789
	5	165.02	165.14	164.86	164.88	164.88
	6	168.87	168.98	168.78	168.78	168.78

Table E.9 Lower bound operating speed frequencies.

	F1	F2	F3	F4	F5	F6	Units
Lamda_operating LB	261.7994	261.7993878	261.7993878	261.7993878	261.7993878	261.7993878	[rad/sec]
lamda_critcal	0.000837	0.94235	210.2675	218.5925	1,036.46	1,060.84	[rad/sec]
lamda_margin	261.7986	260.8570378	51.5318878	43.2068878	774.6606122	799.0406122	[rad/sec]
Frequency Margin_L	0.000711	0.8009975	178.727375	185.803625	880.991	901.714	[rad/sec]
Frequency Margin_U	0.000962	1.0837025	241.807625	251.381375	1191.929	1219.966	[rad/sec]
Frequency Ratio (%)	31280569	27681.54484	24.50777595	19.76595162	74.74100421	75.32150109	[-]

Table E.10 Upper bound operating speed frequencies.

	F1	F2	F3	F4	F5	F6	Units
Lamda_operating UB	314.1593	314.1592654	314.1592654	314.1592654	314.1592654	314.1592654	[rad/sec]
lamda_critcal	0.000837	0.94235	210.2675	218.5925	1036.46	1060.84	[rad/sec]
lamda_margin	314.1584	313.2169154	103.8917654	95.56676536	722.3007346	746.6807346	[rad/sec]
Frequency Margin_L	0.000711	0.8009975	178.727375	185.803625	880.991	901.714	[rad/sec]
Frequency Margin_U	0.000962	1.0837025	241.807625	251.381375	1191.929	1219.966	[rad/sec]
Frequency Ratio (%)	37536703	33237.85381	49.40933114	43.71914195	69.68920505	70.38580131	[-]

Table E.11 Lower bound runaway test speed frequencies.

	F1	F2	F3	F4	F5	F6	Units
Lamda_Runaway_LB	408.407	408.407045	408.407045	408.407045	408.407045	408.407045	[rad/sec]
lamda_critcal	0.000837	0.94235	210.2675	218.5925	1036.46	1060.84	[rad/sec]
lamda_margin	408.4062	407.464695	198.139545	189.814545	628.052955	652.432955	[rad/sec]
Frequency Margin_L	0.000711	0.8009975	178.727375	185.803625	880.991	901.714	[rad/sec]
Frequency Margin_U	0.000962	1.0837025	241.807625	251.381375	1191.929	1219.966	[rad/sec]
Frequency Ratio (%)	48797744	43239.20995	94.23213048	86.83488453	60.59596656	61.50154171	[-]

Table E.12 Upper bound runaway test speed frequencies.

	F1	F2	F3	F4	F5	F6	Units
Lamda_Runaway_UB	555.0147	555.0147021	555.0147021	555.0147021	555.0147021	555.0147021	[rad/sec]
lamda_critcal	0.000837	0.94235	210.2675	218.5925	1036.46	1060.84	[rad/sec]
lamda_margin	555.0139	554.0723521	344.7472021	336.4222021	481.4452979	505.8252979	[rad/sec]
Frequency Margin_L	0.000711	0.8009975	178.727375	185.803625	880.991	901.714	[rad/sec]
Frequency Margin_U	0.000962	1.0837025	241.807625	251.381375	1191.929	1219.966	[rad/sec]
Frequency Ratio (%)	66314918	58796.87506	163.956485	153.9038174	46.45092892	47.68158232	[-]

Appendix F – Initial Concept Block Diagram & Ideation

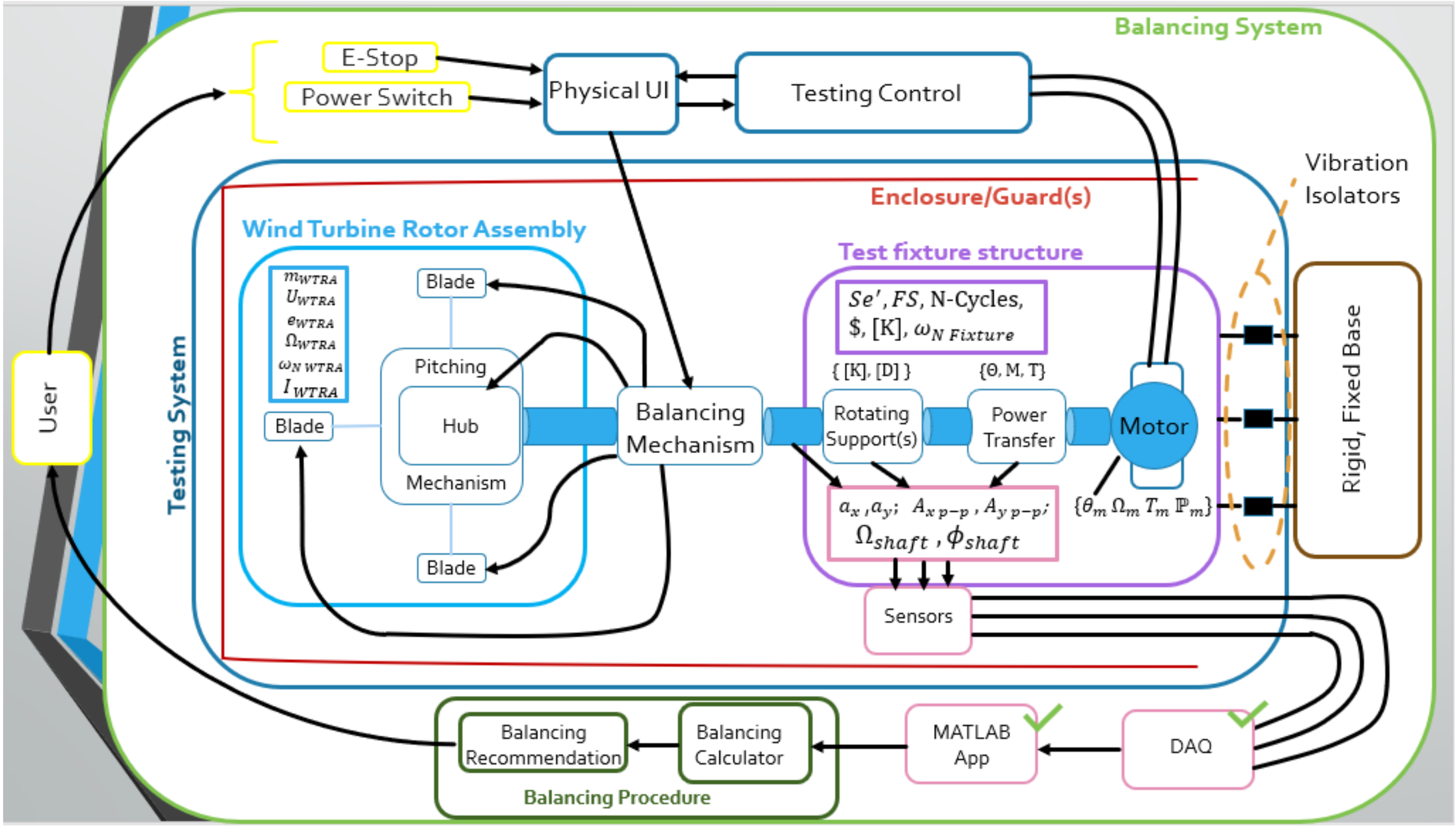

Figure F.1 Enlarged view of concept design block diagram. A flow chart like representation of our design space was employed as we have not yet selected a final concept for our balancing system and mechanism nor finalized the balancing procedure. Parameters in color coated boxes represent variables that characterize dynamic behavior or will drive design as well as concept selection in our system. Parameters in curly braces attached to various components shown on the flow chart represent system/model inputs. Again, our three primary deliverables are the balancing system, the balancing mechanism, and the balancing procedure.

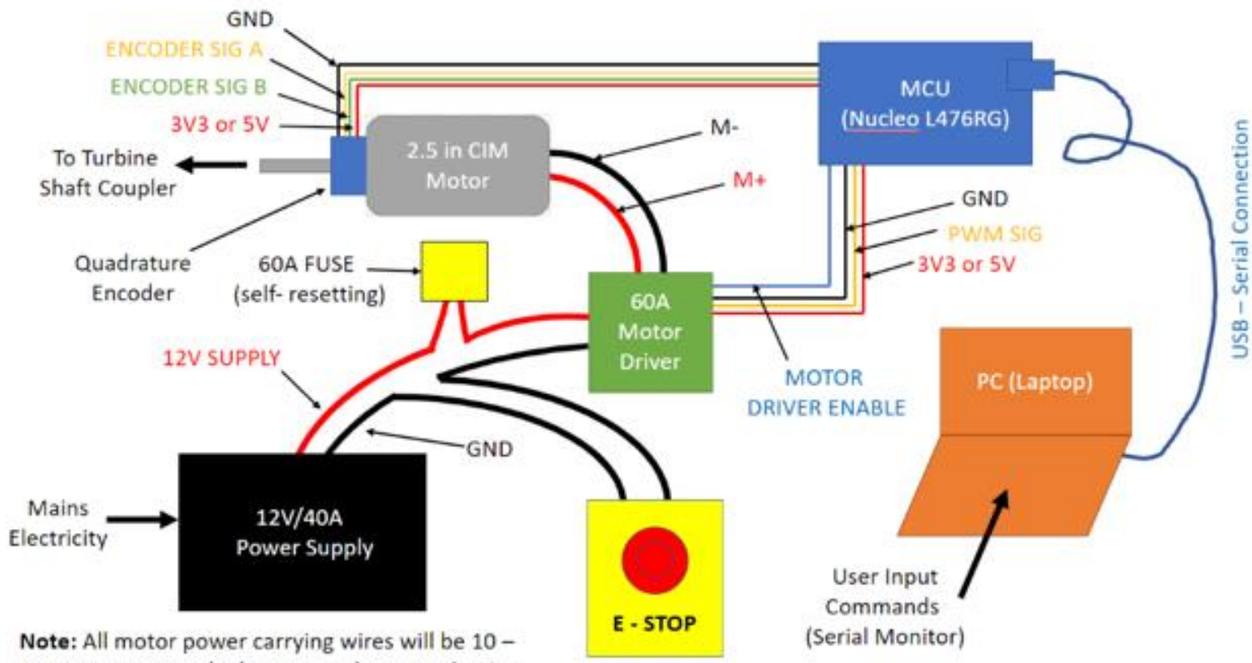
GND
ENCODER SIG A
ENCODER SIG B
3V3 or 5V
To Turbine
Shaft Coupler
2.5 in CIM
Motor
M-
M+
MCU
(Nucleo L476RG)
GND
PWM SIG
3V3 or 5V
USB – Serial Connection
Quadrature
Encoder
60A FUSE
(self- resetting)
60A
Motor
Driver
MOTOR
DRIVER ENABLE
PC (Laptop)
12V SUPPLY
GND
Mains
Electricity
12V/40A
Power Supply
E - STOP
User Input
Commands
(Serial Monitor)
Note: All motor power carrying wires will be 10 –
12 AWG to ensure high currents do not melt wires

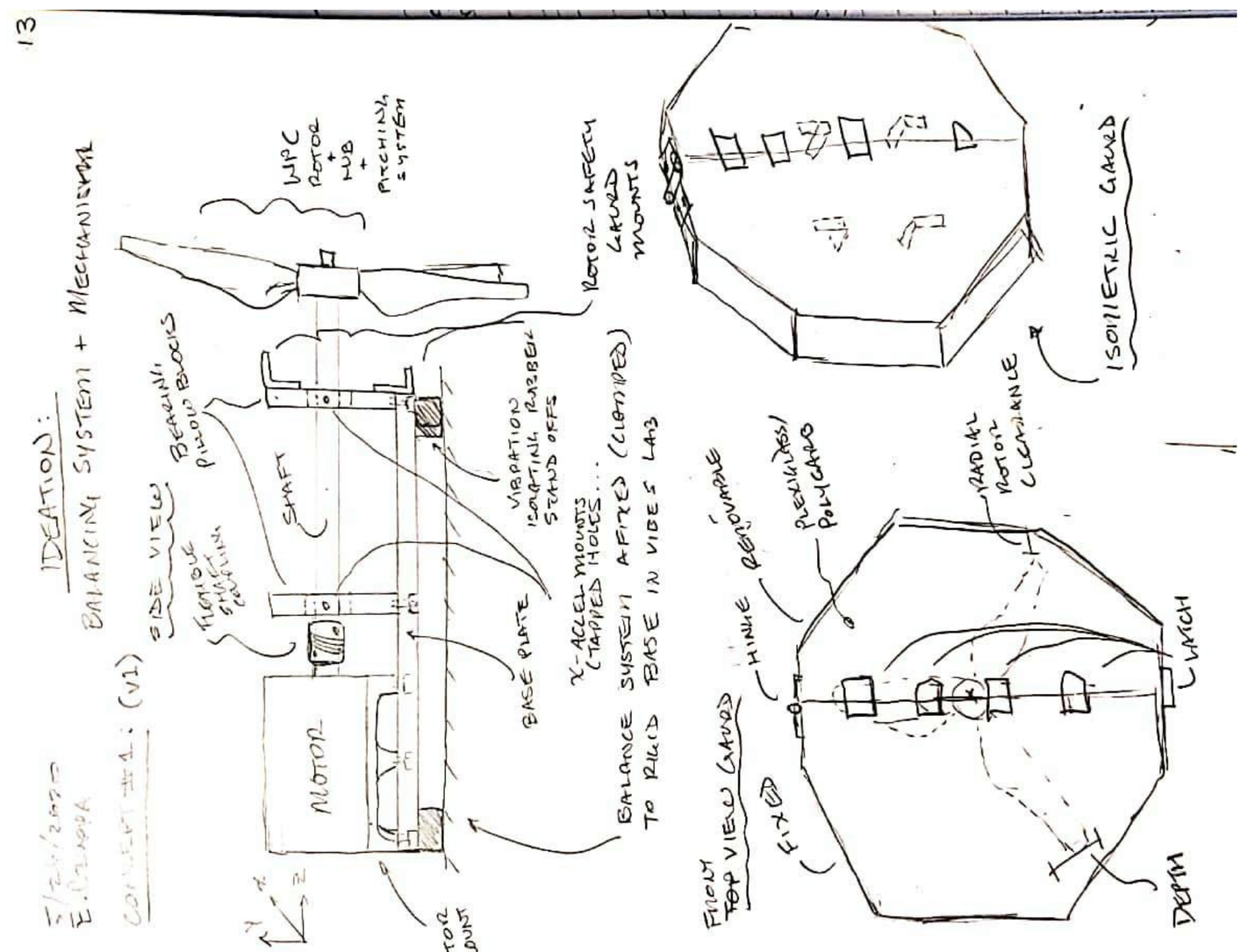
13
IDEATION:
BALANCING SYSTEM + MECHANISM
CONCEPT #1: (V1)
SIDE VIEW
MOTOR
BEARING
PILLOW BLOCKS
SHAFT
WPC
ROTOR
HUB
+
MECHANISM
SYSTEM
ROTOR SAFETY
GUARD
MOUNTS
VIBRATION
ISOLATING RUBBER
STAND OFFS
BASE PLATE
MOTOR
MOUNT
X-ACCEL MOUNTS
(TAPPED HOLES...
BALANCE SYSTEM AFFIXED (CLAMPED)
TO RIGID BASE IN VIBES LAB
FINAL
TOP VIEW GUARD
HINGE
REMOVABLE
FIXED
PLEXIGLASS/
POLYCARB
RADIAL
MOTOR
CLEARANCE
ISOMETRIC GUARD
LATCH
DEPTH

IDEATION (CONT)

BALANCING MECHANISM

CONCEPT #1: TRIM BALANCING OF BLADES

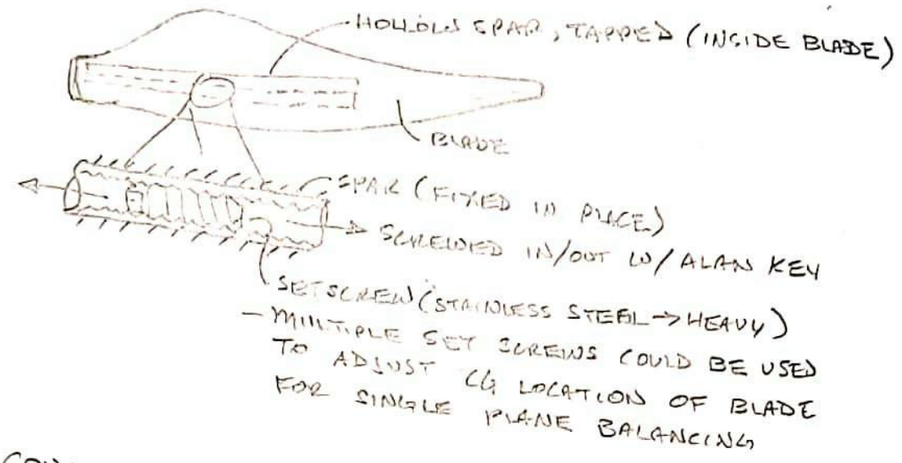

- MULTIPLE SET SCREWS COULD BE USED TO ADJUST CG LOCATION OF BLADE FOR SINGLE PLANE BALANCING

CONCEPT #2:

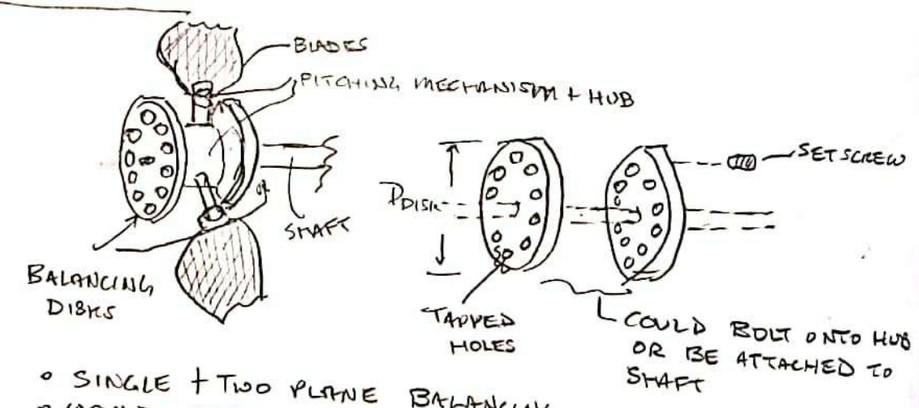

- SINGLE + TWO PLANE BALANCING
- WOULD NEED SPECIALIZED WEIGHTED SET SCREWS
- $D_{DISK} \geq D_{PITCH\ MECHANISM}$, DON'T WANT TO INTERFERE WITH BLADE AERODYNAMICS

ME 428-01 | Contoured Blade Casing | C. Croll, 05/27/20 | 1/1

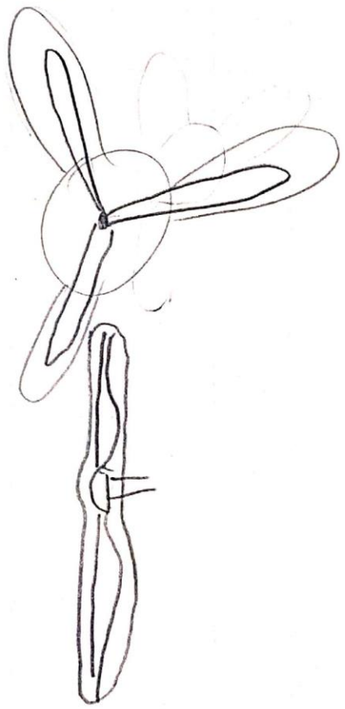

ME 459-01 | Blade Masses | C. Croll, 05/26/20

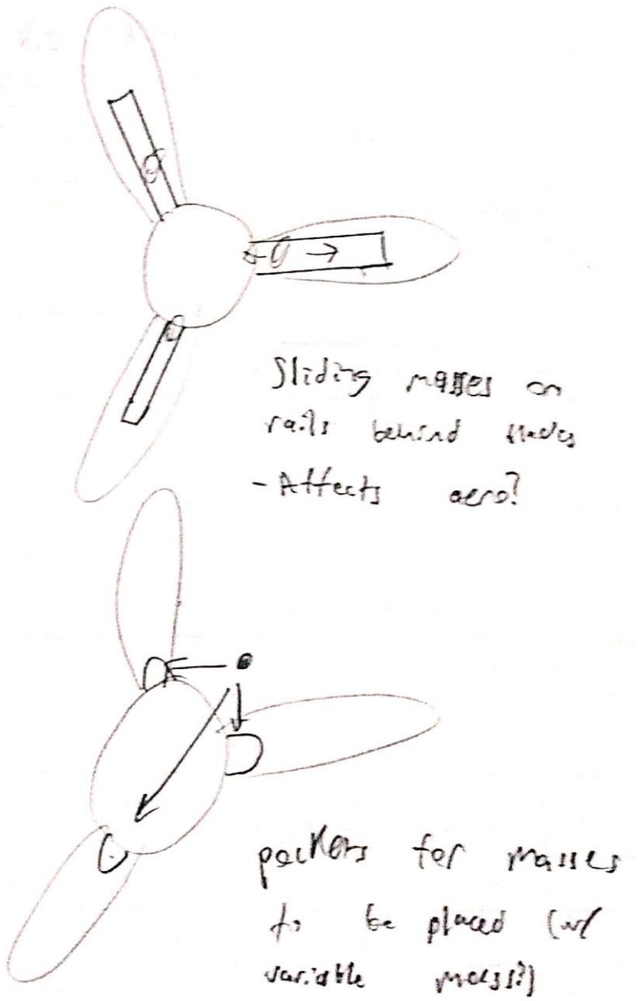

ME 429-01 | Grooved Plate | C. Croll 05/21/19 | 1/

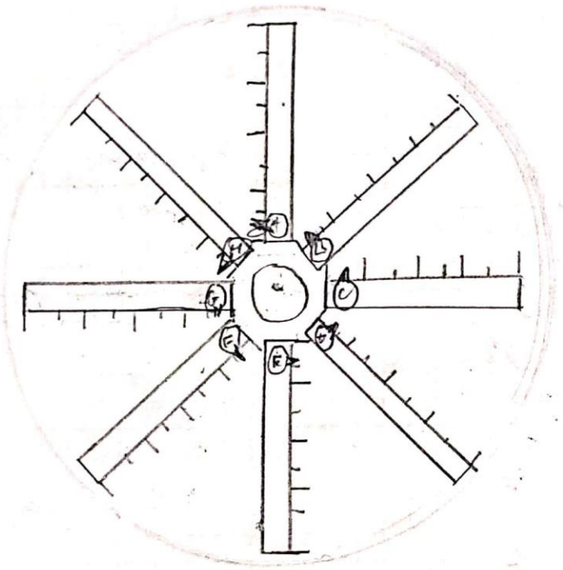

Software analyzes rotor imbalance and recommends mass movements to certain locations to eliminate imbalance

ME 428-01 | Imbalance Ring | C. Croll 05/20/19 | 1/

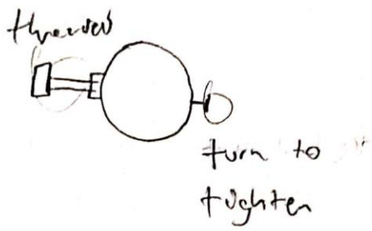

ME 429-01 | Mass Ring | C. Crosl, 05/22/20 | 1/1

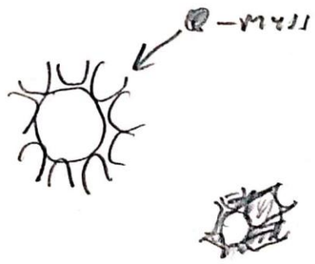

Counter ring with pockets for masses

ME 429-01 | Magnetic Casings | C. Crosl, 05/27/20 | 1/1

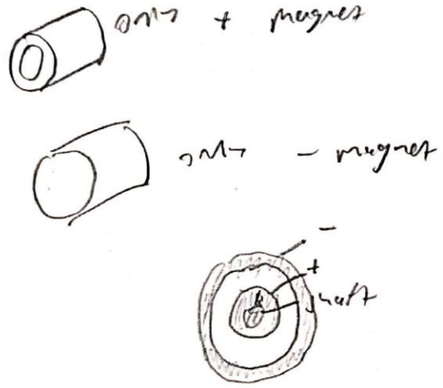

ME 427-01 | Rubber bumperplate | C. Crow, 05/22/20 | 1/1

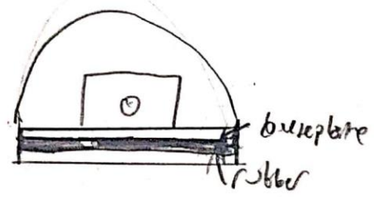

rubber bumperplate between nacelle and shaft assembly

ME 428-01 | Shaft traverser | C. Crow, 05/21/20 | 1/1

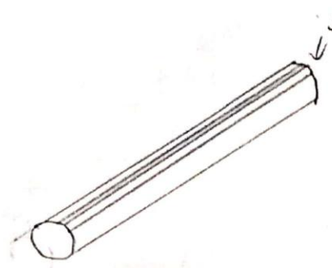

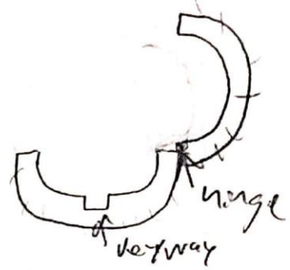

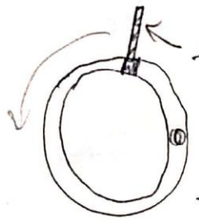

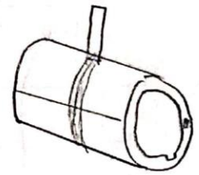

weighted nut attached.

ME 428-91 | Support Lengthener | C. Crell 05/27/29 | 1/1

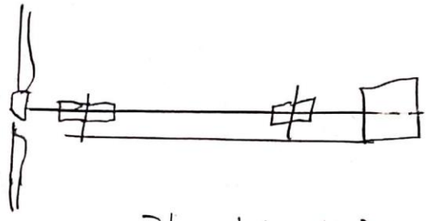

Elongated casing to support shaft

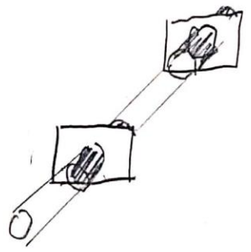

ME 428-91 | Shaft Damper | C. Crell 05/27/29 | 1/1

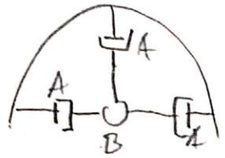

A = Dampener
B = Shaft

Dampers attached to race or springs?

Thick rubber casing

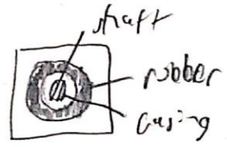

ME 428-91 | Threaded Plate | C. Croft 05/21/20 | 1/

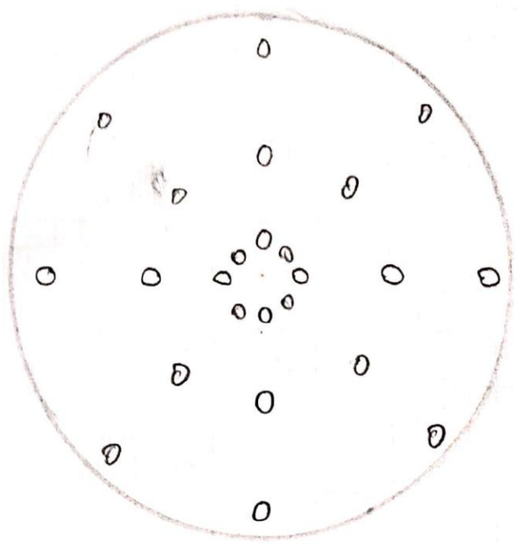

Each hole is threaded so weighted bolts can be screwed in at each location to counteract imbalances

ME 428-91 | Bending shaft notes | C. Croft 05/24/20 | 1/

How to balance?

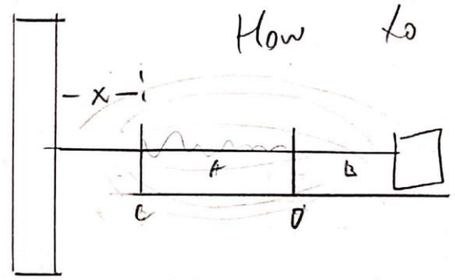

- rigid bearings?
- short overhang (x)?
- heat warped shaft w/ attachments → increase diameter for A and/or B?

- Increase C and/or D wall thicknesses

2E) [2D ; 2F ON PG. 14]

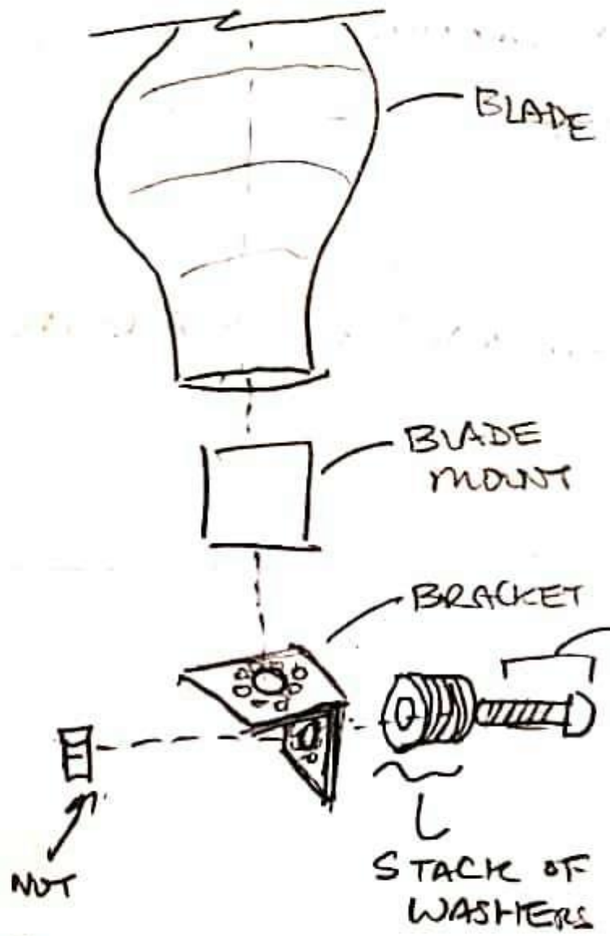

EXPLODED VIEW:
(SIMPLIFIED)

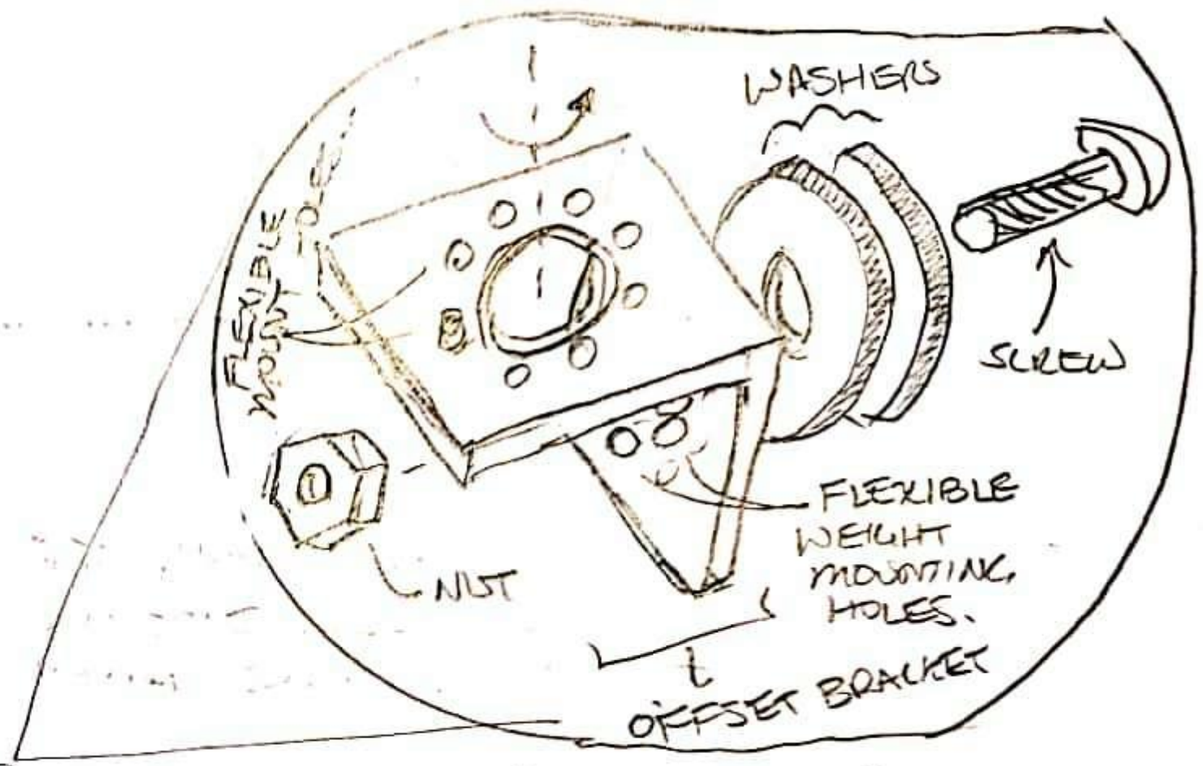

DETAIL VIEW:

BRACKET ROTATED SO WEIGHT ADDED BY WASHERS CAN WORK TO COUNTERACT BLADE/HUB/PITCHING MECHANISM MASS ECCENTRICITIES

9/28/2020

IDEATION SKETCHES:

2A)

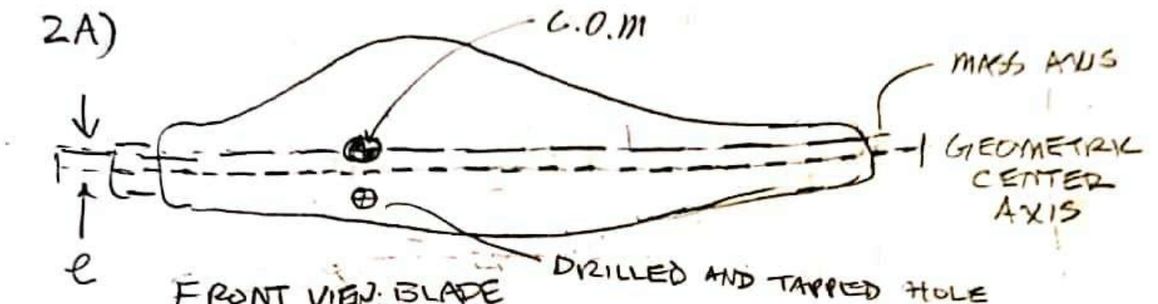

FRONT VIEW: BLADE

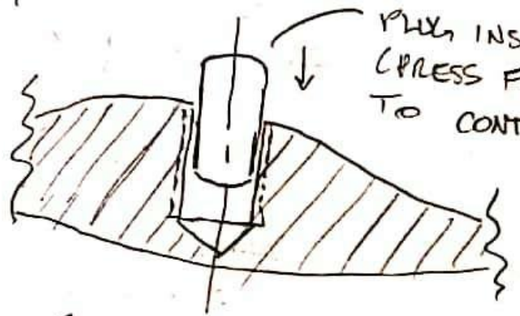

SECTION VIEW: DRILLED HOLE + PLUG

REMIX: PRINT BLADE W/ LOTS OF HOLES WHERE BRASS THREADED INSERTS COULD BE PRESSED IN WITH A SOLDERING IRON AND THREADED STEEL PINS (CNC LATHE?) COULD BE INSERTED

SKETCH... ↳

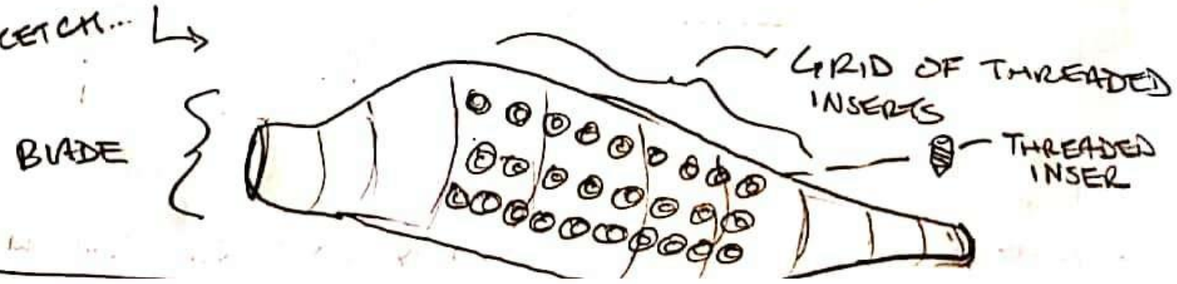

IDEATION SKETCHES:

9/28/2020 19

2C)

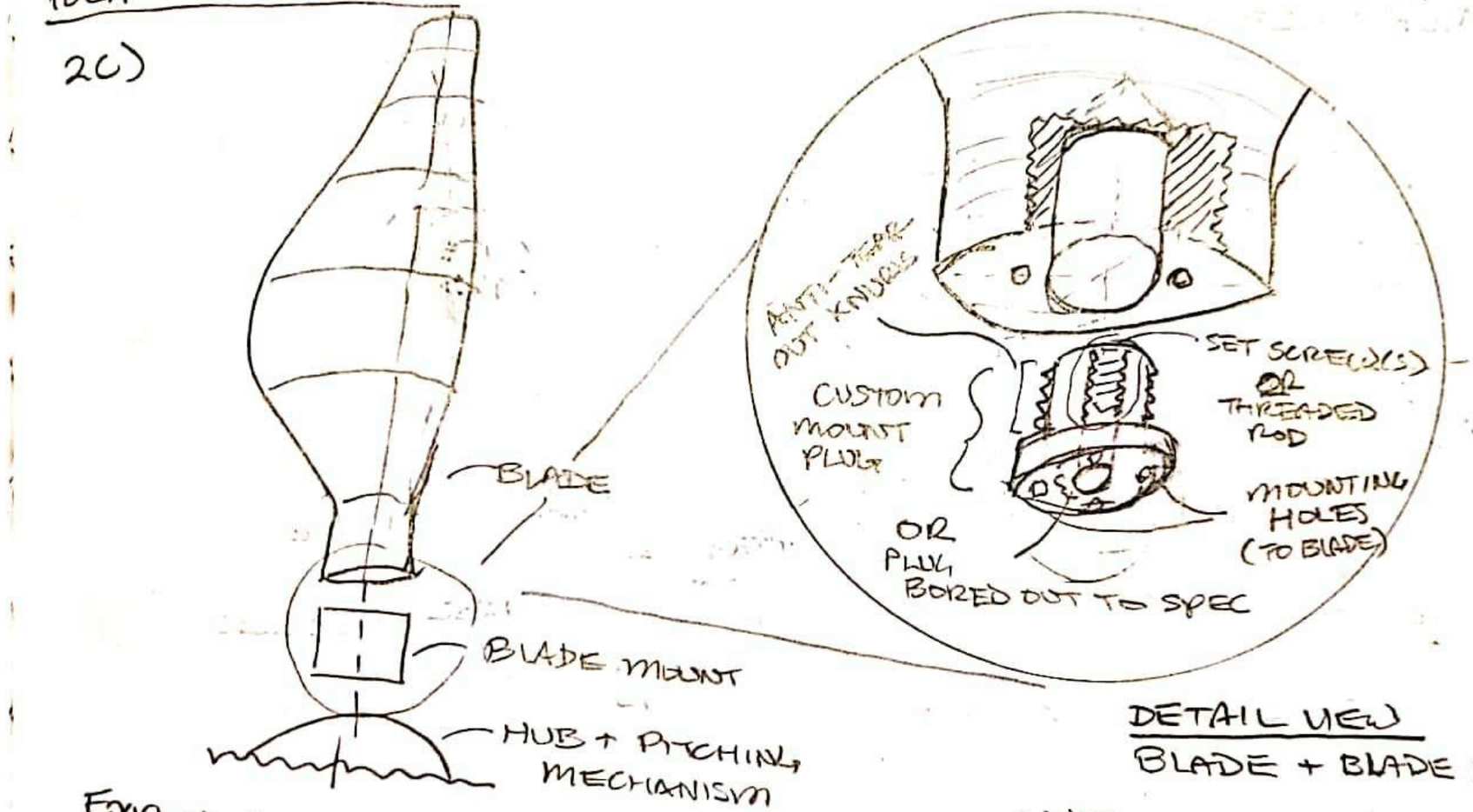

EXPLODED VIEW: (SIMPLIFIED) BLADE + PITCHING MECH + HUB

+ ADJUSTS POSITION OF CENTER OF MASS ONLY ALONG ONE AXIS... DEPENDENT ON LOCATIONS OF BLADE C.O.M's (FROM MOI SWING)

DETAIL VIEW
BLADE + BLADE MOUNT

- WEIGHT ADDED/REMOVED FROM MOUNT PLUG BY BORING OUT CENTRAL HOLE IN PLUG OR THREADING IN SET SCREWS / A THREADED ROD.

2B)

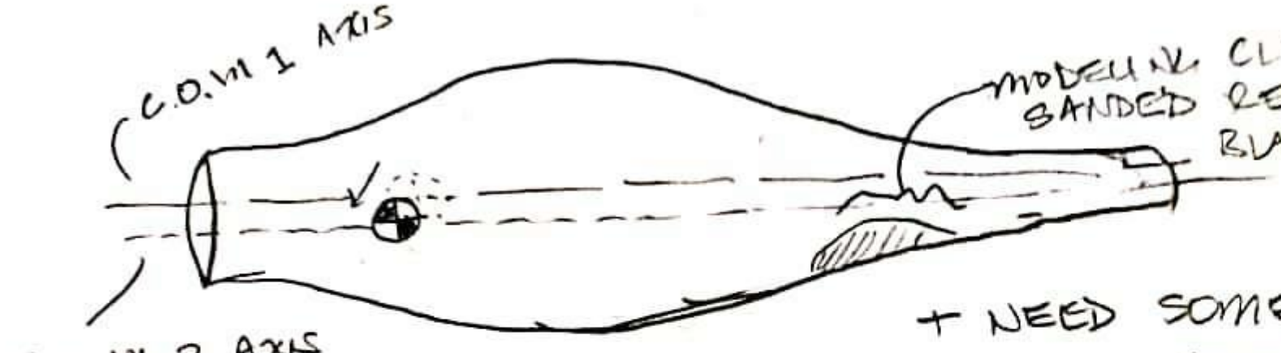

MODELING CLAY PLACED OVER SANDED RECESS IN 3D PRINTED/COMPOSITE BLADE ...

FRONT VIEW : BLADE

FOOT CORRECTION

+ NEED SOME WAY TO SEAL THE SURFACE
+ NEED METHOD TO CALCULATE SIZE/LOCATION OF RECESS FOR MODELING CLAY AND ACCURATE WAY TO CREATE RECESS

IDEATION SKETCHES:

9/28/2020

3C)

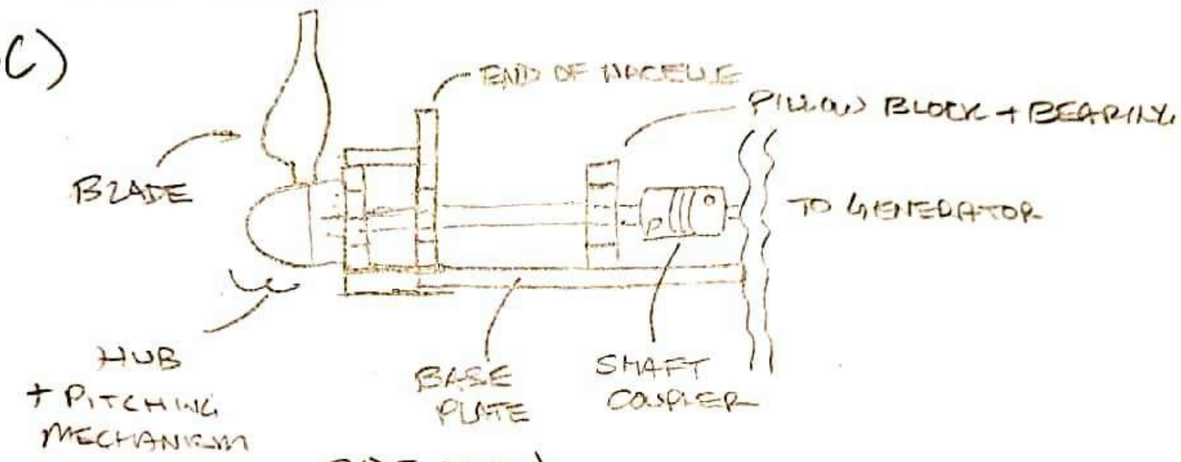

SIDE VIEW

EXTRA PILLOW BLOCK TO MINIMIZE OVERHANG,
IF PITCHING MECHANISM SLIDES ALONG SHAFT
EXTRA PILLOW BLOCK SLIDES W/ IT

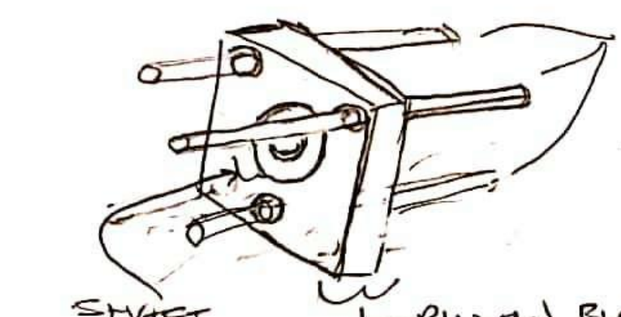

LINEAR RODS (x3 SINGULAR PLANE AND MAXIMUM STIFFNESS

+ AS PITCHING MECHANISM TRAVERSES ALONG SHAFT OUTBOARD (OF NACELLE) PILLOW BLOCK CONTINUOUSLY MINIMIZES OVERHANG.

+ COULD BE USED TO HELP ACTUATE PITCHING MECHANISM

— WHAT MOMENTS (GYRO MOMENTS) ARE CREATED W/ SLIDING?

— HOW MUCH IS ANALYSIS COMPLICATED BY 3RD BEARING [VIBRATIONAL]

— WHAT FIT DOES 3RD BEARING NEED W/ TURBINE SHAFT?

3D)

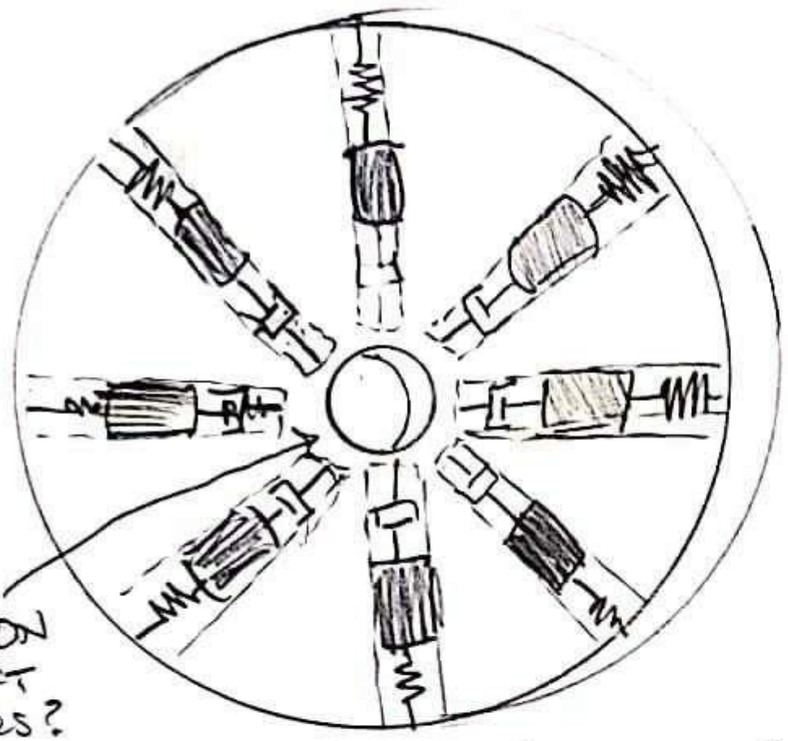

HELD ON W/ SHAFT COLLARS?

CUT-AWAY ISOMETRIC VIEW

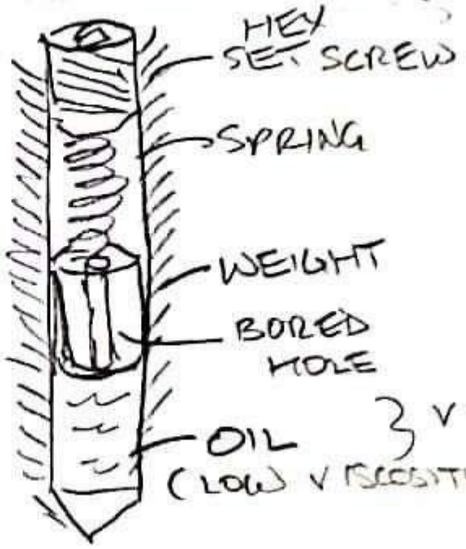

☆ DISCMOUNTED AS CLOSE TO FRONT OF NACELLE AS POSSIBLE (?)

3 VISCOUS DAMPER

CHANNEL DETAIL

+ SHAFT WHIRL "SHOCK ABSORBER"
→ WEIGHTS, SPRINGS, DAMPERS ADJUSTED TO COUNTERACT NATURAL SHAFT WHIRL
→ CORRECT MASS IMBALANCE (?)

IDEATION SKETCHES:

9/20/2020

3A/B)

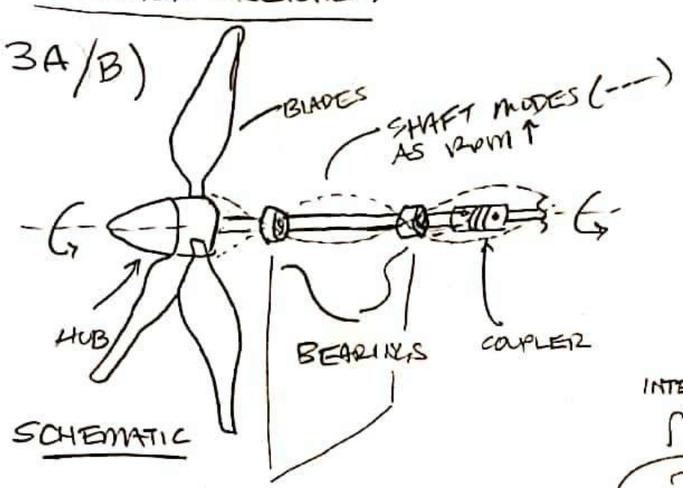

SCHEMATIC

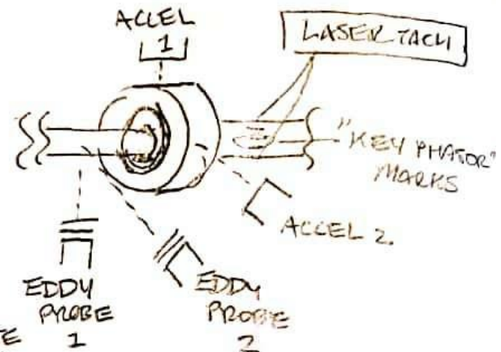

INSTRUMENTED BEARING

INTEGRATE BACK

AT BEARINGS MEASURE $x, \dot{x}, \ddot{x}$, LASER TACHOMETER ON SHAFT, NON-CONTACT EDDY SENSORS (PROXIMITY)

→ MODE SHAPE (EDDY) + PHASE (TACHOMETER)

→ IMBALANCE (ACCELEROMETERS (x2))

+ GRIND

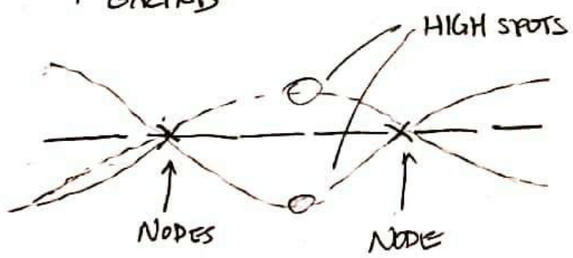

GRIND/MILL OFF MATERIAL FROM HIGH SPOTS OF MODE SHAPES...

+ REQUIRES MORE COMPLICATED MODAL BALANCING APPROACH, SHAFT; MORE SENSORS TO BE INTEGRATED IN BEARING PILLOW BLOCKS / FACE OF NACELLE

+ PRECISELY MILLING/GRINDING OFF RIGHT AMOUNT OF MATERIAL WOULD BE MORE/LESS DIFFICULT DEPENDING ON SHAFT MATERIAL... (e.g. CAN'T SURFACE GRIND ALUMINUM).

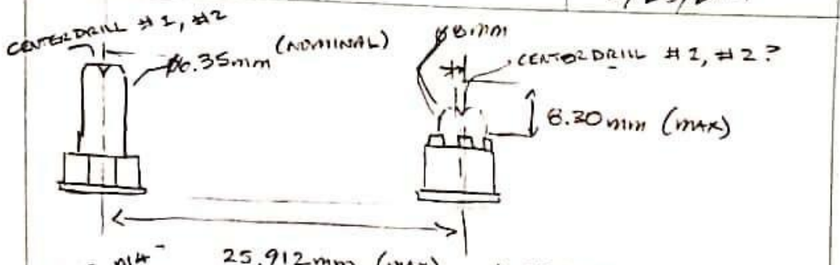

-> MAKE ONE FIXED AND THE OTHER ADJUSTABLE

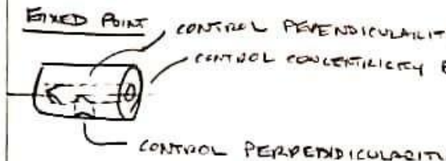

0.7 mm MODULE (mm/THREAD)

MACHINING OPS (30mm - 10mm)

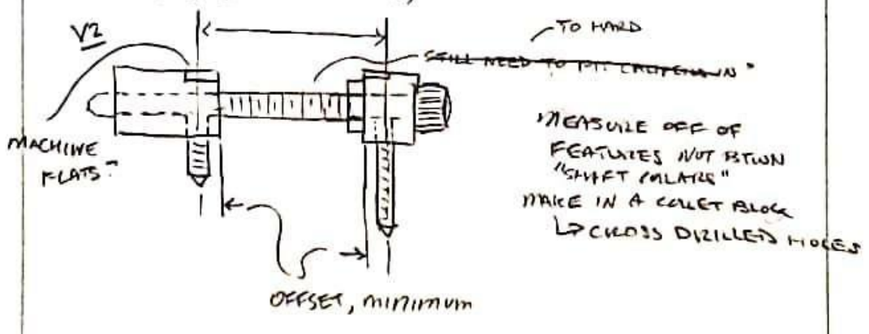

V2.1

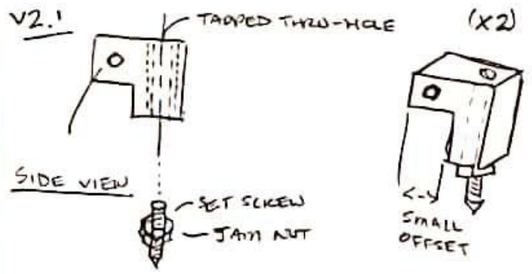

SET SCREW HEIGHT ADJUSTMENT BUILT IN
-> ALUMINUM? / STEEL
-> WATER JET PROFILE?

KEEP IT SIMPLE!

V3

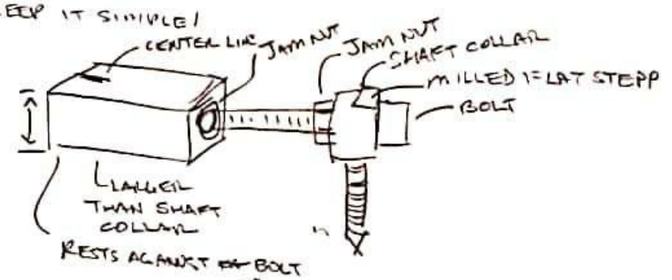

V4

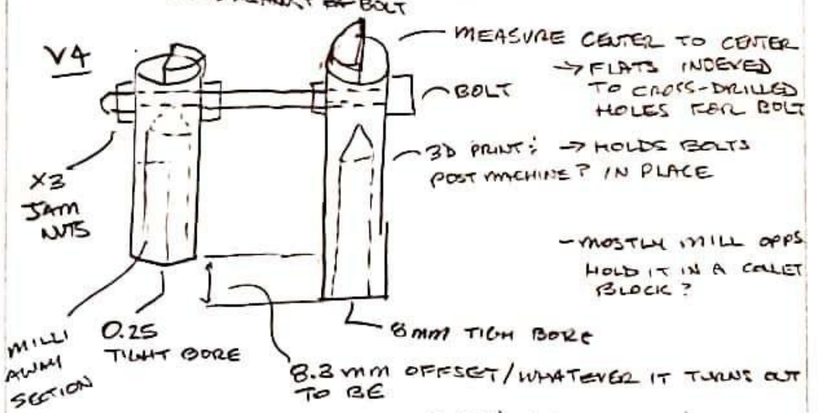

X CAN'T ACCESS OD OF 8MM THREADED SHAFT END ~~THE NE~~

X COTTER PIN BLOCKS ACCESS TO NUT

-> WE NEED TO LOCATE OFF OF "CENTER" DRILLED HOLE IN END OF SHAFT.

TEST MASS POSITIONING BRAINSTORMING

E. CZUPPA ME 430 3/5/2021

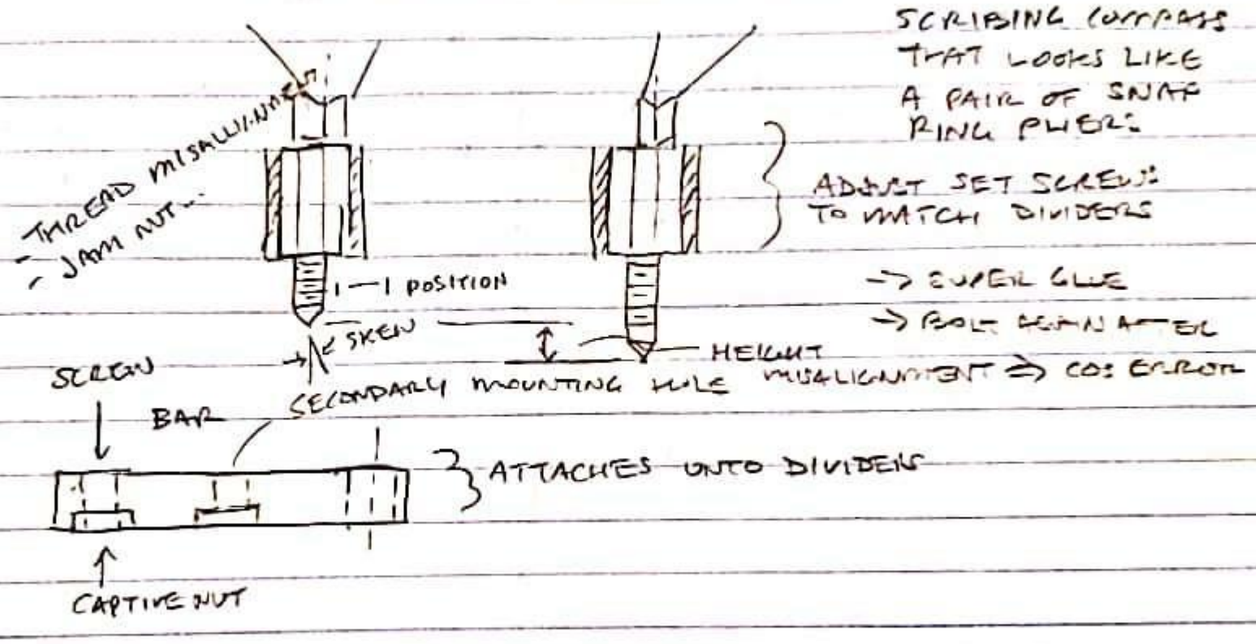

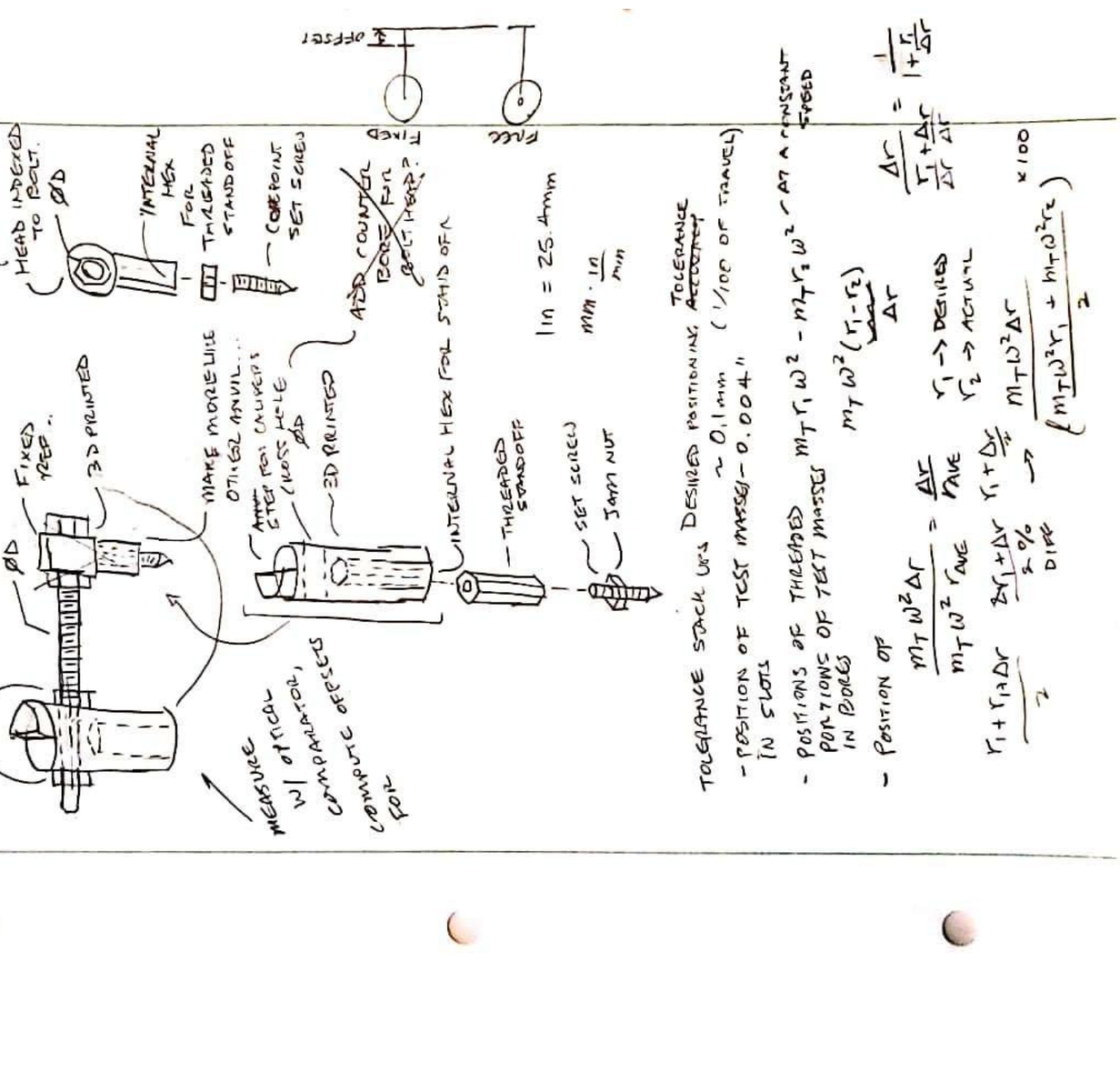

Appendix G – Mass Eccentricity Derivation

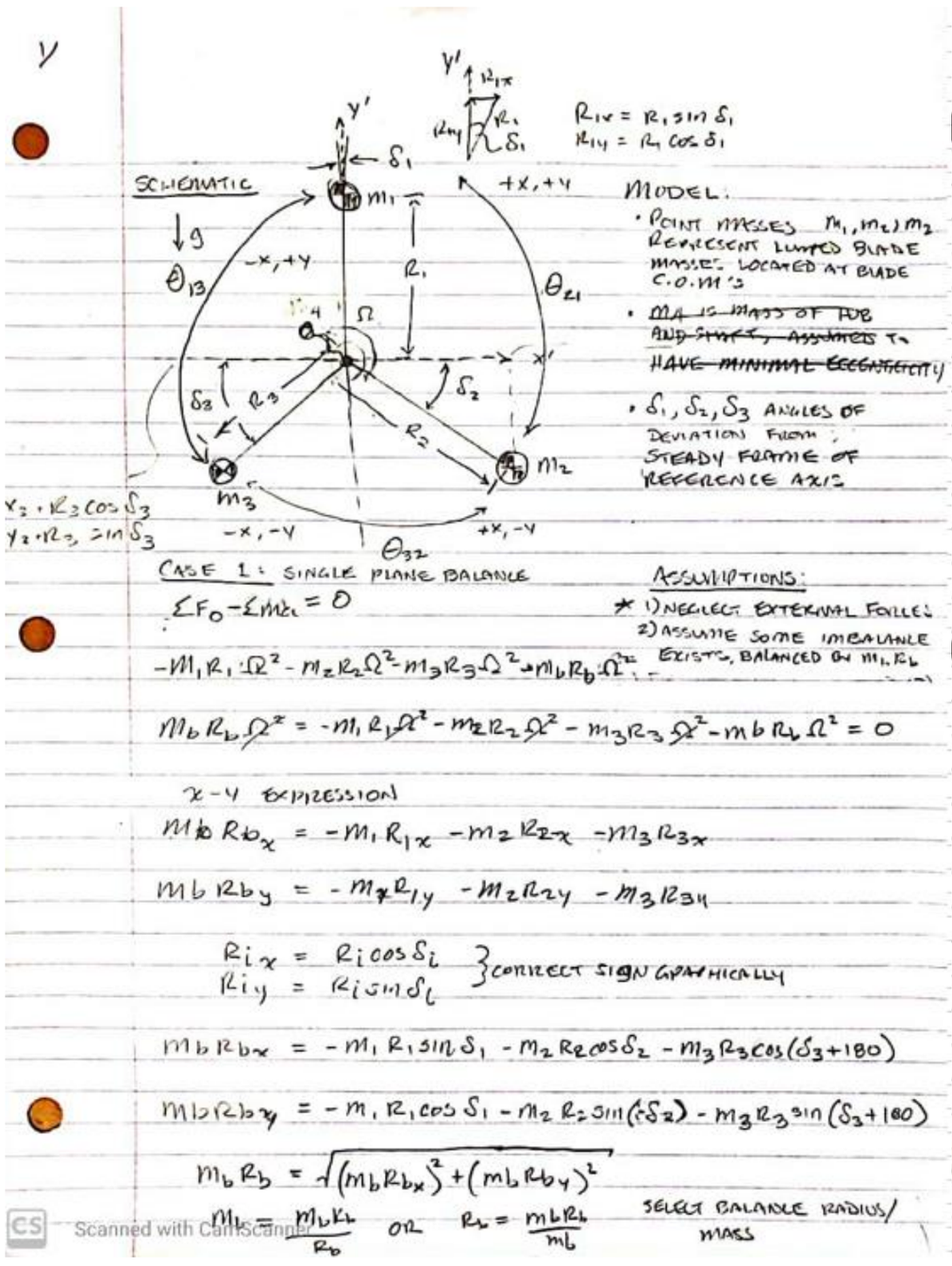

CENTER OF MASS LOCATION FOR SINGLE PLANE BALANCE
[FROM CALC II BALANCING A LAMINA]

$(\bar{x}, \bar{y})$

$$\bar{x} = \frac{\Sigma m_i x_i}{\Sigma m_i} \qquad \bar{y} = \frac{\Sigma m_i y_i}{\Sigma m_i}$$

LET $e_x = \bar{x}$ OF C.O.M ECCENTRIC LOCATION
LET $e_y = \bar{y}$ OF C.O.M ECCENTRIC LOCATION
LET $|e_r| = \sqrt{(e_x)^2 + (e_y)^2}$ RADIUS OF C.O.M ECCENTRICITY

$$e_x = \frac{m_1 R_1 \sin\delta_1 + m_2 R_2 \cos\delta_2 + m_3 R_3 \cos(\delta_3 + 180^\circ)}{(m_1 + m_2 + m_3)}$$

$$e_y = \frac{m_1 R_1 \cos\delta_1 + m_2 R_2 \sin(-\delta_2) + m_3 R_3 \sin(\delta_3 + 180^\circ)}{(m_1 + m_2 + m_3)}$$

Appendix H – Go-No-Go Down Selection

Table H.1 Cost/complexity and scope/effectiveness index.

Aspect	Design	Blade Bracket	Hollow Spar	Balancing Discs	Custom Balancing Rig	Blade Masses	Plug Grid	Grooved Plate	Imbalance Ring	In-Blade Plug	Magnetic Casing	Mass Ring	Sliding Pillow Block	Support Lengthener	Shaft Damper	Threaded Plate	Blade Clay	Rubber Baseplate	Shaft Modal Balance	Shock Absorber
Complexity (1-3)	Manufacturing	2	2	2	3	2	1	2	2	2	2	2	2.5	1.5	2	2	1.5	2	1	3
	Analysis	1	1	2	2	1	1	2	1	1	2	1	3	2	2	2	1	2	1	2
	Simulation	2	3	1	2	1	1	1	1	1.5	3	1	3	2	2	1	1.5	2	2.5	3
	Implementation	2	3	2	1	2	3	2	1	2.5	3	1	2	1	2	2	3	2	2	2
	Total	**7**	**9**	**7**	**8**	**6**	**6**	**7**	**5**	**7**	**10**	**5**	**10.5**	**6.5**	**8**	**7**	**7**	**8**	**6.5**	**10**
Cost (1-3)	Time	1	3	1	3	2	1	2	1	2	2	1.5	3	2	2.5	1.5	1	2.5	3	3
	Price	1	3	1	3	2	2	2	1	2	1.5	2	2	1	2	1.5	1	1	1	2
	Total	**2**	**6**	**2**	**6**	**4**	**3**	**4**	**2**	**4**	**3.5**	**3.5**	**5**	**3**	**4.5**	**3**	**2**	**3.5**	**4**	**5**
Effectiveness (1-3)	Qualitative	2	1.5	2.5	x	1.5	1	3	1	1.5	2	2	2	2	2	2.5	1.5	1	3	?
Scope (1-3)	Does it capture *it*?	2	1.5	3	x	1.5	1.5	3	3	1.5	1	3	1	1	1	3	1.5	1	1.5	3

Table H.2 Cost/complexity and scope/effectiveness index, normalized.

	Blade Bracket	Hollow Spar	Balancing Discs	Blade Masses	Plug Grid	Grooved Plate	Imbalance Ring	In-Blade Plug	Magnetic Casing	Mass Ring	Sliding Pillow Block	Support Lengthener	Shaft Damper	Threaded Plate	Blade Clay	Rubber Baseplate	Shaft Modal Balance	Shock Absorber
Normalized Complexity	0.583333333	0.75	0.583333333	0.5	0.5	0.583333333	0.416666667	0.583333333	0.833333333	0.416666667	0.875	0.541666667	0.666666667	0.583333333	0.583333333	0.666666667	0.541666667	0.833333333
Normalized Cost	0.333333333	1	0.333333333	0.666666667	0.5	0.666666667	0.333333333	0.666666667	0.583333333	0.583333333	0.833333333	0.5	0.75	0.5	0.333333333	0.583333333	0.666666667	0.833333333
Normalized Effectiveness	0.666666667	0.5	0.833333333	0.5	0.33333333	1	0.333333333	0.5	0.666666667	0.666666667	0.666666667	0.666666667	0.666666667	0.833333333	0.5	0.333333333	1	#VALUE!
Normalized Scope	0.666666667	0.5	1	0.5	0.5	1	1	0.5	0.333333333	1	0.333333333	0.333333333	0.333333333	1	0.5	0.333333333	0.5	1

Appendix I – Notes on Imbalance Determinants

Important determinants of imbalance:

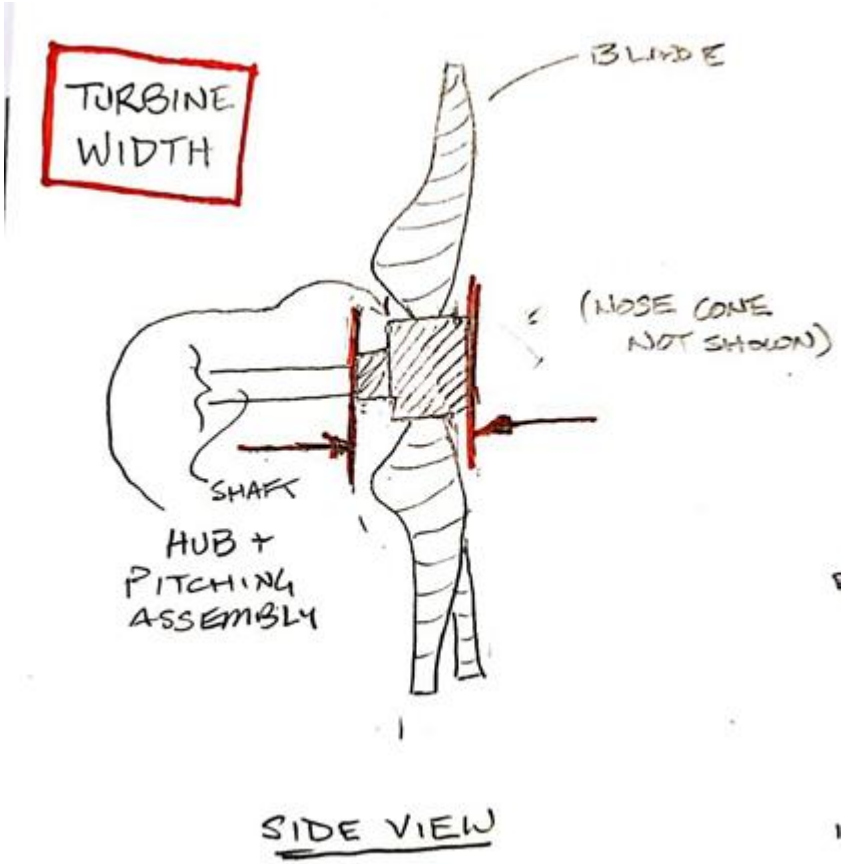

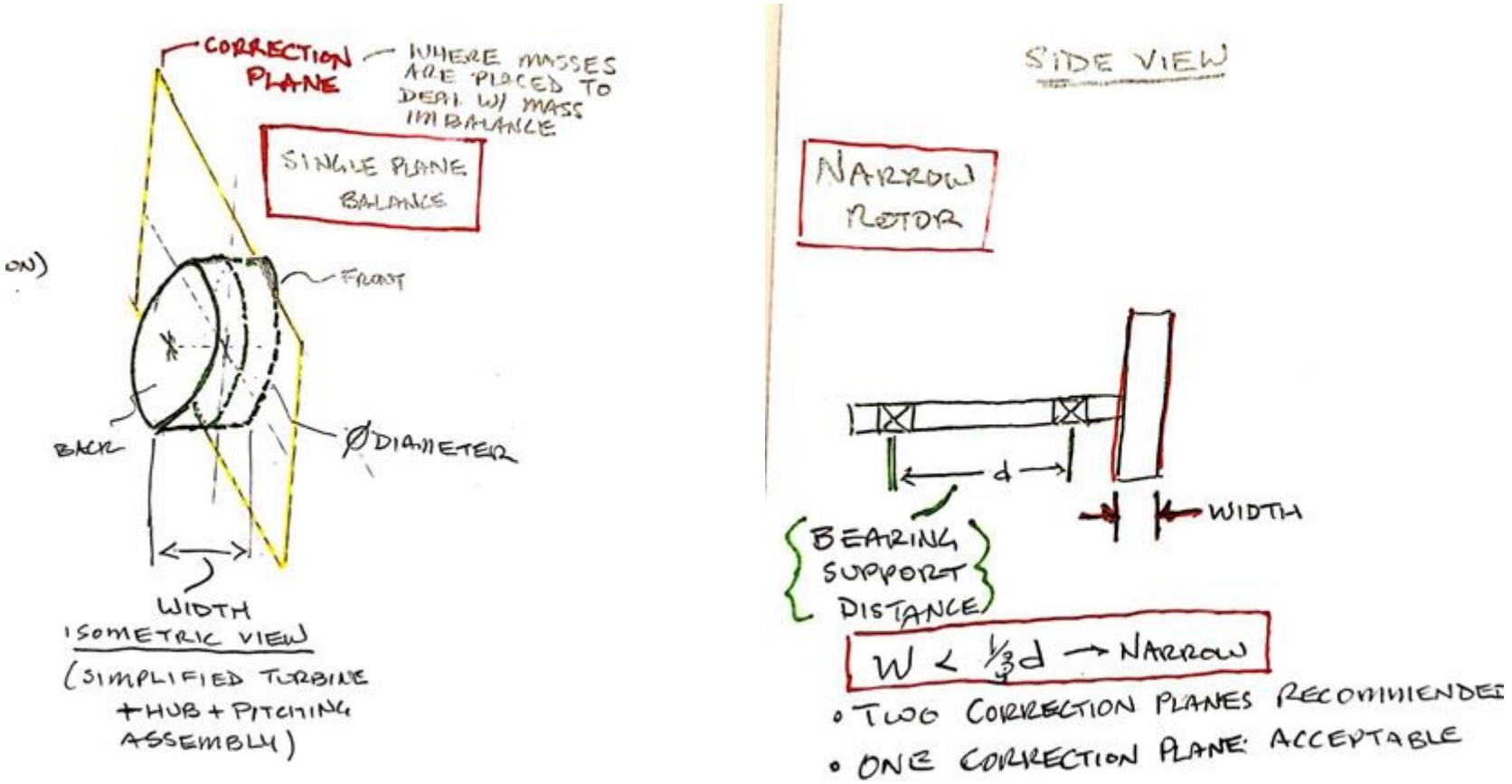

- Pitching Team
  - Blades mounted such that they are each **120 degrees apart from each other** and **in a single plane normal to the axis of rotation of the shaft** within an achievable (tight) tolerance of each other
    - Blades are mounted such that their axes of rotation normal to the rotation of the shaft intersect at the same point on the rotational axis of the shaft
  - Minimize overhang from end of nacelle to prevent excessive shaft whirl.
    - Likely requires a small form factor pitching mechanism
    - Desired that the width of the turbine is minimized to prevent having to do 2-plane balancing (single plane preferred).
  - Modal shapes and critical frequencies of the turbine shaft are affected by bearing placement (how much of the shaft is supported vs. overhung) and mass distribution of rotating elements (primarily of hub, blades, and pitching mechanism).

        - If pitching mechanism must traverse shaft to change pitch angle of blades mass distribution changes, which could worsen shaft whirl or even excite damaging critical frequencies for the rotating shaft.
            - If it must move, minimize linear movement along the shaft
- Blades Team
    - Mass centers for blades within an achievable (tight) tolerance of each other with similar moments of inertia.
        - Moment of inertia swings used to find blade mass properties; center of mass found by the following method in Section 3.2 of https://digitalcommons.calpoly.edu/theses/837/
    - Axis-symmetrical mounting 120 degrees apart in the same plane. (See pitching team)
- CPWP Mechanical Team (Zach)
    - Go for axisymmetric parts not a-symmetric
    - Avoid mounting hardware that does not sit flush with outer diameter of hub (where the hub attaches to the turbine shaft outside of the nacelle)
- CPWP Turbine Design Senior Project (Sophie)
    - Thickness of wind turbine baseplate.
        - Fatigue analysis on plate (material dependent Aluminum vs. Steel)
    - Width of wind turbine to prevent 2-plane balancing (determined via vibrational analysis)
    - Bearing Placement
        - Distance between bearings – the distance over which the shaft is supported
        - Bearing bores are mounted as concentric with each other as possible...
            - Tolerance for bores of pillow blocks
            - Mounting for accelerometers/gyros in pillow blocks
    - Coupler from turbine shaft to generator shaft
        - Mounting hardware should be flush with outer diameter of coupler (picture)
            - We need to know the specs/ratings for the coupler once you make some initial selections

Appendix J – Notes on Michael Mullen's Recommended Testing Procedure

- Equipment list:
  - Bentley Nevada 208 DAQ
  - BNC cables
  - Amplifier (with white cables)
  - Proximity probe
  - Proximitor assembly
  - Accelerometers

- Vibration Data Measurement 1:
  - 2 accelerometers – 1 placed on top (horizontal) and 1 to the side (vertical), as close to the fan as possible.
    - Connect accelerometer to amplifier box using thin white cables.
    - Use BNC cables to connect amplifier box to Bentley Nevada 208 DAQ
    - Use Windows XP software (guide should be included in ME 318 lab manual) and configure from proximity probe to accelerometer with correct factor (from 200 mV/m to 100 mV/G, check lab manual)
- Vibration Data Measurement 2:
  - Proximity probe:
  - Connect proximity probe to proximitor assembly.
  - Connect proximitor assembly to Bentley Nevada 208 with BNC cables.
    - Shaft Phase and Speed Data Measurement 1:
      - Laser tachometer: (EE department may have one, Michael also offered his possibly)
  - Put reflective tape on shaft.
  - Use laser tachometer to measure rotations
  - Connect tachometer to AUX->BNC adapter, and connect to 208 DAQ
  - Output should be polar plot.
  - Must configure ADRE expected key phaser input for the laser tachometer.
  - Use more channels for more data if wanted.

- Shaft Phase and Speed Data Measurement 2:
    - Bently Nevada Keyphaser ® Probe:
      - Instrument keyway or other notch in turbine shaft
      - Connect keyphaser ® probe to ADRE 208 DAQ with BNC cable.

- Alternative (?):

- Use Scout sensor (contact Aaron Hampton for access / details) in junction with laser tachometer to predict counteractive weight placements.
    - Location: top shelf of vibes lab equipment storage in pelican box.
    - Assume functioning below 1st natural frequency, lagging by 45 degrees. If above, assume lagging by 135 degrees.
    - Will output 1X amplitude and phase.

- Logistics
    - Michael Mullen available after October 28th for possible in person assistance.

- Balancing Recommendations from Michael:
    - To balance your wind turbine there are several different approaches you could use with the instrumentation within the Cal Poly vibes lab. The first recommendation which I believe will be the easiest and most effective is to use the Bently Nevada ADRE 208 DAQ and the ADRE for Windows software.

    - The minimum hardware you would need would be a single accelerometer (preferably a small one to avoid influencing the mass of the turbine mount), the amplifier (blue box) for the accelerometer, and a laser tachometer and mount. For cables you would need two BNC cables for the tachometer and accel, then an adapter for the laser tach (probably 3.5mm to bnc). The bnc cables from the back of the ADRE 208 go to the Proximiter assembly. You could just unplug the proximeter assembly and connect to those BNC cables. The accelerometer would be mounted on the bearing cap closest to the fan with either a stud mount, magnetic (if ferrous) or wax mount. The laser tachometer reads off of a piece of reflective tape and acts as the keyphaser ®. Everything except for the laser tachometer and adapter cable is in the vibes lab or storage closet between the vibes and controls lab.

    - If you want to measure more complex dynamics of the turbine you could easily add more accels later with this method. Configuring the ADRE 208 and ADRE for Windows software will be a bit of a challenge but pretty do-able with the ME318 lab manual as a reference.

    - Another method which I believe will end up being more work for you would be to use the Bently Nevada Scout and configure it to read synchronous data and take a tachometer input for keyphaser ® probe (still with the same laser tach). This method won't give you a polar plot like in ME318 but you can guess the running speed relative to the first critical frequency and then estimate the position of the heavy spot enough for a trial run. This method is very good if you have to balance equipment in place or out in the field since the Scout is portable. However, if you can spin your turbine inside the vibes lab, I believe the first method would be easier.

    - If you wish to use my MATLAB app and national instruments DAQ, you could but the setup and configuration to get it to do what you want will end up being more difficult than just using ADRE 208 in my opinion. You could also use the newer Bently Nevada

software System1 and the ADAPT 3701 but again I think this would be much more complicated than what you need just for balancing.

- Again my recommendation for what would be best for your application would be to use the ADRE 208 already in the vibes lab.

Appendix K – ABAQUS Simulation Plan

NOTE: The following simulations represent an incremental increase in simulation complexity to avoid creating a simulation that is too difficult to troubleshoot/debug at the outset. Thus, the linear static (1) analysis will serve as a sanity check and be the first stage in mesh refinement in preparation for the 2nd stage of analysis – critical frequency identification. Mesh refinement will again be performed in the second simplest of cases likely with approximated flexible bearings and no mass imbalance to ensure the mesh is sufficiently refined to capture the vibrational modes the system will experience from 0 –2500 RPM. For critical frequency identification, 10 – 15 modes will be polled with the hope that the modes of interest will be identified within that larger sample size. Finally, the third and most complicated stage of the analysis will be the linear, dynamic transient analysis to examine actual system behavior. The stages of complexity for this model are still being determined and require further research as it requires characterization of the damping of the system. It should be noted that the entirety of this analysis will be performed on the shaft with its supporting bearings tied to a simplified model for the balancing mechanism and pitching mechanism and blades. This simplification is necessary for the timeline of the project but comes at the cost of reduced accuracy or the potential for slightly more divergent behavior of the model when compared to the physical system.

1. Linear, Static analysis sanity check – shaft and simplified rotor assembly
    a. no unbalance
    b. Static Loads:
        i. Concentrated load/ distributed load on overhung portion of shaft from pitching mechanism and blades
        ii. Bearing Reactions
        iii. Thrust Load from wind
        iv. Assuming steady state condition, so no angular acceleration of shaft, resistive torque from rotor inertia terms and torque applied from wind cancel out – thus allowing for approximation by static analysis.
2. Linear, Dynamic (Normal Modes Analysis) critical frequency identification
    a. no unbalance, rigid bearings, flexible shaft
3. Linear, Dynamic (Normal Modes Analysis) critical frequency identification
    a. no unbalance, flexible bearings, flexible shaft
4. Linear, Dynamic (Normal Modes Analysis) critical frequency identification
    a. added mass imbalance, flexible bearings, flexible shaft
5. Linear, Dynamic (Transient Analysis) – dynamic behavior characterization
    a. Added mass imbalance, and resulting loads
        i. Mass load transverse to shaft in addition to load from weight of hub and pitching assembly
        ii. Moment load on overhung portion of shaft, perpendicular to axis of shaft
        iii. Dynamic forces showing up at bearings
    b. Flexible shaft
    c. Flexible bearings
        i. Axial Stiffness

ii. Radial Stiffness
iii. Damping…
iv. Neglecting torsional terms…

d. Goals:
i. Check balance ceiling (hand calculation based on yaw moment)
ii. Check against experimental data
iii. Check that mechanism actually works
iv. Identify critical frequencies and approve shaft design

Appendix L – ABAQUS Simulation Report

Natural Frequency Extraction of Small-scale Wind Turbine Rotating Assembly

ME 404 Project

11/29/2020

By: Ethan Czuppa

1.0 Abstract

The following report documents the development of a linear dynamic natural frequency extraction model of the rotating assembly of the Cal Poly Wind Power (CPWP) club's competition, small-scale wind turbine. As the testing of the CPWP's competition turbine at both the Collegiate Wind Competition and in the Cal Poly mechanical engineering labs requires spinning the turbine in excess of 3000 RPM, the identification of the rotating assembly's natural frequencies is requisite to the safety of both testing efforts. It was found that maximum testing speed of the turbine was well below the model's first natural frequency. While this result strengthens the case that the competition turbine will be safe to test, the scope of this report's results are limited by not exploring the effects of mass imbalance in the rotor and modeling choices that require further refinement.

2.0 Introduction:

My senior project is to develop a single-plane dynamic mass balancing mechanism and procedure for the Cal Poly Wind Power Club's (CPWP) 2021 competition turbine. Imbalances resulting from aerodynamic loads are not within the scope of this project. In pursuit of designing these deliverables, my senior project team has chosen to perform vibrations analysis on a simplified version of the competition turbine's rotor assembly, including but not limited to the identification of the rotor assembly's natural frequencies. I previously completed approximate natural frequency identification using SOLIDWORKS frequency studies – this was also attempted in ADAMS but proved to be too difficult to accomplish. However, due to my lack of experience with FEA and normal modes analysis while using a non-native FEA tool my senior project partner and I reached the consensus that better modeling was needed. The goal of this project is to build the basis of our simplified rotor + shaft assembly in ABAQUS with incrementally increasing complexity, and acquire a better estimate for the system's natural frequencies to help provide proof of safe operating conditions for balancing mechanism testing in Winter quarter 2021.

3.0 Model Development:

The desired result of the project is a more accurate estimate of the natural frequencies of the rotating assembly – the shaft and simplified rotor. As a result, the complex geometries associated with the rotor and hub for the competition turbine were simplified to prevent the need for many more convergence studies. Instead of trying to capture the behavior of individual components in the rotor assembly (shown below in figure 3.1) I simplified the rotor to a disc of equal size and mass and used tie constraints to rigidly join it with the shaft (shown in figure 3.2). Similarly, I removed the fillet on the competition shaft and added a partition to reduce the effect this stress concentration would have on the model's results. While we often idealize the supports for our models as rigid, in this case the bearings which carry this shaft, have dynamic behavior that is loading, frequency, and fit dependent [1]. To simplify the bearing behavior while still allowing them to be somewhat flexible I used Gargiulo's approximation of bearing radial and axial stiffness as a function of applied load and bearing geometry [2] to specify the coefficient spring/dashpot engineering feature in ABAQUS. The values of the desired radial stiffness were calculated from bearing geometries of an angular contact and deep grooved ball bearing that would be press fit onto the 8mm stepped portion of the competition shaft. I then took the radial stiffness values for both bearings and converted them to X and Y components for use with the SPRING1 elements in ABAQUS (the engineering spring/dashpot feature). I have provided the equations used for this stiffness calculation and the table of resulting stiffness values in Appendix C. Though I initially intended to try and analyze the effect of mass imbalance present in the rotor on the whirling of the shaft near its natural frequencies, this proved to be too complicated as well as time consuming to complete for this project.

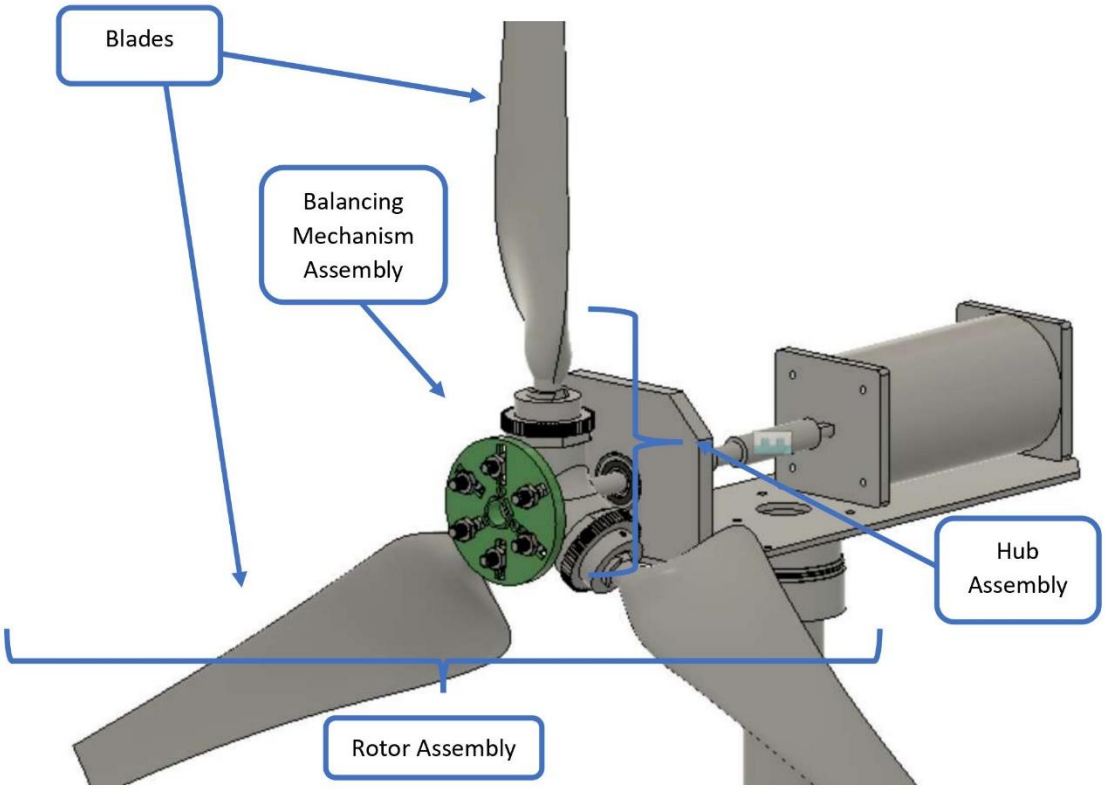

Figure 3.1. Competition Rotor Assembly CAD

To clarify, whenever I mention the term rotor assembly in this report, I am referring to the total assembly of the blades, hub assembly, and the balancing mechanism. Similarly, my simplified representation of this overall assembly aims to capture its mass and approximate size without the need for a convergence study in ABAQUS on the simplified rotor part. This is why all the components here – even those not shown within the hub assembly – were collapsed into a disc with the same diameter as the blade diameter, identical width as the combined width of the hub assembly and balancing mechanism assembly, and made to have an identical mass as the entire rotor assembly.

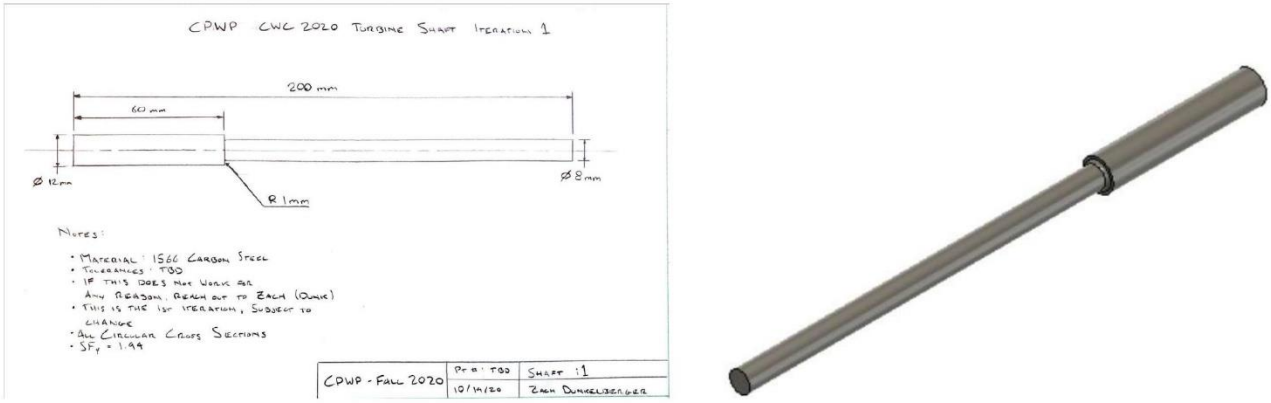

Figure 3.2. (R) Dimensioned Drawing of competition turbine shaft (L) Isometric view of competition shaft CAD model.

Shown immediately above is the competition turbine shaft designed by the CPWP's mechanical team. As mentioned previously, the 1mm fillet at the interface between the 8 and 12mm steps in the shaft was removed and replaced with a partition in the actual finite element model. Additionally, the rotor assembly, described in figure 3.1 mounts on the 12mm

step of the shaft with a keyway. I modeled the effect of the keyway by using Tie constraints without the more complicated contact conditions and stress concentrations that arise from actually modeling the keyway with an appropriate interaction between it, the shaft, and the rotor assembly.

The CPWP has provided my senior project team with the preliminary competition shaft dimensions, material properties, loads, and approximate boundary conditions. The dimensions and material properties for the simplified versions of the competition shaft and rotor that I modeled in ABAQUS are provided in tables 3.1.1 and 3.1.2 respectively. A quick note on notation: the parameters starting with an L refer to a length, with a D refer to a diameter, with a T refer to thickness, and all parameters under the "Material" heading are the elastic modulus (E_...), Poisson's ratio (v_...), the yield strength (Sy_...), the ultimate strength (Su_...), and the density (Rho_...).

Table 3.1.1 Shaft Properties

Parameter	Value	Units
L	0.200	m
L_1	0.125 – 0.140	m
L_2	0.040	m
L_3	0.060	m
L_4	0.200	m
D_1	0.008	m
D_2	0.012	m
Material	ASI 1566 Steel	-
E_shaft	200.0E9	Pa
v_shaft	0.285	-
Sy_shaft	517.0E6	Pa
Su_shaft	875.0E6	Pa
Rho_shaft	7865	kg/m^3

Table 3.1.2 Simplified Rotor Properties

Parameter	Value	Units
D_rotor	0.450	m
T_rotor	0.040	m
D_shaft_hole	0.012	m
m_rotor	1	kg
Material	Fictitious	-
E_rotor	68.9E09	Pa
v_rotor	0.33	-
Rho_rotor	157.3019	kg/m^3

The enumerated length parameters (L_1, etc.) refer to lengths used in the hand calcs and in the load case diagram (figure 3.3). Additionally, the strengths and stiffness used for the shaft material properties (AISI 1566 steel) that were selected by the CPWP represent the median behavior of this alloy of steel – a relatively conservative engineering assumption. So, I chose to also use their selected properties. It should also be noted that the density of the fictitious rotor material I created is derived from the mass and volume of the simplified rotor. Also, to satisfy the element property requirements in ABAQUS, the stiffness of 6061 aluminum was used for the young's modulus value for the simplified rotor as the aluminum hub assembly is the most massive portion of the un-simplified rotor assembly and the assembly which transfers torque to the competition shaft.

Since I simplified the rotor assembly geometry to as high aspect ratio cylinder, the loading from the wind was also simplified to just a thrust load acting axially on the shaft – assumed to be taken entirely by the first bearing – and the resulting torque on the shaft from the wind which acts along the axis of rotation of the shaft. Since the thrust loading effect is decoupled from the transverse deflection of the shaft under static load and during natural frequency identification, I did not account for the thrust loading in my finite element model. In the same way, though the load due

to the weight of the simplified rotor is distributed over 40mm of the larger 12mm diameter and 60mm long competition shaft step, the weight was modeled a concentrated force acting through the centroid of the simplified rotor. Finally, neither the mass eccentricity nor its loading affects or the torque on the shaft were considered in the finite element model. I also neglected the torque from the wind on the competition shaft and considered the rotor be balanced for the natural frequency identification step as it relies on model stiffness and mass and neglects the applied loads. In Table 3.2 I have provided the all the loading conditions needed for the linear static and linear modal dynamic (transient and steady state) for reference.

Table 3.2 Loadings on Turbine Shaft

Parameter	Value	Units
T_w (Wind Torque on Shaft)	0.604 – 0.804	N-m
F_Tw (Wind thrust load)	89.5	N
F_W_MT (Simplified Rotor Weight - Conservative)	50	N
F_W_MT (Simplified Rotor Weight – Actual)	9.81	N
F_W_Me (Weight force of Eccentric mass)	1% to 20% of F_m_T	N
T_J_MT (Resistive Inertial Torque from Rotor)	5% to 10% of T_w	N-m

My linear static analysis case uses only the rotor weight load (F_W_MT), while my linear modal dynamic analyses would have incorporated the remaining loads. Following Table 3.2 I have also provided the linear static load case schematic, Figure 3.3, where the dimensions on this schematic reference Table 3.1.1. Additionally, to ease the visualization of the boundary conditions and loads on the finite element model I have removed simplified rotor from Figure 3.3. Lastly, See Appendix B, figure B.1 for a larger view of the linear static load case.

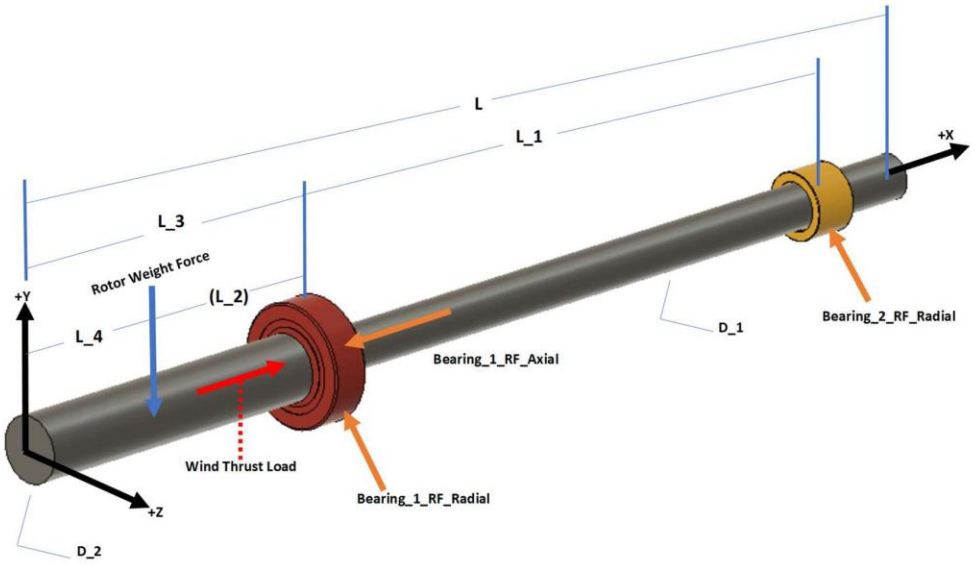

Figure 3.3. Linear static load case schematic.

The competition shaft and bearings are shown while the simplified rotor, due to its large size has been hidden. The bearings present are place holders for the boundary conditions used in this model. To allow for complexity to be incrementally added, I first took the bearings to be rigid and described bearing 1 with a 3D pin boundary condition – constrained displacement in X,Y,Z with all rotational degrees of freedom released – and bearing 2 with a 3D roller boundary condition – constrained displacement in the Y and Z directions with all rotational degree of freedom released.

4.0 Mesh Development and Mesh Convergence

Initially, I considered modeling the simplified shaft and rotor assembly with 3D solid hexahedral elements (linear and non-linear), but realized that issues with distorted elements and element quality could be avoided by using 3D wire planar elements and assigning appropriate beam sections. Since the shaft is 200mm long and 12mm wide at its largest step, the L/D ratio is > 15 and qualifies the use Euler-Bernoulli beams [3]. Also, as bending is the loading of interest – as I am attempting to extract the natural frequencies, which ABAQUS provides coupled with their corresponding mode shape [4], beam elements are an ideal choice to use in this case. I also chose to model the rotor as 3D wire with the corresponding beam section and material properties to match the size and mass of the actual rotor assembly as I wanted to avoid having to tie components together with meshes that cannot be mixed when using the tie constraint [5].

Here I have provided several views of the model with and without beam profiles rendered to clarify the following and previous discussions. When the beam profiles are not rendered, the two parts are indistinguishable – since they were both modeled as 3D deformable wires. However, this view is useful as it provides a better view of the rigid and spring boundary conditions used. Figure 4.1 Is the linear static model with rigid boundary conditions and the concentrated load applied 40mm out from the start of the 12mm shaft step to represent the rotor weight. Figure 4.2 is the linear static model with spring boundary conditions and the same load as the previous figure. Finally, figure 4.3 is the linear dynamic natural frequency extraction model with spring boundary conditions.

Figure 4.1. Linear static wire shaft model with rigid boundary conditions and rotor weight load.

The first boundary condition (the leftmost of the BCs in the unrendered version of the linear static model) is the 3D roller boundary condition. The second boundary condition (at the interface of the 8- and 12-mm steps) is the 3D pin boundary condition.

Figure 4.2. Linear static wire shaft model with spring boundary conditions and rotor weight load.

The rendered beam profile of the shaft is not shown in figure 4.2 as it is identical to the rendering in figure 4.1. In figure 4.2 the rigid boundary conditions, shown in figure 4.1, have been replaced by SPRING1 elements which connect to the same nodes the rigid 3D pin and Roller boundary conditions did, and provide an approximate representation of the bearing stiffnesses between these nodes and ground in the X,Y, and Z directions.

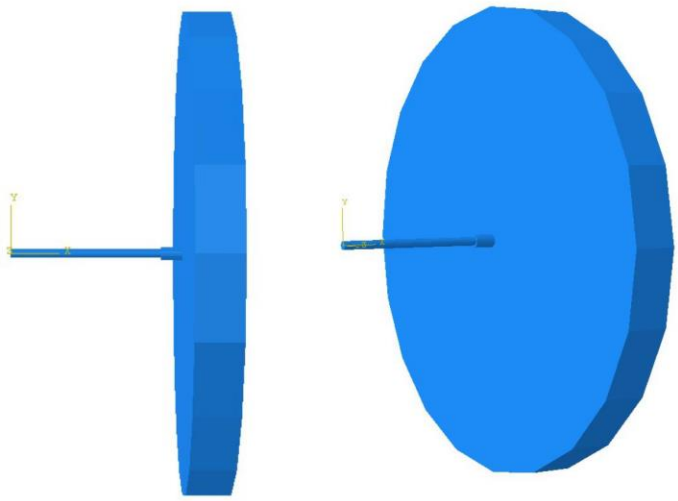

Figure 4.3. Linear dynamic natural frequency extraction model with rendered beam profiles.

In figure 4.3 the boundary conditions are identical to the those in figure 4.2 so, they have not been shown here. Also, the larger rotor part has distorted edges, however, this is only a limitation of the graphics when rendering the rotor (pipe profile) beam section and does not impact the natural frequency extraction or the section properties.

Since I chose to perform both linear static and dynamic analysis, mesh convergence was performed twice. First mesh convergence was checked for the beam element model of the competition shaft in the case of the linear static study where the applied load was the static weight of the simplified rotor and the desired result was the static deflection curve of the simply supported shaft (in 3D) with the load applied to the overhung portion that I predicted with my hand calculations (see appendix A). I started very coarse with my global mesh size for the beam elements as 70mm and found that they converged to within 5% of the theoretical values immediately. However, to provide further evidence of convergence for the linear static case, I reduced the element size by about half until I reached a global element size of 1mm. At about 50 mm global element size with a quadratic beam formulation the deflection at the point of the applied load converged. The max transverse deflection in the supported, 8mm step diameter section continued to improve its convergence with decreasing element size as the location of the max deflection point in this region of the shaft is located at the point given by the length of that section divided by the square root of three. While a near exact global element seed size that corresponds closely to this length value could have been specified to exactly match this value, there was no real need as convergence to the theoretical values was already well within 5% by the time a global element size of 1mm was reached. In figure 4.4 below I have provided the mesh convergence plots for the two parameters of interest during the linear static analysis phase of this modeling effort: 1) U,U2 Max in 8mm step region and 2) U,U2 @ location of applied load in 12 mm step region. Tabulated data from the linear static mesh convergence studies and checks are available in Appendix A.

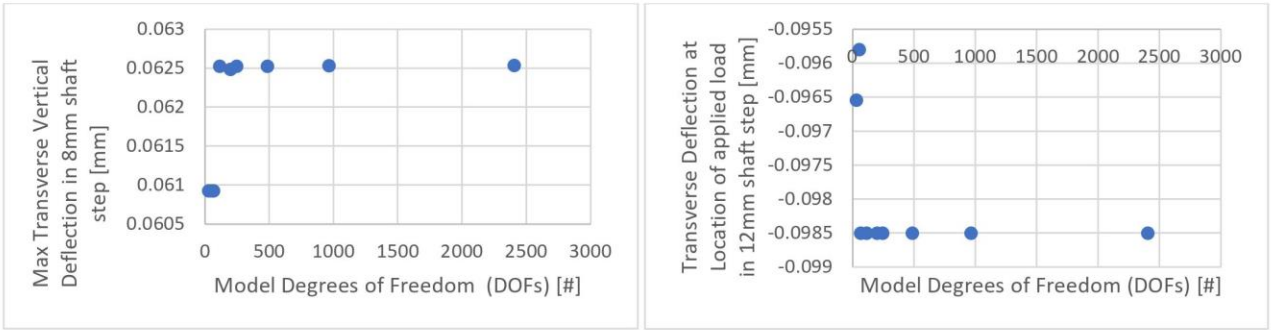

Figure 4.4 Linear static shaft model mesh convergence – 8mm and 12mm step region.

Prior to moving to the linear dynamic analysis, I changed the rigid boundary conditions to flexible and confirmed that the two deflections of interest in the 8 and 12mm step regions of the shaft matched within 5% of the previously converged rigid model with the same global seed size of 2mm. This allowed me to move forward with the linear dynamic natural frequency extraction without an intermediate mesh convergence study. However, I still needed to complete a mesh convergence study for the frequency extraction analysis.

The Dynamic natural frequency extraction mesh convergence study gave me similar results as the linear static analysis. As the degrees of freedom were increased, the % difference between modal frequencies remained under 5% for all but the 23rd modal frequency out of the 30 I requested. The first modal frequency was ignored as it was determined by the solver to be a rigid body mode and not an actual vibrational mode of interest. There were four other rigid body-like modes - where the shaft seems to extend and compress along its axis of rotation – that the solver did not identify as rigid body modes but, are likely an artefact of the way the axial thrust bearing stiffness was calculated. For natural frequency extraction, the mesh does not need to be especially fine to get the correct eigenvalues [6][7]. However, to better capture the actual mode shape a finer mesh is preferred [6][7]. Thus, I used the 2mm global seed size mesh for all the linear dynamic studies as it was the finest mesh that sufficiently described all requested modal frequencies and converged identically to the 1mm global seed size with half the computational cost. Immediately below, in figure 4.5 I have provided selected modal frequency convergence plots that show (exaggerated) divergence as the mesh was refined of the first 6 unique bending modes. All % difference values between the coarsest and finest meshes shown below are less than 0.2%.

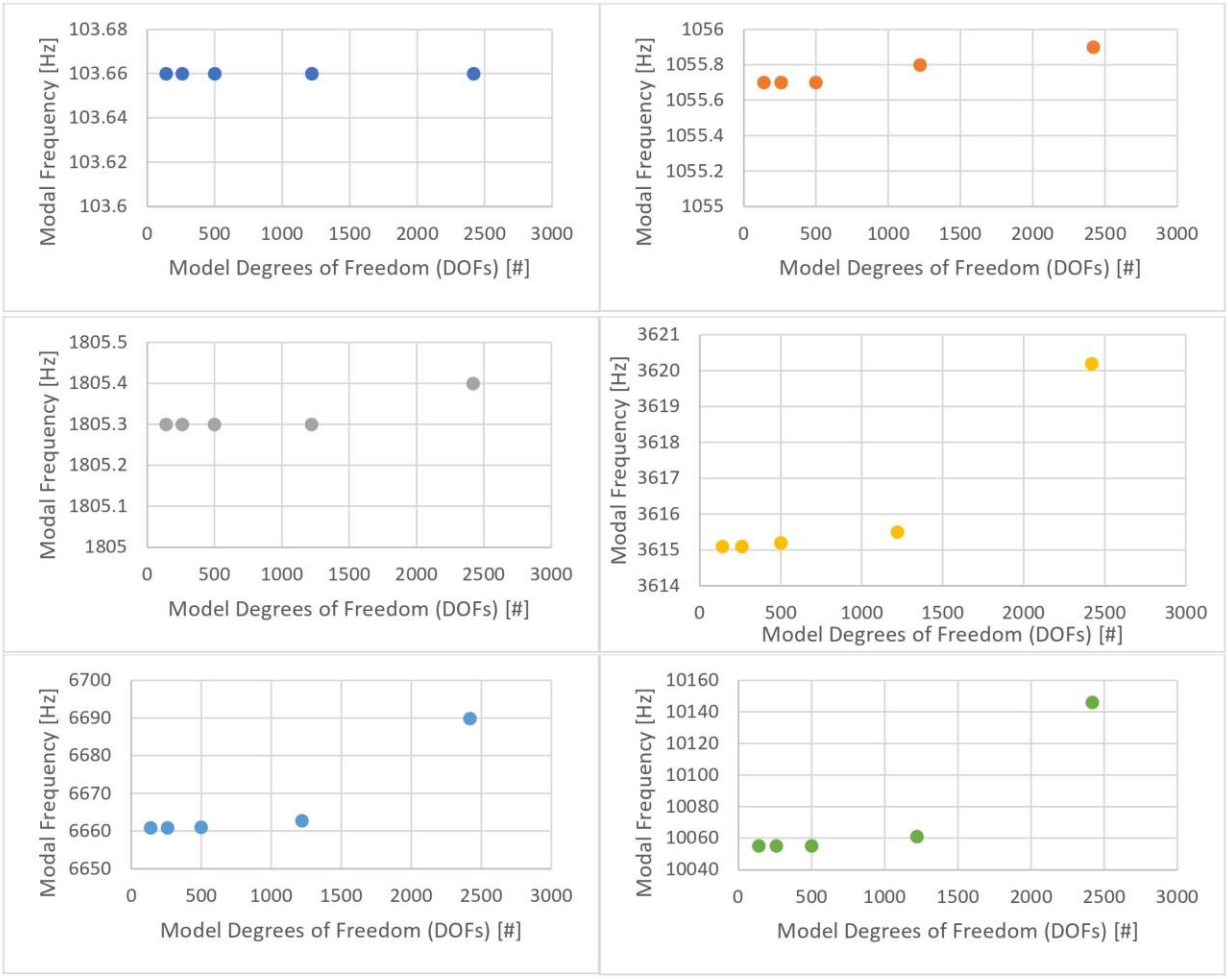

Figure 4.5. Natural frequency extraction mesh convergence – 1st – 6th unique bending modes

5.0 Analysis

I performed both linear static and linear dynamic analysis for this modeling project. The linear static analysis was used to verify model behavior and get preliminary mesh convergence before proceeding to the linear dynamic natural frequency extraction phase of the analysis. The linear dynamic analysis I used was the linear perturbation frequency analysis with the Lanczos solver, which was told to find the first 30 eigenvalues (modal frequencies and mode shapes) of the simplified rotor and shaft assembly. I requested the first 30 modes from the solver to ensure that all the modal frequencies strongly described by the eigenvalue (based on the modal effective mass for that modal frequency were at least 90% of the assembly's mass) were captured by the solver [6][7][8].

While conducting the linear static analysis, specifically during my mesh convergence study, I encountered several simultaneous zero-pivot (over-constrained) and numerical singularity solver problems (under-constrained) on a node that was not selected as a boundary condition or the application point of a load. The zero-pivot errors disappeared as the mesh was refined but, the numerical singularity problems for a single node in the 8mm step region of the shaft remained. Since the results were converging and the problem node was neither at nor near the point of interest, I ignored the remaining warnings. Additionally, when I changed the boundary conditions on the model from the rigid 3D pin and roller to springs representing the radial and thrust stiffnesses of the supporting bearings, the numerical singularity warnings disappeared. Adding the Tie constraint for the linear dynamic natural frequency extraction analysis came with warnings of the nodes having to be adjusted, stress and strain inaccuracy due to selected surfaces, and that an element-based surface approach was preferred. To resolve these warnings, I remodeled the part and made the tie constraint before meshing either component with no adjustment allowed [9]. I was not able to eliminate the stress inaccuracy error or the element-based surface error. However, since both errors are linked to concerns with contact interactions and the resulting stresses/strains not the mass or stiffness of the assembly, I decided to disregard them as they were unlikely to affect the mode shapes and frequencies yielded by natural frequency extraction.

6.0 Results

I originally estimated the first natural frequency of the simplified rotor and shaft assembly using Dunkerely's and Rayleigh's method. Under the conservative rotor weight loading of 50 N the first critical frequency was predicted to be between 3003 RPM and 1325 RPM (the operating speed of the rotor is 2500 RPM). However, during the project, the pitching senior project team responsible for designing the hub finished their first revision of final CAD which gave a new rotor weight load. This new load was 9.81 N (a 1 kg rotor) and gave the estimate for the first natural frequency to be between 6633 RPM and 2991 RPM (See Appendix A). The wire shaft and rotor model with flexible boundary conditions converged on a 1st modal frequency of 103.6 Hz or 6216 RPM showing that the estimation techniques used in the hand calculations were somewhat accurate in predicting the first mode. In table 6.1 below, I have provided the first 10 unique modal frequencies from the natural frequency extraction analysis. A complete table of all 30 modal frequencies is available in Appendix C.

Table 6.1 Unique Bending Modal Frequencies of simplified rotor + shaft model

Mode No.	Frequency	Frequency	Rotational Speed
(#)	(rad/sec)	(Hz)	(RPM)
2	651.33	103.66	6219.6
5	6633.4	1055.7	63342
7	11343	1805.3	108318
9	22715	3615.1	216906
12	41851	6660.8	399648
15	63176	10055	603300
17	88154	14030	841800
20	118528	18864	1131840
22	154577	24602	1476120
24	157536	25073	1504380

The CPWP has specified three rotational speeds as areas for concern with natural frequencies of the rotating assembly: 1) the operating speed of the rotor at 2500 RPM, 2) the max test speed of the rotor at 3103 RPM, and 3) the analysis speed of the rotor at 5253 RPM (these rotational speeds correspond to wind speeds of 11 m/s, 13 m/s, and 22 m/s). The safety of testing the competition turbine at the operating and max test speeds is in part driven by the force amplification factor, which is a function of the ratio of the driven frequency and the natural frequency of interest of the system. To further qualify the safety of performing the physical testing I generated three transmissibility vs. frequency ratio plots and have provided them here below in figure 6.1.

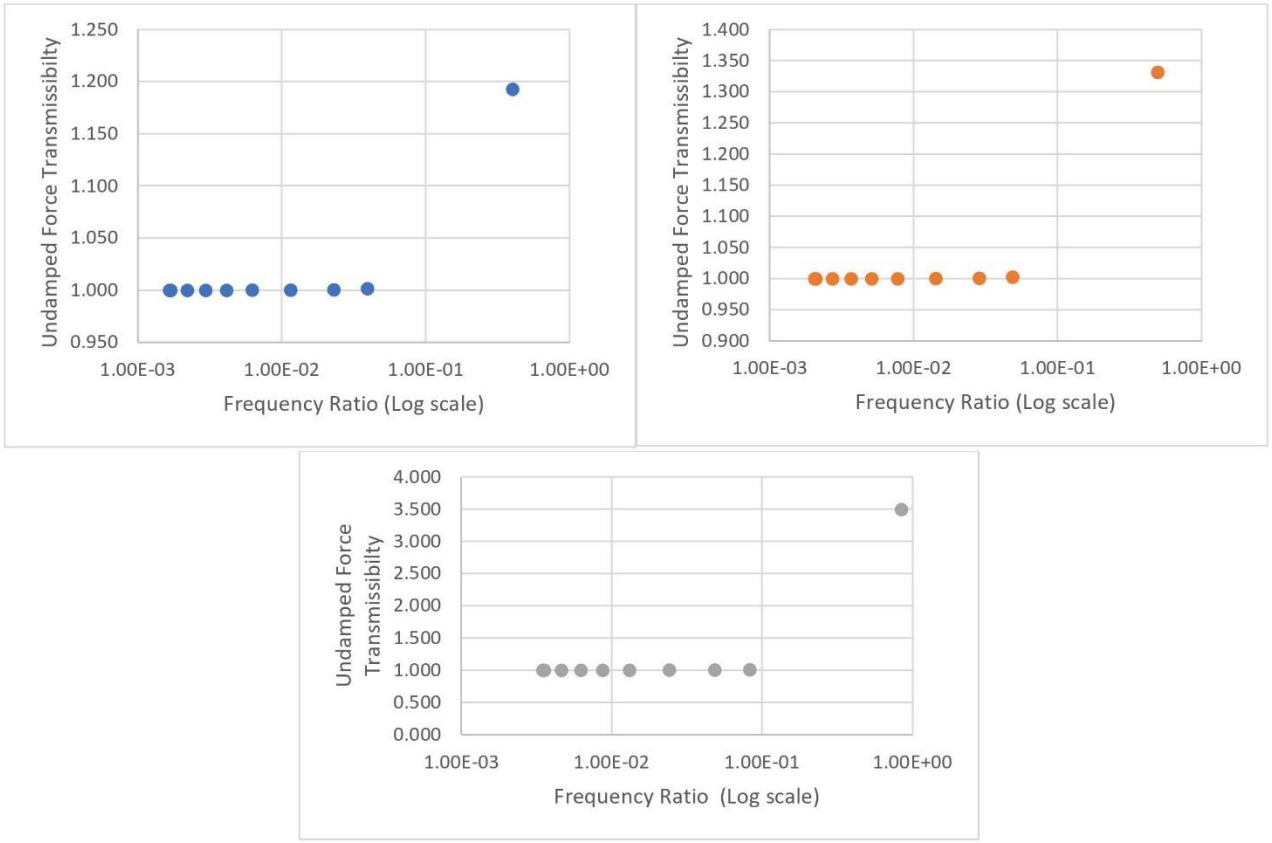

Figure 6.1. Force transmissibility amplification factor as a function of frequency ratio

Top Left: the reference driven frequency is the operating speed – 2500 RPM; Top Right: the reference driven frequency is the max test speed – 3103 RPM; Bottom Center: the reference driven frequency is the analysis speed – 5253 RPM. I employed a log scale on all x-axes of these plots as the frequency ratios were all considerably less than 0.1 for natural frequencies beyond the first bending mode. In the case of the operating and max test speed the force amplification factor gives a response that only slightly exceeds the static response (an undamped force transmissibility factor of 1). In contrast, the amplification factor for the analysis speed, for the first critical frequency, is ~3.5 which is above the maximum allowable factor of 2 [10]. So, vibrations testing of the competition turbine will be safe at operating and max test speeds, however further shaft design refinement may be needed to increase the first natural frequency of the rotating assembly to reduce the amplification factor to below the allowable threshold.

7.0 Discussion

At the outset of this project my objectives were to lay the ground work for a better finite element model and estimate of the natural/critical frequencies of a simplified, but representative rotor and shaft assembly to help verify that vibrations testing on the mass imbalance characterization test bed is safe to do. ABAQUS is by far way more user friendly than

MCS/ADAMS. Even so, my modeling skills after taking only a single dedicated FEA course focused primarily on linear static analysis are still behind what is needed for the more complicated transient dynamic model I originally intended to attempt. While I was able to identify the modal frequencies of the system and estimate which modes must be avoided based on their corresponding modal effective mass values, I was unable to determine what effects mass imbalance in the rotor has on the dynamic behavior of the system around the operating speed of the extracted modal frequencies.

On the other hand, the resulting modal frequencies all start at around 104Hz or 6240 RPM. This makes the frequency ratio between the driven and natural frequencies less than 0.5 for both the operating and max test speed of the competition wind turbine. Even with an undamped amplitude magnification factor, the resulting dynamic force amplification factor gives a dynamic response for these speeds that is approximately the static response meaning that transient dynamic analysis may not be needed in the case of this project. More importantly, since the rotating assembly is operated below its first natural frequency, the shaft can be considered rigid, and it is highly unlikely that any natural frequencies will be excited during testing. As a result, the vibrations test bed will not only be safer to use but it is highly unlikely that even with mass imbalance present in the rotor a resonance condition will be excited.

It was my hope to compare the results from the transient dynamic model with experimental results of the competition wind turbine being balanced, but currently the competition turbine has not yet been manufactured and the ongoing COVID-19 pandemic made accessing the Cal Poly mechanical engineering vibrations lab far more logistically difficult/time consuming than I expected. Though I fell short of my initial, lofty analysis goal, I was able to extract natural frequencies that are at minimum a decent estimate of the natural frequencies of the competition turbine's rotating assembly. I remain convinced that more refinement work is needed to further verify these results. The initial phase of that work would include making a 3D hexahedral element version of this model to try and capture the stiffening effect that the hub has on the shaft which makes it more resistant to whirling (this also would provide better grounds to continue neglecting the gyroscopic effects from a whirling overhung rotor) [1][9]. This was supposed to be accomplished by modeling the rotor as a single quadratic beam element, but it deflected with the shaft with ease instead of further stiffening it. Finally, I was only able to get the Lanczos solver to work reliably and unable to change normalization option from mass to displacement as the reported displacements when viewing the mode shapes at their corresponding natural frequency are meaningless and only intended to give a sense of shape not scale. Consequently, the mode shapes were not provided in this report as the displacement scale is misleading, but they are provided in the model file.

8.0 Conclusion

In sum, natural frequencies for a simplified but representative model of the rotating assembly of the CPWP's competition wind turbine were extracted and found to be well above the max rotational speed of the competition turbine. I removed transient dynamic analysis from my project's scope due to its complexity and potential for extremely time-consuming debugging. Further verification of my model is needed to take the level of certainty of these extracted natural frequencies from decent estimate to reasonably approximate. Additionally, I would like to find some way to make the model more readily adaptable to design changes from the CPWP perhaps by implementing a design-study like model in ABAQUS – if that feature is supported. It currently appears to be the case that CPWP's competition wind turbine is both safe to test in the wind tunnel and on the vibrations measurement test bed my senior project is currently designing.

Works Cited

[1] Wu, X., C. Naugle, and J. Meagher. "A full spectrum analysis methodology applied to an anisotropic overhung rotor." J Appl Mech Eng 5 (2016): 232.[Online].

[2] Gargiulo E.P. Jr., "A Simple Way to Estimate Bearing Stiffness." *Machine Design.* (1980). pp.107-110. [Online]. https://dyrobes.com/help1800/Rotor/html/dyro17qs.htm

[3] (2020) "Choosing a beam element." *ABAQUS User Manual*. MIT. [Online]. https://abaqus-docs.mit.edu/2017/English/SIMACAEELMRefMap/simaelm-c-beamelem.htm

[4] (2020) "Natural frequency extraction." *ABAQUS User Manual*. MIT. [Online]. https://abaqus-docs.mit.edu/2017/English/SIMACAEANLRefMap/simaanl-c-freqextraction.htm

[5] (2020) "Mesh tie constraints." *ABAQUS User Manual*. MIT. [Online]. https://abaqus-docs.mit.edu/2017/English/SIMACAECSTRefMap/simacst-c-tiedconstraint.htm

[6] Abney, T. "SOLIDWORKS Simulation: Dynamic Analysis." video recording. LinkedIn Learning (2018). Viewed 27 May, 2020. [Online]. https://www.linkedin.com/learning/solidworks-simulation-dynamic-analysis/mass-participation-background?u=2121556

[7] "Abaqus Standard: Fundamentals and Modal analysis." *Abaqus Acumen.* YouTube. [Online]. https://www.youtube.com/watch?v=T5MhK-MuGMQ

[8] (2020) "Modifications to the model." *Cargo Crane Example* – Getting Started with Abaqus. MIT. [Online]. https://abaqus-docs.mit.edu/2017/English/SIMACAEGSARefMap/simagsa-c-dynmodeldata.htm

[9] Schuster, J. (2017) "Abaqus Tutorial 2 (Beams and Constraints)." *Schuster Engineering*. YouTube. [Online]. https://www.youtube.com/watch?v=rY4cNbXHV0U&list=PLBwQ5Llf4Q_Vj8xKcxsbzIfdqrtzcHLbe&index=3

[10] E.J. Gunter. "Introduction to Rotor Dynamics - Critical Speed and Unbalance Response Analysis." (2001). Dyrobes Rotordynamics Software ©. [Online]. https://dyrobes.com/wp-content/uploads/2016/04/Introduction-to-Rotor-Dynamics-Critical-Speed-and-Unbalance-Response-Analysis-E.-J.-Gunter_linked.pdf

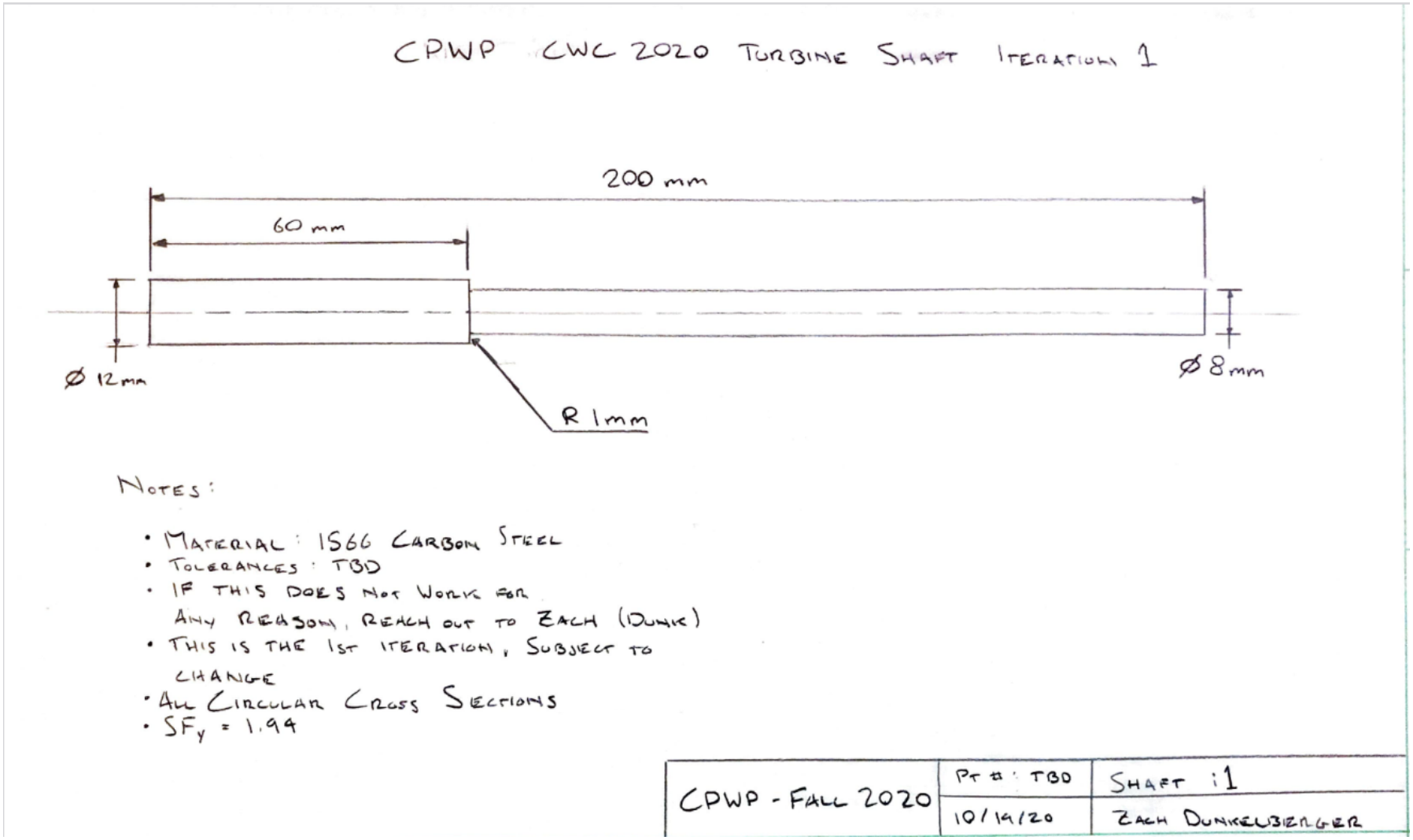

Figure L.1(A.1) Dimensioned Competition Shaft Drawing. Courtesy of Z. Dunkelberger, CPWPC mechanical team lead

STATIC DEFLECTION

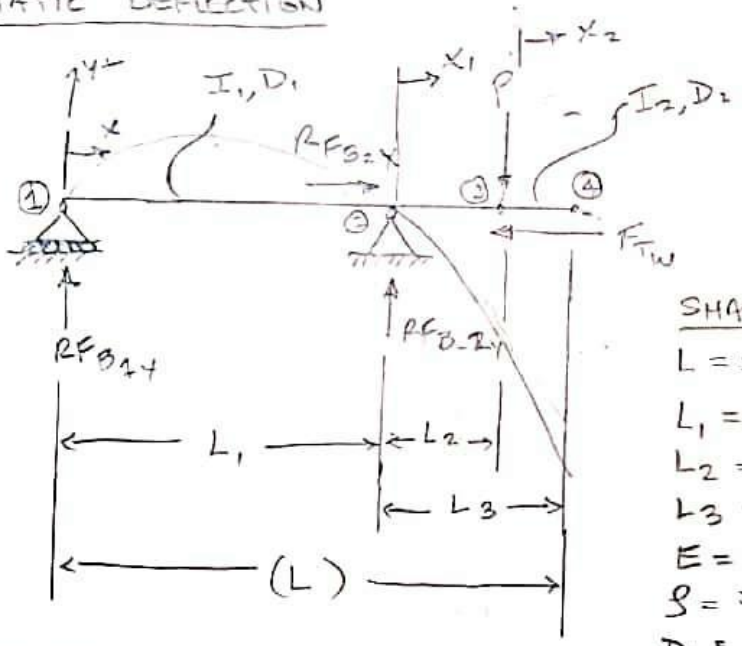

SHAFT PROPERTIES

$L = 200\ mm$

$L_1 = 140\ mm$

$L_2 = 40\ mm$

$L_3 = 60\ mm$

$E = 200 \times 10^9\ Pa$

$\rho = 7850\ kg/m^3$

$D_1 = 8\ mm$

$D_2 = 12\ mm$

ASSUME:

(1) STEADY STATE, SHAFT NOT ACCELERATING, APPLIED TORQUES/INERTIAS VANISH

(2) BALANCED ROTOR, NEGLIGIBLE ECCENTRICITY,

(3) ECCENTRIC MASS NEGLECTED

(4) LINEAR ISOTROPIC MATERIAL BEHAVIOR

(5) RIGID SUPPORTS, FLEXIBLE SHAFT

(6) BEARING 2 RF_x TAKES THRUST LOAD F_{TW}

(7) BEARING 1 ONLY SUPPORTS RADIAL LOADS

(8) SHAFT IS SIMPLY SUPPORTED

(9) STATIC DEFLECTION CURVE $\approx$ TO 1ST CRITICAL FREQUENCY MODE SHAPE

(10) NEGLECT STRESS CONCENTRATIONS

(11) AXIAL DEFLECTION DECOUPLED FROM TRANSVERSE

ANALYSIS:

APPLY SUPERPOSITION:

1)

+

$$\theta_{23\_comp} = \theta_{23\_2} + \theta_{2\_1}(L_1)$$

$$\therefore \theta_{23\_comp} = \frac{P}{6EI_2}(3x_1^2 - 6L_2x_1) + -\frac{PL_2L_1}{3EI_1}$$

$$= \frac{PI_1}{6EI_1I_2}(3x_1^2 - 6L_2x_1) + \frac{-2PL_2L_1I_2}{6EI_1I_2}$$

$$\therefore \boxed{\theta_{23\_comp} = \frac{P}{6EI_1I_2}(3x_1^2I_1 - 6L_2x_1I_1 - 2L_2L_1I_2)}$$

$$\int_0^{L_2} \theta_{23\_comp}\, dx_1 = \frac{P}{6EI_1I_2}(I_1x_1^3 - 3L_2I_1x_1^2 + \dots - 2L_2L_1I_2x_1)$$

$$\boxed{v_{23\_comp} = \frac{P}{6EI_1I_2}(I_1x_1^3 - 3I_1L_2x_1^2 - 2L_2L_1I_2x_1)} \quad (0 \le x_1 \le L_2)$$

EXTRAPOLATED ELASTIC CURVE 2 - COMPLETE:

ASSUME

(12) SMALL ANGLE APPROXIMATION - SMALL DEFLECTIONS

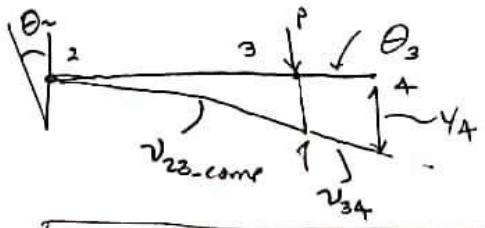

$$\therefore \boxed{v_{34} = \theta_{3\_comp}(x_2 - L_2) \quad (L_2 \le x_2 \le L_3)}$$

$$\theta_{3\_c} = \frac{P}{6EI_1I_2}(3x_1^2I_1 - 6L_2x_1I_1 - 2L_2L_1I_2)\Big|_{x_1 = L_2}$$

$$= \frac{P}{6EI_1I_2}(3L_2^2I_1 - 6L_2^2I_1 - 2L_2L_1I_2)$$

$$\boxed{\theta_{3\_c} = \frac{P}{6EI_1I_2}(-3L_2^2I_1 - 2L_2L_1I_2)}$$

ANALYSIS (CONT):

2)

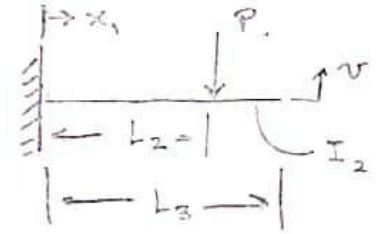

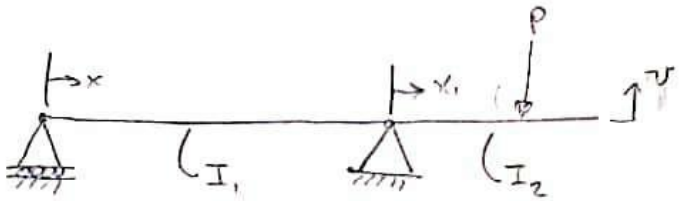

ORIGINAL)

ELASTIC CURVE 1. $(0 \leq x \leq L_1)$

$$v'_{12} = \frac{-PL_2}{6EI_1L_1}(x^3 - L_1^2 x)$$

SINCE UNLOADED IN THIS REGION, THIS ELASTIC CURVE IS UNCHANGED..

ELASTIC CURVE 2

$$v_{23} = \frac{P}{6EI_2}(x_1^3 - 3L_2x_1^2)$$

THIS CURVE MUST BE MODIFIED SUCH THAT

$$\theta_{2\_1} = \theta_{2\_2} \quad (1)$$

θ_{2_1} IS GIVEN BY: $\frac{-PL_2L_1}{3EI_1}$

$$\frac{d}{dx_1}(v_{23}) = \theta_{23\_2}$$

$$\theta_{23\_2} = \frac{P}{6EI_2}(3x_1^2 - 6L_2x_1)$$

CONDITION (1) STIPULATES THAT $\theta_{23\_2}(0) = \theta_{12\_1}(L_1)$

MAXIMUM DEFLECTIONS:

$$v_{12\_max} = \frac{P L_2 L_1}{9\sqrt{3} E I_1}$$ (FROM CE 201 EQN SHEET)

$$v_{23\_max} = \frac{P}{6EI_1I_2}\left(I_1 x_1^3 - 3I_1 L_2 x_1^2 - 2L_2^2 L_1 I_2 x_1\right)\Big|_{x_1 = L_2}$$

$$= \frac{P}{6EI_1I_2}\left(I_1 L_2^3 - 3I_1 L_2^3 - 2L_2^2 L_1 I_2\right)$$

$$= \frac{P}{6EI_1I_2}\left(-2I_1 L_2^3 - 2L_2^2 L_1 I_2\right)$$

$$v_{23\_max} = \frac{-P}{3EI_1I_2}\left(I_1 L_2^3 + L_2^2 L_1 I_2\right)$$

SHAFT PROPERTIES (CONT)

$$I_1 = \frac{\pi}{4}\left(\frac{D_1}{2}\right)^4 = \frac{\pi}{4}\left(\frac{0.008\,m}{2}\right)^4$$

$$I_2 = \frac{\pi}{4}\left(\frac{D_2}{2}\right)^4 = \frac{\pi}{4}\left(\frac{0.012\,m}{2}\right)^4$$

$$\forall_1 = \frac{\pi D_1^2}{4} \cdot L_1 = \frac{\pi}{4}(0.008\,m)^2 \cdot 0.14\,m$$

$$\forall_2 = \frac{\pi D_2^2}{4} \cdot L_3 = \frac{\pi}{4}(0.012\,m)^2 \cdot 0.06\,m$$

$$W_1 = \forall_1 \rho_{1566}$$

$$W_2 = \forall_2 \rho_{1566}$$

$$I_1 = 2.01 \times 10^{-10}\ m^4$$
$$I_2 = 1.02 \times 10^{-9}\ m^4$$
$$\forall_1 = 7.04 \times 10^{-6}\ m^3$$
$$\forall_2 = 6.79 \times 10^{-6}\ m^3$$

SHAFT PROPERTIES (CONT)

$$W_1 = \frac{\pi}{4}(0.008\,m)^2 \cdot 0.14m \cdot 7850\,\frac{kg}{m^3} \cdot 9.81\,\frac{m}{s^2}$$

$$W_2 = \frac{\pi}{4}(0.012\,m)^2 \cdot 0.06m \cdot 7850\,\frac{kg}{m^3} \cdot 9.81\,\frac{m}{s^2}$$

$$\begin{bmatrix} W_1 = 5.42 \times 10^{-1}\,N \\ W_2 = 5.23 \times 10^{-1}\,N \end{bmatrix}$$

$$v_{12\_max} = \frac{(50\,N)(0.04m)(0.14m)^3}{9\sqrt{3}(200E9\,\frac{N}{m^2})(2.01E{-}10\,m^4)}$$

$$\begin{bmatrix} v_{12\_max} = 6.25 \times 10^{-5}\,m \quad (\text{FOR } 50N \downarrow) \\ -6.25 \times 10^{-5}\,m \quad (\text{FOR } 50N \uparrow) \\ \star \text{ STATIC DEFLECTED BEAM SHAPE SYMMETRIC ABOUT UNDEFORMED BEAM WHEN UNDER EQUAL, BUT OPPOSITE LOADING} \end{bmatrix}$$

$$v_{23\_max} = \frac{-50N}{3(200E9\,\frac{N}{m^2})(2.01\times10^{-10}m^4)(1.02\times10^{-9}\,m^4)}$$

$$\cdot\left[2.01\times10^{-10}m^4 \cdot (0.04m)^3 + (0.04m)^2(0.14m) \cdot 1.02\times10^{-9}\,m^4\right]$$

$$\begin{bmatrix} v_{23\_max} = 9.81 \times 10^{-5} \quad (\text{FOR } 50N \downarrow) \\ -9.81 \times 10^{-5} \quad (\text{FOR } 50N \uparrow) \\ \star \quad " \quad " \end{bmatrix}$$

CRITICAL SPEED:

RAYLIEGH:

DESCRITIZED SYSTEM $\omega_1 = \sqrt{\frac{g\sum W_i y_i}{\sum W_i y_i^2}}$

CRITICAL SPEED ESTIMATE (CONT)

DISCRETIZE STEPPED SHAFT AS FOLLOWS:

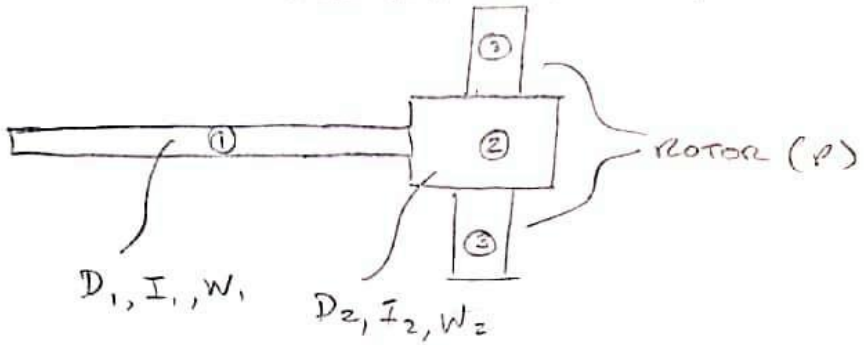

SINCE ROTOR IS ONLY APPLIED (EXTERNAL LOAD) y_i's ALREADY KNOWN

$$\therefore \omega_{1_{ALL}} = \sqrt{\frac{g\left|\left(W_1 v_{12\text{-}max} + (W_2 + P)\, v_{23\text{-}max}\right)\right|}{\left|\left(W_1 v_{12\text{-}max}^2 + (W_2 + P) v_{23\text{-}max}^2\right)\right|}}$$

$$\omega_{1_{SHAFT}} = \sqrt{\frac{g\left|\left(W_1 v_{12\text{-}max} + W_2 v_{23\text{-}max}\right)\right|}{\left|\left(W_1 v_{12\text{-}max}^2 + W_2 v_{23\text{-}max}^2\right)\right|}}$$

$$\left[\omega_{1_{ALL}} = 314 \frac{rad}{sec} = 3003 \text{ RPM}\right] \longrightarrow \text{UPPER BOUND } \omega_1$$

$$\omega_{1_{SHAFT}} = 154 \frac{rad}{sec} = 1474 \text{ RPM}$$

DUNKERLEY'S METHOD IS USED TO GET THE LOWER BOUND $\omega_{1_{ALL}}$

$$\omega_{11\_D} = \sqrt{\left[\frac{P}{g} v_{23\text{-}max}\right]^{-1}}$$ INITIAL ESTIMATE (NEGLECTING SHAFT WEIGHT)

$$\frac{1}{\omega_{11}} \approx \sum \frac{1}{\omega_{ii}^2}$$

CRITICAL SPEED ESTIMATE

DUNKERLEY'S CONT

$$\frac{1}{\omega_{11\_ALL}} = \frac{1}{\omega_{11}^2} + \frac{1}{\omega_s^2}$$

$$\omega_{11\_all\_D} = \sqrt{\left[\frac{1}{\omega_{11\_D}^2} + \frac{1}{\omega_{1_{SHAFT}}^2}\right]^{-1}}$$

$\omega_{11\_D} = 3020$ RPM

$\left[\omega_{11\_ALL\_D} = 1325 \text{ RPM}\right] \rightarrow$ LOWER BOUND ω_1

Table L.1(A.1) Excel output using hand calculations – conservative loading condition

Givens		
Parameter	Value	Units
Rho_1566	7850	kg/m^3
E_1566	2E+11	Pa
D_1	0.008	m
D_2	0.012	m
W_R	50	N
L_1	0.14	m
L_2	0.04	m
L_3	0.06	m
L	0.2	m
g	9.81	m/s^2

Shaft Properties		
Parameter	Value	Units
A_1	5.03E-05	m^2
A_2	1.13E-04	m^2
Vol_1	7.04E-06	m^3
Vol_2	6.79E-06	m^3
I_1	2.01E-10	m^4
I_2	1.02E-09	m^4
W_1	5.42E-01	N
W_2	5.23E-01	N
y_1_max	-6.25E-05	m
y_2_max	9.81E-05	m

Raighleigh's Method			
Parameter	Value	Units	
Sig_Wi_yi	4.92E-03	N-m	Shaft + Rotor
Sig_Wi_yi^2	4.88E-07	N-m^2	
omega_1	314	rad/sec	
N_1_all	3003	RPM	
Sig_Wi_yi	1.736E-05	N-m	Shaft Only
Sig_Wi_yi^2	7.15E-09	N-m^2	
omega_1	154	rad/sec	
N_1_shaft	1474	RPM	

Dunkerley's Method			
Parameter	Value	Units	
del_1	-1.25E-06		
del_2	1.96E-06		
omega_1_rotor	316.3	rad/sec	
N_1_rotor	3020	RPM	Rotor Only
omega_1_all	1325	RPM	Rotor + Shaft

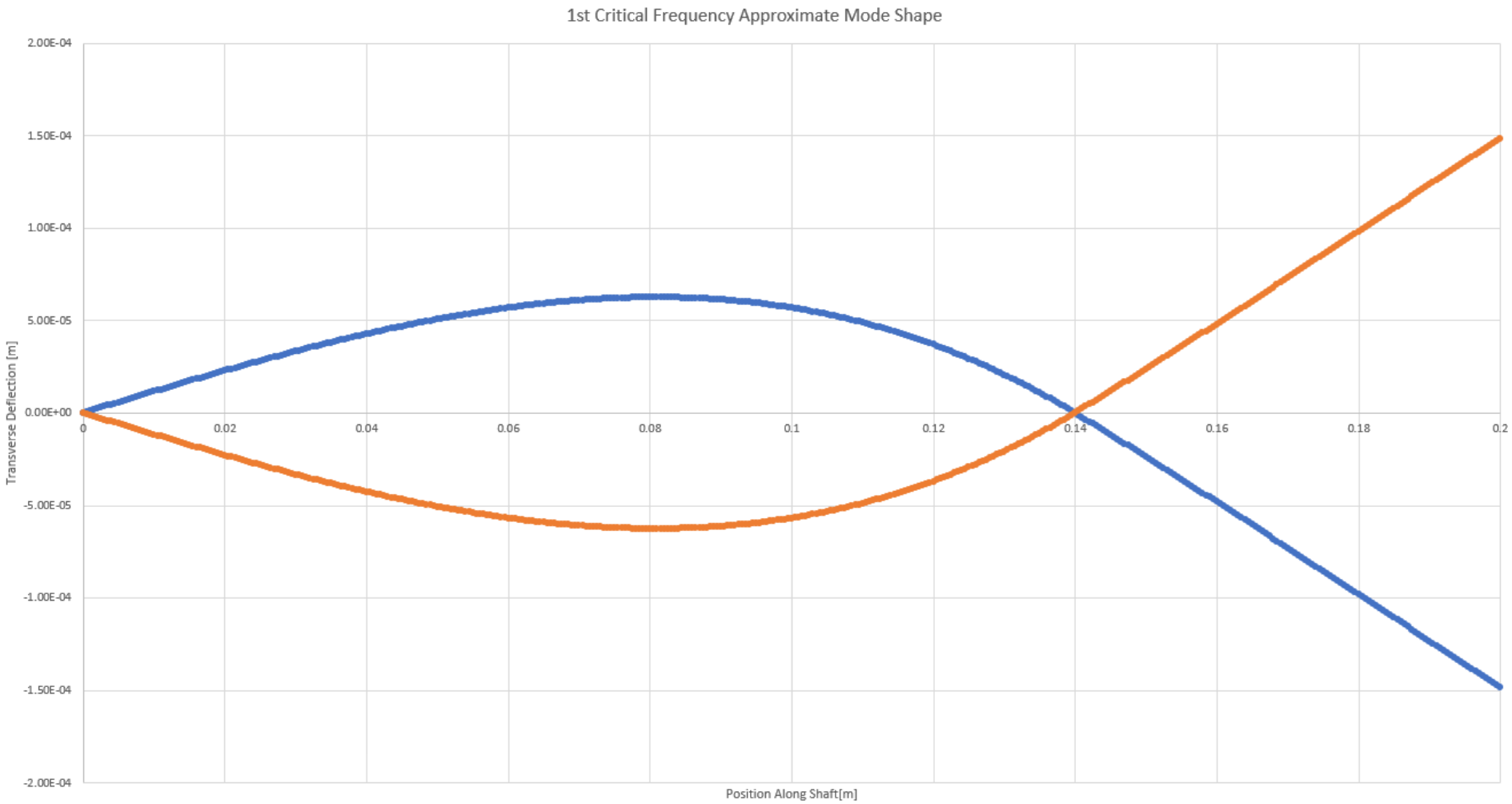

Figure L.2(A.2) Elastic Curve of Shaft - Approximated Shape of 1st Mode from Superposition (50N Rotor weight loading condition)

Table L.2(A.2) Excel output using hand calculations – actual loading condition

Givens		
Parameter	Value	Units
Rho_1566	7850	kg/m^3
E_1566	2E+11	Pa
D_1	0.008	m
D_2	0.012	m
W_R	9.81	N
L_1	0.14	m
L_2	0.04	m
L_3	0.06	m
L	0.2	m
g	9.81	m/s^2
Shaft Properties		
Parameter	Value	Units
A_1	5.03E-05	m^2
A_2	1.13E-04	m^2
Vol_1	7.04E-06	m^3
Vol_2	6.79E-06	m^3
I_1	2.01E-10	m^4
I_2	1.02E-09	m^4
W_1	5.42E-01	N
W_2	5.23E-01	N
y_1_max	-1.22694E-05	m
y_2_max	1.92433E-05	m

Raighleigh's Method			
Parameter	Value	Units	
Sig_Wi_yi	1.92E-04	N-m	Shaft + Rotor
Sig_Wi_yi^2	3.91E-09	N-m^2	
omega_1	695	rad/sec	
N_1_all	6633	RPM	
Sig_Wi_yi	3.407E-06	N-m	Shaft Only
Sig_Wi_yi^2	2.75E-10	N-m^2	
omega_1	349	rad/sec	
N_1_shaft	3328	RPM	

Dunkerley's Method			
Parameter	Value	Units	
del_1	-1.25E-06		
del_2	1.96E-06		
omega_1_rotor	714.0	rad/sec	
N_1_rotor	6818	RPM	Rotor Only
omega_1_all	2991	RPM	Rotor + Shaft

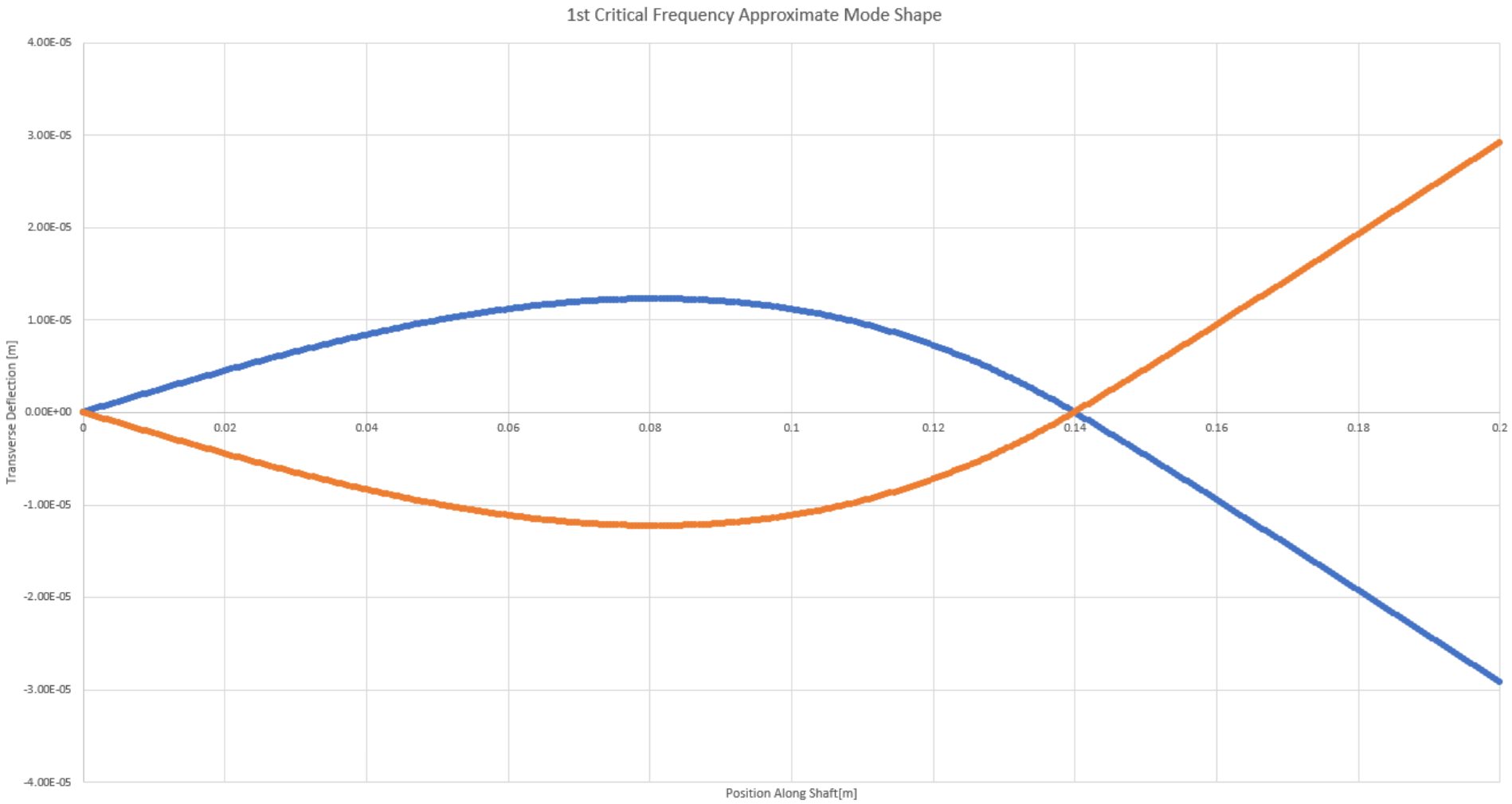

Figure L.3(A.3) Elastic Curve of Shaft - Approximated Shape of 1st Mode from Superposition – (9.81 N rotor weight loading condition)

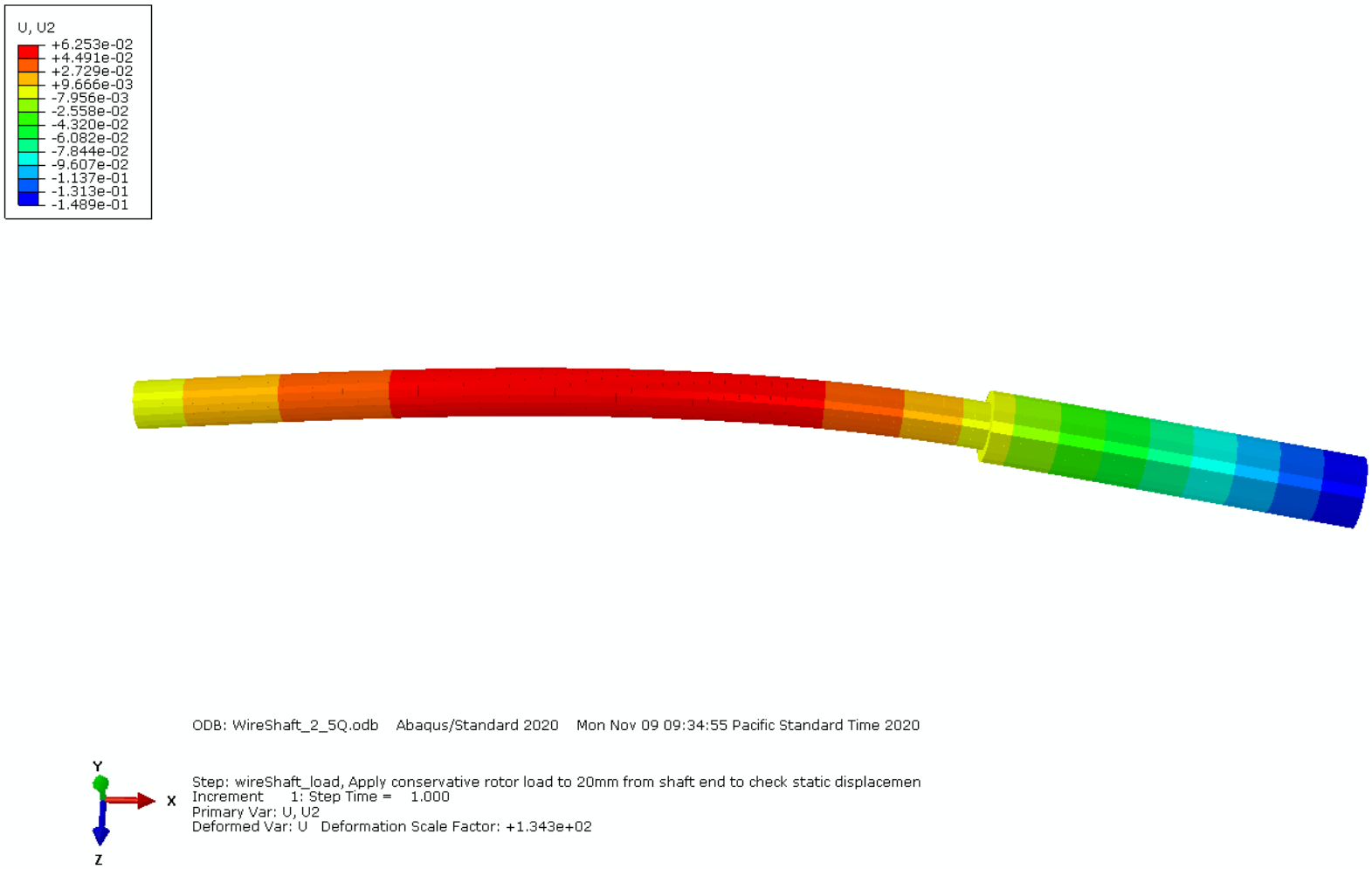

Figure L.4(A.4). Static deflection of the wire shaft quadratic beam model under conservative rotor load

Pictured immediately above is the converged linear static model under the more conservative 50 N rotor weight loading. The beam element formulation used for this wire shaft model was quadratic and had 2.5mm global seed size. This model also made use of rigid displacement only boundary conditions – acting as a 3D roller and pin from left to right on the ends of the smaller shaft step.

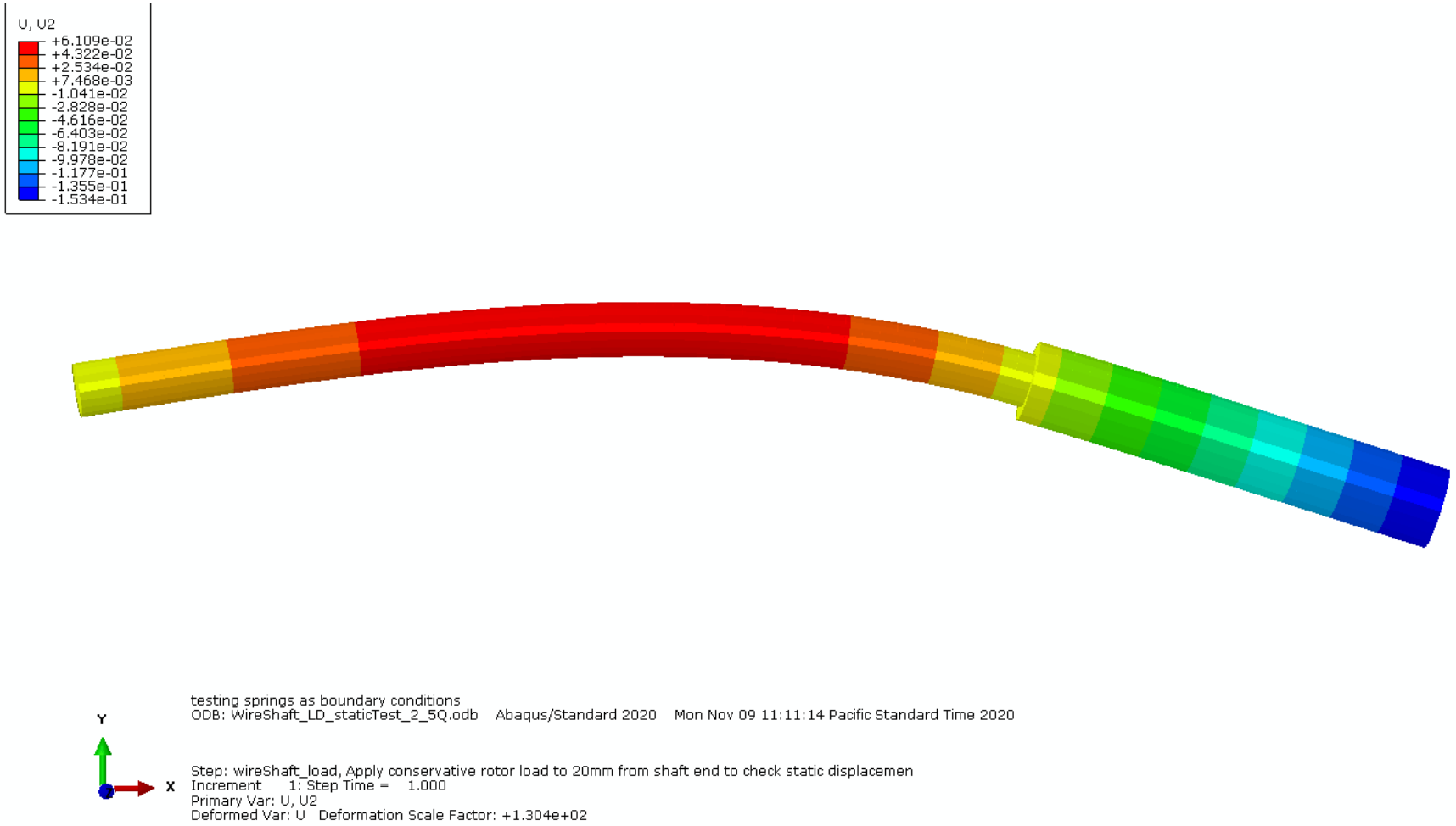

Figure L.5(A.5). Static deflection of the wire shaft quadratic beam model under conservative rotor load

Here we have the same mesh on the wire shaft model with only modified boundary conditions. The ends of the small step of the stepped competition shaft are held by SPRING1 elements in ABAQUS that connect the specified nodes to ground and match the load dependent behavior of the bearing stiffness approximation from Gargiulo [2]. The percent difference between the maximum point of deflection in the 8mm shaft step region and the point of application of the rotor weight load in the 12mm shaft step region was less than 5% for each, so this modified boundary condition version of the previous model also converged.

Table L.3 (A.3). Tabulated Linear Static mesh convergence study

Element Type	Seed Size	# Elements	#DOFs	U,U2 Max in 8mm Step	U,U2 Max in 12mm Step	U,U2 8mm Theoretical	U,U2 12mm Theoretical	%Error 1	%Error 2
(description)	(mm)	(#)	(#)	(mm)	(mm)	(mm)	(mm)	(%)	(%)
Linear Beam	70	4	30	0.0609265	-0.0965432	0.062535	-0.0980801	-2.57	-1.56
Quadratic Beam	70	4	54	0.0609265	-0.0958013			-2.57	-2.32
Quadratic Beam	50	5	66	0.0609265	-0.0985012			-2.57	0.429
Quadratic Beam	25	9	114	0.0625249	-0.0985012			-0.0161	0.429
Quadratic Beam	12.5	16	198	0.0624829	-0.0985012			-0.0833	0.429
Quadratic Beam	10	20	246	0.0625252	-0.0985011			-0.0156	0.429
Quadratic Beam	5	40	486	0.0625252	-0.0985011			-0.0156	0.429
Quadratic Beam	2.5	80	966	0.0625324	-0.0985011			-0.0041	0.429
Quadratic Beam	1	200	2406	0.0625334	-0.0985011			-0.00255	0.429

Table L.4 (A.4). Proof of convergence for Linear static mesh with SPRING1 boundary conditions.

Element Type	Seed Size	# Elements	#DOFs	U,U2 Max in 8mm Step	U,U2 Max in 12mm Step	U,U2 8mm Theoretical	U,U2 12mm Theoretical	%Error 1	%Error 2
(description)	(mm)	(#)	(#)	(mm)	(mm)	(mm)	(mm)	(%)	(%)
Quadratic Beam	2.5	80	966	0.0610924	-0.102466	0.062535	-0.0980801	-2.31	4.47

This study was not repeated when the rotor loading weight decreased as the mesh was sufficiently fine to accurately describe the static deflection curve of the beam under a lower magnitude of loading as well as capable of describing the extracted mode shapes without unacceptable distortion.

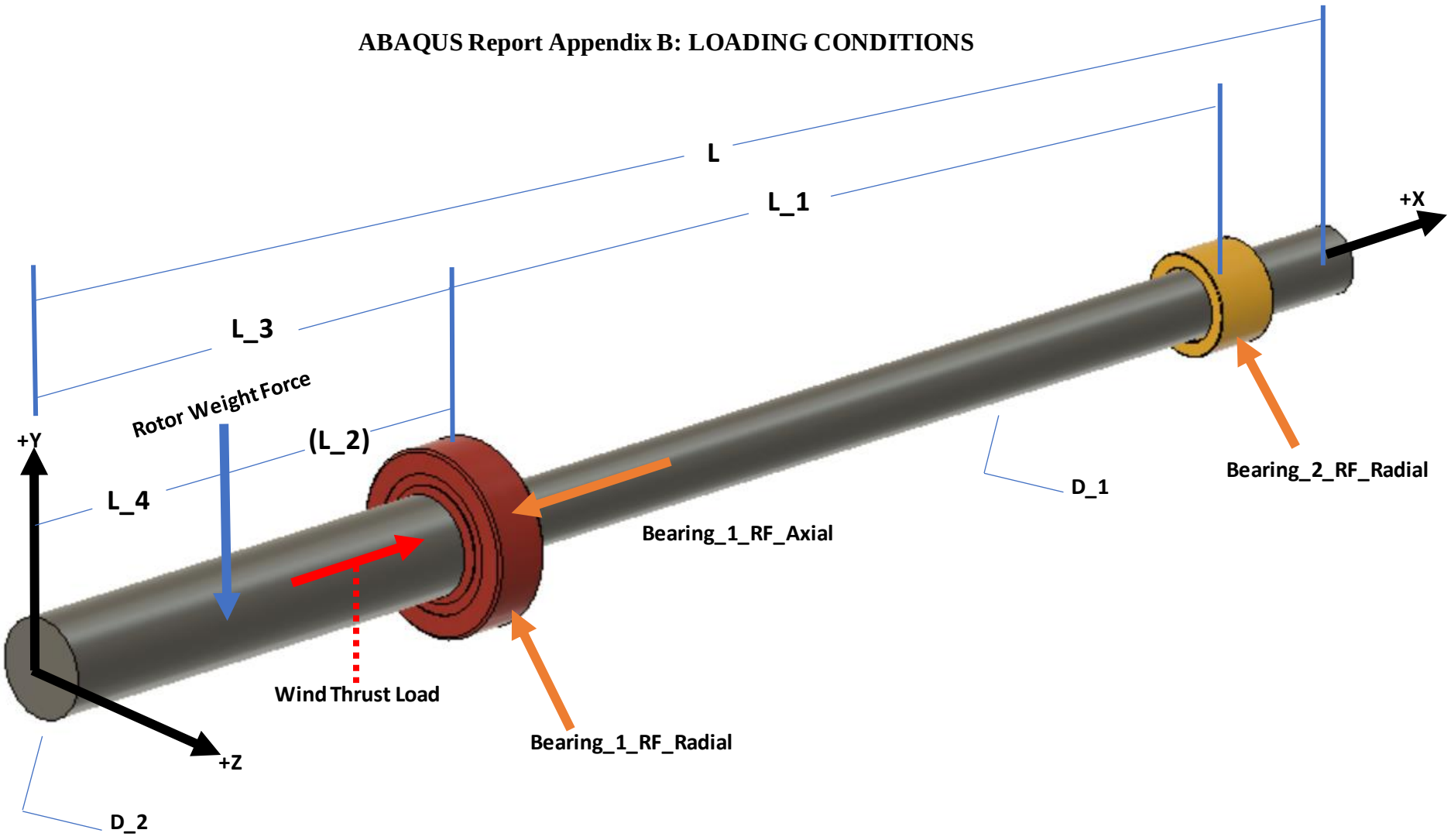

Figure L.6 (B.1). Static Loading Case for Small Wind Turbine Shaft

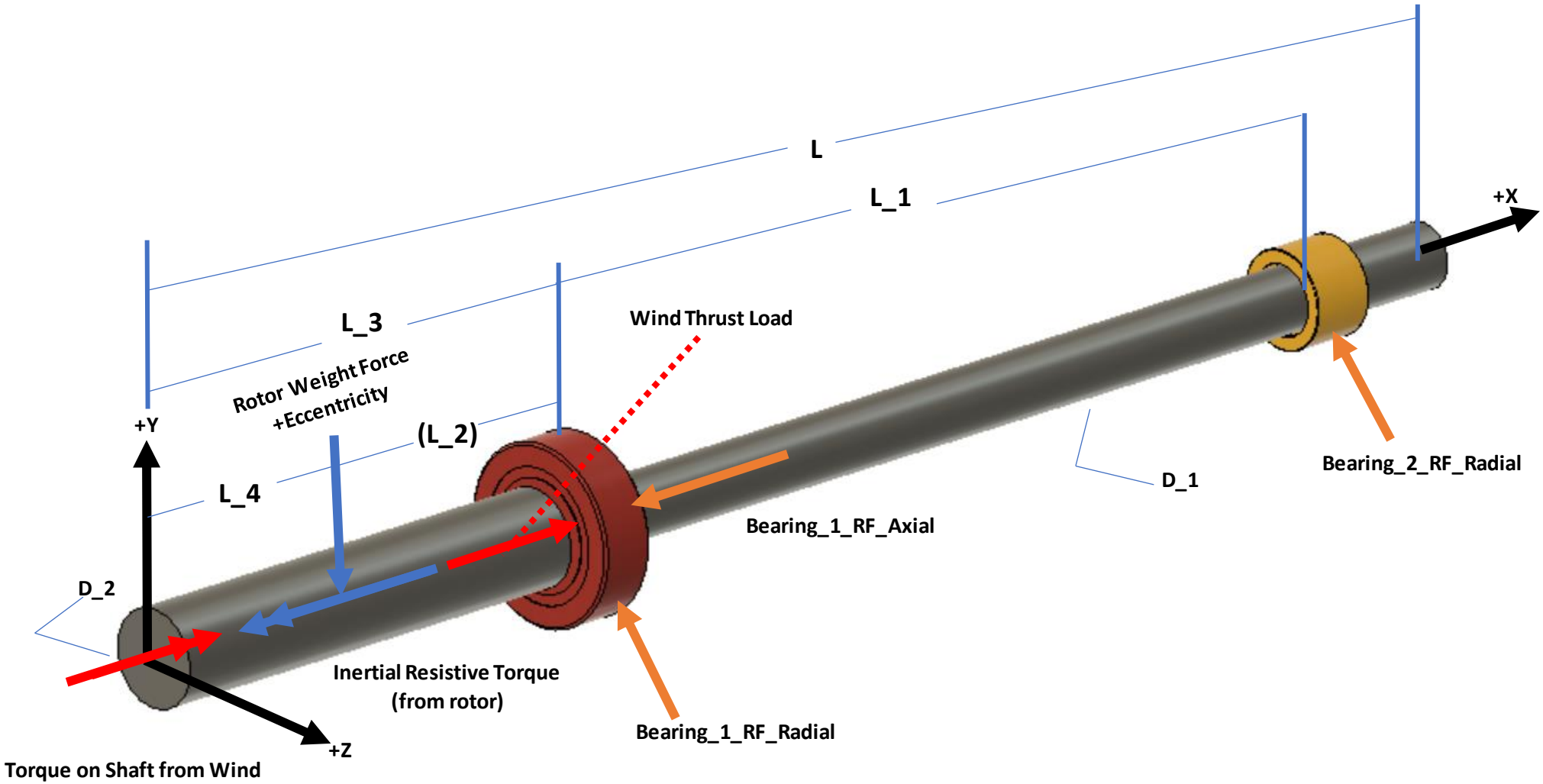

Figure L.7 (B.2) Dynamic Loading Case for Small Wind Turbine Shaft – (unused)

Deep-Groove or Angular-Contact Radial Ball Bearings

$$\delta = 46.2E-06\ \sqrt[3]{\frac{F^2}{DZ^2\cos^5\alpha}}$$

$$K = 0.0325E06\ \sqrt[3]{DFZ^2\cos^5\alpha}$$

where	δ	Radial Deflection
	K	Radial Stiffness (Lbf/in)
	F	External Radial Force (Lbf)
	D	Ball Diameter (in)
	Z	Number of Rolling Elements
	L	Roller Effective Length (in)
	α	Contact Angle (rad)

See also Generalized non-linear isotropic bearing.

Reference on roller element bearing stiffness estimation

Gargiulo, E.P.,Jr., A Simple Way to Estimate Bearing Stiffness, Machine Design, 1980, pp.107-110.

Figure L.8 (C.1) Deep Groove and Angular Contact Bearing Stiffness Approximation

To get axial stiffness from Gargiulo's approximation it was assumed that by looking at the SIN() of the contact angle alpha raised to the fifth power instead of COS() the axial component would be produced. This is likely not the case in the reality but, was the simplest possible way to estimate axial stiffness based on size without determining the stiffness matrix for both support bearings. In Table C.1 on the next page, I have provided the excel output of these calculations for the conservative and actual rotor weight loads.

Table L.5 (C.1). Stiffness calculations for SPRING1 element representations of front and rear bearings

Radial Stiffness Estimate for Deep Groove Ball Bearings										
		EE Units					SI Output			
Bearing Location	Bearing Type	D	F	Z	alpha	K	K	K	K_val	K_val
(description)	(description)	[in]	[lbf]	[#]	[degrees]	[lbf/in]	[N/m]	[N/mm]	[N/m]	[N/mm]
back	deep groove	0.133	11.24	12	0	1.95E+05	3.41E+07	3.41E+04	34111137	34111.14
front	angular contact rad	0.133	11.24	12	20	1.76E+05	3.08E+07	3.08E+04	30751943	30751.94
front	ang. Cont axial	0.133	20.24	12	20	3.96E+04	6.94E+06	6.94E+03	6941666	6941.666
back	deep groove	0.133	2.205	12	0	1.13E+05	1.98E+07	1.98E+04	19820303	19820.3
front	angular contact rad	0.133	2.205	12	20	1.02E+05	1.79E+07	1.79E+04	17868441	17868.44
front	ang. Cont axial	0.133	20.24	12	20	3.96E+04	6.94E+06	6.94E+03	6941666	6941.666

These values of radial and axial stiffness were than broken into X, Y, and Z components such that the resultant stiffness in the YZ plane at both bearing locations was equal to the calculated radial stiffness. Since the axial stiffness already acted along the axis of rotation of the shaft (the X-axis) no further calculations were needed. I have provided the results of these calculations, which represent the actual SPRING1 coefficients in the applicable ABAQUS models in tables C.2 and C.3 on the next page. Table C.2 corresponds to the SPRING1 coefficients used with the conservative rotor weight loading condition, while table C.3 corresponds to the SPRING1 coefficients used with the actual rotor weight loading condition.

Table L.6 (C.2). Calculated SPRING1 element stiffness coefficients under conservative loading condition

Spring BCs (Description)	DOF (x,y,z)	K (N/m)	K (N/mm)	Transverse Load (Cons) (N)	Axial Load (Cons) (N)
Back Bearing - rad-y	y	24112300	24112.3	50	0
Back Bearing - rad-z	z	24112300	24112.3	50	0
Net Radial Back Bearing	radial (YZ)	34099942	34099.94	N/A	N/A
Front Bearing - rad-y	y	21779000	21779	50	0
Front Bearing - rad-z	z	21779000	21779	50	0
Front Bearing - thrust - x	x	6940000	6940	0	85.92
Net Radial Front Bearing	radial (YZ)	30800157	30800.16	N/A	N/A

Table L.7 (C.3). Calculated SPRING1 element stiffness coefficients under actual loading condition

Spring BCs (Description)	DOF (x,y,z)	K (N/m)	K (N/mm)	Transverse Load (Act.) (N)	Axial Load (Act.) (N)
Back Bearing - rad-y	y	14015069	14015.07	9.81	0
Back Bearing - rad-z	z	14015069	14015.07	9.81	0
Net Radial Back Bearing	radial (YZ)	19820300	19820.3	N/A	N/A
Front Bearing - rad-y	y	12634895	12634.9	9.81	0
Front Bearing - rad-z	z	12634895	12634.9	9.81	0
Front Bearing - thrust - x	x	6942000	6942	0	85.9
Net Radial Front Bearing	radial (YZ)	17868440	17868.44	N/A	N/A

Table L.8 (C.4) Dynamic frequency extraction mesh convergence study

#DOFs	2420	1220	500	260	140	Coarse vs. Fine mesh
Mode (#)	Frequency (Hz)	Frequency (Hz)	Frequency (Hz)	Frequency (Hz)	Frequency (Hz)	%Difference (%)
2	103.66	103.66	103.66	103.66	103.66	0
3	103.66	103.66	103.66	103.66	103.66	0
4	397.09	397.09	397.09	397.09	397.09	0
5	1055.7	1055.7	1055.7	1055.8	1055.9	0.018942982
6	1055.7	1055.7	1055.7	1055.8	1055.9	0.018942982
7	1805.3	1805.3	1805.3	1805.3	1805.4	0.005539092
8	1805.3	1805.3	1805.3	1805.3	1805.4	0.005539092
9	3615.1	3615.1	3615.2	3615.5	3620.2	0.140975495
10	3615.1	3615.1	3615.2	3615.5	3620.2	0.140975495
11	5460.7	5460.7	5460.7	5460.7	5460.7	0
12	6660.8	6660.8	6661	6662.7	6689.8	0.434437404
13	6660.8	6660.8	6661	6662.7	6689.8	0.434437404
14	8656.5	8656.5	8656.5	8656.5	8656.5	0
15	10055	10055	10055	10061	10146	0.900945498
16	10055	10055	10055	10061	10146	0.900945498
17	14030	14030	14031	14048	14285	1.80116546
18	14030	14030	14031	14048	14285	1.80116546
19	16316	16316	16316	16316	16318	0.012257155
20	18864	18864	18867	18910	19504	3.336113428
21	18864	18864	18867	18910	19504	3.336113428
22	24602	24602	24609	24708	25320	2.87648732
23	24602	24602	24609	24708	25988	5.479343744
24	25073	25073	25076	25134	25988	3.58394861
25	25073	25073	25076	25134	26166	4.266281543
26	25317	25317	25317	25317	26166	3.298176097
27	26841	26841	26841	26842	26864	0.085653105
28	31280	31281	31296	31511	35063	11.40436821
29	31280	31281	31296	31511	35063	11.40436821
30	35885	35885	35885	35891	35980	0.26438461

Table L.9. Converged extracted Natural Frequencies for simplified rotor + competition shaft model

Mode (#)	Frequency (rad/sec)	Frequency (Hz)	Rotational Speed (RPM)	Notes (description)
1	0.00E+00	0.00E+00	0.00E+00	Rigid Body mode
2	651.33	103.66	6.22E+03	Y-bending
3	651.33	103.66	6.22E+03	Z-bending
4	2495	397.09	2.38E+04	X- extensive mode
5	6633.4	1055.7	6.33E+04	Y-bending
6	6633.4	1055.7	6.33E+04	Z-bending
7	11343	1805.3	1.08E+05	Y-bending
8	11343	1805.3	1.08E+05	Z-bending
9	22715	3615.1	2.17E+05	Y-bending
10	22715	3615.1	2.17E+05	Z-bending
11	34310	5460.7	3.28E+05	X- extensive mode
12	41851	6660.8	4.00E+05	Y-bending
13	41851	6660.8	4.00E+05	Z-bending
14	54390	8656.5	5.19E+05	X- extensive mode
15	63176	10055	6.03E+05	Y-bending
16	63176	10055	6.03E+05	Z-bending
17	88154	14030	8.42E+05	Y-bending
18	88154	14030	8.42E+05	Z-bending
19	1.03E+05	16316	9.79E+05	X- extensive mode
20	1.19E+05	18864	1.13E+06	Y-bending
21	1.19E+05	18864	1.13E+06	Z-bending
22	1.55E+05	24602	1.48E+06	Y-bending
23	1.55E+05	24602	1.48E+06	Z-bending
24	1.58E+05	25073	1.50E+06	Y-bending
25	1.58E+05	25073	1.50E+06	Z-bending
26	1.59E+05	25317	1.52E+06	YZ-bending
27	1.69E+05	26841	1.61E+06	YZ-bending
28	1.97E+05	31281	1.88E+06	Y-bending
29	1.97E+05	31281	1.88E+06	Z-bending
30	2.25E+05	35885	2.15E+06	YZ-bending

Appendix M – Grooved Plate & Vibrations Test Bed Design Calculations

Table M.1: Static Sliding Mass Clamping Force Calculation

Fx=0

Parameter	Variable	Value	Units	Notes	Equation
Bolt mass and nut mass	m	0.0132	kg	https://www.valentazt.com/carr	Fcent=(mv2)/r
Rotational speed	w	3101	RPM		
Distance from center to bolt location	r	20	mm		
Translational velocity	v	6494.71	mm/s		
Centripital force	Fcent	27.8397	N		
Coefficient of friction	m	0.22	-	https://github.com/superjamie/l	f=mN
Normal force	N	126.544	N		

Fy=0

Parameter	Variable	Value	Units	Notes	Equation
Bolt rating	R	1.46095	N/mm2	Indicate torque using split washers	Fclamp=RA
Bolt rating	R	211.838	PSI	Most hex bolts are rated for above 10000 PSI	
Cross-sectional area of bol	A	86.6175	mm2		
Side length of hex	s	5.774	mm	https://www.valentazt.com/carriage-bolts.html	
Clamping force	Fclamp	126.544	N		
Normal force	N	126.544	N		

Fclamp	126.414	N	This accounts for the mass of the bolt. Pretty much negligible. Also minimizes clamping, safer to assume needs to do all clamping

Parameter	Variable	Value	Units	Notes	Equation
Coefficient of friction	m	0.22	-	For PETG	t=mNd
Hex bolt head length	d	10	mm		
Normal force	N	126.544	N		
Applied torque	t	278.397	N-mm		
Torque arm	d	15	mm	Assuming using hex wrench	t=rF
Applied force	Fapp	18.5598	N	This is about 4lbs. Humans can exert their body weight as a force... Good enough	

Table M.2: Static Sliding Mass Clamping Force Calculation Revised for Square Head Bolt.

Fx=0

Parameter	Variable	Value	Units	Notes	Equation
Bolt mass and nut mass	m	0.0132	kg	https://www.valentazt.com/carr	Fcent=(mrW^2)
Rotational speed	w	3101	RPM		
Distance from center to bolt location	r	28	mm		
Translational velocity	w	324.736	rad/sec		
Centripital force	Fcent	38.9756	N		
Coefficient of friction	m	0.22	-	https://github.com/superjamie/l	f=mN
Normal force	N	177.162	N		

Fy=0

Parameter	Variable	Value	Units	Notes	Equation
Bolt rating	R	1.24314	N/mm2	Indicate torque using split washers	Fclamp=RA
Bolt rating	R	180.255	PSI	Low strength grade A min Sy ~30ksi	
Cross-sectional area of bol	A	142.511	mm2		
Side square head	s	9.525	mm	https://www.valentazt.com/carriage-bolts.html	
Clamping force	Fclamp	177.162	N		
Normal force	N	177.162	N		

Fclamp	0.09648	N	This accounts for the mass of the bolt. Pretty much negligible. Also minimizes clamping, safer to assume needs to do all clamping

Parameter	Variable	Value	Units	Notes	Equation
Coefficient of friction	m	0.22	-	For PETG	t=mNd
Hex bolt head length	d	10	mm		
Normal force	N	177.162	N		
Applied torque	t	389.756	N-mm		
Torque arm	d	25.4	mm	Assuming using hex wrench	t=rF
Applied force	Fapp	15.3447	N	This is about 4lbs. Humans can exert their body weight as a force... Good enough	

SLOT YIELDING BASED ON BOLT CLAMPING FORCE

SCHEMATIC

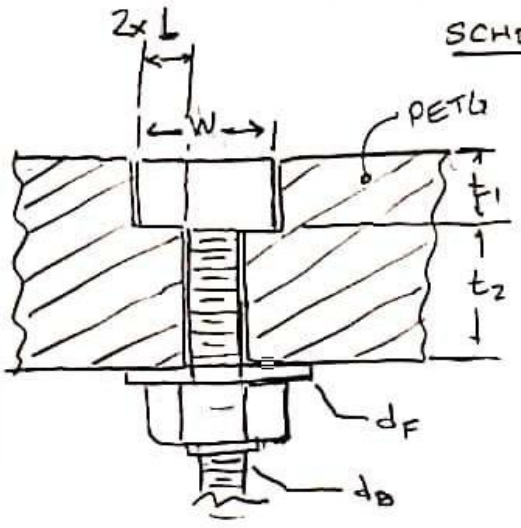

SLOT AND BOLT BROKEN-OUT SECTION

$W = 9.52\,mm$
$L = 1.75\,mm$
$t_1 = 4.4\,mm$
$t_2 = 7.6\,mm$
$d_F = 14.2\,mm$
$d_B = 6.35\,mm$

CLAMPING / FRICTION FORCE REQUIREMENT

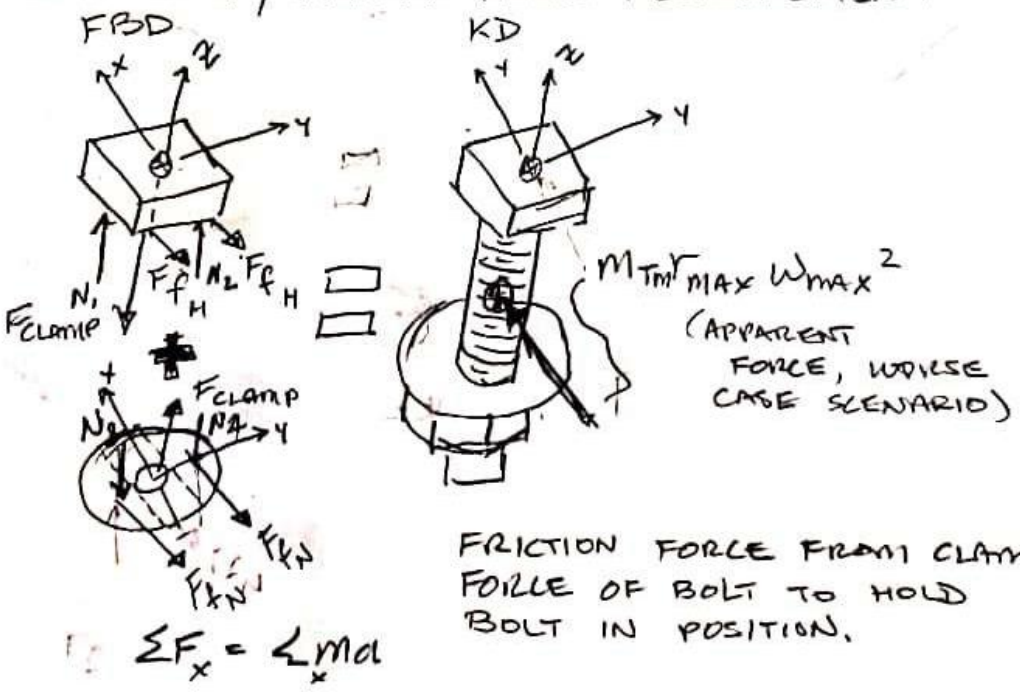

FRICTION FORCE FROM CLAMPING FORCE OF BOLT TO HOLD BOLT IN POSITION.

$\Sigma F_x = \sum_x ma$

$$2F_{f_H} + 2F_{f_N} = m_{Tm} r_{max} \omega_{max}^2$$

BEFORE SLIDING, ASSUMING FRICTION FORCE IS SUFFICIENT FROM CLAMPING

$F_{f_H} = \mu_s N_{1,2}$ → ASSUME EACH NORMAL IS AN EQUAL FRACTION OF CLAMPING FORCE OPPOSING)

$F_{f_N} = \mu_s N_{3,4}$

$N_1 \equiv N_2 = N_3 = N_4 = F_{CLAMP}/4$

$F_{f_H} = F_{f_N}$

$F_{f_{NET}} = 2F_{f_H} + 2F_{f_N} = 4F_f$, FRICTION ON 4 DIFFERENT SURFACES

$F_{f_{NET}} = 2(\mu_s \cdot \frac{F_{CLAMP}}{4}) + 2(\mu_s \frac{F_{CLAMP}}{4}) = \mu_s F_{CLAMP}$

$F_{f_{NET}} = m_{TM} r_{MAX} \omega^2_{MAX}$

$+(\mu_s F_{CLAMP}) = m_{TM} r_{MAX} \omega_{MAX}^2$

$+F_{CLAMP_{REQ}} = \frac{m_{TM} r_{MAX} \omega_{MAX}^2}{\mu_s}$

SINCE KINETIC FRICTION IS PRIMARILY DOCUMENTED AND THE 3D PRINTED SURFACES ARE RELATIVELY ROUGH (EVEN THE SIDE PRINTED ON GLASS) THE μ_s WILL BE APPROXIMATED BY μ_D TO REQUIRE A MORE CONSERVATIVE CLAMPING FORCE

m_{TM} = NOMINAL TEST MASS, MASS

r_{MAX} = CENTER TO CENTER DISTANCE FROM BOLT TO CENTER OF RADIUS AT END OF SLOT.

ω_{MAX} = MAX TEST SPEED OF SHAFT

$$F_{CLAMP} = \frac{(0.0132 Kg)(0.028 mm)(3101 RPM \cdot \frac{2\pi \ RAD}{60 \cdot SEC \cdot REV})^2}{+(0.22)}$$

$\therefore F_{CLAMP_{REQ}} = \underline{177 N}$

COMPRESSIVE STRESS IN CLAMPING SURFACES

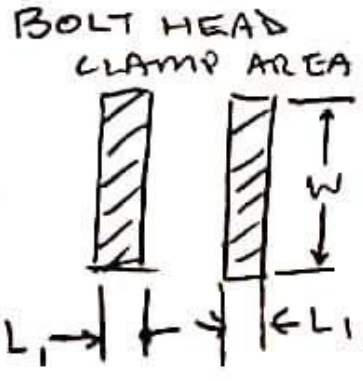

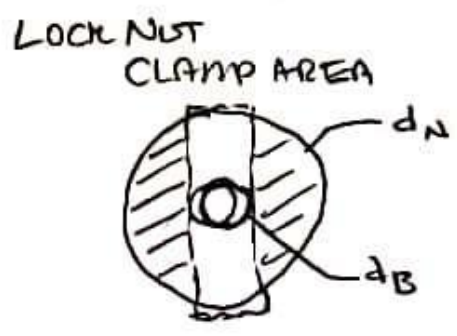

CLAMP AREAS:

$A_{BOLT\ HEAD} = 2 \cdot L_1 \cdot W$

$A_{LOCKNUT} = \frac{\pi d_N^2}{4} - d_{BC} d_N$

THESE ARE THE MINIMUM CLAMPING AREAS TEST MASSES IN MIDDLE OF SLOTS

$\sigma = \frac{F_{CLAMP}}{A_{CLAMP}}$, $\sigma = \frac{S_y}{n_{sd}}$

$F_{CLAMP_{LIM}} = \frac{S_y \cdot A_{CLAMP}}{n_{sd}}$

$F_{CLAMP_{LIM_{BH}}} = \frac{S_y \text{ PEEK} (2 L_1 W)}{n_{sd}}$

$F_{CLAMP_{LIM_{LN}}} = \frac{S_y \text{ PEEK} \left(\frac{\pi d_N^2}{4} - d_{BC} d_N \right)}{n_{sd}}$

$F_{CLAMP_{LIM_{BH}}} = \frac{(49 \times 10^6 Pa)(2 \cdot 0.00175 m \cdot 0.00952 m)}{3}$

$F_{CLAMP_{LIM_{LN}}} = \frac{(49 \times 10^6 Pa)\left[\left(\frac{\pi (0.0142 m)^2}{4} - (0.0142 m \cdot 0.00635 m) \right)\right]}{3}$

$F_{CLAMP_{LIM_{BH}}} = 544\ N$, $F_{CLAMP_{LIM_{LN}}} = 1114\ N$

$F_{CLAMP_{LIM_{BH}}}$ LIMITS, GIVEN REQ'D CLAMPING FORCE OF 177 N

$\therefore\ FOS_{Y,CLAMP} = \frac{544 N}{177 N} = \boxed{3}$ → FACTOR OF SAFETY ON YIELD DUE TO CLAMPING FROM TIGHTENING OF TEST MASSES

SHAFT TORQUE LOAD CASE ANALYSIS

CENTER BORE + MOUNTING HOLES SCHEMATIC

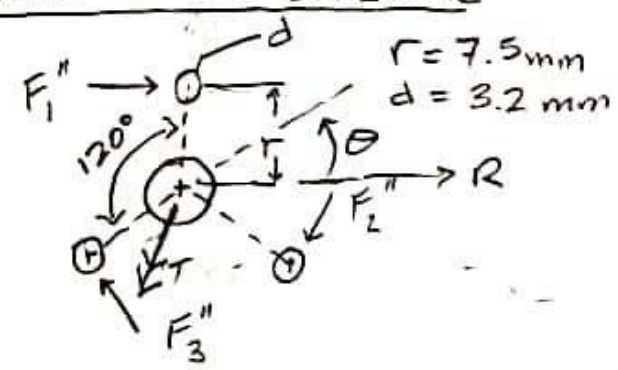

WHERE

$r_1 = r_2 = r_3 = r$

$d_1 = d_2 = d_3 = d$

$F_1'' = F_2'' = F_3'' = F''$

THUS: $F'' = \frac{Tr}{3r^2}$

AND

$T = \frac{F'' \cdot 3r^2}{r}$

r = 7.5mm

- ASSUMING:
  - STATIC EQUILIBRIUM
  - ALL BOLTS SHARE LOADS EQUALLY
  - INTERESTED IN MATERIAL FAILURE NUT BOLTS
  - SUFFICIENTLY SIMILAR CASE TO THAT FOR WHICH SHEAR FORCE FROM ECCENTRIC LOADINGS IN BOLTED JOINTS WAS DEVELOPED

$$F_n'' = \frac{M_1 r_n}{r_A^2 + r_B^2 + \dots r_n^2}$$

(8-57 SHIGLEY'S 10th ed)

- TORQUE T TREATED AS SHAFT TORQUE WHILE DRIVEN BY WIND/MOTOR

LET F" BE SET BY BEARING STRESS LIMIT ON MATERIAL YIELD. $n_{sd} = 3$ APPLIED SINCE 3D PRINTED PETG IS NOT ISOTROPIC.

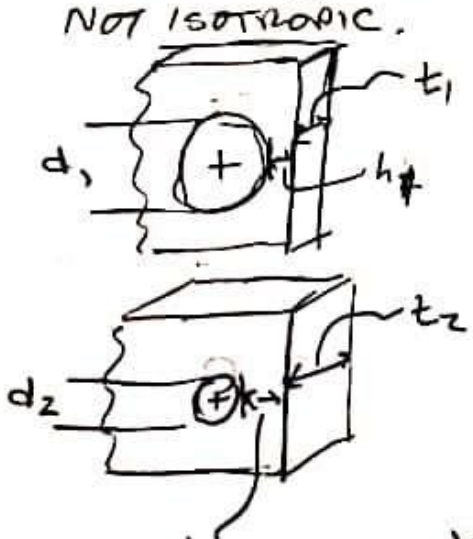

SCHEMATICS (SIMPLIFIED)

COUNTER BORE BEARING/ SHEAR SCHEMATIC

THRU HOLE BEARING/ SHEAR SCHEMATIC

CURRENT MODEL PARAMS

$d_1 = 5.5mm$

$t_1 = 4.4mm$

$h_1 = 6.135mm$

$d_2 = 3.2\ mm$

$t_1 = 7.6\ mm$

$h_1 = 5.895\ mm$

h_1 AND h_2 MEASURED ON CAD MODEL AND TAKEN FROM EDGE OF HOLE TO NEAREST DISCONTINUITY ALONG LINE OF ACTION.

$$\sigma_b = \frac{F''}{t_n d_n}, \quad \sigma_b = \frac{S_y}{n_{sd}}$$

$$\therefore \quad F'' = S_y (t_n d_n) / n_{sd}$$

$$F''_{CB} = \frac{S_y(t_1 d_1)}{n_{sd}} \Rightarrow \frac{(49\times10^6 Pa)(0.0044m \cdot 0.0055\ m)}{3}$$ (S_y PETG?)

$$F''_{M3} = \frac{S_y(t_2 d_2)}{n_{sd}} \Rightarrow \frac{(49\times10^6 Pa)(0.0044_m \cdot 0.0032_m)}{3}$$

$\therefore F''_{CB} = 395\ N$, $F''_{M3} = 397\ N$

$\therefore F''_{CB}$ LIMITS, THOUGH BEARING FORCE IS NEARLY IDENTICAL. IN THIS CASE

CHECK SHEARING OF MEMBER

$$\sigma_{TEAROUT} = \frac{F''_s}{d_n h_n} \qquad \sigma_{TEAROUT} = \frac{0.577 S_{y\,PETG}}{n_{sd}}$$

$$\therefore F''_s = \frac{0.577\, S_{y\,PETG} \cdot (d_n \cdot h_n)}{n_{sd}}$$

$$F''_{CB_s} = \frac{0.577\, S_{y\,PETG}\,(d_1 \cdot h_1)}{n_{sd}}$$

$$F''_{M2_s} = \frac{0.577\, S_{y\,PETG}\,(d_2 \cdot h_2)}{n_{sd}}$$

$$F''_{CB_s} = \frac{0.577\,(49\times10^6 Pa)(0.0055m \cdot 0.006135\,m)}{3}$$

$$F''_{M3_s} = \frac{0.577\,(49\times10^6 Pa)(0.0032\ m \cdot 0.005875m)}{3}$$

$F''_{CB_s} = 318\ N$, $F''_{M3_s} = 178\ N$

F''_{M3_s} LIMITS HERE AND OVERALL, LET $F'' = F''_{M3_s}$

THUS OUR RATED TORQUE TO PREVENT YIELD OF 3D PRINTED PART AT MOUNTING CONNECTIONS IS:

$$T_{RATED} = \frac{F'' \cdot 3r^2}{r}, \quad F'' = F_{M3_s}''$$

$r = 7.5mm$
(CENTER TO CENTER DISTANCE MOUNTING HOLE TO CENTER BORE)

$$T_{RATED} = \frac{178N \cdot 3(0.0075m)^2}{(0.0075m)}$$

$$T_{RATED} = 4.0\ N\text{-}m$$

$T_{WIND\ SHAFT} \approx 0.6\ N\text{-}m$ (FROM WPC)

$T_{MOTOR} \approx 1.2\ N\text{-}m$ (DATA SHEET FOR MY1016 MOTOR)

$$\therefore SF_{TORQUE_1} = \frac{4.0\ N\text{-}m}{0.6\ N\text{-}m} = \boxed{6.7}$$ → SAFETY FACTOR ON MATERIAL YIELD FROM TORQUE LOAD INCOMING WIND

$$\therefore SF_{TORQUE_2} = \frac{4.0\ N\text{-}m}{1.2\ N\text{-}m} = \boxed{3.3}$$ → SAFETY FACTOR ON MATERIAL YEILD FROM TORQUE LOAD MOTOR

A CONSERVATIVE CALCULATION APPROACH IS TAKEN HERE SINCE THE PART IS 3D PRINTED. ADDITIONALLY YIELD IS CONSIDERED OVER TENSILE FAILURE AS WE DO NOT WANT THE GROOVED PLATE TO PLASTICALLY DEFORM AS THIS COULD EFFECT TEST MASS 'C' ADJUSTMENT AND ∴ CALIBRATION/BALANCING OVERALL

Table M.2: Static Sliding Mass Specification Calculation

ROT of test mass imbalance force = 10% of rotor weight — Michael Mullen

Equation

m_e * r_e * omega_rotor^2 = nockdown * rototating assembly mass * accel_gravity

Inputs

Parameter	Value	Units	Description
m_e	13.1	[g]	test mass added - too heavy
r_e	14	[mm]	location of test mass (radial)
omega_rotor	2500	[RPM]	rotational speed of rotor
nockdown	0.4	[% exp as decimal]	balancing margin
m_rotor	1	[kg]	total rotor mass (including test mass added)
g	9.81	[m/s^2]	acceleration due to gravity

Preprocessing

Parameter	Value	Units	Description
m_e	0.0131	[kg]	
r_e	0.014	[m]	
omega_rotor	261.799388	[rad/sec]	

Ouput

Parameter	Value	Units	Description
Solving for mass	0.00408944	[kg]	
	4.08943877	[g]	Mass of bolt, washer and nut
solving for radius	0.00437039	[m]	
	4.37039258	[mm]	radial poisition of carriage bolt, washer and nut

Table M.3 Balancing Limit Calculations

Table 4 — Vibration-levels limit for test in manufacturer's work-shop

Fan application category	Rigidly mounted mm/s		Flexibly mounted mm/s	
	Peak	r.m.s.	Peak	r.m.s.
BV-1	12,7	9,0	15,2	11,2
BV-2	5,1	3,5	7,6	5,6
BV-3	3,8	2,8	5,1	3,5
BV-4	2,5	1,8	3,8	2,8
BV-5	2,0	1,4	2,5	1,8

NOTE 1 Refer to Annex A for conversion of velocity units to displacement or acceleration units for filter-in readings.

NOTE 2 The r.m.s. values given in this Table are preferred. They are rounded to a R20 series as specified in ISO 10816-1. Peak values are widely used in North America. Being made up of a number of sinusoidal wave forms, these do not necessarily have an exact mathematical relationship with the r.m.s. values. They may also depend to some extent on the instrument used.

NOTE 3 The values in this Table refer to the design duty of the fan and its design rotational speed and with any inlet guide vanes "full-open". Values at partial load conditions should be agreed between the manufacturer and user, but should not exceed 1,6 times the values given.

From ISO Standard for Fan Balancing ISO 14694:2003(en)

Assuming Flexibly Mounted - since shaft is rigid this may make considering the bearings to be flexible a non-conservative assumption

$$U = \frac{Ma}{\omega^2}$$

U is the unbalance

M is the mass in motion
a is the acceleration
ω is the circular speed in radians per second

From: Wowok, K. Professional Engineer, Balancing and Its Effects.
https://www.machinedyn.com/docs/articles/Balancing_and_its_Effects_on_Vibration_Response.pdf

STI Sinusoidal Waveform Vibration Calculator

1. Frequency Value: (Enter Only One Data Value)	Data	Results
Enter Frequency in Hertz	0.00	0.00 Hertz
Enter Frequency in CPM/RPM	0.00	0.00 CPM/RPM

2. Vibration Value: (Enter Only One Data Value)	Data	Results
Enter Mils Displacement (mils)	0.000	0.000 mils P/P
Enter mm Displacement (millimeters)	0.000	0.000 mm P/P
Enter in/sec Peak	0.000	0.000 in/sec Peak
Enter mm/sec Peak	0.000	0.000 mm/sec Peak
Enter in/sec RMS	0.000	0.000 in/sec RMS
Enter mm/sec RMS	0.000	0.000 mm/sec RMS
Enter g's Peak	0.000	0.000 g's Peak
Enter g's RMS	0.000	0.000 g's RMS

Figure M.1. Calculator for converting measured vibration, to velocity, and accelerations and vice versa.

The user enters the speed of rotation as a frequency or in RPM and then provides one of the listed vibration values. The calculator returns all other vibration values. From: https://www.stiweb.com/Vibration_Calculator_s/104.htm

Assuming Flexibly Mounted – (natural frequency of entire assembly is below operating speeds)

Operating Speed BV-2 (2500 RPM 11 m/s)

Parameter	Description	Value	Units
U	m_e * r_e	17.3746	g-mm
M	(rotating mass)	0.61	kg
a	vibrational accel	1.95219	m/s^2
v	vibrational vel	7.5	mm/s
omega	rad/s	261.799	rad/s

Operating Speed BV-3 (2500 RPM 11 m/s)

Parameter	Description	Value	Units
U	m_e * r_e	11.874	g-mm
M	(rotating mass)	0.61	kg
a	vibrational accel	1.3342	m/s^2
v	vibrational vel	5.1	mm/s
omega	rad/s	261.8	rad/s

Max Test Speed BV-2 (3103 RPM 13 m/s)

Parameter	Description	Value	Units
U	m_e * r_e	13.9983	g-mm
M	(rotating mass)	0.61	kg
a	vibrational accel	2.42307	m/s^2
v	vibrational vel	7.5	mm/s
omega	rad/s	324.945	rad/s

Max Test Speed BV-3 (3103 RPM 13 m/s)

Parameter	Description	Value	Units
U	m_e * r_e	9.5211	g-mm
M	(rotating mass)	0.61	kg
a	vibrational accel	1.6481	m/s^2
v	vibrational vel	5.1	mm/s
omega	rad/s	324.95	rad/s

Assuming Rigidly Mounted – (natural frequency of entire assembly is above operating speeds)

Operating Speed BV-2 (2500 RPM 11 m/s)

Parameter	Description	Value	Units
U	m_e * r_e	8.11979	g-mm
M	(rotating mass)	0.61	kg
a	vibrational accel	0.91233	m/s^2
v	vibrational vel RMS	3.5	mm/s
omega	rad/s	261.799	rad/s

Operating Speed BV-3 (2500 RPM 11 m/s)

Parameter	Description	Value	Units
U	m_e * r_e	6.4609	g-mm
M	(rotating mass)	0.61	kg
a	vibrational accel	0.72594	m/s^2
v	vibrational vel RMS	2.8	mm/s
omega	rad/s	261.799	rad/s

Max Test Speed BV-2 (3103 RPM 13 m/s)

Parameter	Description	Value	Units
U	m_e * r_e	6.51742	g-mm
M	(rotating mass)	0.61	kg
a	vibrational accel	1.12815	m/s^2
v	vibrational vel RMS	3.5	mm/s
omega	rad/s	324.945	rad/s

Max Test Speed BV-3 (3103 RPM 13 m/s)

Parameter	Description	Value	Units
U	m_e * r_e	5.21394	g-mm
M	(rotating mass)	0.61	kg
a	vibrational accel	0.90252	m/s^2
v	vibrational vel RMS	2.8	mm/s
omega	rad/s	324.945	rad/s

Table M.4 Enclosure Penetration Thickness Calculation

Parameter Name	Symbol	Value	Units	Notes
Mass of the blade	m_{blade}	9.48	g	
Translational velocity of blade	V_{blade}	5.85	m/s	
Smallest projected cross-sectional area of blade	$A_{P,blade}$	1.964E-05	mm^2	Assuming at tip, $A_{p,blade}$ is ~5mm diameter circle.
Absolute energy of blade	$E_{abs,blade}$	8261505	$mN\text{-}m/mm^2$	
Particle penetration severity factor	$f_{P,ref}$	1	-	Recommended value of 1 for "standard projectile."
Penetration capability	P_{cap}	8261505	$mN\text{-}m/mm^2$	
Material resistance factor	$f_{m,std}$	8055	-	
Material tearing resistance	R_m	39300	N/mm^2	Reference calc.
Breaking elongation	e_B	0.05	-	Reference calc.
Thickness	t	12.7	mm	Using 1/2" plywood.
Penetration resistance	P_{res}	201016553	$mN\text{-}m/mm^2$	
Safety factor	$S_{F,spec}$	3.0	-	
True penetration resistance	$P_{res,qual}$	67005518	$mN\text{-}m/mm^2$	Need: $P_{cap} < P_{res,qual}$
Penetration capability and resistance ratio	$P_{cap}/P_{res,qual}$	0.1232959	-	Need to be <1 to be considered safe.

Relevant Formulas

The area-specific energy E_{spec} (see Figure A.1) is a measure of the penetration capability of a particle flying off the rotor.

The area-specific energy of a particle or part E_{spec} ($mN\cdot m/mm^2$) is given by

$$E_{spec} = \frac{E_{abs}}{A_p} = \frac{mv^2}{2A_p} \quad \text{(A.1)}$$

where

E_{abs} is the absolute energy of the particle [see A.3.1 and equation (A.6)], but here with the dimension $mN\cdot m$ to satisfy the designation convention according to A.4;

A_p is the smallest cross-section of the particle (mm^2);

m is the mass of the particle (g);

v is the translational velocity of the particle (m/s).

The penetration capability P_{cap} of a particle ($mN\cdot m/mm^2$) in terms of that of a standard projectile (see Figure A.3 and Table A.1) with identical area-specific energy is given by

$$P_{cap} = f_{P,rel} \cdot E_{spec} \quad \text{(A.2)}$$

where

$f_{P,rel}$ is the particle penetration severity factor relative to the standard projectile, which reflects the influence of the material and form of a particle (dimensionless);

E_{spec} is the area-specific energy of a particle ($mN\cdot m/mm^2$).

For the standard projectile (see Figure A.3), $f_{P,rel}$ would be 1.

As a result of penetration tests, the penetration resistance P_{res} of the material ($mN\cdot m/mm^2$), which is the area-specific energy of the particle that can be absorbed when retaining it, can be approximated by

$$P_{res} = f_{m,std} \cdot R_m \cdot \varepsilon_B \cdot t \quad \text{(A.3)}$$

where

$f_{m,std}$ is the material resistance factor of the enclosure material (see A.2.2) for a standard projectile (dimensionless);

R_m is the tearing resistance of the enclosure material (N/mm^2);

ε_B is the breaking elongation of the enclosure material (dimensionless);

t is the thickness of the enclosure material (mm).

An enclosure is qualified for an area-specific energy if for its penetration resistance $P_{res,\ qual}$ (mN·m/mm²) the following holds true:

$$P_{res,\ qual} \leq \frac{P_{res}}{S_{F,\ spec}} \tag{A.4}$$

where

P_{res} is the area-specific energy which can be absorbed when retaining the particle (mN·m/mm²);

$S_{F,\ spec}$ is the adequate safety factor concerning area-specific energy, e.g. 2 (dimensionless).

From ISO 7475 (2002) Section A

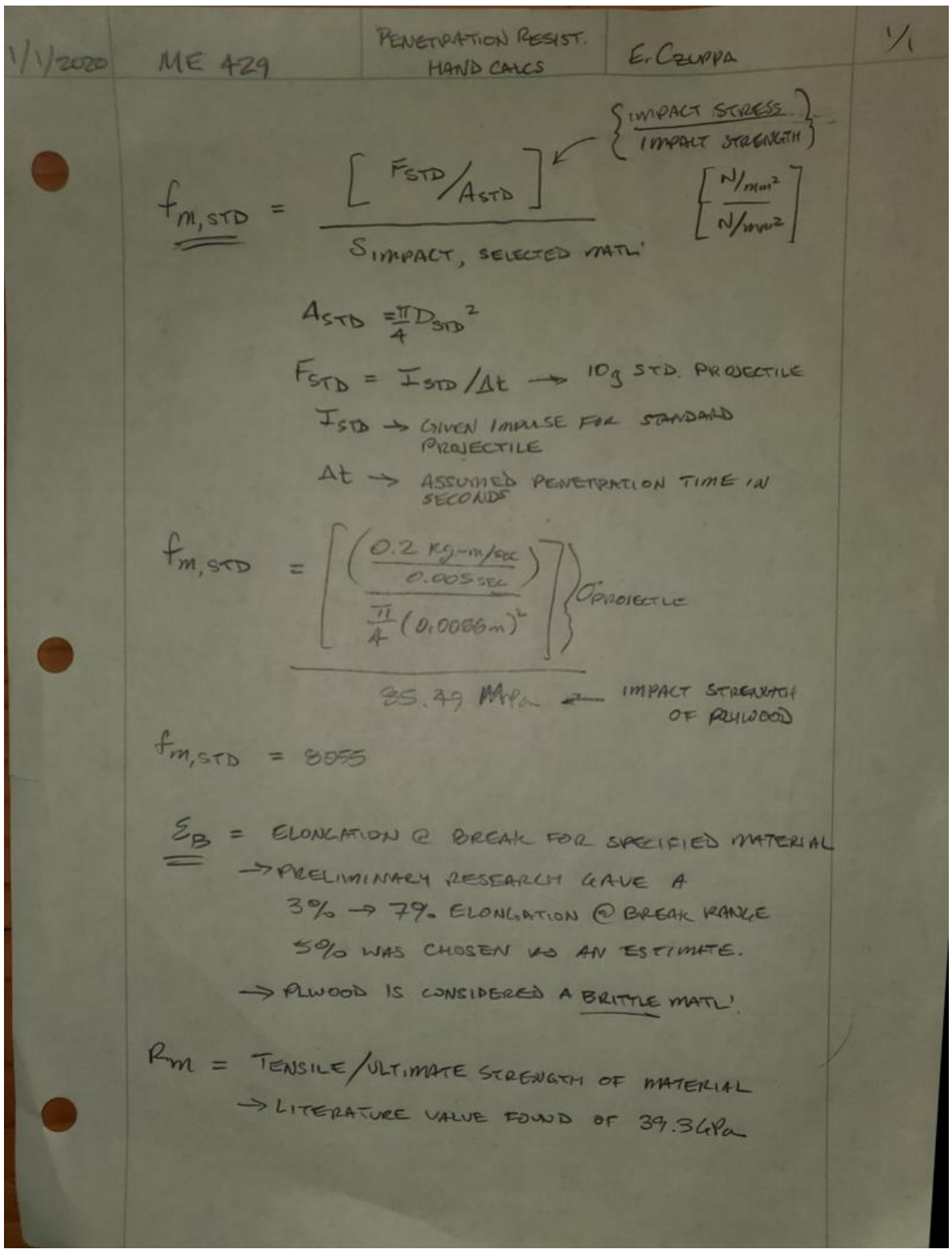

Supporting hand calculations to table M.4

Table M.5 Rotor assembly mass and mass moment of inertia about axis of shaft rotation estimates.

Component Description	I_com_component	d	mass	I_resolved	I_resolved
(Name)	(g-mm^2)	(mm)	(g)	(g-mm^2)	(kg-m^2)
Rotor Connection Assm.	1.16E+05	0	270.985	1.16E+05	1.16E-04
Blades (x3)	2.25E+05	33.383	51.17	8.45E+05	8.45E-04
Rotating Actuation Assm.	2.15E+04	0	39.891	2.15E+04	2.15E-05
Pitching Forks (Rack Carriers) (x3)	27.461	32.384	2.708	8.60E+03	8.60E-06
Grooved Plate Balancing Mechanism Assm.	5.30E+04	0	137.2	5.30E+04	5.30E-05
			609.71	1.04E+06	1.04E-03

Using the most current revision of the pitching CAD available, the mass properties of all subassemblies within the rotor assembly were taken from Fusion 360. The inertias were taken at the components origin or center of mass and the distance from that reference point and the axis of rotation was measured using the inspection tool. Some of the component materials may be incorrect or updated from the mostly-finalized CAD our senior project team had received from the pitching senior project team. Therefore, the assembly mass and rotary moment of inertia estimate should be treated as approximate. Note: the mass values for the blades and rack carriers have been multiplied by three so that the entire mass of their subassemblies has been accounted for in the total mass estimate. The same is true of the resolved inertias.

Table M.6.1 Rotor startup torque (treated as a propeller) estimate – calculator input.

Inputs

Description	Parameter	Value	Units
Number of blades	N_b	3	[-]
Shaft Speed (High)	omega_RPM	3103	[RPM]
Shaft Speed	omega_R/s	324.9454	[rad/sec]
Shaft Speed (low)	omega_RPM	500	[RPM]
Shaft Speed	omega_R/s	52.35988	[rad/sec]
Air density	rho_air	1.21	[kg/m^3]
Blade Radius	R_max	0.1764	[m]
Hub Radius	R_hub	0.0036	[m]
Change in Radius	delta_R	0.0072	[m]

Table M.6.2 Rotor startup torque (treated as a propeller) estimate – numerical integration.

Numerical Integration

radius	Chord	Chord	C_d_Low speed	C_d_high speed	integrand_low	integrand_high	T_startup_low	T_startup_high
(m)	(cm)	(m)	(-)	(-)	(m^5)	(m^5)	(N-m)	(N-m)
0.0036	2.7	0.027	0.073	0.311	1.701E-11	8.935E-11	3.28E-03	9.93E-02
0.0108	6.225	0.06225	0.0579	0.3065	1.111E-10	6.132E-10		
0.018	7.875	0.07875	0.0474	0.2662	3.446E-10	2.066E-09		
0.0252	8.363	0.08363	0.039	0.2461	7.320E-10	4.682E-09		
0.0324	8.288	0.08288	0.0351	0.2277	1.445E-09	5.829E-09		
0.0396	7.875	0.07875	0.0416	0.0686	2.708E-09	4.133E-09		
0.0468	7.388	0.07388	0.0456	0.063	4.520E-09	5.747E-09		
0.054	6.9	0.069	0.052	0.0591	6.998E-09	7.543E-09		
0.0612	6.375	0.06375	0.0557	0.0555	9.894E-09	9.409E-09		
0.0684	5.925	0.05925	0.0591	0.0523	1.325E-08	1.147E-08		
0.0756	5.55	0.0555	0.06	0.0502	1.665E-08	1.378E-08		
0.0828	5.175	0.05175	0.0595	0.0483	2.003E-08	1.623E-08		
0.09	4.838	0.04838	0.0586	0.0474	2.358E-08	1.889E-08		
0.0972	4.538	0.04538	0.058	0.0457	2.742E-08	2.158E-08		
0.1044	4.275	0.04275	0.0572	0.0449	3.152E-08	2.450E-08		
0.1116	4.05	0.0405	0.0567	0.0433	3.593E-08	2.736E-08		
0.1188	3.825	0.03825	0.0561	0.0425	4.044E-08	3.058E-08		
0.126	3.638	0.03638	0.0555	0.0418	4.528E-08	3.373E-08		
0.1332	3.45	0.0345	0.0552	0.0403	5.032E-08	3.671E-08		
0.1404	3.3	0.033	0.0545	0.0397	5.549E-08	4.011E-08		
0.1476	3.15	0.0315	0.0539	0.0384	6.058E-08	4.271E-08		
0.1548	3	0.03	0.0531	0.0367	6.571E-08	4.492E-08		
0.162	2.888	0.02888	0.0524	0.0351	7.115E-08	4.893E-08		
0.1692	2.775	0.02775	0.0513	0.037	7.501E-08	6.649E-08		
0.1764	2.663	0.02663	0.0482	0.0583	6.592E-07	5.181E-07		

Sophie Spencer, CPWPC president, provided us with the drag coefficients for the "low speed" and "high speed" columns. These coefficients are valid for 2 m/sec wind speed and a pitching angle of 8 degrees and 12 m/sec with a pitching angle of 1 degree, respectively. For rotor balancing, the blades will be kept at pitching angle of zero degrees. The graph of torque versus pitching angle is provided in figure M.6.2. This calculation was done to attempt to determine the difference in aerodynamic loads from the turbine's operation as a propeller. The resulting restive torques of the rotor (under propeller operation) were much lower than the torque on the rotor from incoming wind. To be conservative in our analysis we opted to use the rotor torque resulting from wind loading for the load torque in our motor selection analysis.

2/10/21	ME 430	TURBINE AS FAN TORQUE APPROX.	E. CZUPPA C. CROSS	V

TREATING TURBINE AS PROPELLER

W/ HELP FROM N. BANKS

$$T_{STARTUP} \simeq \left[\frac{1}{2}\rho_{AIR} W_{START}^2 \int_{R_{HUB}}^{R} c C_D r^3 dr\right] N \quad \leftarrow \#\text{ OF BLADES}$$

FROM FOX & MCDONALD 9th ed
EXAMPLE 10.6

NUMERICALLY INTEGRATE OVER BLADE

$C_D(R, \cancel{\alpha})$

$C(R)$ CHORD LENGTH

$N \cdot m \quad \frac{kg \cdot m^2}{s^2} \cdot m$

C_D FROM AIRFOIL DATA XFOIL @ CPWP

~~EDPE~~ CPWP →

- CHORD LENGTH
- α
- AIRFOIL

} @ EACH CROSS SECTION

→ XFOIL DATA
→ BLADE DATA

NUMERICALLY INTEGRATE: $\int_{R_{HUB}}^{R} c C_D r^3 dr$

$$\rho W^2 \sum \left\{ \Delta r \left[\frac{C(i) \cdot C_D(i)\, r(i)^3 + C(i+1) \cdot C_D(i-1)\, r_{(i-1)}^3}{2} \right] \right\}$$

INTEGRAND NUMERICAL FORM OF TRAPEZOID RULE

$$\frac{C_{(i+1)} C_{D(i+1)} r_{(i+1)}^3 + C(i)\, C_D(i)\, r_{(i)}^3}{2} (r_{i+1} - r_i)$$

Figure M.6.1 Supporting derivation of propeller startup torque numerical integration formula.

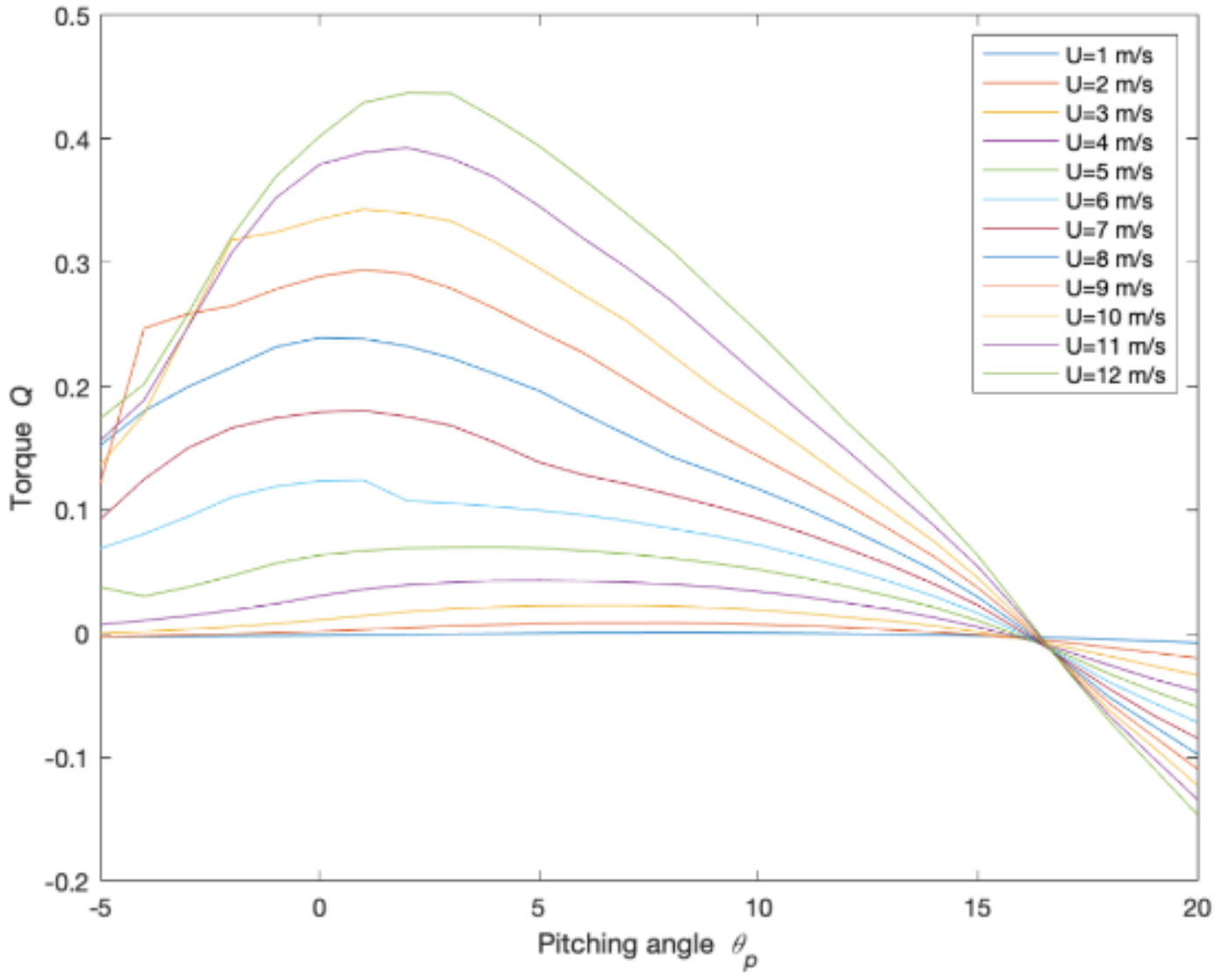

Figure M.6.2 Torque on wind turbine rotor as a function of the pitching angle. Courtesy of Sophie Spencer (CPWPC President).

The MATLAB code that generated this graph only worked up to 12 m/sec wind speed. Since the balancing will be conducted with the blades at a zero degree pitching angle, the torque at the maximum windspeed is about 0.4 N-m. This values will be used as the load torque on the rotor in the calculation of required motor torque.

Table M.7 Required Motor Torque Calculation

Inputs

Description	Parameter	Value	Units
Initial Shaft Speed	V_1	0	RPM
Final Shaft Speed	V_2	3103	RPM
Ramp Rate	a_r	5	RPM/sec
Safety Factor	SF	2	-
Change in Shaft Speed	Vm	3103	RPM
accerleration time	t_a	620.6	sec

Required Motor Torque

T_interia	T_rotor_aero	T_required	Notes
(N-m)	(N-m)	(N-m)	(Description of wind torque on rotor)
5.47E-04	9.93E-02	0.20	Propeller Startup Estimate
5.47E-04	4.00E-01	0.80	12 m/s wind speed at 0 degree pitch angle
5.47E-04	4.29E-01	0.86	12 m/s wind speed at 1 degree pitch angle

T_inertia is the acceleration torque required to overcome the rotary inertia of the rotor assembly. T_rotor_aero is the load torque from the incoming wind on the turbine. T required is the summation of T_inertia and T_rotor_aero multiplied by a safety factor of two. The equations for all these torque values are provided on the following page and were taken from Oriental Motor Corp USA's motor sizing tool and technical reference.

EQUATION REFERENCE

$$T_{REQ} = (T_{ACCEL} + T_{LOAD}) \cdot SF$$

(T_{LOAD}: AERO LOADS)

$$T_a = J_{TOT}\left[\frac{\Delta N}{9.55 \cdot t_a}\right]$$

ΔN = CHANGE IN SPEED [RPM]
t_a = ACCELERATION TIME [SEC]

$$J_{TOT} = J_{ROTOR} + J_{SHAFT} + J_{LOAD}$$

$J_{LOAD} \Rightarrow 0$ IN OUR CASE

J_{ROTOR}: ESTIMATED FROM CAD MODEL

SHAFT APPROX DIMS:

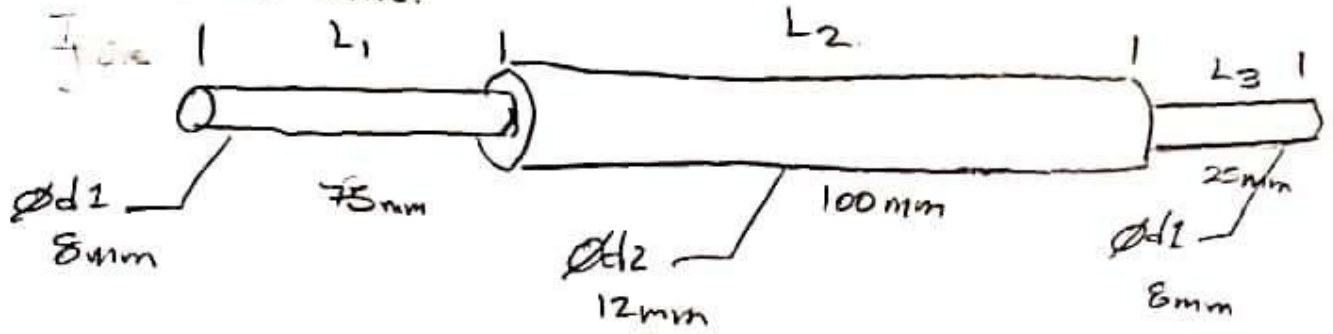

$$J_{SHAFT} = \sum \frac{\pi}{32} \rho L_i d_i^4$$

$$= \frac{\pi \rho_{1E6}}{32}\left(d_1^4 L_1 + d_2^4 L_2 + d_1^4 L_3\right)$$

$$= \frac{\pi \cdot 7865 \frac{kg}{m^3}}{32}\left((0.008m)^4 \cdot 0.075m + (0.012m)^4 \cdot 0.1m + (0.008m)^4 \cdot 0.025m\right)$$

$$J_{SHAFT} = 1.92 \times 10^{-6}\ kg\text{-}m^2$$

Equation reference for motor torque calculation adapted from Oriental Motor Corp USA's Rotary Device Sizing Tool.

Table M.8 MY1016 36V 350W brushed DC motor performance data.

Performance Data for MY1016 36V 350W Electric Scooter Motor

Ref. Point [description]	Torque [N-m]	Speed [RPM]	Speed [Rad/sec]	P-out [W]	Voltage [V]	Current [A]	P-in [W]	Efficiency [%]
No Load.	0.02	3584	375.3156	7.5	36.1	1.64	59.2	12.7
Max Efficiency	0.82	3051	319.5	262.0	36.14	8.86	320.2	81.8
Rated Load	1.2	2800	293.2153	351.9	36.17	12.28	444.2	79.2
Max Load	1.46	2626	274.9941	401.5	36.18	14.64	529.7	75.8
Estimated Stall Condition	5.39	0	0	0	36	50.28	1810.0	0.0

Note: the estimate stall condition was calculated from the estimated motor parameters (Table M.9) and was not a part of the original performance data taken from: https://www.mat-con.eu/epages/62158737.sf/en_GB/?ObjectPath=/Shops/62158737/Products/my1016b4m6_36V

Table M.9 MY1016 36V Motor estimated parameters.

Estimated Motor Parameters

Description	Parameter	Value	Units
Torque Speed Slope	C_1	-6.96E+01	[rad/sec / N-m]
Torque Current Slope	C_2	9.02E+00	[A/Nm]
Extrapolated Stall Torque	T_stall	5.39E+00	[N-m]
Extrapolated Stall Current	I_stall	5.03E+01	[A]
Estimated Torque Constant	kt_est	1.07E-01	[N-m/A]
Esitmated Motor Resistance	R_motor	7.16E-01	[Ohms]
Rotational Inertia of Rotor	J_equiv_motor	1.04E-03	[kg-m^2]
Estimated motor time const.	Tau_motor	6.51E+01	[msec]
Motor Torque @ Max test speed	T_motor	7.23E-01	[N-m]

At the maximum test speed, the motor produces less torque than required by our very conservative torque estimate. A safety factor of two may be excessive, but since the required life of this balancing system has not been determined, we decided to error on the side of caution, perhaps too much in this case.. Despite this, the motor we have selected, is still likely over specified and should be suitable for a use in our proposed balancing system.

MOTOR PARAMETER ESTIMATION FORMULAS

$N = G_1 T + N_{NL}$ TORQUE - SPEED LINE

$$G_1 = \frac{N_{NL} - N_{MAX\ TORQUE}\ [RAD/SEC]}{T_{NL} - T_{MAX}\ [N-m]}$$

NL → NO LOAD

$I = G_2 T + I_{NL}$ TORQUE-CURRENT LINE

$$G_2 = \frac{I_{MAX,RATED} - I_{NL}\ [A]}{T_{MAX} - T_{NL}\ [N-m]}$$

EXTRAPOLATED STALL TORQUE & CURRENT:

$$T_{STALL\ EST.} = \frac{(-1 \cdot N_{NL})}{G_1}$$

$$I_{STALL\ EST.} = G_2 \cdot T_{STALL\ EST} + I_{NL}$$

ESTIMATED TORQUE CONSTANT:

$$K_t = \frac{T_{STALL}\ [N-m]}{I_{STALL}\ [A]}$$

ESTIMATED MOTOR RESISTANCE:

$$R_{MOTOR} = \frac{V_{SUPPLY,\ NOMINAL}}{i_{STALL}}$$

ESTIMATED MOTOR TIME CONSTANT (MECHANICAL):

$$\tau_{MOTOR\ [SECONDS]} = \frac{J_{TOT} R_{MOTOR}}{K_t^2}$$

TIME REQUIRED FOR MOTOR TO RESPOND TO STEP INPUT.

WHERE: $J_{TOT} = J_{MOTOR} + J_{LOAD}$

AND $J_{LOAD} >> J_{MOTOR}$

Equation reference for table M.9.

Note: This first six equations are based on motor modeling as taught by ME 506 System modeling. The last four equations taken from simplified brushed DC motor modeling as taught in ME 405 Mechatronics. The torque-speed and torque-current slopes was initially calculated as shown above and later verified with the line of best fit slope in excel (see figure M.9.)

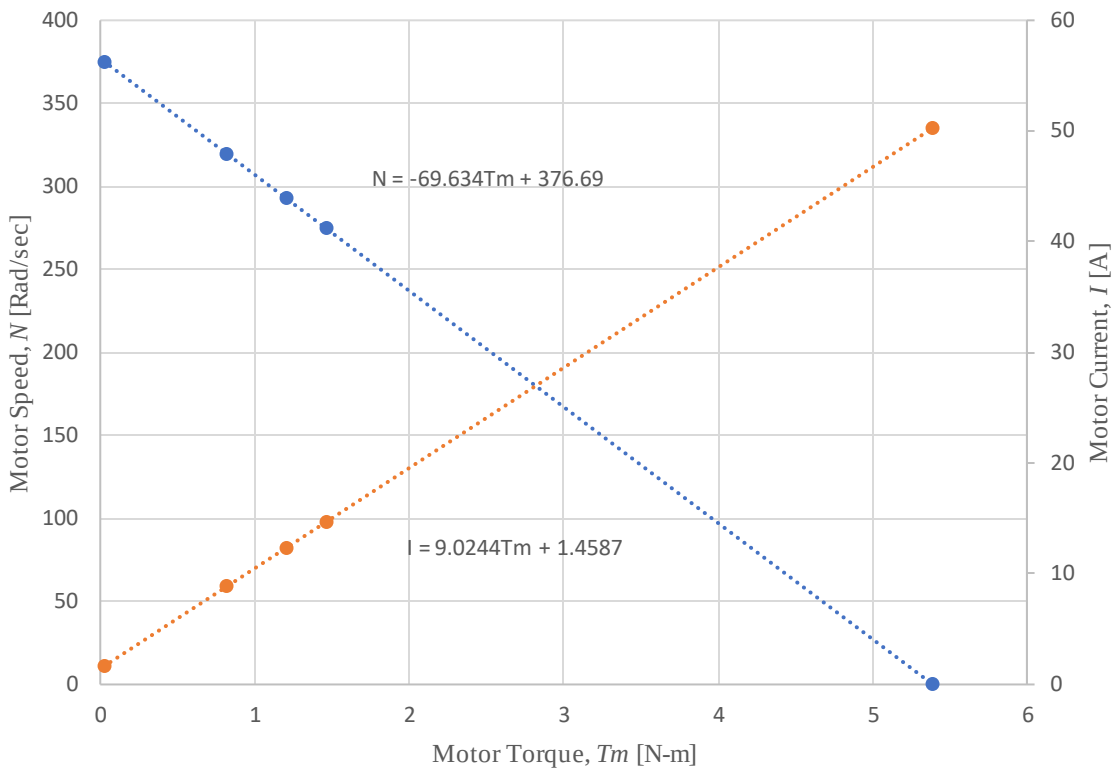

Figure M.9 Torque-speed and torque-current curves for MY1016 36V motor (plotted from performance data, extrapolated data points shown).

Appendix N – Drawing Package & BOM

Table N.1 Grooved Plate BOM

Assembly Level	Part Number	Level					Cost in Sold Quantities							
							Qty.	Cost	Total Cost	Package of	Source	Part #	Link	Notes
		lvl 0	lvl 1	lvl 2	lvl 3		(#)	($)	($)	(#)	(description)	(#)	URL	(-)
0	1000	Final Asm									-			
1	1100		Balancing Mechanism				1				-	-	-	
2	1110			Grooved Plate Body			1	22.99	22.99	1.75mm 1kg roll of PETG	3D Printed in PETG	-	amazon	ALREADY PURCHASED
2	1120			Test Mass Sub Asm			6				-	-	-	
3	1121				1/4"x20x1" Squarehead bolt		1	5.11	5.11	25	McMaster-Carr/ACE Hardware	91465A101	https://www.mcmaster.com/91465A101/	NEEDS TO BE PURCHASED
3	1122				1/4"X20 Flanged Nylock nut		1	7.48	7.48	100	McMaster-Carr/ACE Hardware	93298A110	https://www.mcmaster.com/93298A110/	NEEDS TO BE PURCHASED
2	1130			Mounting Sub Asm			3				-	-	-	
3	1131				M3 x 15mm x 0.5mm Socket Head Cap Screws		1	10.00	10.00	50	McMaster-Carr/ACE Hardware	91290A572	https://www.mcmaster.com/91290A572/	NEEDS TO BE PURCHASED
							16	45.58	45.58	-				

Table N.2 Test Mass Positioner BOM

Assembly Level	Part Number	Level					Cost in Sold Quantities				Source	Part #	Link	Notes
							Qty.	Cost	Total Cost	Package of				
		lvl 0	lvl 1	lvl 2	lvl 3		(#)	($)	($)	(#)	(description)	(#)	URL	(-)
0	2000	Final Asm												
1	2100		3" Scribing Compass				1	18.32	18.32	1	-	2060A29	https://www.mcmaster.com/2060A29/	NEEDS TO BE PURCHASED
1	2200		Positioner Asm				2				-	-	-	
2	2210			Set Screw Arm			1	22.99	22.99	1.75 mm 1kg roll of PETG	acconunted for on Grooved plate iBOM	-	-	
2	2220			Set Screw Sub Asm			1				-	-	-	
3	2221				M4x0.7x10 90 deg cone point set screw		1	8.19	8.19	50	McMaster-Carr/ACE Hardware	91210A114	https://www.mcmaster.com/91210A114/?SrchEntryWebPart_InpBox=dividers	NEEDS TO BE PURCHASED
3	2222				M4X0.7x10 standoff		1	3.15	12.6	4	McMaster-Carr/ACE Hardware	94868A038	https://www.mcmaster.com/94868A038/?SrchEntryWebPart_InpBox=dividers	NEEDS TO BE PURCHASED
3	2223				M4X0.7 hex jam nut		1	2.26	2.26	100	McMaster-Carr/ACE Hardware	90695A035	https://www.mcmaster.com/90695A035/?SrchEntryWebPart_InpBox=dividers	NEEDS TO BE PURCHASED
2	2230			Mounting Sub Asm			1							
3	2231				M3x0.5X18 SHCS		1	11.45	11.45	50	McMaster-Carr/ACE Hardware	91290A121	https://www.mcmaster.com/91290A121/?SrchEntryWebPart_InpBox=dividers	NEEDS TO BE PURCHASED
3	2232				M3X0.5 Nylock hex nut		1	3.57	3.57	100	McMaster-Carr/ACE Hardware	90576A102	https://www.mcmaster.com/90576A102/?SrchEntryWebPart_InpBox=dividers	NEEDS TO BE PURCHASED
							13	69.93	79.38	-				

Table N.3 Testing Equipment

Item Description (Description)	QTY. (#)	Price ($)	Notes (-)	Link (URL)
Monarch PLT200 Laser Tachometer	1	215.00	NEEDS TO BE PURCHASED. THE SOONER THE BETTER.	https://monarchinstrument.com/products/pocket-laser-tach-200
Monarch Remote Optical Sensor	1	159.00	NEEDS TO BE PURCHASED. THE SOONER THE BETTER.	https://monarchinstrument.com/products/remote-optical-led-sensor-with-8-ft-cable-and-mounting?variant=32117233160
T-5 Reflective Tape 5ft x 0.5 in single pack roll	1	15.00	If we need extra refelctive tape	https://monarchinstrument.com/collections/tachometer-accessories/products/t-5-tape-single-pack

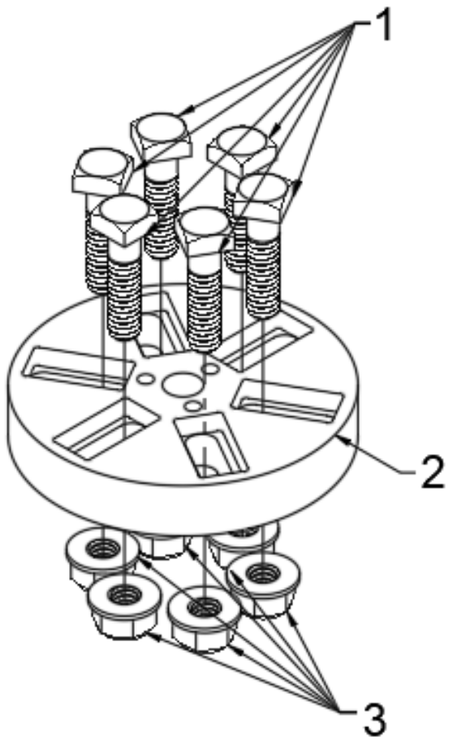

ASSEMBLY OF TEST MASSES ONTO GROOVED PLATE BODY

NOTE: TEST MASSES MUST BE INSTALLED PRIOR TO MOUNTING OF ASSEMBLY TO TURBINE SHAFT AND ROTOR HOUSING

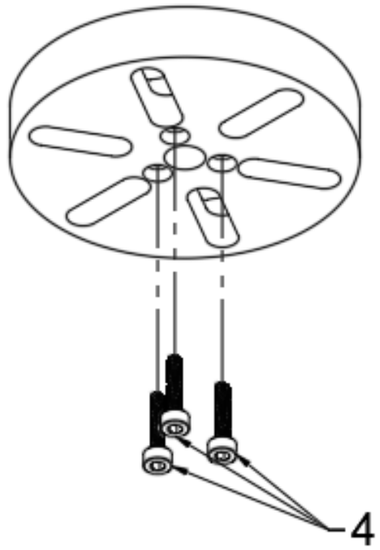

PLACEMENT OF MOUNTING BOLTS FOR ATTACHING GROOVED PLATE TO ROTOR HOUSING

NOTE: TEST MASSES NOT SHOWN FOR CLARITY

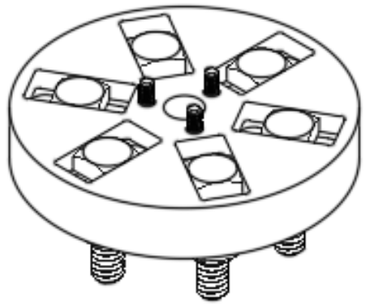

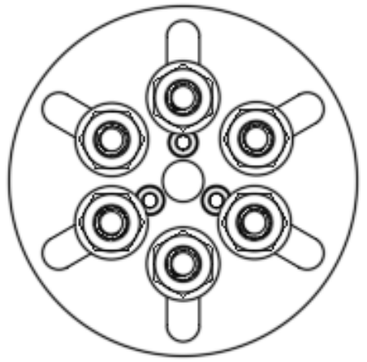

ITEM NO.	QTY.	DESCRIPTION	PART NUMBER	MATERIAL
4	3	M3X0.5X15 SHCS	1131	ALLOY STEEL
3	6	¼"X20X1" SQUARE HEAD BOLTS	1121	ALLOY STEEL
2	1	GROOVED PLATE BODY	1100	3D PRINTED PETG
1	6	¼"X20 FLANGE NYLOCK LOCK NUTS	1122	ALLOY STEEL

PARTS LIST

PROJECT
WPC BALANCING SENIOR PROJECT

TITLE
GROOVED PLATE BALANCING MECHANISM ASSEMBLY DRAWING

APPROVED		SIZE	CODE	DWG NO / REV
CHECKED	CALEB CROSS 3/19/2021	B		3
DRAWN	ETHAN OZUPPA 3/18/2021	SCALE 1:1	WEIGHT	SHEET 1/1

-

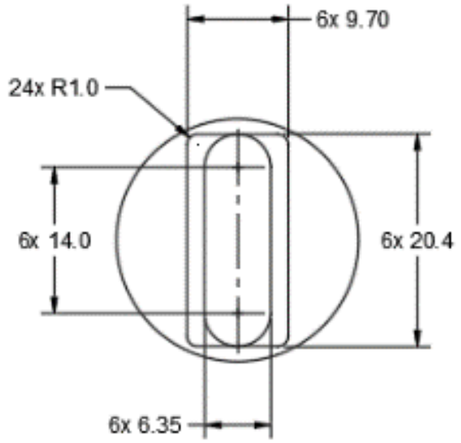

DETAIL B
SCALE 2:1

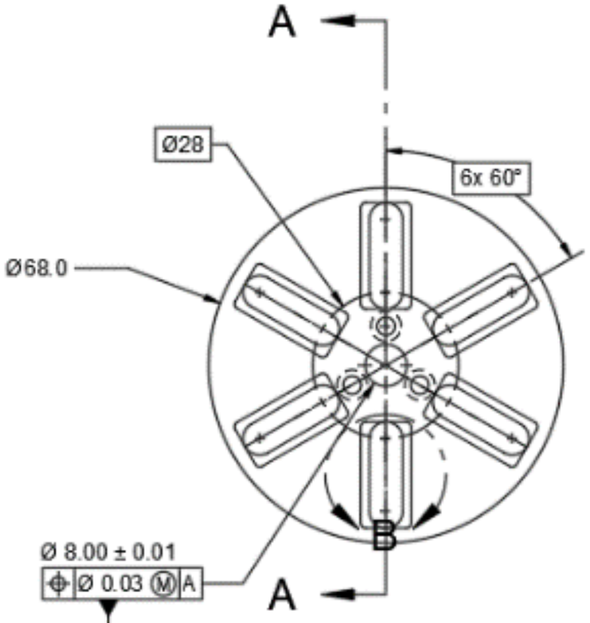

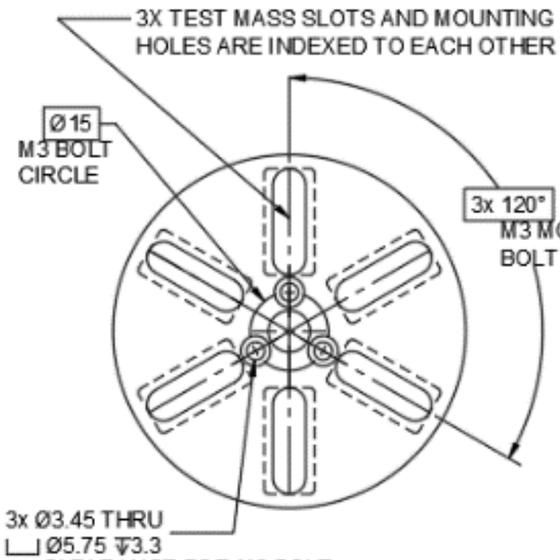

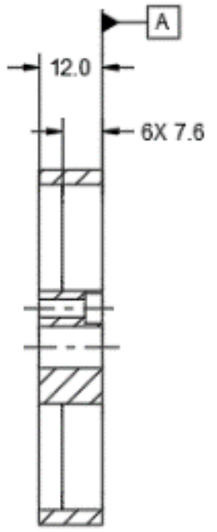

SECTION A-A
SCALE 1:1

NOTES:
UNLESS OTHERWISE SPECIFIED:

1. ALL DIMS IN MILLIMETERS
2. TOLERANCES
   - X ± 1
   - X.X ± 0.1
   - X.XX ± 0.05
   - ANGLES ± 2°
3. REMOVE STRINGING/ SUPPORT MATERIAL IF PRESENT FROM ALL SLOTS AND HOLES WITH AN EDGE DEBUR OR EXACTO KNIFE
4. CURRENT DIMENSIONS HAVE BEEN ADJUSTED TO COMPENSATE FOR SHRINKING OF PETG WHILE COOLING (~0.25 MM). BE ADVISED SHRINK RATES DIFFER FOR EVERY PRINTER.
5. PRINT WITH DATUM A LAYING FLAT ON THE PRINT BED
6. REAM Ø8 NOMINAL BORE TO MATCH SHAFT, HOLE WILL BE UNDERSIZED DUE TO SHRINKING FROM PRINTING
7. IF THE TOP SURFACE IS NOTICEABLY ROUGH OR BUMPY, REPRINT WITH THE IRONING SETTING ENABLED TO SMOOTH THE TOP SURFACE

			PROJECT: WPC Balancing Senior Project			
			TITLE: Grooved Plate Body (3D Printed)			
APPROVED			SIZE: B	CODE:	DWG NO: 1	REV: 5
CHECKED	Caleb Cross	3/17/2021				
DRAWN	Ethan Czuppa	3/17/2021	SCALE: 1:1	WEIGHT:	SHEET: 1/1	

7	2	2223	M4X0.7X10 STANDOFFS	ALUMINUM
6	2	2222	M4X0.7 HEX JAM NUTS	ALLOY STEEL
5	2	2221	M4X0.7X10 90° CONE POINT SETSCREWS	ALLOY STEEL
4	2	2232	M3X0.5 NYLOCK HEX NUT	ALLOY STEEL
3	2	2200	SET SCREW ARMS	3D PRINTED PETG
2	2	2231	M3X0.5X18 SHCS	ALLOY STEEL
1	1	2100	3 IN SCRIBING COMPASS	ALLOY STEEL
ITEM NO.	QTY.	PART NUMBER	DESCRIPTION	MATERIAL
PARTS LIST				

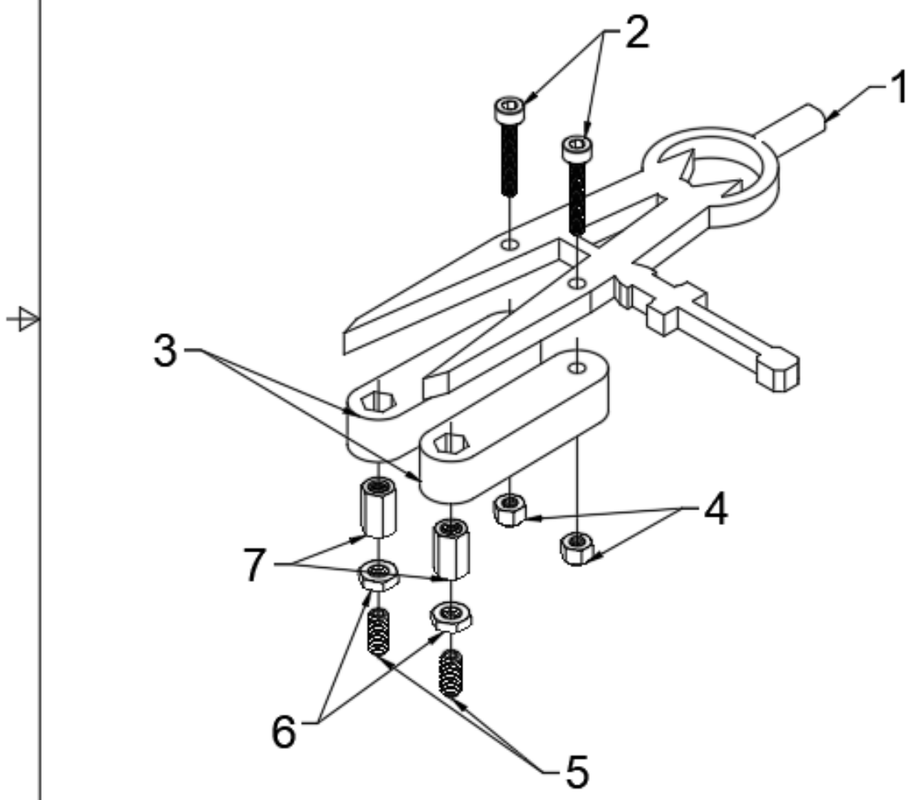

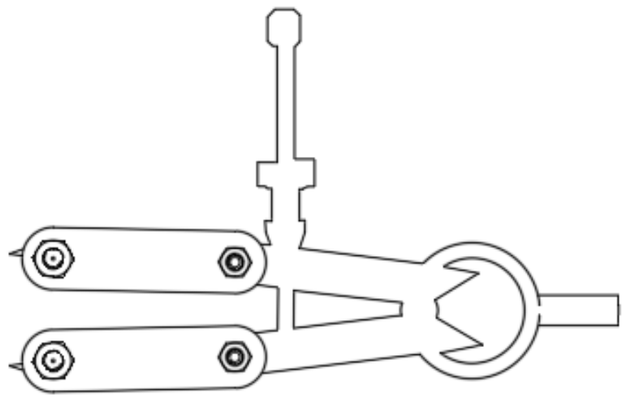

	PROJECT: WPC BALANCING SENIOR PROJECT			
	TITLE: TEST MASS POSITIONER			
APPROVED	SIZE: B	CODE	DWG NO	REV: 1
CHECKED CALEB CROSS 3/19/2021				
DRAWN ETHAN CZUPPA 3/19/2021	SCALE 1:1	WEIGHT	SHEET 1/1	

NOTES:
UNLESS OTHERWISE SPECIFIED

1. ALL DIMS IN MILIMETERS
2. TOLERANCES
   X.X ± 0.1
   X.XX ± 0.05
3. REMOVE STRINGING/ SUPPORT MATERIAL IF PRESENT FROM ALL SLOTS AND HOLES WITH AN EDGE DEBUR OR EXACTO KNIFE.
4. PRINT WITH DATUM A LAYING FLAT ON THE PRINT BED
5. CURRENT DIMENSIONS ARE NOMINAL AND HAVE NOT BEEN ADJUSTED FOR SHRINKAGE (ADD ~0.25 TO HOLES, HEXAGONAL CUT OUTS AND OTHER PROFILES DO NOT ALWAYS SHRINK THE SAME AMOUNT).
6. THIS INTERNAL 6 HEX IS INTENDED TO BE A TRANSITION LOCATION FIT WITH A 4X0.7X10 STANDOFF, WHICH HAS A SYMMETRIC TOLERANCE SPAN OF 0.26. THE POSITIONING TOLERANCE THAT APPLIES TO THE 3 THRU CLEARANCE HOLE ALSO APPLIES TO THIS HEX

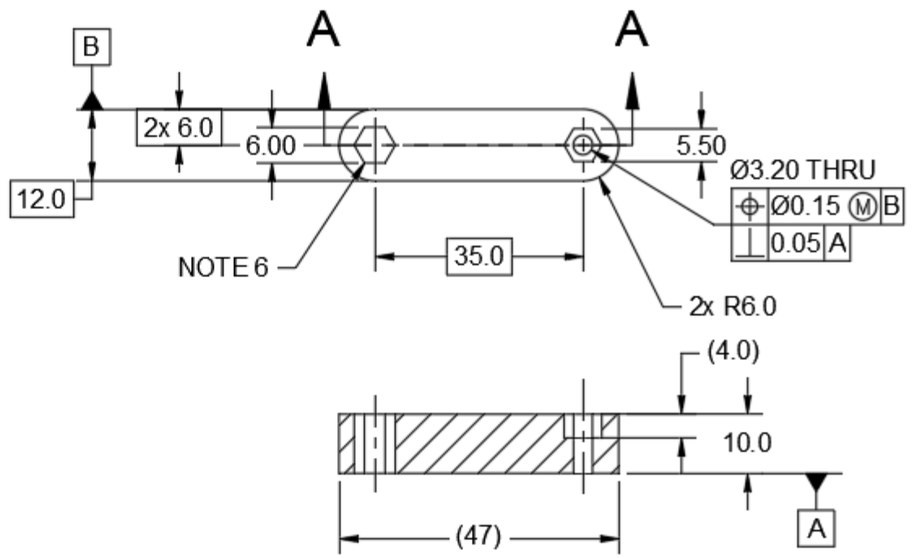

SECTION A-A
SCALE 1:1

	PROJECT: WPC BALANCING SENIOR PROJECT			
	TITLE: SET SCREW ARM			
APPROVED	SIZE	CODE	DWG NO	REV
CHECKED CALEB CROSS 3/19/2021	A			1
DRAWN ETHAN CZUPPA 3/18/2021	SCALE 1:1	WEIGHT		SHEET 1/1

Appendix O – Manufacturing Inspection Log

Test Print Name	Date	Duration	Filament Used	Mass	Infill Density	Quality	Notes
(Name)	(ctlr+;)	(hr:min)	(m)	(g)	(%)	(mm)	(text)
Shrink Test	1/3/2021	2hr 55min	7.28	19.2	20	0.2	PETG is a very stringy material prone to defects, but remarkably resilient when it comes to survining stringing or poor adhesion during the printing of the first layer. The shrink seems to be on par with PLA in the vertical direction, but not in the horizontal directions.
Shrink Test 2 No Brim	1/3/2021	2hr 53min	7.29	19.2	20	0.2	Adjusted dimensions of c-bores and they shrunk as predicted to almost exactly the right dimension. Used grid support for the counter bores and they were much easier to remove and significantly cleaner the M3 screws with correct socket head height should have no issue sitting flush in the counter bore. No brim is needed. The first layer was extraordinarily clean with the same exact settings save increasing the retraction slightly to 25 mm/s
Final Print Tes 1 20% IF	3/9/2021	2hr 54 min	7.29	19.1	20	0.2	Adjusted dimensions of rectangular slot cutouts to achieve a closer fit, the result was a much tighter fit that prevented the bolt heads from sliding freely.

Inspection	Slot Width	Slot length	Slot depth	Rect. Slot Width	Rect. Slot Length	Rect. Slot Depth	Overall Diameter	Overall Depth	Bore Diam	C-Bore Diam	C-Bore Depth	M3 Clearance Fit	M3 Socket Head Flush	Square Head Bolt Flush	Square Head Bolt Slot	Inspection Notes
(Name)	(mm)	(mm)	(mm)	(mm)	(mm)	(mm)	(mm)	(mm)	(mm)	(mm)	(mm)	(Go / No-Go)	(Go / No-Go)	(Go / No-Go)	(Go / No-Go)	
Nominal	6.4	20.4	7.6	9.9	20.4	4.4	68	12	8.00	5.6	3					N/A
Shrink Test	6.4 +/- 0.1	20		9.9 +0.1/ -0	20.3 +/- 0.1	4.4	68	11.8 +/- 0.05	7.83	5.45	2.6 +/- 0.1	Go	No-Go	Not Tested	Not Tested	It seems that there is a bit of a draft/taper in many of the features with the feature being the widest at the top and narrowest at the bottom. It is possible that layer adhesion was not as it should be or that the print speed was too high. Additionally, this test print had a first layer with several defects. The brim made the overall diameter harder to measure and may not be necessary for the actual print.
Shrink Test 2	6.40 +/- 0.05	19.75 +/- 0.05		9.91 +/- 0.05	20.3 +/- 0.1	4.42	67.75	11.9	7.8	5.65 +/- 0.05	3.05 +/- 0.05	Go	Go	Not Tested	Not Tested	it is printed on is not super flat, nor is the top surface of the print- that which mounts to the boss on the pitching housing free of blemishes. I may try irroning the top to make it a cleaner, flatter (?) surface. Overall this test went much better than the first. The dimensions seem to be relatively stable and repeatable - enough that 3D printing should be suitable for making the grooved plate. I was talking with Niko about infills and how they might affect the eccentricity of the grooved plate body. I am nervous about using an infill other than cubic like concentric due to how it could effect the strenght of the part as well as layer adhesion.
Final Print Test 1	-	-		9.70 +/- 0.05	-	-	-	-	-	-	-	Go	Go	Go	Go,	good fit does not slide freely, a little more adjustment and it should be just right...

Appendix P – MATLAB Calibration Code

```
%% Import information
xim = 0 ; % x value of imbalance from import
yim = 0 ; % y value of imbalance from import
rim = 0 ; % radial value of imbalance from import
degim = 0 ; % degree of imbalance from import

%% Balancing requirements
% res = 0.01 ; % desired resolution for balancing [kg-mm]

%% Balancing mechanism data
degA = 30 ; % [deg]
degB = 90 ;
degC = 150 ;
degD = 210 ;
degE = 270 ;
degF = 330 ;
mass = .012 ; % mass of sliding mass [kg]
mindis = 15.628 ; % distance from center of rotation to center of mass of bolt in zero position [mm]
maxdis = 26.372 ; % distance from center of rotation to center of mass of bolt in farthest position [mm]

%% Wind turbine data
massim = 0 ; % mass of rotating assembly

%% Base equations
% mass * mindis * ( cos(degA) + cos(degB) + cos(degC) + cos(degD) +
% cos(degE) + cos(degF) ) = massim * xim
% eqABx = mass * ( ( mindis * ( cos(degC) + cos(degD) + cos(degE) + cos(degF) ) ) + ( ( A + mindis ) * cos(degA) ) + ( ( B + mindis ) * cos(degB) ) ) - massim * xim

%% iterative solving method
% if 0 <= degim < 30 || degF <= degim < 360 % [deg]
%     % use closest masses in Q1 (A) and Q6 (F)
%     eqAFx = mass * ( ( mindis * ( cosd(degB) + cosd(degC) + cosd(degD) + cosd(degE) ) ) + ( ( A + mindis ) * cosd(degA) ) + ( ( F + mindis ) * cosd(degF) ) ) - massim * xim ;
%     eqAFy = mass * ( ( mindis * ( sind(degB) + sind(degC) + sind(degD) + sind(degE) ) ) + ( ( A + mindis ) * sind(degA) ) + ( ( F + mindis ) * sind(degF) ) ) - massim * yim ;
%     % must iteratively solve, use zeroes as initial guess because of linear
%     % system
%     % how to properly incorporate limits
%     while abs( eqAFx ) > res || abs( eqAFy ) > res % [kg-mm]
%
% end
%
%% linear matrix solve
% pros:
% - easy
```

```
% - does not need resolution, just finds closest number
% cons:
% - error due to cartesian conversion
% - will run into issues with inability to meet certain imbalances?
if 0 <= degim < degA || degF <= degim < 360
    matAF1 = [ -mass * cosd(degA) , -mass * cosd(degF) ;
            -mass * sind(degA) , -mass * sind(degF) ] ;
    matAF2 = [ mass * mindis * ( cosd(degA) + cosd(degB) + cosd(degC) + cosd(degD) + cosd(degE) + cosd(degF) ) - massim * xim ;
            mass * mindis * ( sind(degA) + sind(degB) + sind(degC) + sind(degD) + sind(degE) + sind(degF) ) - massim * yim ] ;
    matAF3 = matAF1 \ matAF2 ;
    A = matAF3(1) ;
    F = matAF3(2) ;
    display( [ 'A' , 'B' , 'C' , 'D' , 'E' , 'F' ;
             A  ,  0  ,  0  ,  0  ,  0  ,  F ] ) ;
end
% ERROR: MATRIX IS SINGULAR, MATLAB is having trouble with matriz division, not sure why exactly
% ======= May be due to zero elements in matrix,
%
if degA <= degim < degB
    matAB1 = [ -mass * cosd(degA) , -mass * cosd(degB) ;
            -mass * sind(degA) , -mass * sind(degB) ] ;
    matAB2 = [ mass * mindis * ( cosd(degA) + cosd(degB) + cosd(degC) + cosd(degD) + cosd(degE) + cosd(degF) ) - massim * xim ;
            mass * mindis * ( sind(degA) + sind(degB) + sind(degC) + sind(degD) + sind(degE) + sind(degF) ) - massim * yim ] ;
    matAB3 = matAB2 \ matAB1 ;
    A = matAB3(1) ;
    B = matAB3(2) ;
    display( [ 'A' , 'B' , 'C' , 'D' , 'E' , 'F' ;
             A  ,  B  ,  0  ,  0  ,  0  ,  0 ] ) ;
end

if degB <= degim < degC
    matBC1 = [ -mass * cosd(degB) , -mass * cosd(degC) ;
            -mass * sind(degB) , -mass * sind(degC) ] ;
    matBC2 = [ mass * mindis * ( cosd(degA) + cosd(degB) + cosd(degC) + cosd(degD) + cosd(degE) + cosd(degF) ) - massim * xim ;
            mass * mindis * ( sind(degA) + sind(degB) + sind(degC) + sind(degD) + sind(degE) + sind(degF) ) - massim * yim ] ;
    matBC3 = matBC2 \ matBC1 ;
    B = matBC3(1) ;
    C = matBC3(2) ;
    display( [ 'A' , 'B' , 'C' , 'D' , 'E' , 'F' ;
             0  ,  B  ,  C  ,  0  ,  0  ,  0 ] ) ;
end

if degC <= degim < degD
    matCD1 = [ -mass * cosd(degC) , -mass * cosd(degD) ;
            -mass * sind(degC) , -mass * sind(degD) ] ;
    matCD2 = [ mass * mindis * ( cosd(degA) + cosd(degB) + cosd(degC) + cosd(degD) + cosd(degE) + cosd(degF) ) - massim * xim ;
```

```
            mass * mindis * ( sind(degA) + sind(degB) + sind(degC) + sind(degD) + sind(degE) + sind(degF) ) - massim * yim ] ;
    matCD3 = matCD2 \ matCD1 ;
    C = matCD3(1) ;
    D = matCD3(2) ;
    display( [ 'A' , 'B' , 'C' , 'D' , 'E' , 'F' ;
             0 , 0 , C , D , 0 , 0 ] ) ;
end

if degD <= degim < degE
    matDE1 = [ -mass * cosd(degD) , -mass * cosd(degE) ;
            -mass * sind(degD) , -mass * sind(degE) ] ;
    matDE2 = [ mass * mindis * ( cosd(degA) + cosd(degB) + cosd(degC) + cosd(degD) + cosd(degE) + cosd(degF) ) - massim * xim ;
            mass * mindis * ( sind(degA) + sind(degB) + sind(degC) + sind(degD) + sind(degE) + sind(degF) ) - massim * yim ] ;
    matDE3 = matDE2 \ matDE1 ;
    D = matDE3(1) ;
    E = matDE3(2) ;
    display( [ 'A' , 'B' , 'C' , 'D' , 'E' , 'F' ;
             0 , 0 , 0 , D , E , 0 ] ) ;
end

if degE <= degim < degF
    matEF1 = [ -mass * cosd(degE) , -mass * cosd(degF) ;
            -mass * sind(degE) , -mass * sind(degF) ] ;
    matEF2 = [ mass * mindis * ( cosd(degA) + cosd(degB) + cosd(degC) + cosd(degD) + cosd(degE) + cosd(degF) ) - massim * xim ;
            mass * mindis * ( sind(degA) + sind(degB) + sind(degC) + sind(degD) + sind(degE) + sind(degF) ) - massim * yim ] ;
    matEF3 = matEF2 \ matEF1 ;
    E = matEF3(1) ;
    F = matEF3(2) ;
    display( [ 'A' , 'B' , 'C' , 'D' , 'E' , 'F' ;
             0 , 0 , 0 , 0 , E , F ] ) ;
end
```

Appendix Q – Product Literature

3D PRINTING FILAMENT

3D PRINTING PHOTOPOLYMER RESIN SERIES

（Filament Specification：1.75mm / 2.85mm）（Specification of Resin：500ML / 1000ML）

Filament Type	Print Temp (℃)	Bed Temp (℃)	Density (g/cm³)	Heat Distortion Temp (℃,0.45MPa)	Melt Flow Index (g/10min)	Tensile Strength (MPa)	Elongation at Break (%)	Flexural Strength (MPa)	Flexural Modulus (MPa)	IZOD Impact Strength (kJ/㎡)
PLA	190-210	No Heat/(60-80)	1.25	56	5(190℃/2.16kg)	65	8	97	3600	4
PLA+	205-225	No Heat/(60-80)	1.25	52	4(190℃/2.16kg)	65	12	75	2102	8.5
ABS	220-260	90-110	1.04	78	12(220℃/10kg)	43	22	66	2348	19
ABS+	220-260	90-110	1.06	73	15(220℃/10kg)	40	30	68	2443	42
ABS Odorless	220-260	100-110	/	/	/	40.4	34	61	2377	12.2
eABS MAX	220-240	90-110	1.05	85	60(220℃/10kg)	45	30	58	2400	48
eASA	220-260	90-110	1.00	54	10-15(220℃/10kg)	50	30	35	4300	19
HIPS	220-260	90-110	1.05	80	2(200℃/5kg)	27	55	39	2280	11
PETG	230-250	No Heat/(60-80)	1.23	64	20(250℃/2.16kg)	49	225	68	1800	7.6
PVA	180-210	No Heat/(60-80)	1.25	/	/	22	360	/	/	/
ePVA+	190-210	No Heat/(60-80)	1.14	/	/	26	190	/	/	/
eSmooth	190-220	No Heat/(60-80)	/	63.5	4-6(190℃/2.16kg)	46	273	71	2799	4
Wood	190-220	No Heat/(60-80)	0.7	45	17(190℃/2.16kg)	/	/	/	/	/
Color Change	190-220	No Heat/(60-80)	1.24	58	10(190℃/2.16kg)	65	5	97	3600	4
eClean	160-300	/	0.95	45	/	23	580	/	/	29
Bronze	180-210	No Heat/(60-80)	1.27	50	62(190℃/2.16kg)	66	16	106	4442	4
eCopper	200-220	No Heat/(60-80)	2.46	52	20(190℃/2.16kg)	40	4	64	4954	4
eAl-fill	200-220	No Heat/(60-80)	1.48	52	8(190℃/2.16kg)	45	5	74	4885	4
eSteel	200-220	No Heat/(60-80)	2.46	52	14(190℃/2.16kg)	45	5	63	4452	5
ePA (Nylon)	230-260	80-90	1.12	50	5(230℃/2.16kg)	57	196	57	1495	15
ePA-CF	240-260	80-90	1.24	120	6(250℃/5kg)	85	26	122	5160	15.5
ePA6-CF	240-280	60	1.4	240	/	170	2	/	15	/
ePA-GF	240-260	80-90	1.35	120	7(250℃/5kg)	101	17	160	4300	8
ePC	235-260	80-110	1.12	80	5(230℃/2.16kg)	57	196	57	1495	15
eFlex (TPU)	210-230	No Heat	1.12	/	/	52	500	/	/	/
eLastic (TPE)	210-230	No Heat	1.14	/	/	32	420	/	/	/
eTPU-95A	210-240	No Heat	1.43	/	8.4g/10min(190℃/2.16kg)	/	780	/	/	/
eMate (PCL)	70-100	≤40	1.16	45	0.5(70℃/2.16kg)	18	>800	13	345	Don't break
ePeek	380-410	90-150	1.30	152	10(380℃/5kg)	100	40	170	3500	7
eSilk-PLA	190-220	No Heat/(60-80)	1.43	67	2.5(190℃/2.16kg)	58	300	75	4000	4
eTwinkling	190-220	No Heat/(60-80)	1.41	67	2.5(190℃/2.16kg)	58	/	70	2100	4
eMarble	190-220	No Heat/(60-80)	1.24	67	/	60	6.0	/	/	/

LCD Resin Type	Wavelength (nm)	Density (g/cm³)	Viscosity (25℃, MPa•s)	Hardness (Shore D)	Tensile Strength (MPa)	Elongation at Break(%)	Flexural Strength(MPa)	Flexural Modulus (MPa)	IZOD Impact Strength (J/m)
eResin-PLA	395-405	1.07-1.13	200-300	75-80	35-50	20-50	40-60	600-800	15-32
Standard Resin	395-405	1.08-1.13	150-250	80-82	46-67	28-35	46-72	1000-1400	18-40
Hard-Tough Resin	395-405	1.10-1.15	200-300	81	55-60	30-50	70-80	1300-1400	67-100
Rigid Resin	395-405	1.10-1.15	200-300	83	60-70	25-35	80-85	1400-1500	15-42
Castable Resin for Jewelry	395-405	1.05-1.12	100-150	60	42-62	11-20	49-58	1860-2640	44-49
Castable Resin for Dental	395-405	1.05-1.12	100-150	80	42-62	11-20	49-58	1180-2520	44-49

DLP Resin Type	Wavelength (nm)	Density (g/cm³)	Viscosity (25℃, MPa•s)	Hardness (Shore D)	Tensile Strength (MPa)	Elongation at Break(%)	Flexural Strength(MPa)	Flexural Modulus (MPa)	IZOD Impact Strength (J/m)
eResin-PLA	395-405	1.07-1.13	200-300	70-75	30-40	20-40	/	/	15-32
Non-castable Resin	395-405	1.05-1.13	100-150	88	36-52	11-20	59-70	1882-2385	44-49
Castable Resin for Jewelry	395-405	1.05-1.13	100-150	60	42-62	11-20	49-58	1862-2645	44-49
Castable Resin for Dental	395-405	1.05-1.13	100-150	81	42-62	11-20	49-58	1192-2525	44-49

Table Q.1 Proposed Electrical Subsystem Selected Components (Reference Only).

Item Description	Voltage Rating	Current Rating	Quantity	Price	Link
(Description)	(V)	(A)	(#)	($)	(URL)
MY1016 Brushed DC electric scooter motor	36	12.5	1	53.99	https://www.monsterscooterparts.com/36v35mowisp.html?gclid=Cj0KCQjw9YWDBhDyARIsADt6sGbhg4jdDX2MAiaMZl2DZPuvp7ADeAy469kJW-dxB6HxFPNjcTT-YkEaAioWEALw_wcB
DC-DC Solid State Relay	60	100	1	13.99	https://www.amazon.com/TWTADE-SSR-40-3-32V-5-60V-Solid/dp/B079BBZL7F/ref=psdc_6374820011_t1_B07PFDJQLV?th=1
Automotive Slow-Blow Blade type fuse	58	10	10	2.62	https://www.mouser.com/ProductDetail/Littelfuse/0891010NXS?qs=%252BIl6bbVulsqibooUuRKf8w%3D%3D
Inline blade type fuse holder			2	11.84	https://www.amazon.com/Littelfuse-0FHA0030XP-Carded-Inline-Holder/dp/B000COA2ZW?ref_=fspcr_pl_dp_2_6355937011
Thermal Circuit Breaker (Emergency Stop)	48	20	1	21.99	https://www.amazon.com/Lumision-Waterproof-Circuit-Resettable-12-48VDC/dp/B074TBMW3G
High Power Brushed DC Motor Driver	44	20	1	64.95	https://www.pololu.com/product/1457
Nucleo L476RG Microncontroller	N/A	N/A	1	14.60	https://www.mouser.com/ProductDetail/STMicroelectronics/NUCLEO-L476RG?qs=PRtH0mD6DWbM6mRV5DKjBQ%3D%3D&mgh=1&gclid=CjwKCAjwu5CDBhB9EiwA0w6sLfoQNdjjBElejX2rkw_pZzja6H0IY3oUNCKjb5lMzbxnYS2zs2k-khoCQUQQAvD_BwE
Monarch PLT200 Laser Tachometer	N/A	N/A	1	215.00	https://monarchinstrument.com/products/pocket-laser-tach-200
Monarch Remote Optical Sensor	N/A	N/A	1	159.00	https://monarchinstrument.com/products/remote-optical-led-sensor-with-8-ft-cable-and-mounting?variant=32117233160
T-5 Reflective Tape 5ft x 0.5 in single pack roll	N/A	N/A	1	15.00	https://monarchinstrument.com/collections/tachometer-accessories/products/t-5-tape-single-pack
			20	398.98	

Table Q.2 Electrical Component Literature and Documentation

Component Name	Data Sheet/Literature Link
(Name)	(URL)
TWTADE SSR-25 DD	https://cdn.sparkfun.com/datasheets/Components/General/SSR40DA.pdf
58V Rated Low Profile Blade Fuses	https://www.mouser.com/datasheet/2/240/Littelfuse_LowProfileMINI_Datasheet-523217.pdf
Little Fuse Inline Fuse Holder	https://media.digikey.com/pdf/Data%20Sheets/Littelfuse%20PDFs/FHA_FHAC_Series.pdf
High Power Motor Driver Board Current Sensor	https://www.pololu.com/file/0J388/IPD048N06L3_Rev2.0.pdf
High Power Motor Driver Board MOSFETs	https://www.pololu.com/file/0J196/ACS714.pdf
High Power Motor Driver Board Documentation	https://www.pololu.com/product/1457
Monarch PLT200 Laser Tachometer	https://monarchserver.com/Files/pdf/manuals/PLT200English.pdf
Monarch Remote Optical Sensor	https://monarchserver.com/Files/pdf/manuals/1071-4854-124%20ROS%20Instruction%20Sheet.pdf

Appendix R – Final Project Budget

	Item	Part #	Quantity	Cost	Total
Balancing Mechanism	Grooved plate body	1110	1	22.99	22.99
	1/4"x20x1 Squarehead bolt	1121	1	5.11	5.11
	1/4"x20 Flanged Nylock nut	1122	1	7.48	7.48
	M3x15x0.5 Socket Head Cap Screw	1131	1	10.00	10.00
Test Mass Positioner	Standoff (M4x0.7x10)	2223	2	9.11	9.11
	Hex Jam Nuts (M4x0.7)	2222	2	8.76	8.76
	Cone Point Setscrews (M4x0.7x10) 90deg	2221	2	0.76	1.52
	NY Lock Hex Nut (M3x0.5)	2232	2	0.98	1.96
	Set Screw Arms	2200	2	2.98	5.96
	SHCS (M3x0.5x18)	2231	2	0.96	1.92
	3 inch Scribing Compass	2100	1	13.48	13.48
Total	-	-	-	-	88.29

Appendix S – Failure Modes & Effects Analysis + Risk Assessment (DesignSafe and Preliminary FMEA)

designsafe Report

Application:	CPWP Rotor Balancing Testing Procedure	Analyst Name(s):	Ethan Czuppa, Caleb Cross
Description:	Risk assesment of testing procedure including mechatronic system, balancing procedure, measurement procedure, etc.	Company:	Cal Poly Wind Power Senior Project Vibrations Testing Procedure
Product Identifier:		Facility Location:	California Polytechnic State University, SLO. Mechanical Engineering Department Vibrations laboratory.
Assessment Type:	Detailed		
Limits:			
Sources:			
Risk Scoring System:	ANSI B11.0 (TR3) Two Factor		

Guide sentence: When doing [task], the [user] could be injured by the [hazard] due to the [failure mode].

Item Id	Sub-process / User / Task	Hazard / Failure Mode	Initial Assessment Severity Probability	Risk Level	Risk Reduction Methods /Control System	Final Assessment Severity Probability	Risk Level	Status / Responsible /Comments /Reference
1-1-1-1	Calibration of Vibration Measurement Testbed adult first use / test	mechanical : product instability Imbalance inherent in rotor exceeds safe threshold	Moderate Likely	Medium	fixed enclosures / barriers, prevent energy buildup /Not Applicable	Moderate Unlikely	Low	Ethan Czuppa, Caleb Cross, Trained Operator
1-1-1-2	Calibration of Vibration Measurement Testbed adult first use / test	electrical / electronic : energized equipment / live parts Power is applied to motor control system	Serious Unlikely	Medium	lock out / tag out	Serious Remote	Low	Ethan Czuppa, Caleb Cross, Trained Operator
1-1-1-3	Calibration of Vibration Measurement Testbed adult first use / test	electrical / electronic : unexpected start up / motion Cascading control system failure due to hardware defects across the board	Catastrophic Remote	Low	instruction manuals - Check mechatronics system before testing	Catastrophic Remote	Low	Ethan Czuppa, Caleb Cross, Trained Operator
1-1-1-4	Calibration of Vibration Measurement Testbed adult first use / test	electrical / electronic : power supply interruption Accidental disconnect of power cable	Minor Likely	Low	separate hazard / people in time or space, warning sign(s)	Minor Unlikely	Negligible	Ethan Czuppa, Caleb Cross, Trained Operator
1-1-2-1	Calibration of Vibration Measurement Testbed adult normal use	mechanical : product instability Imbalance inherent in rotor exceeds safe threshold	Moderate Unlikely	Low	fixed enclosures / barriers, prevent energy buildup	Minor Unlikely	Negligible	Ethan Czuppa, Caleb Cross, Trained Operator
1-1-2-2	Calibration of Vibration Measurement Testbed adult normal use	electrical / electronic : energized equipment / live parts Power is applied to motor control system	Moderate Unlikely	Low	lock out / tag out	Moderate Remote	Negligible	Ethan Czuppa, Caleb Cross, Trained Operator

Item Id	Sub-process / User / Task	Hazard / Failure Mode	Initial Assessment Severity Probability	Risk Level	Risk Reduction Methods /Control System	Final Assessment Severity Probability	Risk Level	Status / Responsible /Comments /Reference
1-1-2-3	Calibration of Vibration Measurement Testbed adult normal use	electrical / electronic : unexpected start up / motion Cascading control system failure due to hardware defects across the board	Catastrophic Remote	Low	instruction manuals - Check mechatronics system before testing	Catastrophic Remote	Low	Ethan Czuppa, Caleb Cross, Trained Operator
1-1-2-4	Calibration of Vibration Measurement Testbed adult normal use	electrical / electronic : power supply interruption Accidental disconnect of power cable	Minor Likely	Low	separate hazard / people in time or space	Minor Unlikely	Negligible	Ethan Czuppa, Caleb Cross, Trained Operator
1-1-3-1	Calibration of Vibration Measurement Testbed adult maintenance / lubrication	mechanical : drawing-in / trapping / entanglement Turbine runs while maintenace is being performed with the enclosure removed	Catastrophic Unlikely	Medium	lock out / tag out	Catastrophic Remote	Low	Ethan Czuppa, Caleb Cross, Trained Operator
1-1-3-2	Calibration of Vibration Measurement Testbed adult maintenance / lubrication	mechanical : pinch point Tightening bolts and clamps	Minor Likely	Low	standard procedures	Minor Unlikely	Negligible	Ethan Czuppa, Caleb Cross, Trained Operator
1-1-3-3	Calibration of Vibration Measurement Testbed adult maintenance / lubrication	mechanical : product instability Adjustment made to correct mass imbalance introduced more imbalance	Serious Unlikely	Medium	E-stop control, special procedures	Moderate Unlikely	Low	Ethan Czuppa, Caleb Cross, Trained Operator
1-1-3-4	Calibration of Vibration Measurement Testbed adult maintenance / lubrication	electrical / electronic : unexpected start up / motion Power supply was not turned off	Serious Unlikely	Medium	lock out / tag out, unplug power supply unless testing	Serious Remote	Low	Ethan Czuppa, Caleb Cross, Trained Operator
1-1-4-1	Calibration of Vibration Measurement Testbed adult trouble-shooting / problem solving	mechanical : product instability Adjustment made to correct mass imbalance introduced more imbalance	Serious Likely	High	slow ramp speed controller input, fixed enclosures, barriers	Serious Unlikely	Medium	Ethan Czuppa, Caleb Cross, Trained Operator

Item Id	Sub-process / User / Task	Hazard / Failure Mode	Initial Assessment Severity Probability	Risk Level	Risk Reduction Methods /Control System	Final Assessment Severity Probability	Risk Level	Status / Responsible /Comments /Reference
1-1-4-2	Calibration of Vibration Measurement Testbed adult trouble-shooting / problem solving	electrical / electronic : energized equipment / live parts Some troubleshooting may require the power to be left on	Serious Unlikely	Medium	Unplug power supply if able to / protective wear from electrocutions	Serious Remote	Low	Ethan Czuppa, Caleb Cross, Trained Operator
1-1-4-3	Calibration of Vibration Measurement Testbed adult trouble-shooting / problem solving	electrical / electronic : shorts / arcing / sparking Continuity tests on live wires when power was not removed, hot-swapping connections	Serious Unlikely	Medium	Inspecting wiring before usage and referring to procedural schematic, standard eletrical testing procedures	Serious Remote	Low	Ethan Czuppa, Caleb Cross, Trained Operator
1-1-4-4	Calibration of Vibration Measurement Testbed adult trouble-shooting / problem solving	electrical / electronic : unexpected start up / motion Power supply was not turned off and commands are inadvertantly sent to MCU	Serious Unlikely	Medium	Turn off power supply unless testing, lock out/ tag out	Serious Remote	Low	Ethan Czuppa, Caleb Cross, Trained Operator
1-1-4-5	Calibration of Vibration Measurement Testbed adult trouble-shooting / problem solving	slips / trips / falls : trip larger diameter power and signal cables loose or in high foot-traffick areas	Minor Likely	Low	separate hazard / people in time or space, warning sign(s)	Minor Unlikely	Negligible	Ethan Czuppa, Caleb Cross, Trained Operator
1-1-5	Calibration of Vibration Measurement Testbed adult cleaning	<None>						
1-1-6-1	Calibration of Vibration Measurement Testbed adult assemble	mechanical : cutting / severing sharp edges (enclosure/assembled components)	Moderate Unlikely	Low	Deburr sharp edges, sand plywood to removed splinters, wear gloves while handling (only)	Minor Remote	Negligible	Ethan Czuppa, Caleb Cross, Trained Operator
1-1-6-2	Calibration of Vibration Measurement Testbed adult assemble	mechanical : pinch point Tight fits on assembled components	Moderate Unlikely	Low	Standard assembly procedure, special procedures for stuck components	Moderate Remote	Negligible	Ethan Czuppa, Caleb Cross, Trained Operator

Item Id	Sub-process / User / Task	Hazard / Failure Mode	Initial Assessment Severity Probability	Risk Level	Risk Reduction Methods /Control System	Final Assessment Severity Probability	Risk Level	Status / Responsible /Comments /Reference
1-1-6-3	Calibration of Vibration Measurement Testbed adult assemble	ergonomics / human factors : lifting / bending / twisting properly locating plywood enclosure by hand (weight approx 10-20lbf)	Minor Likely	Low	proper lifting practices, use mechanical transport	Minor Unlikely	Negligible	Ethan Czuppa, Caleb Cross, Trained Operator
1-1-7-1	Calibration of Vibration Measurement Testbed adult disassembly	mechanical : cutting / severing force to remove tight-fitting components with sharp edges	Minor Likely	Low	Deburr sharp edges, wear gloves while handling (only)	Minor Unlikely	Negligible	Action Item Ethan Czuppa, Caleb Cross, Trained Operator
1-1-7-2	Calibration of Vibration Measurement Testbed adult disassembly	ergonomics / human factors : lifting / bending / twisting removing plywood enclosure by hand	Minor Likely	Low	proper lifting practices, use mechanical transport	Minor Unlikely	Negligible	Ethan Czuppa, Caleb Cross, Trained Operator
1-1-8	Calibration of Vibration Measurement Testbed adult storage	<None>						
1-1-9-1	Calibration of Vibration Measurement Testbed adult misuse	mechanical : cutting / severing enclosure removed, thin spinning turbine blades exposed	Moderate Likely	Medium	fixed enclosure / barriers	Moderate Unlikely	Low	Ethan Czuppa, Caleb Cross, Trained Operator
1-1-9-2	Calibration of Vibration Measurement Testbed adult misuse	mechanical : drawing-in / trapping / entanglement personnel loose clothing contact with spining rotor with enclosure removed	Serious Likely	High	no loose clothing, proper PPE (closed toed shoes, long pants, snag hazards tied back or removed)	Serious Unlikely	Medium	Ethan Czuppa, Caleb Cross, Trained Operator
1-1-9-3	Calibration of Vibration Measurement Testbed adult misuse	mechanical : stabbing / puncture catastrophic blade failure with enclosure removed	Serious Likely	High	fixed enclosure / barriers, proper PPE (face shield / safety glasses)	Serious Unlikely	Medium	Ethan Czuppa, Caleb Cross, Trained Operator

Item Id	Sub-process / User / Task	Hazard / Failure Mode	Initial Assessment Severity Probability	Risk Level	Risk Reduction Methods /Control System	Final Assessment Severity Probability	Risk Level	Status / Responsible /Comments /Reference
1-1-9-4	Calibration of Vibration Measurement Testbed adult misuse	mechanical : unexpected start power to system improperly applied	Serious Likely	High	lock out / tag out, unplug power supply unless testing	Serious Unlikely	Medium	Ethan Czuppa, Caleb Cross, Trained Operator
1-1-9-5	Calibration of Vibration Measurement Testbed adult misuse	mechanical : product instability unsafe amount of correction masses added / improper adjustment of balancing mechanism	Serious Likely	High	slow ramp speed for motor, standard calibration procedure, Hardware/Software E-Stop	Serious Unlikely	Medium	Ethan Czuppa, Caleb Cross, Trained Operator
1-1-9-6	Calibration of Vibration Measurement Testbed adult misuse	electrical / electronic : energized equipment / live parts power left on	Moderate Likely	Medium	Unplug power supply unless testing - in accordance with standard procedure	Moderate Unlikely	Low	Ethan Czuppa, Caleb Cross, Trained Operator
1-1-9-7	Calibration of Vibration Measurement Testbed adult misuse	electrical / electronic : shorts / arcing / sparking unsafe electrical testing methods	Catastrophic Unlikely	Medium	standard eletrical testing procedures	Catastrophic Remote	Low	Ethan Czuppa, Caleb Cross, Trained Operator
1-1-9-8	Calibration of Vibration Measurement Testbed adult misuse	electrical / electronic : improper wiring improper troubleshooting/setup inexperienced operator	Catastrophic Likely	High	instruction manual - check wiring against schematic before applying power and/or testing	Catastrophic Unlikely	Medium	Ethan Czuppa, Caleb Cross, Trained Operator
1-1-9-9	Calibration of Vibration Measurement Testbed adult misuse	electrical / electronic : overloading motor is forced into stall condition and current limiting measures fail	Moderate Likely	Medium	hardware/ software E-Stop	Moderate Unlikely	Low	Ethan Czuppa, Caleb Cross, Trained Operator
1-1-9-10	Calibration of Vibration Measurement Testbed adult misuse	electrical / electronic : overvoltage /overcurrent power supply current and voltage limits improperly set	Moderate Likely	Medium	verify proper power supply settings before testing	Moderate Unlikely	Low	Ethan Czuppa, Caleb Cross, Trained Operator

Item Id	Sub-process / User / Task	Hazard / Failure Mode	Initial Assessment Severity Probability	Risk Level	Risk Reduction Methods /Control System	Final Assessment Severity Probability	Risk Level	Status / Responsible /Comments /Reference
1-1-9-11	Calibration of Vibration Measurement Testbed adult misuse	slips / trips / falls : impact to / with correction mass not properly torqued / locked in place in balancing mechanism	Serious Likely	High	fixed enclosure / barriers, proper PPE (face shield / safety glasses), standard balancing mechanism adjustment procedure	Serious Unlikely	Medium	Ethan Czuppa, Caleb Cross, Trained Operator
1-1-9-12	Calibration of Vibration Measurement Testbed adult misuse	heat / temperature : burns / scalds personnel bodily contact with heated surface of stalled motor or motor that has been run for a prolonged period of time.	Serious Likely	High	visible warnings, allow cool down period for motor before dissasembly	Serious Unlikely	Medium	Ethan Czuppa, Caleb Cross, Trained Operator
1-1-9-13	Calibration of Vibration Measurement Testbed adult misuse	heat / temperature : inadequate heating / cooling current motor is sealed and has no cooling mechanisms	Moderate Likely	Medium	Insepct motor during testing for smoking or squealing noises, add heat sink to motor	Moderate Unlikely	Low	Ethan Czuppa, Caleb Cross, Trained Operator
1-1-9-14	Calibration of Vibration Measurement Testbed adult misuse	noise / vibration : product / equipment damage improper balancing mechanism adjustment leads to resonance condition in system - large deflections and plastic deformation of turbine components	Moderate Likely	Medium	fixed enclosure / barrier, slow ramping speed	Moderate Unlikely	Low	Ethan Czuppa, Caleb Cross, Trained Operator
1-2-1-1	Calibration of Vibration Measurement Testbed passer-by / non-user walk near	mechanical : cutting / severing observer gets to close to spinning turbine without enclosure	Serious Likely	High	fixed enclosure / barrier, visible warning of danger zone, visible warning of permitted observer area	Serious Unlikely	Medium	Ethan Czuppa, Caleb Cross, Trained Operator
1-2-1-2	Calibration of Vibration Measurement Testbed passer-by / non-user walk near	mechanical : stabbing / puncture catastrophic blade failure with enclosure removed and observer in damaging range of blade shrapnel	Serious Likely	High	fixed enclosure / barrier, visible warning of danger zone, visible warning of permitted observer area	Serious Remote	Low	Ethan Czuppa, Caleb Cross, Trained Operator

Item Id	Sub-process / User / Task	Hazard / Failure Mode	Initial Assessment Severity Probability	Risk Level	Risk Reduction Methods /Control System	Final Assessment Severity Probability	Risk Level	Status / Responsible /Comments /Reference
1-2-1-3	Calibration of Vibration Measurement Testbed passer-by / non-user walk near	electrical / electronic : energized equipment / live parts power is applied to system during operating conditions	Moderate Likely	Medium	Observers not permitted to approach testing apparatus area or interact with mechanisms in those areas	Moderate Unlikely	Low	Ethan Czuppa, Caleb Cross, Trained Operator
1-2-1-4	Calibration of Vibration Measurement Testbed passer-by / non-user walk near	slips / trips / falls : trip larger diameter power and signal cables loose or in high foot-traffick areas	Minor Likely	Low	separate hazard / people in time or space, warning sign(s)	Minor Unlikely	Negligible	Ethan Czuppa, Caleb Cross, Trained Operator
1-2-2	Calibration of Vibration Measurement Testbed passer-by / non-user observe / watch	<None>						

Description of Hazard	Planned Corrective Action	Planned Date	Actual Date
Some parts will have tight fits and may have burrs on them from manufacturing or just from the nature of their constructed materials	Special assembly instructions will be used to put together the testing fixture and PPE such as gloves will be used during testing – specifically when moving or handling the sanded plywood enclosure. Finally, the tight-fitting parts will be deburred as much as is possible before use.	03/19/2021	03/19/2021
The rotor on the small-scale turbine spins at a max test speed of 3100 RPM and a standard test speed of 2500 RPM	An ½" thick plywood enclosure, that completely incases the rotor with enough margin to allow the whirl will be implemented	03/19/2021	N/A
The rotor vibrations test bed will be made of aluminum sheet and plate and a large, brushed DC motor with a total weight maximum of 10lbf	The test bed will be clamped to a heavy, sturdy table with several C-Clamps	03/19/2021	N/A
The rotor has a mass of ~1kg and will be spinning at a max speed of 3100RPM, and no braking mechanism	A fixed enclosure will encase the rotor any time testing is being conducted, the ramp rate in RPM/sec will be limited by the control system to prevent unsafe accelerations from a low energy state to a dangerous one	03/19/2021	N/A
An inexperienced user could make a balancing mechanism adjustment that puts the rotor into a resonance condition	If vibration levels of rotor become easily observable (e.g. the user can see/here/feel the vibration) the user will rapidly depress the E-Stop button to cut power to the motor driver and allow the rotor to decelerate inside of	03/19/2021	N/A

An inexperienced operator could troubleshoot unsafely and test live wires causing a short to ground An inexperienced operator could try to run a test without the enclosure	it's enclosure. Additionally, the operator will be wearing safety glasses and a face shield while running vibration tests. Standard electrical testing procedures will be used and documented for future operators Two operators (minimum) will be present to run a test and will go through a pre/post test safety checklist to ensure all proper guards were in place.		
Cascading failure of the safety hardware and control system (E-Stop, Fuse, over current/voltage protection on power supply, MCU running closed loop PI control on drive motor)	Hardware and software E-Stops will be implemented and if all of those fail the power supply will be located a safe distance from the rotor so it can be turned off/or unplugged to de-energize the system.	03/19/2021	N/A

Appendix T – Design Hazard Checklist

DESIGN HAZARD CHECKLIST

Team: CPWP ROTOR BALANCE Faculty Coach: PROF. FABIJANIC

Y	N	
☒	☐	1. Will any part of the design create hazardous revolving, reciprocating, running, shearing, punching, pressing, squeezing, drawing, cutting, rolling, mixing or similar action, including pinch points and sheer points?
☒	☐	2. Can any part of the design undergo high accelerations/decelerations?
☐	☒	3. Will the system have any large moving masses or large forces?
☐	☒	4. Will the system produce a projectile?
☒	☐	5. Would it be possible for the system to fall under gravity creating injury?
☐	☒	6. Will a user be exposed to overhanging weights as part of the design?
☐	☒	7. Will the system have any sharp edges?
☐	☒	8. Will any part of the electrical systems not be grounded?
☐	☒	9. Will there be any large batteries or electrical voltage in the system above 40 V?
☒	☐	10. Will there be any stored energy in the system such as batteries, flywheels, hanging weights or pressurized fluids?
☐	☒	11. Will there be any explosive or flammable liquids, gases, or dust fuel as part of the system?
☐	☒	12. Will the user of the design be required to exert any abnormal effort or physical posture during the use of the design?
☐	☒	13. Will there be any materials known to be hazardous to humans involved in either the design or the manufacturing of the design?
☐	☒	14. Can the system generate high levels of noise?
☐	☒	15. Will the device/system be exposed to extreme environmental conditions such as fog, humidity, cold, high temperatures, etc?
☒	☐	16. Is it possible for the system to be used in an unsafe manner?
☒	☐	17. Will there be any other potential hazards not listed above? If yes, please explain on reverse.

For any "Y" responses, add (1) a complete description, (2) a list of corrective actions to be taken, and (3) date to be completed on the reverse side.

Appendix U – Testing Procedure

I. Pre-Calibration Setup

Before going into the Cal Poly vibrations lab and calibrating the part, testing access must be approved and a testing date and time must be scheduled. This section will detail how to gain access to the Cal Poly vibrations lab and outline any tools or equipment you will need to bring to the testing site.

i. Cal Poly Vibrations Lab Access

1. E-mail the Cal Poly vibrations lab coordinator(s) to get approval for lab access. This procedure—and any revisions made for the current year of testing—must be submitted to the lab coordinators for verification. Below is the relevant contact information you can use to gain lab access (last updated 02/03/2021).
   - Lab Director: Dr. Julia Wu (xwu@calpoly.edu)
   - Lab Coordinator: Professor Hermanth Porumamailla (hporumam@calpoly.edu)
   - M.E. Department Senior Project Safety: Eric Pulse (epulse@calpoly.edu)

2. Schedule a date and time for lab testing. After approval from the lab coordinator(s) is obtained, select a date and time for in-lab testing and calibration from the dates provided. ///any additional steps needed to acquire lab access.

ii. Get Equipment

3. Obtain needed equipment for testing. While the Cal Poly lab will provide most equipment and tools needed for testing, the WPC is accountable for a few key items, listed below.
   - Wind turbine nacelle assembly.
     It is recommended to conduct the test with the completed nacelle design to ensure that the final calibration completely balances the wind turbine assembly. However, please ensure that the nacelle assembly used for calibration has an open line of sight to the shaft. This will be required for testing.
   - Power supply.
     A suitable power supply can be checked out from the Cal Poly EE Department on the Cal Poly campus.
   - Driving motor.
     /// supplied or bought each year? Can ours be reappropriated? Spec motor beforehand?
   - Controls system.
     /// supplied or made each year? Can ours be reappropriated? Spec supply beforehand?
   - Laser tachometer.
     A laser tachometer can be checked out from the Cal Poly EE Department on the Cal Poly campus. Alternatively, one can be purchased, or borrowed from a Cal Poly professor or graduate student.
   - Reflective tape.
     /// specific kind?
   - BNC-AUX adapter.
   - C-Clamps. ///provided by testers or lab?
   - Plywood enclosure
   - Controls interface
     i. Personal laptop with controls software installed
     ii. Microcontroller
     iii. Electrical panel
     iv. Voltmeter

II. Testing Apparatus Setup

Once arriving to the Cal Poly vibrations lab, all equipment must be checked to ensure that testing is ready to safely start. This section will outline the procedures conducted before testing to secure all testing apparatus.

To make the testing experience as smooth as possible, we recommend that the tasks during testing be split between three people.

- (1) Test Administrator
  - in charge of running the test, notifying all personnel when the test is about to start as well as when the test is complete, sending commands to the microcontroller via the laptop.
- (2) Data Collector
  - in charge of using ADRE for Windows to retrieve and display the data from the test as well as running the MATLAB script to analyze the results
- (3) Safety Officer
  - in charge of completing all pre-test inspection checklists and making sure all those present at the test are adhering to lab safety and testing safety personnel requirements.

However, prior to the slow roll test and completion of the pre-test inspection checklist, these roles are not needed.

i. Equipment Checklist

1. Complete the equipment checklist below to verify that all equipment is present for testing. If something supplied by the Cal Poly vibrations lab is not present, contact the Lab Coordinator to retrieve the needed item.
   - Supplied by Cal Poly vibrations lab:
     - ADRE 208/408 DAQ (x1)
     - ADRE 208/408 DAQ power cable (x1)
     - ADRE 208/408 DAQ serial cable (x1)
     - BNC cables (x3)
     - Amplifier box (x1)
     - White amplifier box cables (x2)
     - Accelerometer (100 mV/G) (x1)
     - Computer with ADRE Software (x1)
     - Table (x1)
     - Mounting wax (x1)
   - Supplied by testers:
     - Wind turbine nacelle assembly (x1)
     - Power supply (x1)
     - Driving motor (x1)
     - Controls system (x1)
     - Reflective tape roll (x1)
     - Laser tachometer (x1)
     - AUX feed cable (x1)
     - BNC-AUX adapter (x1)
     - C-Clamps (x3) ///provided by lab or testers?
     - ALL controls systems equipment (see sec. I.ii.3.i.)

ii. Nacelle Preparation

2. Fasten wind turbine nacelle assembly to testing table. Use the provided table set out by the Lab Coordinator. Clamp the nacelle assembly to the table using three C-clamps at each corner of the nacelle. Do not overtighten these clamps, as overtightening can cause damage to the table or nacelle base. Below is a diagram of the recommended clamp configuration.

///clamp diagram

3. Inspect nacelle assembly, ensuring that all components are securely fastened and correctly assembled. Verify that the shaft it is secured to the rotor hub, nacelle body and motor mount. Also verify that the motor is tightly mounted to the motor mount, as any loose mounting will cause undesired vibrations during testing.

4. Place the balancing mechanism securely onto the wind turbine shaft. Ensure that all bolt masses are fastened in the “zeroed” position, closest to the center of the balancing mechanism. Tighten all nuts on the mechanism to ensure that sliding masses are secure.

iii. Accelerometer Setup

5. Mount accelerometer to front plate of nacelle as close to the wind turbine shaft as possible. The accelerometer can be mounted in one of two ways:
   - Wax can be used to apply the accelerometer directly to the front plate of the nacelle. The accelerometer can be mounted horizontally, or vertically to the front plate.
   - The accelerometer can be placed into a pre-tapped hole on the front plate of the nacelle.

///accelerometer mounting diagram

6. Connect the accelerometer to the amplifier box using the thin, white wire provided with the amplifier box. Handle these wires with care, as they are delicate and prone to connection issues. If the meter on the amplifier box reads in the reg re, replace the wiring and retry the connection.

7. Connect the amplifier box to the ADRE 208 DAQ using a provided BNC cable. ///insert criteria for clear connection ///insert exactly which hole to put cable into

iv. Laser Tachometer Setup

8. Place a strip of reflective tape parallel to the shaft, on the shaft of the wind turbine in an open location. The tape should be located between the front bearing block, and the rear bearing block or motor coupler. ///does tape need to cover all of shaft or only part?

9. Suspend the laser tachometer over the shaft where the reflective tape is located. ///insert what tools to use to mount tachometer.

10. Connect the laser tachometer to the AUX-BNC adapter using the personally provided AUX cable.

11. Connect AUX-BNC adapter to the ADRE 208 DAQ using a provided BNC cable. ///insert criteria for clear connection ///insert exactly which port to put cable into

v. ADRE 208 DAQ Setup

12. Connect the ADRE 208 DAQ to the provided Cal Poly vibrations lab computer using the ///insert what cable needed to connect to which DAQ port and desktop port

13. Power on the ADRE 208 DAQ. ///insert where on button is?

14. Turn on the provided computer monitor and desktop. Once prompted, login to the Cal Poly servers.

15. Open the ADRE(R) for Windows software program. This program can be located ///give exact location on desktop, or found by searching "ADRE(R)" in the search bar at the bottom left hand of the monitor.

16. Configure the accelerometer to measure shaft vibrations. ///Insert how to navigate to program and pull up necessary windows Once open, substitute the provided value under "///which designation" of [200 mV/G] with the recommended value of [100 mV/G]. Save changes and return to the main program.

vi. System Power and Motor Driver Setup

17. Power on the personally provided laptop with ///insert software needed installed.

18. Connect motor encoder connector from microcontroller to encoder module on motor. Inspect connection on the microcontroller and verify that all connectors are completely seated, match the port names, and match the color code provided.

///color code diagram for microcontroller status LED

19. Connect three PWM servo cables between the motor driver and microcontroller. Below is a diagram of the recommended wiring configuration.

///PWM wiring setup

20. Inspect the power control panel fuse to ensure that the metal connections are not melted before usage. Once the integrity of the fuse is confirmed, connect the power supply outputs to the corresponding positive (+) and negative (-) inputs of the provided power control panel.

21. Connect the signal relay control wire to the microcontroller at the ///specify port port.

22. Connect the positive (+) and negative (-) outputs of the crimp connectors on the power control panel to the corresponding crimp connectors on the DC motor driver supply. Carefully insert the male supply connector to the female motor driver connector. Confirm that both red, positive (+) wires and both black, negative (-) wires are securely connected, so that both insulated portions of each wire overlap completely.

23. With the circuit breaker switched OFF, turn on the DC power supply. Set the input voltage to [///get value V] and current to [///get value A]. ///specify more power supply specs here

24. Test voltage feed to the motor. Set the digital voltmeter to the VDC setting option and select a voltage of ///insert voltage for voltmeter. Connect one voltmeter probe to the positive (+) and negative (-) feeds of the driving motor.
    - If the voltmeter reads [0 V] with minimal noise between [10-100 mV], the system is ready for testing and you may proceed to the next step.
    - If the voltmeter reads [0 L], overload is present in the system for the selected voltage range on the voltmeter. Remove the probes immediately and turn off the power supply. Disconnect the power supply from the power control panel, then reconnect, inspect all electrical connections and retry.

- If the voltmeter reads out [0.5 V] or more, grounding issues are present in the system. Remove the probes immediately and turn off the power supply. Disconnect the power supply from the power control panel, inspect all connections, then reconnect and retry.

25. Conduct the electrical system “smoke-check” test. Disable the microcontroller using the ///specify terminal command terminal command. Disconnect the motor from the motor driver. While keeping a safe distance from the testing apparatus, turn ON the circuit breaker and ensure that the following criteria are met. If a criterion listed below is not met, turn OFF the circuit breaker, investigate all associated connections, consult the troubleshooting appendix if needed, then retry.
    - Check the status lights pattern on the motor driver. If the light pattern matches ///provide pattern for motor driver in idle/ready state, the subsystem is ready for testing.
    - Check the power lamp on the control panel. If it is on, the subsystem is ready for testing.
    - Check the fuse on the control panel to ensure that it has not failed and is not failing. If the fuse is not glowing white with heat, the subsystem is ready for testing.
    - Check the status lights on the microcontroller. If the color and blinking pattern remains consistent after connected to the personal laptop, the subsystem is ready for testing.
    - Measure the input voltage on the supply side of the motor driver by placing the voltmeter probes on the positive (+) and negative (-) input terminals of the motor driver. While set to its active low state, the voltage of the motor driver should read [///Nominal Motor voltage V]. While disabled, the voltage of the motor driver should read [0 V]. If the motor driver meets both measurements, then the subsystem is ready for testing.
    - Measure the output voltage of the motor driver by placing the voltmeter probes on the positive (+) and negative (-) output terminals of the motor driver. While set to its active low state, the voltage of the motor driver should read [0 V], with allowance for minimal electrical noise between [10-100 mV]. If the Motor driver meets this criterion, the subsystem is ready for testing.

26. Switch OFF the circuit breaker, then connect the crimp connectors on the motor leads to the motor driver. To complete the connection, tighten the screw onto the forked or ringed end of the crimp connector. ///info on polarity?

27. Ensure that all wiring connections match the diagram provided below.

///complete controls wiring diagram

III. Safety Check and Pre-Calibration Inspection

The required testing apparatus is now in place. Before conducting the test however, we want to ensure that all equipment is being correctly utilized and is safe to operate. In this section, we will conduct an in-depth inspection of the testing setup to confirm that the whole system is ready for testing. For each section, visually inspect each outlined connection or apparatus interface. Make physical inspections when designated to. If inspecting, wear safety goggles. If inspecting wiring, wear rubber gloves.

i. Mechanical Inspection

1. C-Clamps.

☐ Physically inspect the clamps holding the nacelle to the table. Jostle the nacelle base to look for loose edges. Modify clamp tightening as needed.

2. Bolt tightness check.

☐ Physically examine all bolts and nuts used to fix the testing apparatus. Check tightness by slightly loosening the selected bolt with the applicable tool (appropriately sized combination wrench or an Allen/Hex wrench). Then retighten before testing. A comprehensive list of the items can be found below. This step can be completed in tandem with the testing mechanical setup.

- Balancing mechanism's test mass bolts. (///Reference to section)
  NOTE: verify that each test mass (1/4x20 square head bolt) is in the zeroed position, placed closest to the shaft.
- Balancing mechanism's mounting bolts. (///Reference to section)
- Castle nut with cotter pin/safety wire on end of shaft. (///Reference to section)
- Bearing block mounting bolts (///Reference to section)
- Motor mount bolts (///Reference to section)

☐ Be advised that bolts and nuts under vibrational loadings may loosen over time. If repeating this test, please re-examine the bolts and nuts to ensure stability before rebeginning the test.

3. Grooved plate configuration.

☐ Ensure that all the test masses in the grooved plate are equidistant from the center with the test mass positioning gauge such that they are as close to the center axis of the shaft as the slots that guide the test masses will allow.
NOTE: This step is essential for the measurement run the initial characterization of the turbine's mass imbalance.

4. Rotor Enclosure.

☐ Retrieve plywood enclosure and secure around wind turbine rotor. ///enclosure closing instructions Confirm that the enclosure sits flush against the testing table.

☐ Ensure that the shaft and rotor blades do not interfere with the enclosure. Once the enclosure is closed, rotate the wind turbine shaft by hand [360°]. If any interference is detected between the blades and enclosure, adjust the enclosure, and conduct the test again until no interference is detected.

☐ Ensure that the base of the rotor enclosure is weighed down with

ii. Electrical Inspection

5. Circuit breaker.

☐ Circuit breaker portion of smoke-test completed successfully.

6. Fuse.

☐ Visual inspection complete.

☐ Fuse portion of smoke-test completed successfully.

7. Wiring connections.

☐ Visually inspect all wire connections and verify that everything is connected properly. If physical inspection is needed, use rubber gloves before checking wiring.

☐ If loose wiring or cables are present on the floor of the lab, tape them down with electrical tape before testing to prevent trip hazards.

☐ If adjustments to the wiring or electrical configuration need to be made, turn off the power supply before making any changes. Disconnecting linkages while the power is on—also referred to as hot-swapping—is dangerous to the handler and can damage the electrical system.

8. Power supply.

☐ Confirm that voltage on the LCD screen of the power supply matches the voltage measured with the voltmeter.

9. Motor driver.

☐ Visually inspect supply side connections to driver, ensure the polarity is not reversed but the red (+) to red (+) and black (-) to black (-) convention is followed.

☐ Motor driver portion of smoke-test completed successfully.

iii. Software Inspection

///will be inserted after lab access and interface can be relayed

iv. Personnel safety

10. Disease prevention.

- ☐ In the event of a pandemic, all testing participants must be compliant with Cal Poly's pandemic regulations. If needed, wear masks, socially distance, and follow any in-lab signage or additional rules provided by Cal Poly, or the vibrations lab's coordinator.
- ☐ If testing is required before lab access can be granted, schedule for disease testing. Negative test results must be provided within two weeks prior to lab access.

11. Lab attire.

- ☐ Ensure that all testing participants are in accordance with Cal Poly lab attire policies.
  - Safety glasses or ANSI z81 face shields.
  - Close toed shoes.
  - Hair pulled back in a bun.
  - No dangling accessories or clothing.

12. Emergency evacuation route.

- ☐ In the unlikely event of a lab emergency, we recommend consulting the lab's evacuation procedure—posted as a placard at ///exact location—and learning the lab's evacuation route.

13. During testing.

- ☐ Test participants should distance themselves [///tbd feet] from the wind turbine nacelle during testing. This distance can be outlined with electrical tape on the floor to verify safe distancing.
- ☐ Do not touch the wind turbine nacelle, motor, or [
- ☐ or interference. If anything unsteady is observed, turn off the motor, the power supply, and wait for the wind turbine to come to a complete stop before approaching the testing area and making the necessary adjustments.
- ☐ Before starting the test, verbally verify that each testing participant is ready. Also verify that all participants are compliant with the previously mentioned safety directions.

IV. Measurement and Calibration Procedure

The following is the suggested procedure for a series of calibration runs to trim balance the Cal Poly wind power club turbine using the grooved plate. Now that everything is properly prepared, we can finally calibrate the balancing mechanism. This section will outline the calibration procedure needed to effectively balance the wind turbine using the provided balancing mechanism. For simplicity and safety purposes, each step of the testing procedure will be completed by a different, designated role. The three roles for testing are the test administrator, data collector, and safety officer.

The Test Administrator will interact with testing apparatus during testing.

The Data Collector will ensure that data is being reliably obtained during test.

The Safety Officer will certify that the test is being conducted in a safe manner throughout.

Several Steps from each of these procedures make use of and reproduce instructions from the Handbook and Reference for the ME 318 Laboratory manual, specifically Exercise 9 Single Plane Balancing and Phase Measurement, section "Balancing Procedure" pages 9-07 to 9-10.

i. Measurement Run Procedure

Measurement run refers to the characterization of the inherent mass imbalance present in the wind turbine without any mitigation from adjustment of the test masses in the grooved plate balancing mechanism.

1. (Safety Officer) Ensure that inspection checklist has been successfully completed.

2. (Data Collector) Ensure that the accelerometer connection quality is in the green region as indicated by the amplifier box indicator.

3. (Safety Officer) Ensure that every item on the inspection checklist has been completed successfully and give verbal confirmation to the Test Administrator.

4. (Test administrator) Before the start of a test run give and receive verbal confirmation between all those present that they are ready for the test to start. This includes verbal confirmation of "checklist completed successfully" from the Safety Officer.

5. (Test Administrator) Instruct those who assisted with the assembly and setup of the testbed step back to a safe distance of [ft] while remaining socially distant.

6. (Test administrator) Instruct observers to clear away from the enclosure to a safe distance of [///tbd ft] while remaining socially distant.

7. (Test Administrator) Send (/// terminal command) to the microcontroller via laptop to set control system to the Active Low Enabled state

8. (Test Administrator) Send (/// terminal command) to the microcontroller via laptop to spin up the motor at the default ramp rate [5 RPM/second] and tell Data Collector to start recording the run in the ADRE for Windows program.

9. (Data Collector) once the motor starts turning, click on "STORE ENABLE" from the ADRE for Windows program main menu. The real time data output of the sensors should be visible (///portion of the ADRE software GUI to check) and whenever prompted to overwrite your current run, select "NO, CONTINUE WITHOUT SAVING."

10. While the motor is ramping up to speed, listen for any abnormal noises and look for any abnormal vibrations.

11. (Safety Officer) If something goes wrong, immediately switch the circuit breaker to the off position and then turn off the power supply. Wait for all motion to cease before approaching the testing area. Adjust the testing setup, and once the issue is identified eliminated, re-secure all testing components and power up the power supply again.

12. (Test Administrator) Ramp motor slowly from [0 RPM] to [3000 RPM] (no more than 5 RPM/s) this will take about 10 minutes to complete

13. (Test Administrator) Once the turbine reaches the target speed of [2500/3100 RPM] (constant power threshold for shaft speed, max shaft speed for max testing wind speed), the controller will provide a notification via the terminal. Instruct the Data Collector to stop collecting data.

14. (Data Collector) on the Test Administrator's signal, stop collecting data by clicking Stop in the ADRE for Windows menu.

15. (Test Administrator) send (///terminal command) to the microcontroller via the laptop to ramp down the motor. When the motor has slowed sufficiently the controller will send a notification via the terminal and then proceed to brake the motor.

16. (Data Collector) Once the test run is complete, click on the button that looks like a miniature polar plot in the ADRE for Windows to view the collected Data.
    - If a full circle is not completed, but only an arc exists on the polar plot, this indicates that the shaft behavior is rigid (operating below its 1st natural frequency). This is still useable data, do not discard it.

    - If the plot is offset from the origin this indicates that a new SLOW ROLL vector needs to be selected to account for the non-ideal state of the system. From the main menu, select [Edit], [Reference Data], and finally [Vector Reference]. View all samples by

using the [Up/Down] arrows in the upper window. Select a representative sample at about [250 RPM], then "freeze" the sample by clicking the button in the first row of the lower half of the window. Record the 1X slow roll vector, then hit [OK]. Return to the initial polar plot to verify that the origin has been shifted [1].

- ///description of how to verify polar plot

17. (Data Collector) Once the polar plot is fully generated, extract the data from the polar plot and export it as a .csv to the Vibrations Calibration MATLAB Program. Once the data is properly imported, run the MATLAB file.
    - ///Troubleshooting for code and more on how to insert plot

18. (Safety Officer & Data Collector) After the MATLAB code has finished running, adjust each test mass in its corresponding groove according to the output of the MATLAB code.
    - ///Adjustment procedure – using the positioning gauge and loosening/tightening the bolts

ii. Calibration Run Procedure

Calibration refers to the adjusting the test masses in the grooved plate to reduce the measured imbalance (from the previous run(s)) to within a safety factor of the maximum imbalance threshold.

1. Repeat steps 1-15, excluding step 16 as the SLOW ROLL vector determined before hand is based on the rotor's uncalibrated state and all subsequent calibrations must have the same reference to ensure the balancing is done correctly.

2. Repeat steps 17 and 18 to apply the new calibration to the grooved plate.

3. The goal of balancing is to reduce the amplitude of vibration as much as possible, but realize that it is impossible to eliminate it entirely. We recommend the following threshold for considering a the rotor to be properly balanced [///safety factor dividing rigid fan balancing limit g-mm].

[1] Meagher, J., Ridgely, J., Garner, E., Iannce, M., Porumamilla, H., Cooper, M. (2015). Handbook and Reference for the ME 318 Laboratory. California Polytechnic State University San Luis Obispo.

V. Teardown and Clean-Up

After verifying that the balancing mechanism sufficiently eliminates imbalance in the wind turbine shaft, it will be time to deconstruct the test. This section outlines the steps necessary to safely disassemble the testing assembly and specifies the clean-up that needs to be done before leaving the vibrations lab.

Will this be followed during testing? Or should teardown/cleanup just have some general recommendations about teardown? Tell to consult equipment checklist to verify rather than walking through each thing.

i. Motor and Power Supply

1. Ensure that the motor and power supply are turned OFF. After the motor and power supply are OFF, disconnect the power supply.
2. Remove all electrical connections from the motor and power supply.
3.

ii. Laser Tachometer

4. Disconnect laser tachometer from AUX cable and remove from fixture. Safely return tachometer to its case and store away.
5. Remove AUX-BNC adapter

i. Motor and Power Supply

1. Ensure that the motor and power supply are turned OFF. After the motor and power supply are OFF, disconnect the power supply. Remove all electrical connections from the motor and power supply. After this is completed, general disassembly can begin.

ii. Disassembly

2. Disconnect all electrical wiring between testing apparati.

3. Disassemble or collect all testing apparatus. Consult the Equipment Checklist to ensure that all components are retrieved or properly stored for future lab usage.

iii. Clean-Up

4. Clean the wind turbine's shaft to remove any sticky residue left behind by the reflective tape.

5. If the accelerometer was mounted to the wind turbine's front plate using wax, remove any residue was from the accelerometer's mounting position.

6.

References:

[1] Meagher, J., Ridgely, J., Garner, E., Iannce, M., Porumamilla, H., Cooper, M. (2015). Handbook and Reference for the ME 318 Laboratory. California Polytechnic State University San Luis Obispo.

[2]

[3]

Appendix A: Troubleshooting

- If control system or motor driver is damaged, check controls crimp connectors to ensure that red/red and black/black are connected.
- Proper electrical measurement procedure with a digital voltmeter/am-meter (link to external resources)
    - Measure current
    - Measure voltage
    - Continuity Testing
- microcontroller Troubleshooting
- Motor driver Module troubleshooting – attach manual for module selected or link to resource)

Appendix V – The Theory and Practice of Miniature Wind Turbine Balancing

M E M O R A N D U M

To: The Cal Poly Wind Power Club (WPC)

From: Caleb Cross (*ccross01@calpoly.edu*)

Ethan Czuppa (*eczuppa@calpoly.edu*)

Date: 03/19/2021

Subject: **The Theory and Practice of Small-Scale Wind Turbine Balancing**

Introduction

This memo is aimed to provide a fundamental understanding for balancing unbalanced, small-scale wind turbines. Although rotor dynamics is an extraordinarily complicated subject, we will only be discussing elementary theory alongside the practical applications of imbalance correction.

THEORY

This section will discuss the technical concept of rotor imbalances, as well as delve into the specifics of balancing procedures used to eliminate unbalances.

What is mass imbalance?

Mass imbalance in a rotating assembly occurs when the center of mass (C.O.M.) of the rotating object(s) is not coincident to the axis of rotation. If there is a discrepancy between the center of mass and the axis of rotation, the shaft will oscillate between the two points, causing a vibration.

In a wind turbine, mass eccentricities are most often introduced by non-identical blades. However, mass imbalances can also emerge from manufacturing defects or asymmetrical designs.

The resulting vibrations can impede optimal power collection and catalyze fatigue in the system. In severe cases, unchecked vibrations can excite the natural frequencies within the assembly, causing catastrophic system failure.

To mitigate any present imbalances, the system must be manually balanced by artificially displacing the center of mass of the rotating assembly to be in alignment with its axis of rotation.

Rigid vs. Flexible

A rigid system is a mechanical system operating below its first natural frequency. If a system is operating at or above the first natural frequency of the rotating assembly, the system is considered to be flexible.

In most small-scale wind turbines, it is common to operate above the first natural frequency of the system. In spite of this, we are still able to model miniature wind turbines as rigid systems due to the system's scale and the strength of materials. The shaft of the system must be made out of steel—or any stronger material—in order to be properly evaluated as a rigid system. Assuming the system is rigid allows us to utilize the following balancing methods.

Spot Balancing

After an imbalance is quantified, small masses can be placed onto the rotating assembly to counteract present imbalances. This is simply referred to as spot balancing.

Spot balancing is most effectively used to correct residual or small imbalances. It is recommended to primarily use spot balancing to correct notable asymmetries. For example: mismatched blades can be sanded down to become more similar, and therefore, correct imbalance. Alternatively, an asymmetrical hub could effectively balanced by simply putting a setscrew onto the opposite side of the hub. Spot balancing, however, will not be as precise or efficient as some of the following balancing methods.

Single Plane Balancing

The single plane balancing method utilizes one balancing plane to correct eccentricities. This method generally makes use of a balancing disk, placed in or near the plane of imbalance. A balancing disk is a circular disk attached to the shaft which can be calibrated to introduce an opposing imbalance, eliminating all imbalance in the rotor assembly. Below is a diagram which depicts how a balancing disk placed in the plane of imbalance is able to artificially correct the rotating assembly's center of mass (*Figure 1*).

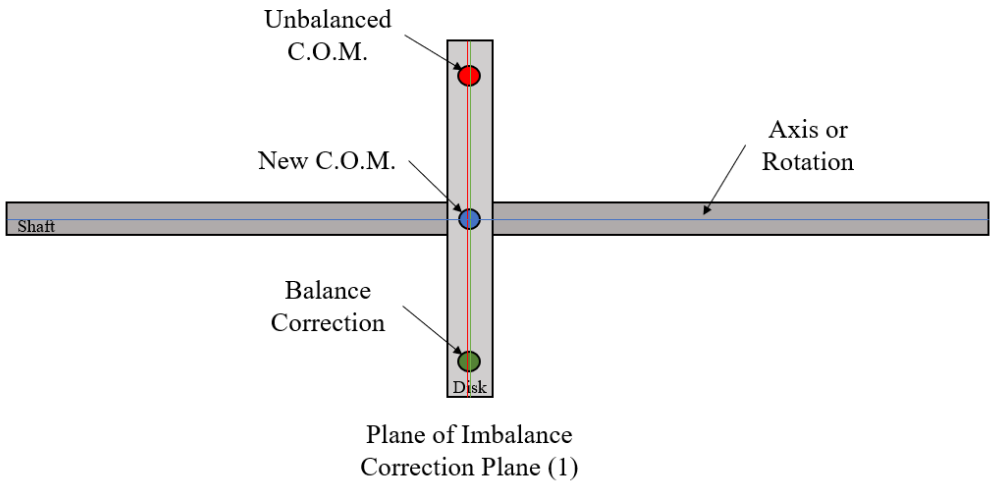

Figure 1: Single Plane Balancing with a Balancing Disk

A few criteria must be met in order for single plane balancing to be effective. Firstly, the diameter of the wind turbine's hub rotor must be twice as large as the length of the hub. If the rotor hub is too long, the plane of correction cannot adequately correct imbalances in the plane of imbalance. Additionally, there cannot be a bisecting bearing block between the plane of imbalance and the plane of correction. While the inclusion of a bearing block would hinder vibrations, it also isolates the plane of imbalance, cementing the initial imbalance of the system. Lastly, the plane of correction must be located within one half of the rotor's diameter, relative to the plane of imbalance. Below is diagram displaying the distancing relationships required for single plane balancing to be justified (*Figure 2*).

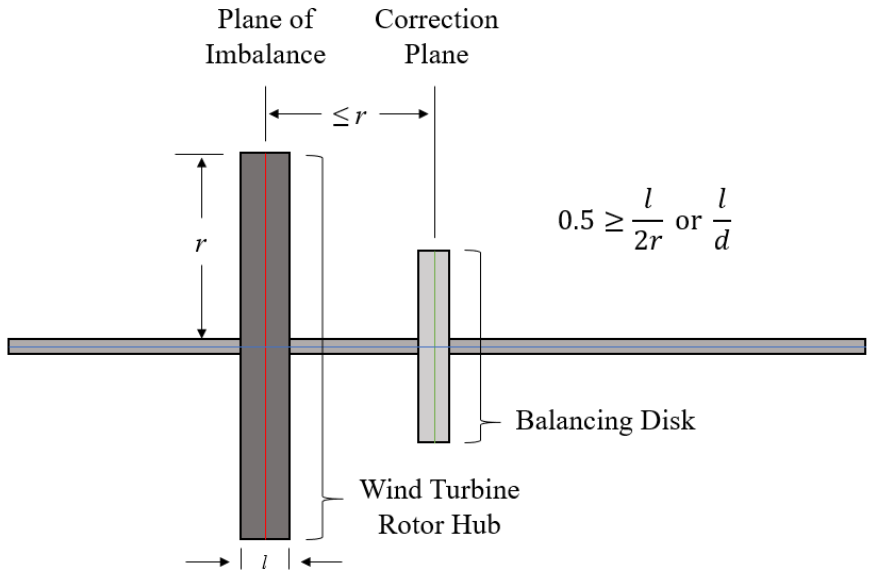

Figure 2: Criteria for Single Plane Balancing

Single plane balancing often offers higher precision than spot balancing, as exact distances or masses can be used to simulate variable imbalances.

Summary of requirements for single plane balancing:

- The wind turbine's hub diameter should be twice as large as the length of the rotor.
- A bearing block cannot be located between the plane of imbalance and the plane of correction.
- The distance between the plane of imbalance and the plane of correction must be less than half of the hub's diameter.

Two Plane Balancing

Much like the name suggests, this balancing method utilizes two balancing planes, which cumulatively correct existing eccentricities. Below is a diagram depicting how two equally distanced balancing disks can be used to artificially modify the system's center of mass (*Figure 3*).

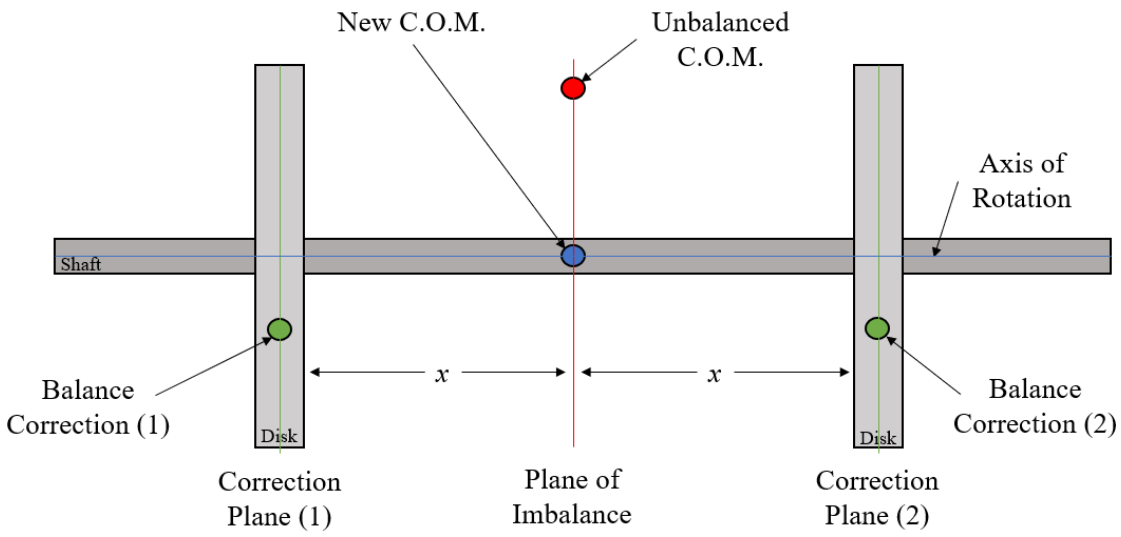

Figure 3: Two Plane Balancing with a Balancing Disk

Similar to single plane balancing, two plane balancing also requires the rotor diameter to be twice as large as the length of the rotor, as well as the absence of a bearing block between the planes of imbalance and correction.

Two plane balancing is often utilized in cases when the plane of imbalance is inaccessible. Generally, the overhung rotor of traditional wind turbines makes two plane balancing unnecessary. However, this method may be efficiently applied to non-traditional wind turbine designs.

Summary of requirements for two plane balancing:

- The wind turbine's hub diameter should be twice as large as the length of the rotor.
- A bearing block cannot be located between the plane of imbalance and the planes of correction.
- The distance between the plane of imbalance and the plane of correction must be less than half of the hub's diameter.

PRACTICE

This section will discuss the logistical applications associated with balancing a small-scale wind turbine, as well as a few crucial design recommendations to optimize performance and minimize imbalance.

Balancing Mechanism Design Considerations

The chief purpose of a balancing mechanism is to be accurately calibrated to oppose the inherit imbalance of the rotating system. A balancing mechanism can take the form of a balancing disk, spot balancing, or an imaginative alternative. Imbalances in the balancing mechanism can be introduced in one of three ways: variable masses, variable displacements, or variability in both mass and displacement. Of these options, variable displacement tends to be the most popular, as mass adjustments can be complicated to integrate and costly.

Although the exact construction of the device is at the designer's discretion, there are a few key requirements for a balancing mechanism to be effectively used. Firstly, the balancing mechanism must be able to correct for any imbalance located at any radial angle from the shaft. Since the system's unbalance can be located between [0°] and [360°] radially from the shaft, the balancing mechanism must be able to generate an imbalance at any given angle.

Secondly, due to the small scale of the system and the respectively modest imbalances, a precise calibration procedure is needed. Without a precise measurement process and calibration options, the balancing mechanism may not be able to efficiently eliminate system unbalances. Allowable residual imbalance in a wind turbine abides by the following equation.

	$U=9459(GW/N)$	(EQ. 1)

G is the balancing grade—simply [6.3 mm/s] for small-scale wind turbines—*W* is the mass of the rotor assembly, and *N* is the maximum rotational speed of the assembly. The final balancing mechanism must be precise to the calculated value of residual imbalance.

Thirdly, each mass used in the balancing mechanism should be approximately weighted as [40%] of the entire rotor assembly. The industry standard for balancing small rotating systems is generally less, however for smaller-scale systems, this must be scaled up.

Lastly, the balancing mechanism must be thoroughly evaluated as safe to utilize. Being an adjustable subsystem on a rotating assembly, parts may be at risk of flying off during testing. Before putting the designed balancing mechanism to the test, calculate the forces holding the subsystem together and holding the subsystem to the rotating assembly. After all forces have been verified to be within a safe threshold, testing can begin.

Summary of requirements for balancing mechanism design:

- Balancing mechanism must be able to correct for imbalance in all angular directions [0°-360°].
- Balancing mechanism should be precise to approximately [10 g-mm].
- Masses used in the balancing mechanism should weight [40%] of the rotor assembly. Note that the rotor assembly includes the shaft, hub, and the balancing mechanism itself.

Measuring Imbalances

Measurement of the wind turbine's imbalance necessitates access to the Cal Poly Vibrations Lab (Vibes Lab), as well as some of its essential tools. Access to the Vibes Lab must be granted to all testing participants prior to testing. Contact the Vibes Lab coordinators, or the ME Department Chair to obtain access for all testing participants.

The WPC is responsible for bringing a few key items to the Vibes Lab for testing, which have been itemized below.

- Wind turbine assembly (1)
- Power supply (1)
- Driving motor (1)
- Controls system (1)
- Laser tachometer (1)
- Reflective tape roll (1)
- AUX feed cable (1)

- BNC-AUX adapter (1)
- C-clamps (3)
- Rotor enclosure (1)

Note that the laser tachometer, reflective tape, AUX feed cable, and the BNC-AUX adapter are not needed if using a keyphaser rather than a laser tachometer. Also note that the rotor enclosure should be designed to not interfere with the rotor hub during testing. [½ inch] plywood is recommended as a sturdy, yet lightweight material for the enclosure which will properly protect against small projectiles.

A comprehensive list of all equipment and testing steps can be found in the WPC Wind Turbine Balancing Procedure [1] document.

Before a rotating system can be balanced, an imbalance must be correctly measured. Measuring vibrations in a system require two identifications: vibration magnitude and phase angle. The magnitude can be measured with either a proximity probe, or an accelerometer. The phase angle of the vibration can be measured with either a keyphasor probe, or a laser tachometer. The WPC Wind Turbine Balancing Procedure [1] utilizes the most simplified system, with an accelerometer and a laser tachometer to measure unbalance. Nonetheless, this measurement process can be modified as needed to use alternative equipment or accommodate for complex turbine designs.

Wind Turbine Design Considerations

There are a few key considerations for wind turbine design that will harbor testing ease and innately mitigate imbalance.

The wind turbine must be properly instrumented to house the measurement tools used in testing. If a proximity probe is used to measure vibration magnitude, then the shaft must be instrumented with a notch which can securely hold the probe while rotating. Alternatively, if an accelerometer is used, it can be attached to the front plate of the wind turbine via an appropriately thread hole, or by using mounting wax in a horizontal or vertical configuration. In addition, the bearing located on the front plate of the wind turbine must be pressed fit to the shaft. An interference fit will provide adequate accelerometer data, but any looser fit would inaccurately model vibration measurements.

If phase data is collected with a keyphasor probe, a notch in the shaft will need to be made to accommodate for the probe. Alternatively, a laser tachometer simply needs a clear line of sight to the shaft in order to obtain phase data. It is recommended to make the shaft of the wind turbine as accessible as possible, ensuring that the laser tachometer has an unobstructed view during testing and allowing for ease of adjustment as necessary.

While imbalances can emerge from a myriad of sources, measures to minimize emergent imbalances can be incorporated into the wind turbine's design. Below is a diagram from ISO 1940 regarding mechanical vibrations in rigid rotors [2] (*Figure 4*). The diagram details the length of the rotor (b), the distance between the back bearing—or coupling—and the plane of imbalance (c), and the distance between the back bearing and the front bearing (d).

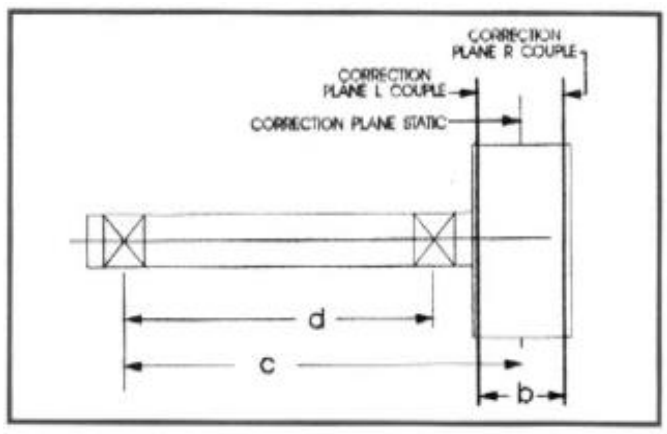

Figure 4: General Diagram for an Overhung Rotor Assembly using Two Plane Balancing [2]

To analyze the effects of each dimension on the allowable imbalance in the system, each parameter was varied to analyze its effect on the allowable imbalance for single plane and two plane balancing. The results of this parametric study can be found below (*Figure 5*, *Figure 6*, *Figure 7*, *Figure 8*).

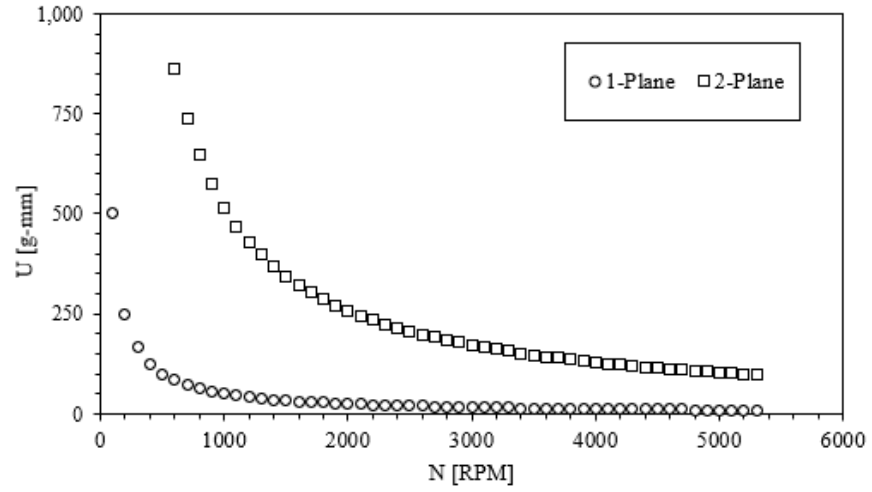

Figure 5: Allowable Residual Imbalance (U) for Varied Rotational Speeds

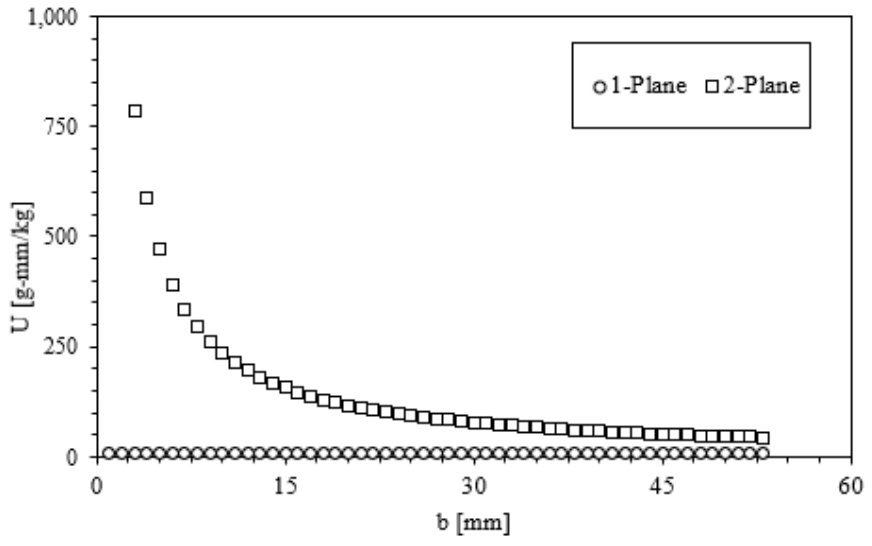

Figure 6: Allowable Residual Imbalance (U) for Varied Rotor Lengths (b)

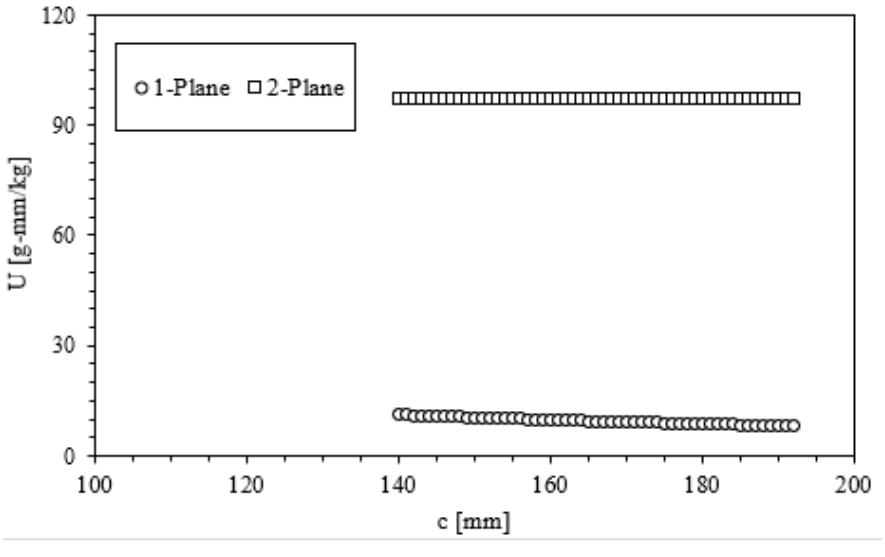

Figure 7: Allowable Residual Imbalance (U) for Varied Distance between Back Bearing and Plane of Imbalance (c)

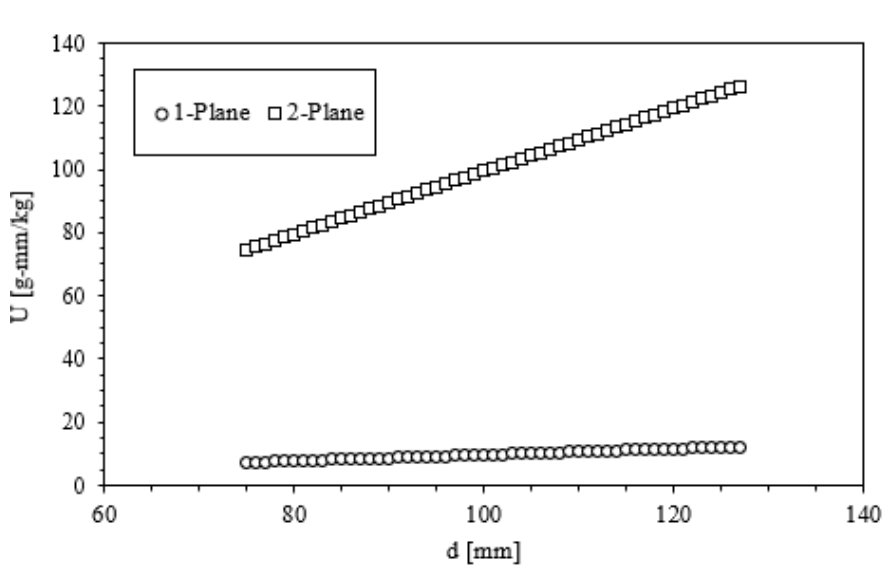

Figure 8: Allowable Residual Imbalance (U) for Varied Distance between Bearings (d)

Unintuitively, it is recommended to design to maximize allowable imbalance in the system, which will inversely make the system less susceptible to existing imbalances. Below are the recommended design considerations which will mitigate imbalances in the system (*Table 1*).

Table 1: Recommended Design Considerations to Mitigate Imbalances

Variable	Minimize or Maximize
b	Minimize
c	Minimize
d	Maximize

Note that these recommendations will not yield a perfectly balanced wind turbine in itself; the system still must be manually balanced. However, designing in-line with these considerations will make the final wind turbine system more stable during operation, and ultimately easier to balance.

In the event that the wind turbine sways during testing, it is recommended to add a counterweight to the back of the wind turbine. However, most sway should be naturally eliminated through the inclusion of a fin, located on the back of the wind turbine.

Lastly, if time permits, it is recommended to perform frequency analysis on the completed CAD model to verify that no natural frequencies are excited. This is an unlikely scenario, but it is important to ensure that the system is not operating at or close to any of its natural frequencies. Alternatively, a brief hand calculation of the shaft's natural frequency should sufficiently evaluate whether any trouble will arise during usage.

Summary of recommendations for wind turbine design:

- Instrument the wind turbine to accommodate for the appropriate testing equipment.
- Minimize the length of the rotor.
- Minimize distance between the rear bearing/coupling and the plane of imbalance.
- Maximize distance between rear bearing and front bearing.
- Use a fin and/or a counterweight in the back of the nacelle to mitigate sway.
- Ensure that no natural frequencies are excited during testing.

Conclusion

The ultimate aim of balancing a wind turbine is to achieve a safe and efficient testing environment. When balancing a wind turbine, it is essential to ensure that all criteria are met for the balancing method to be effective. This requires interconnectivity between the wind turbine design team and the balancing team to work towards designing a safe system that can be readily balanced.

This document should be revised for future reference in the event that the balancing criteria or procedure change.

References

[1] Cross and Czuppa, *WPC Wind Turbine Balancing Procedure*, 1st Edition, Cal Poly ME Department, 2021.

[2] Rieger, Neville F. *Balancing of rigid and flexible rotors*. STRESS TECHNOLOGY INC ROCHESTER NY, 1986.

Appendix W – Cura © 4.7.1 Slicer Settings

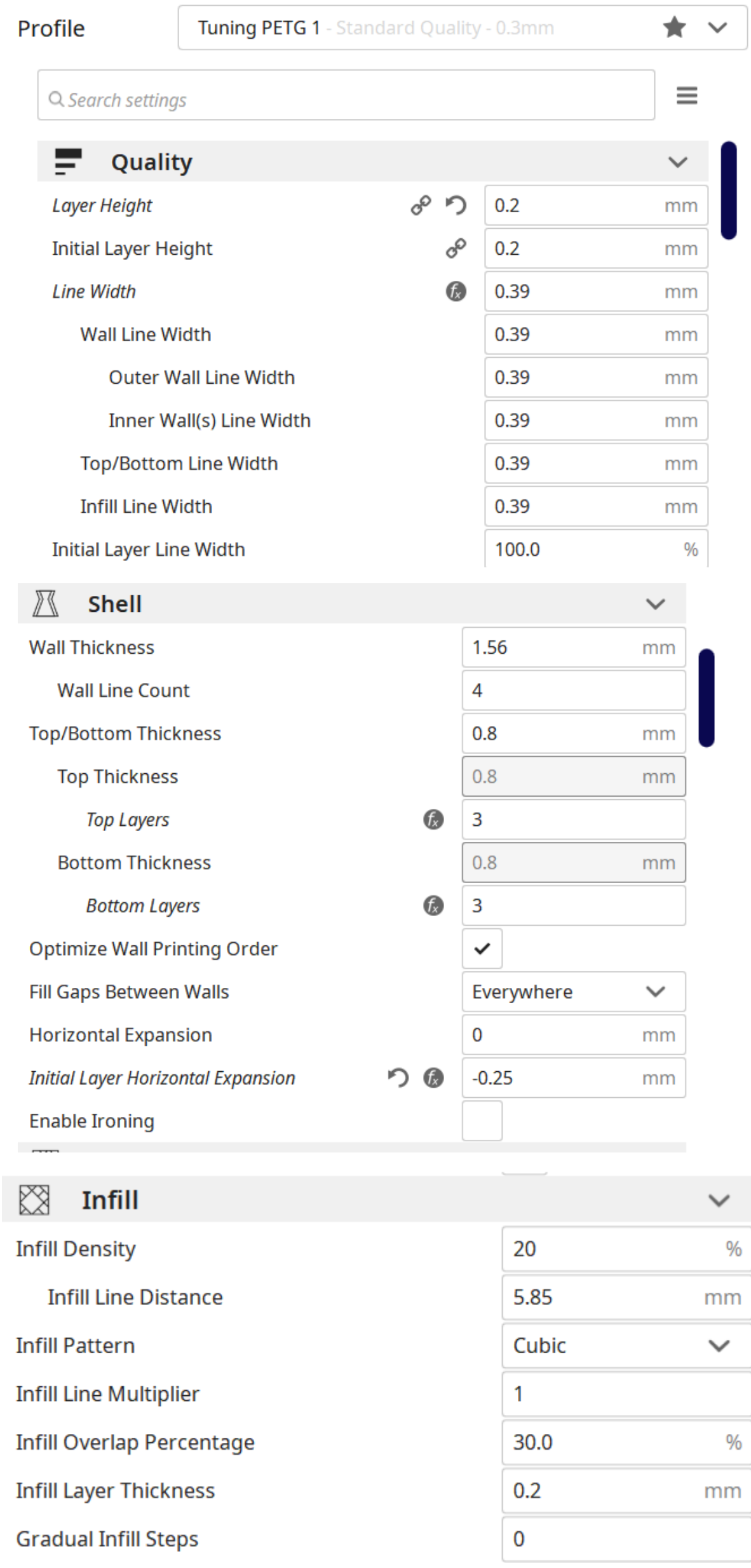

**** Print At 80-100% infill for actual body to be used in testing, this infill setting is for tuning feature dimensions.**

Material

Printing Temperature		225 °C
Printing Temperature Initial Layer		225 °C
Initial Printing Temperature		225 °C
Final Printing Temperature		225 °C
Build Plate Temperature		80 °C
Build Plate Temperature Initial Layer		80 °C
Flow		100 %
Initial Layer Flow		100 %

Speed

Print Speed		60 mm/s
Infill Speed		60 mm/s
Wall Speed		30.0 mm/s
Outer Wall Speed		30.0 mm/s
Inner Wall Speed		30.0 mm/s
Top/Bottom Speed		30.0 mm/s
Travel Speed		150.0 mm/s
Initial Layer Speed		15 mm/s
Skirt/Brim Speed		15 mm/s
Enable Acceleration Control		
Enable Jerk Control		

Travel

Enable Retraction		✓
Retract at Layer Change		
Retraction Distance		3 mm
Retraction Speed		25.0 mm/s
Combing Mode		Not in Skin
Avoid Printed Parts When Traveling		✓
Avoid Supports When Traveling		✓
Travel Avoid Distance		0.625 mm
Z Hop When Retracted		

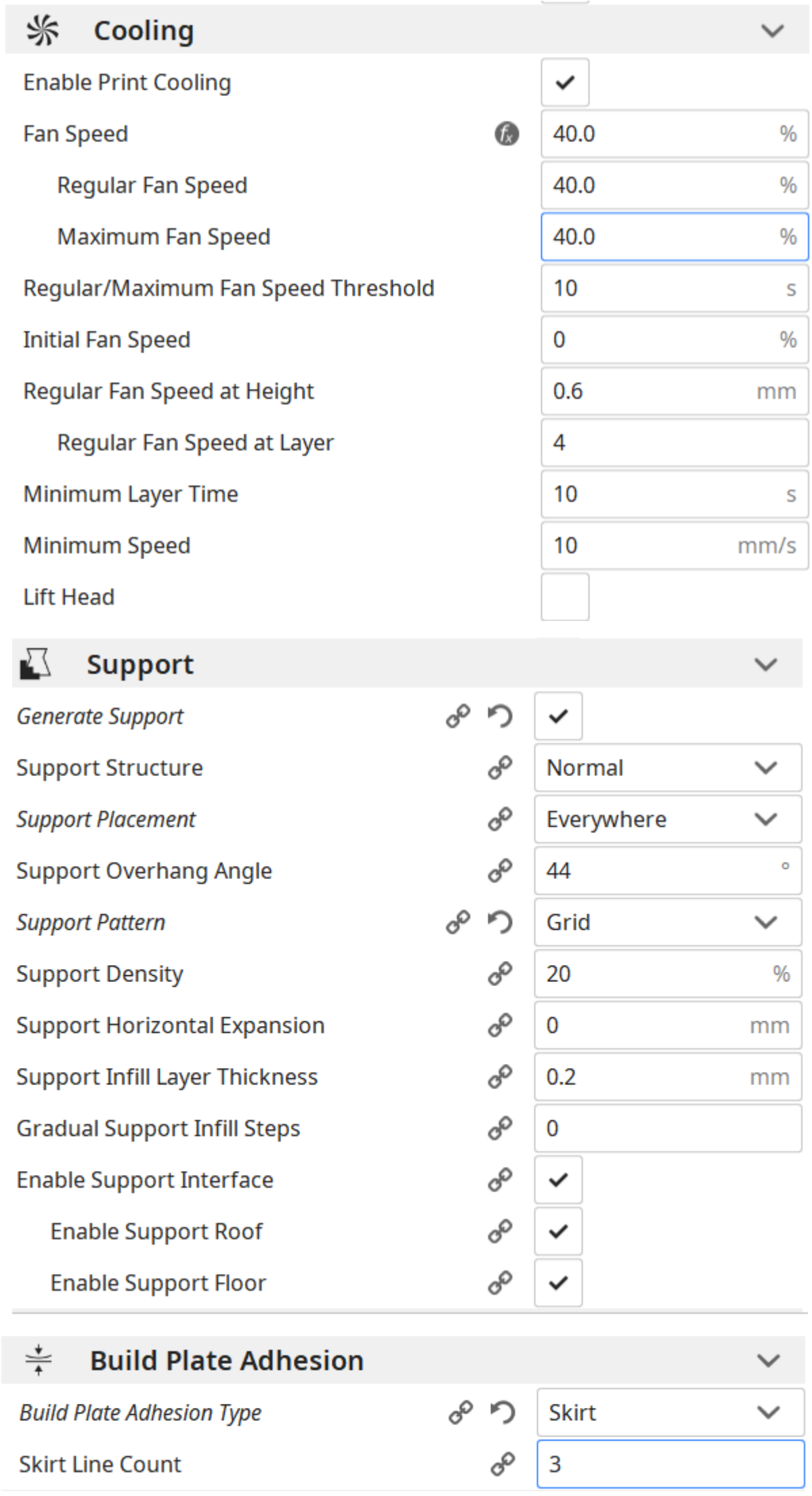

****Default parameters left for "Dual Extrusion", "Special Modes", and "Experimental".**

Note: all printer settings displayed correspond to a Creality Ender – 3 with glass bed plate. This is a hobby level 3D printer that comes as a kit. The settings here may need to be adjusted for your specific printer, but are provided here as a starting point.